Interpretation of the behavior of pile foundations in unsaturated soils subjected to axial and lateral loading

XINTING CHENG

Thesis submitted to the Faculty of Engineering
in partial fulfillment of the requirements for the
Doctorate in Philosophy degree in Civil Engineering

Department of Civil Engineering
Faculty of Engineering
University of Ottawa

ABSTRACT

Many regions in the world are experiencing drying trends due to climate change effects. The cumulative influence of environmental activities associated with rainfall infiltration, evaporation and plant transpiration contributes to a groundwater table (GWT) typically located at a great depth, especially in arid and semi-arid regions. Due to this reason, natural soils are widely found to be in a state of unsaturated condition. Unsaturated soils are tri-phase materials comprised of solids (i.e., soil particles), liquid (i.e., water) and gas (i.e., air), which have more complex hydraulic and mechanical properties in comparison to saturated soils. Pile foundations are widely used to transfer large loads from the superstructure to a deeper stratum with reduced soil settlements. In many scenarios, pile foundations are either entirely or partly embedded in unsaturated soils. For the rational design of pile foundations, it is important to ensure that it can support different types of loads that include axial, lateral or transversal loads arising from the super structures that are safely transmitted to the soil below without undergoing bearing capacity failure in addition to limiting the excessive deformation. However, the load transfer mechanism of piles embedded in unsaturated soils has not been fully investigated in the presently available literature. Unreliable estimations are likely if saturated soil mechanics principles are used to design or analyze the nonlinear response of pile foundations. Therefore, a better understanding of the mechanical properties of unsaturated soils and pile-soil interaction is required for the rational interpretation of the load-displacement behavior of piles in unsaturated soils. The focus of this thesis has been directed towards investigating the influence of varying unsaturated conditions on the behavior of piles under axial and lateral loadings extending the mechanics of unsaturated soils.

To investigate the behavior of laterally loaded piles in unsaturated soils, a nonlinear analytical method is proposed to predict the lateral response of rigid piles considering the influence of matric suction. The lateral load corresponding to lateral displacement is derived considering three different states. Good comparisons are achieved between the

results of the analytical method and measurements from eight published field pile load tests in unsaturated soils. Finite element analyses are then undertaken to model the lateral response of pile foundations. The proposed numerical method is validated against two experimental studies from the literature.

To investigate the behavior of axially loaded piles, an analytical approach is proposed for predicting the end-bearing capacity of driven piles that are subjected to axial loads based on the stress characteristic method. The validation of the analytical method is established using eleven case studies of driven piles in saturated soils and two in unsaturated soils. Numerical analysis is undertaken to simulate a published model test of driven piles in unsaturated sand. Both dynamic and static analysis are involved in the numerical analysis to simulate the pile driving and the following pile loading.

A simplified methodology is first proposed for estimating the load-displacement response of single piles under axial loading using modified hyperbolic function-based load transfer models. Then the proposed model is extended for pile groups considering the interaction effects between individual piles. The validity of the approach for both single pile and pile groups is demonstrated using three pile load tests results from the literature. Furthermore, a three-dimensional (3D) numerical analysis is undertaken to analyze the nonlinear response of pile groups implementing a user-defined subroutine into ABAQUS software. Good comparisons are found between the predictions from both the proposed analytical method and numerical analysis with the measurements.

In addition, a comprehensive numerical technique is proposed for simulating the load-displacement behavior of single piles embedded in unsaturated soils using finite element analysis. A user-defined subroutine is implemented into ABAQUS taking account of nonlinear shear strength and modulus of elasticity of unsaturated soils with respect to matric suction. The numerical analyses are then performed on four pile load tests that include two model pile tests in the laboratory and the remainder two from the field tests that were gathered from the published literature. Reasonably good predictions are achieved for all cases. The proposed numerical technique is a simple and useful tool for use in geotechnical engineering practice for the rational design of pile foundations in unsaturated soils.

The bearing capacity and settlement are two key properties of pile behavior, which should be estimated rigorously considering the influence of matric suction. The studies summarized in this thesis provide valuable insight towards implementing the unsaturated soil mechanics into the rigorous design of pile foundations in unsaturated soils considering the influence of matric suction under axial and lateral loading. The proposed analytical and numerical models are useful for the rational design of pile foundations for both saturated and unsaturated soil conditions.

ACKNOWLEDGMENTS

The studies presented in this Ph.D. thesis were conducted at the Department of Civil Engineering, University of Ottawa under the supervision of Prof. Sai K. Vanapalli. I would like to express my deepest appreciation to Dr. Vanapalli for his significant support and ongoing mentorship. His humble approach to research is truly inspiring, and his philosophy towards both research and life has been invaluable for me. His guidance and consistent feedback were indispensable throughout my Ph.D. journey, particularly during the COVID-19 pandemic, and without his support, this thesis would not have been possible.

The financial supports received from China Scholarship Council (CSC) and University of Ottawa joint scholarship, the Natural Sciences and Engineering Research Council of Canada (NSERC) are gratefully acknowledged. In addition, I would like to thank the Faculty of Engineering at University of Ottawa for providing an opportunity to visit Durham University, the UK for three months to enhance my research experience.

I would like to thank thesis committee members, Prof. Rozalina Dimitrova, Prof. Sedano Julio Angel Infante, Prof. Mohammad Rayhani and Prof. Nadarajah Ravichandran. Special thanks go to Prof. David Toll and Prof. Alexandros Petalas at Durham University for their academic support and kind help.

My appreciations extend to faculty officers, Luc and Jean-Claude. Many thanks also to my colleagues and friends from our research group: Yunlong, Junping, Penghai,Ping, Ruixia, Xiuhan, Mengxi, Mingshu, Hongyu, Maha, Junjie, Yao, Xinye, Aolin, Pan, Ziwen and Hao. Special thanks to BP and my furry friends Juju, Bobo, Indy and Duoduo.

Most importantly, none of this could have happened without my family. I am extremely grateful to my parents for providing me with unfailing support and continuous encouragement throughout my years of study. I would also like to thank my grandmother, who always offered her encouragement and support through video calls.

TABLE OF CONTENTS

LIST OF FIGURES

LIST OF TABLES

CHAPTER 1

INTRODUCTION

1.1 Background

The arid and semi-arid regions cover 1.9×10^7 km^2 and 2.3×10^7 km^2, respectively that account for 13 and 15 % of the Earth's land surface (Huang et al. 2016). Figure 1.1 shows the global distribution of arid and semi-arid regions. Many countries in the world are experiencing drying trends because of global warming, especially those in Africa, Eurasia and eastern Australia (Hoerling and Kumar 2003, Dai 2013, Ma and Yang 2017). The natural groundwater table (GWT) is typically at a great depth below the natural ground surface particularly in semi-arid and arid regions due to the cumulative influence of environmental activities such as rainfall infiltration, evaporation, and plant transpiration. The soil zone between the ground surface and GWT is typically in a state of unsaturated condition. An unsaturated soil is a multiphase continuum system containing soil particles (i.e., solid), water (i.e., liquid) and air (i.e., gas). The behavior of unsaturated soils is significantly influenced by air-water interphase (Fredlund and Rahardjo, 1993). The presence of an air-water interface generates surface tension within the soil skeleton that is strongly related to the soil suction and contributes to improving the mechanical behavior of unsaturated soils. Therefore, the hydraulic and mechanical properties of unsaturated soils complex in comparison to saturated soils and have been interpreted by many researchers considering the influence of matric suction during the past six decades (e.g., Bishop 1959, Fredlund et al. 1978, Escario et al. 1989, Alonso et al. 1990, Vanapalli et al. 1996, Wheeler et al. 2003, Lu and Likos 2006, Sheng et al. 2008).

Pile foundations are long slender axial columns that are widely used to transfer large loads from the superstructure to the soil below and significantly limit the settlements. These foundations are frequently used for supporting infrastructures such as high-rise buildings, embankments, bridges and pavements. In addition, the pile foundations should be capable of supporting vertical, transversal, or lateral loads without causing damage to the superstructure, failing in bearing capacity or causing excessive deformation (Salgado 2006). In other words, the bearing capacity and settlement are two key parameters in the design of pile foundations. Four different methods are widely used for investigating the behavior of pile foundations assuming saturated soil conditions; namely, static pile load tests (Vesić 1970, Altaee et al. 1992, Paik et al. 2003, Karlsrud et al. 2014, Yang et al. 2015), dynamic methods (Hery 1983, Rausche et al. 1985, Fellenius 2006); static analysis (e.g., total and effective stress approach) (Skempton 1959, Vesić 1963, Burland 1973, Vijayvergiya and Focht 1972), and direct or indirect use of results from in situ tests (Nottingham 1975, Schmertmann 1978, Bustamante and Gianeselli 1982, Eslami and Fellenius 1997, Lehane et al. 2005, Jardine et al. 2005).

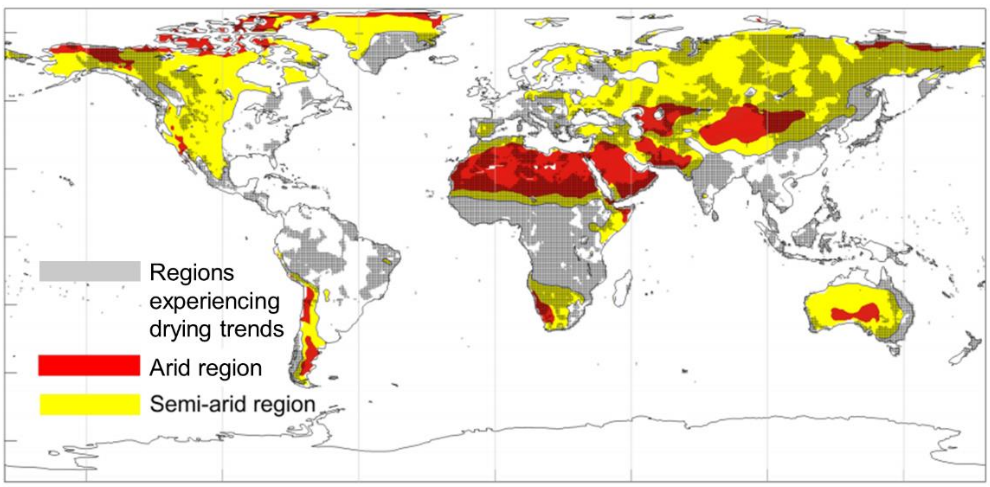

Figure 1.1 The global distribution of arid and semi-arid regions (modified after Ma and Yang, 2017)

Figure 1.2 presents the load transfer mechanism for axially and laterally loaded piles, respectively. As shown in Figure 1.2(a), the ultimate bearing capacity of a single pile Q_u consists of two parts: pile shaft carrying capacity Q_s and end-bearing capacity Q_b. During the pile installation, the soil adjacent to the pile shaft will be disturbed and remoulded to some extent. Thus, the pile shaft carrying capacity Q_s is not equal to the shear strength of soil but can be considered as a function of cohesion and friction angle of the pile-soil interface. When a pile is subjected to a lateral force and moment, the distribution of unit soil stresses normal to the pile shaft would transfer from uniform (dash lines) in Figure 1.2(b) to non-uniform (solid lines). The stress on the side with the pile movement, p_p, will increase and the stress on the back side, p_a, will decrease. The nonlinear behavior of the soil is commonly represented by load-displacement characteristics, which is also known as the *p*-*y* curve, where *p* is the lateral soil resistance per unit length of the pile and *y* is the lateral deflection. The *p*-*y* curves for different types of saturated soils have been developed by many researchers based on either field tests or analytical derivations (Matlock 1970, Reese et al. 1974, Reese and Welch 1975, Georgiadis 1983, Murff and Hamilton 1993, Reese 1997, Rollins et al. 2005, Suleiman et al. 2014). The criterion for the design of foundations under lateral loads is based on a prefixed or limited horizontal displacement that the load can attain and not on the ultimate lateral load capacity (Poulos and Davis 1980, de Albuquerque et al. 2019). Such a design approach is used since it is difficult to identify the rupture of the pile foundation as observed in compression and traction loadings.

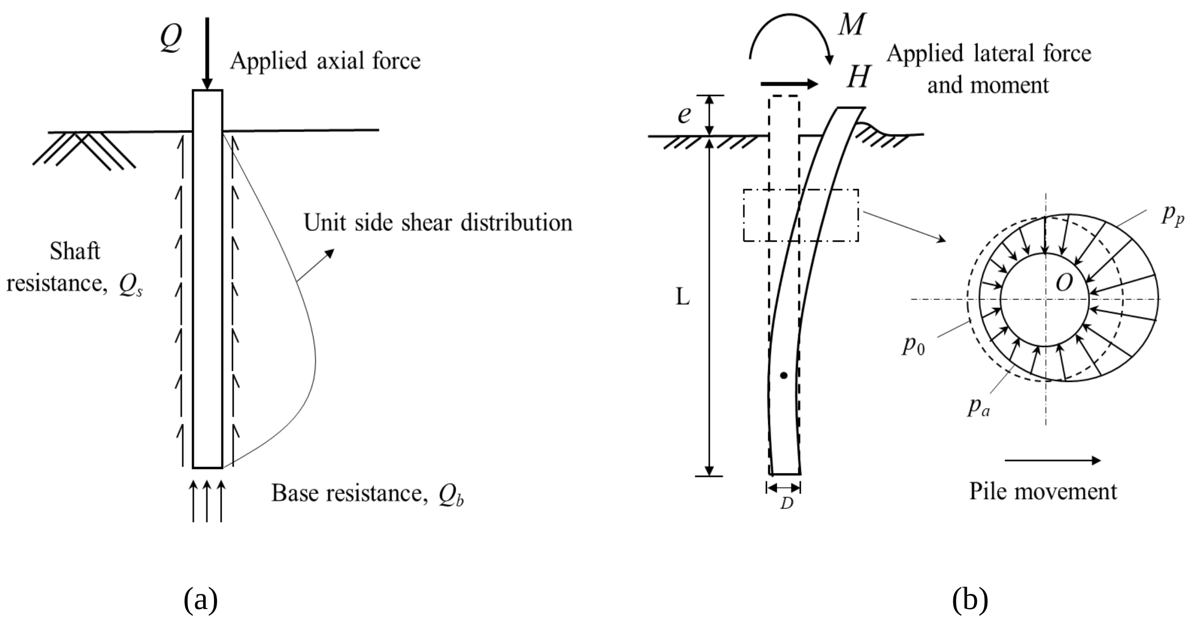

Figure 1.2 Load transfer mechanism of (a) axially loaded pile and (b) laterally loaded pile

Pile foundations are usually installed in closely spaced groups to provide a larger support combining the strength of multiple piles in conventional geotechnical engineering practice applications. The load transfer mechanism of pile groups is different than single piles. The load-carrying capacity of pile group is significantly influenced by the interactions between individual piles in the group. For this reason, it is necessary to take account of the group effects when estimating overall bearing capacity or settlement of pile groups.

In many scenarios, a portion or the entire length of the pile is embedded in the soil zone that is in a state of unsaturated condition. However, the design of pile foundations is typically based on saturated soil mechanics. The ultimate bearing capacity of pile foundations and their settlement behavior may not be reliably estimated because of ignoring the contribution arising from matric suction in unsaturated soils. In the recent years, some researchers have investigated the behavior of single axially loaded piles (Uchaipichat 2012, Vanapalli and Taylan 2012, Fattah et al. 2014, Han et al. 2016, Akrouch et al. 2016, Chung and Yang 2017, Vanapalli et al. 2018), pile group under axial loading (Al-Khazaali and Vanapalli 2019, Al-Omari et al. 2019) and laterally loaded piles (Helmers 1997, Mokwa et al. 2000, Mahmood et al. 2018, Lalicata et al. 2019) in unsaturated soils based on experimental tests and numerical simulations. These studies highlighted the significant influence of the degree of saturation on the load versus displacement behavior of piles. The state-of-the-art understanding of the influence of matric suction on pile foundations in unsaturated soils; however, is still limited for geotechnical engineers to extend it into conventional engineering practice applications. Furthermore, there are no foundation design codes, protocols, or well-established procedures for the rational design of pile foundations in unsaturated soils.

1.2 Objectives and novelty

The focus of the studies summarized in this thesis is directed towards investigating the behavior of single piles and pile groups under axial loading and lateral loading. The four major objectives along with associated novelty of this thesis are summarized below (Figure 1.3):

(i)***To investigate the nonlinear behavior of laterally loaded piles in unsaturated soils considering the influence of matric suction***

Two novel approaches are proposed for evaluating the load versus displacement behavior of laterally loaded piles in unsaturated soils. The first one is a nonlinear analytical method, which considers the variation of lateral soil resistance along the pile length under three different states (i.e., pre-tip yield state, post-tip yield state and ultimate limiting state). The lateral load corresponding to lateral displacement at the ground surface is derived based on force and moment equilibrium equations. The lateral earth pressure coefficient K_c required in the solutions is derived by extending the three-dimensional (3D) effect factor for drained loading. Secondly, a novel numerical technique is proposed which incorporates a user-defined subroutine (USDFLD) into ABAQUS to model the nonlinear shear strength and modulus of elasticity behavior of unsaturated soils. The proposed analytical method and numerical techniques are validated, respectively with the results of eight field studies and two laboratory model tests published in the literature. In both cases, there is a good comparison between numerical results and measured data. Lastly, the results between the proposed analytical method and numerical predictions are also compared and discussed for an example problem with varying GWTs.

(ii) ***To investigate the end-bearing capacity of driven piles in unsaturated soils***

An analytical approach is proposed for predicting the end-bearing capacity of driven piles extending the stress characteristic method that is employed successfully for both saturated and unsaturated soils. An iterative technique computer code is developed for the proposed analytical approach extending the finite difference method to develop solutions with the aid of MATLAB that provides graphical output to visualize the results. The results from the proposed approach are compared against measurements for thirteen pile load tests that include eleven in saturated soils and two in unsaturated soils. In addition, numerical analyses are undertaken using ABAQUS to simulate the driven pile penetration and pile loading by employing the arbitrary Lagrangian–Eulerian (ALE) adaptive mesh methods. The numerical predictions and measurements from a published model pile test are compared and discussed. The proposed analytical method highlighted the need for use in engineering practice applications to estimate the end bearing capacity of pile foundations in both saturated and unsaturated soils.

(iii) ***To investigate the behavior of single piles and pile groups in unsaturated soils under axial loading***

A simplified analytical approach is proposed for predicting the load-displacement response of single piles in unsaturated soils considering the contribution towards the nonlinear shear strength and soil stiffness associated with matric suction. In this approach, the nonlinear relationship between shaft shear stress and pile-soil relative shaft displacement at the pile-soil interface is described by a hyperbolic function-based load transfer model, while the pile base resistance and base displacement follows a bilinear relationship. The proposed model is extended for pile groups considering the interaction effects between individual piles. The validity of the approach for both single pile and pile groups is demonstrated by comparing with the measurements from three pile load tests of which two are single pile tests and the other is a model pile group test. Furthermore, a three-dimensional (3D) numerical analysis is undertaken to analyze the nonlinear response of pile groups in various unsaturated conditions implementing a user-defined subroutine into ABAQUS.

(iv) ***To predict the load-displacement behavior of piles using numerical techniques***

A comprehensive numerical technique is proposed for simulating the load-displacement behavior of single piles embedded in unsaturated soils using finite element analysis. The suggested numerical method takes account of nonlinear shear strength and modulus of elasticity of unsaturated soils with respect to matric suction. The required information for modeling includes only the saturated shear strength parameters, saturated modulus of elasticity and the Soil-Water Characteristic Curve (SWCC). The numerical analyses were then performed on four pile load tests that include two model pile tests in the laboratory and the remainder two from the field tests that were gathered from the published literature. Good comparisons were observed between the measured data and numerical predictions, for all four cases. The proposed numerical method is a promising tool for rational design of pile foundation in both saturated and unsaturated soils.

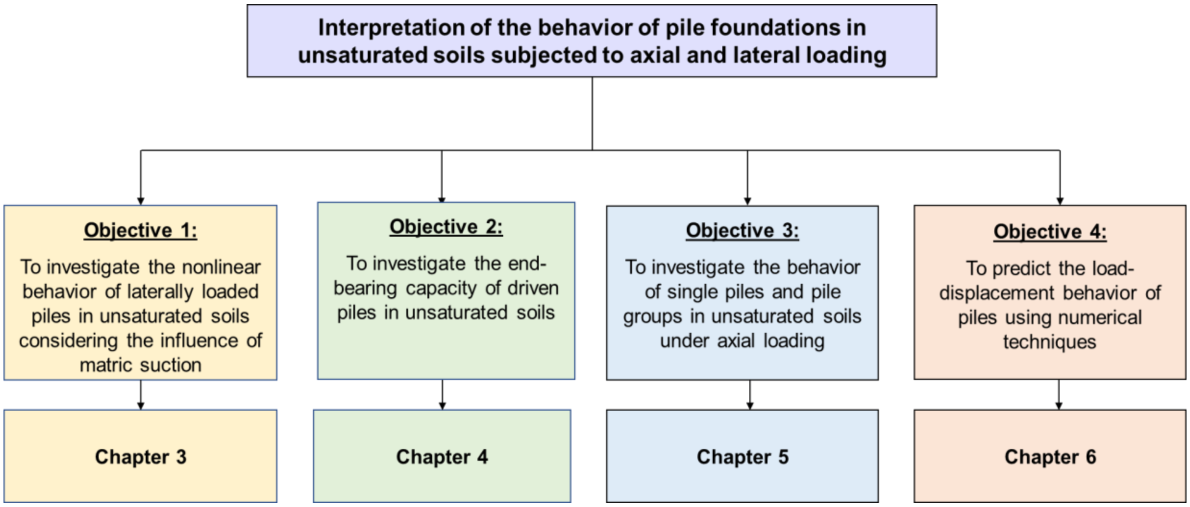

Figure 1.3 Research scope and thesis objectives

1.3 Thesis Layout

This thesis is organized in a format of "a collection of research articles". The thesis consists of seven chapters. The main content of all the chapters is summarized as below:

Chapter 1 presents a general introduction of the undertaken study. The objectives, novelty and layout of this study are then succinctly described.

Chapter 2 presents a comprehensive literature review on the pile behavior in both saturated and unsaturated soils, including (i) the research studies on the variation of shear strength and elasticity of modulus of unsaturated soils; (ii) existing methods for predicting the behavior of pile foundations in saturated soils under vertical loads and lateral loads; (iii) Lastly, the studies that focus on the influence of matric suction on the behavior of pile foundations in unsaturated soils.

Chapter 3 presents two approaches for predicting the lateral response of single piles embedded in unsaturated soils. An analytical method that considers the variation of lateral soil resistance along the pile length under three different states is first presented. Then, a numerical modeling methodology to investigate the nonlinear behavior of laterally loaded piles considering of matric suction is introduced. Both proposed analytical method and numerical techniques are verified, respectively, using eight published field studies and two laboratory model tests. In addition, the results between the proposed analytical method and numerical predictions are compared and discussed for an example problem with varying GWTs.

In Chapter 4, an analytical approach is proposed for predicting the end-bearing capacity of driven piles in saturated and unsaturated soils extending the stress characteristic method. The results from the proposed approach are compared against measurements for thirteen pile load tests that include eleven in saturated soils and two in unsaturated soils, with good agreements. In addition, numerical analyses are undertaken using ABAQUS to simulate the driven pile penetration and pile loading by employing the ALE adaptive mesh methods. The numerical analyses are validated by providing comparisons between the numerical predictions and measurements from a published model pile test.

In Chapter 5, a modified load transfer model is proposed to predict the nonlinear load-displacement behavior at the pile-soil interface for single piles in unsaturated soils considering the influence of matric suction. The analysis for single piles is then extended to pile group accounting for the interaction effect between individual piles. The reliability of the proposed method for single piles and pile groups are validated using two pile load tests in unsaturated residual soils and one model pile group test, respectively. In addition, a 3D numerical analysis of a 2×2 pile group is undertaken to investigate the effects of varying GWT depths and interaction between piles in a group. Good comparisons are found between the predictions from both the proposed analytical method and numerical analysis with the measurements.

In Chapter 6, theoretical background related to the shear strength and modulus of elasticity of unsaturated is first introduced to highlight how it can be used as a tool in the interpretation and prediction of the bearing capacity and settlement behavior of unsaturated soils. A numerical technique is developed by implementing a user-subroutine in the commercial software ABAQUS to model the load-displacement behavior of piles. The developed approach is validated using the results of two model pile load tests and three field studies from the published literature. The comparisons between the measured data and numerical predictions for all the four cases are presented and discussed. The proposed numerical method is a promising tool for rational design of pile foundation in unsaturated soils.

Chapter 7 presents the summary and conclusions of the research undertaken in this thesis.

1.4 Related publications

Journal Publications:

1. **Cheng, X.**, & Vanapalli, S. K. (2023). Prediction of the end-bearing capacity of axially loaded piles in saturated and unsaturated soils based on the stress characteristics method. *International Journal of Geomechanics*, *23*(7), 04023104.

2. **Cheng, X.**, & Vanapalli, S. K. (2021). Prediction of the nonlinear behavior of laterally loaded piles in unsaturated soils. *Computers and Geotechnics*, 140, 104480.

3. Tan, M., **Cheng, X.,** & Vanapalli, S. (2021). Simple approaches for the design of shallow and deep foundations for unsaturated soils I: Theoretical and experimental Studies. *Indian Geotechnical Journal*, 51(1), 97-114.

4. **Cheng, X.,** Tan, M., & Vanapalli, S. (2021). Simple approaches for the design of shallow and deep foundations for unsaturated soils II: Theoretical and experimental Studies II: Numerical Techniques. *Indian Geotechnical Journal*, 51(1), 115-126.

5. **Cheng, X.**, & Vanapalli, S. K. (2023). Nonlinear analysis of load-displacement behavior of single pile and pile groups in unsaturated soils. (*Under review with an International Journal)*

6. **Cheng, X.**, & Vanapalli, S. K. (2023). Numerical analysis of pile foundations in saturated and unsaturated soils. (*Under review with a Special Issue Journal)*

Conference publications:

1. **Cheng, X.**, & Vanapalli, S. K. (2021). A numerical technique for modeling the behavior of single piles in unsaturated soils. *In MATEC web of conferences*. (Vol. 337, p. 03012). EDP Sciences.

CHAPTER 2

LITERATURE REVIEW

2.1 Introduction[1]

In this chapter, a comprehensive review of the shear strength of unsaturated soils (*SSUS*) is presented. The published studies from the literature that are used for interpreting the behavior of axially and laterally loaded piles in saturated soils are then summarized, respectively. Lastly, the studies that focus on the influence of matric suction on the behavior of pile foundations in unsaturated soils under axial and lateral loadings in terms of experimental studies, theoretical approaches and numerical simulations are reviewed.

2.2 The mechanical behavior of unsaturated soils (*SSUS*)

2.2.1 The shear strength of unsaturated soils (*SSUS*)

Bishop (1959) proposed a single-valued effective stress relationship that is widely used for interpreting the *SSUS*:

$$\tau = c' + \left[\left(\sigma_\mathrm{n} - u_\mathrm{a} \right) + \chi \left(u_\mathrm{a} - u_\mathrm{w} \right) \right] \tan\phi' \tag{2.1}$$

where τ is the shear strength of unsaturated soils, c' is effective cohesion, ϕ' is effective internal frictional angle, $(\sigma_\mathrm{n} - u_\mathrm{a})$ is net normal stress, $(u_\mathrm{a} - u_\mathrm{w})$ is matric suction, χ is a soil parameter related to the degree of saturation (between 0 and 1) that depend on many factors.

[1]Some of the contents presented in this chapter are published as journal articles:

Tan, M., **Cheng, X**., and Vanapalli, S. (2021). Simple approaches for the design of shallow and deep foundations for unsaturated soils I: Theoretical and experimental Studies. *Indian Geotechnical Journal*, 51(1), 97-114.

Cheng, X., Tan, M., and Vanapalli, S. (2021). Simple approaches for the design of shallow and deep foundations for unsaturated soils II: Numerical Techniques. *Indian Geotechnical Journal*, 51(1), 115-126.

Several researchers suggested that Bishop's effective stress equation that is based on a single stress state variable has some limitations. For example, Jennings and Burland (1962) suggested that Bishop's effective stress equation has some limitations in interpreting both the shear strength and volume change behavior simultaneously. A more rigorous method for describing the behavior of unsaturated soils is possible using independent stress state variables (e.g., $(\sigma_n - u_a)$ and $(u_a - u_w)$ (Bishop and Blight 1963; Matyas and Radhakrishna 1968; Morgenstern 1979).

Fredlund et al. (1978) provided a theoretical framework extending the Mohr-Coulomb failure criterion for interpreting the *SSUS* in terms of two independent stress state variables: $(\sigma_n - u_a)$ and $(u_a - u_w)$ as given below:

$$\tau = c' + (\sigma_n - u_a)\tan\phi' + (u_a - u_w)\tan\phi^b \tag{2.2}$$

where ϕ^b is the contribution of internal friction angle due to matric suction.

Experimental studies on various soils by several investigators highlight the variation of shear strength with respect to matric suction is nonlinear in nature (e.g., Escario and Juca 1989, Vanapalli et al. 1996, Rassam and Cook 2002, Vilar 2006, Guan et al. 2010). Determination of the *SSUS* from experimental studies is time consuming, complex, and expensive. For this reason, several researchers proposed several empirical or semi-empirical models for interpreting or predicting the shear strength of unsaturated soils. Several widely used shear strength equations and models are summarized in Table 2.1. Some of these equations have been implemented in commercial software such as GeoSlope and SoilVision for numerical modeling of geotechnical infrastructures such as the slopes and foundations in unsaturated soils (GeoSlope International Ltd. 2002, Fredlund et al. 2012, Zhang et al. 2015).

The Soil-Water Characteristic Curve (SWCC) is a useful tool for predicting the *SSUS*. SWCC is referred to as the relationship between the mass (and/or volume) of water in the soil and the soil suction. The terms, soil-water retention curve and soil moisture curve are also used for defining this relationship. Figure 2.1 shows the relationship between the SWCC and shear strength of unsaturated soils.

Table 2.1 Some typical models for predicting *SSUS* (modified after Vanapalli 2009)

Authors	Equations	Remarks
Fredlund et al. (1978)	$\tau = c' + (\sigma_n - u_a)\tan\phi' + (u_a - u_w)\tan\phi^b$	
Lu (1992)	$\tau = c' + (\sigma - u_a)\tan\phi' + P_s \tan\phi'$	P_s: swelling pressure of the soil
Vanapalli et al. (1996)	$\tau = c' + (\sigma - u_a)\tan\phi' + (u_a - u_w)\left(\dfrac{\theta_w - \theta_r}{\theta_s - \theta_r}\right)(\tan\phi')$ $\tau = c' + (\sigma_n - u_a)\tan\phi' + (u_a - u_w)S^{\kappa}\tan\phi'$	θ_w is volumetric water content; θ_s, θ_r is saturated and residual volumetric water content respectively; S: degree of saturation; κ is a fitting parameter
Öberg & Sällfors (1997)	$\tau = c' + (\sigma - u_a) + S(u_a - u_w)\tan\phi'$	
Khalili and Khabbaz (1998)	$\tau = c' + (\sigma - u_a)\tan\phi' + (u_a - u_w)\tan\phi'\left[\dfrac{(u_a - u_w)}{(u_a - u_w)_b}\right]^{\eta}$	η: fitting parameter; $(u_a$-$u_w)_b$ is the air entry value
Lee et al. (2003)	$\tau = c' + (\sigma - u_a)\tan\phi' + \dfrac{(u_a - u_w)}{a_3 + b_3(u_a - u_w)}$	$a_3 = \dfrac{1}{\tan\phi'}$; $b_3 = \dfrac{1}{C_{max}}$; C_{max}: ultimate increment of apparent cohesion
Vilar (2006)	$\tau = c' + (\sigma - u_a)\tan\phi' + \dfrac{(u_a - u_w)}{\dfrac{1}{\tan\phi'} + \left[\dfrac{1}{\tau_m - c'} - \dfrac{1}{(u_a - u_w)_m \tan\phi'}\right]}$	τ_m, $(u_a - u_w)_m$: measured maximum cohesion and suction
Sheng et al. (2008)	$\tau = c' + (\sigma - u_a)\tan\phi' + s\tan\phi'$: $s \le s_{sa}$ $\tau = c' + (\sigma - u_a)\tan\phi' + \tan\phi'\left[s_{sa} + (s_{sa}+1)\ln\dfrac{s+1}{s_{sa}+1}\right]$: $s \ge s_{sa}$	$s = (u_a - u_w)$; s_{sa}: saturation suction

The SWCC can be divided into three distinct zones of saturation; namely, boundary effect zone (BEZ), transition effect zone (TEZ) and residual zone of saturation (RZS), which are influenced by different ranges of soil suction values based on the properties of the soils. In the BEZ, the soil is typically in a state of saturated condition. The soil behavior in this zone can be interpreted extending principles of saturated soil mechanics. The shear strength contribution due to matric suction (ϕ^b) in this zone is equal to the angle of internal friction (ϕ'). When air enters the largest pores of the soil, the soil suction is referred to as the air-entry value (AEV). The soil desaturates rapidly with a further increase in matric suction beyond the AEV. ϕ^b is less than ϕ' in TEZ. In the RZS, there are relatively small changes in the degree of saturation despite greater increases in the matric suction value. The shear strength may increase, decrease, or remain constant depending on the soil types and the amount of drainage in soil pores (Vanapalli, 2009). Similar conceptual behavior can also be extended for explaining the modulus of elasticity of unsaturated soils. Several indirect methods for estimating SWCC were developed utilizing known soil parameters or limited experimental data, such as pedotransfer functions (Schaap et al. 2001, Wösten et al. 1999, Soet and Stricker 2003), physico-empirical method which converts the grain size distribution into a pore size distribution (Arya and Paris, 1981, Rafraf et al. 2016) and empirical mathematical functions (e.g., Brooks and Corey 1964, van Genuchten 1980, Fredlund and Xing 1994, Zhou et al. 2012, Cuomo et al. 2018) to alleviate the time-consuming experimental techniques of direct measurements of SWCC (Fredlund and Rahardjo 1993; Peranić et al. 2018). The empirical mathematical equations are also used to best fit SWCC to obtain a smooth SWCC. Some of these equations are obtained by correlating parameters of fitting models with basic soil properties such as grain size or pore size distribution, dry density and void ratios (Haverkamp et al. 2005, Vanapalli and Catana 2005, Chin et al. 2010). Besides, machine learning and Artificial Intelligence (AI) methods are also used for predicting the SWCC (Schaap and Bouten 1996, Pham et al. 2019, Li and Vanapalli 2022).

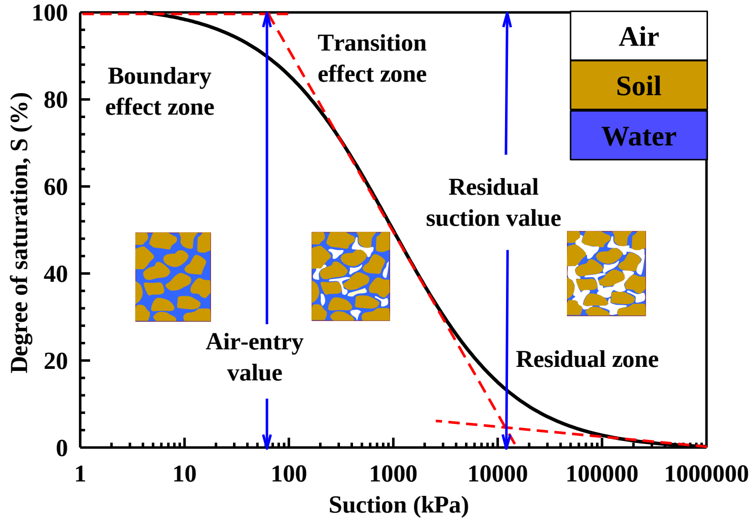

(a) Typical soil water characteristic curve

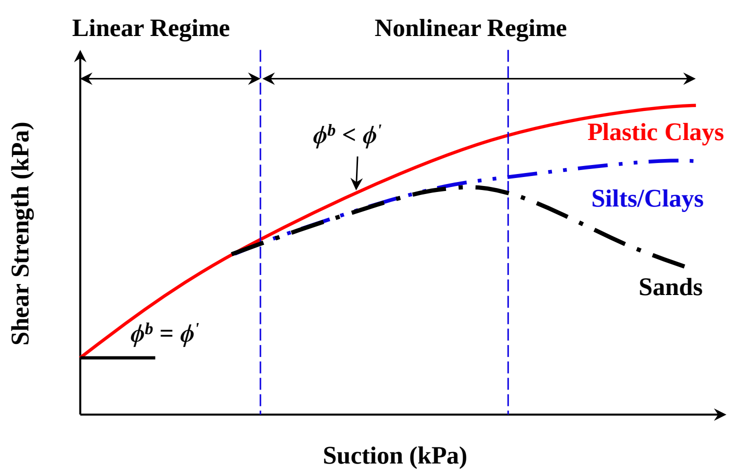

(b) Shear strength of unsaturated soils in various zones

Figure 2.1 Relationship between the SWCC and shear strength of unsaturated soils (Modified after Vanapalli 2009)

2.2.2 The elastic modulus of unsaturated soils

The elastic modulus and shear modulus are two key parameters that are useful in describing the elastic stress-strain relationships for soils that are required in the design of geotechnical structures. The settlement of various foundations embedded in soils can be estimated using the information of elastic modulus. Experimental studies performed on unsaturated soils suggest a strong dependence of elastic modulus on both matric suction and volumetric water content values (Fredlund et al. 1975, Edil et al. 1981, Costa et al. 2003, Sawangsuriya et al. 2009, Oh et al. 2009). Several studies published in the literature suggest that the elastic modulus increases with an increase in matric suction (Edil et al. 1981, Mancuso et al. 2002; Khoury and Zaman 2004, Oh et al. 2009, Morales et al. 2015). Shear modulus has been commonly used for evaluating the soil stiffness in response to shear deformation and it is also an important property required in the dynamic and seismic response analysis of soils. The maximum shear modulus, G_0, refers to the shear modulus at a small strain (typically <0.001%). G_0 of unsaturated soils can be determined from both laboratory tests and seismic field tests (e.g., Kawaguchi et al. 2001, Lee and Santamarina 2005). Bender element and resonant column tests are two widely used laboratory tests that can be modified for both saturated and unsaturated soils (Ng and Menzies 2007). The measurement of G_0 through experimental studies usually requires considerable time to achieve equilibrium conditions of soil volume due to changes in net stress and water content, especially for fine-grained soils. Therefore, several researchers proposed empirical or semi-empirical equations for estimating G_0 in unsaturated soils considering the water content and matric suction (e.g., Mancuso et al. 2002, Mendoza and Colmenares 2006, Sawangsuriya et al. 2009, Lu and Kaya 2014). Sawangsuriya et al. (2009) have proposed two empirical models to describe the relationship between shear modulus of unsaturated soils G and total stress and matric suction:

$$G = A\left(\sigma - u_{\mathrm{a}}\right)^{n1} + C\left(\frac{\theta}{\theta_s}\right)^{\kappa}\left(u_{\mathrm{a}} - u_{\mathrm{w}}\right) \tag{2.3a}$$

$$G = A\left[\left(\sigma - u_{\mathrm{w}}\right) + \left(\frac{\theta}{\theta_s}\right)^{\kappa}\left(u_{\mathrm{a}} - u_{\mathrm{w}}\right)\right]^{n2} \tag{2.3b}$$

where θ is volumetric water content, θ_r is residual volumetric water content, A, n_1, κ, and C are curve-fitting parameters. The first model (Equation 2.3a) was established using two independent state variables (i.e., matric suction and net normal stress) based on the shear strength model proposed by Vanapalli et al. (1996). The second model was established from the effective stress equation by Bishop (1959). The effective stress parameter by Bishop (1959) is replaced by the shear strength model proposed by Vanapalli et al. (1996). The test results on fine-grained soils with varying water content showed that both models can provide reliable predictions of the variation of shear modulus with respect to matric suction and volumetric content.

In addition, Oh et al. (2009) proposed a semi-empirical model to describe the relationship between the modulus of elasticity of unsaturated soils, E_{unsat}, and degree of saturation with respect to matric suction.

$$E_{\mathrm{unsat}} = E_{\mathrm{sat}}\left[1+\alpha\frac{(u_{\mathrm{a}}-u_{\mathrm{w}})}{(P_{\mathrm{a}}/101.3)}\left(S^{\beta}\right)\right] \tag{2.4}$$

where E_{sat} is the modulus of elasticity of soil under saturated conditions, P_{a} is atmospheric pressure (101.3kPa), and α and β are two fitting parameters. The fitting parameter α is related to the plasticity index, I_{p}, for cohesive soils. The value of α for cohesionless soil ranges from 0.5 to 2.5 depending on the footing size. Vanapalli and Oh (2010) suggest that the fitting parameter β equal to 1 for cohesionless soils and 2 for cohesive soils based on the results from model footing tests on unsaturated soils. Extending the same philosophy for elastic modulus, Oh and Vanapalli (2014) proposed a similar model for predicting the variation of G_0 with respect to (u_{a} – u_{w}) in unsaturated sandy soils using the saturated maximum shear modulus, $G_{0(\mathrm{sat})}$ and SWCC.

$$G_{0(\mathrm{us})} = G_{0(\mathrm{sat})}\left[1+\zeta\frac{(u_{\mathrm{a}}-u_{\mathrm{w}})}{(P_{\mathrm{a}}/101.3)}\left(S^{\xi}\right)\right] \tag{2.5}$$

where $G_{0(\mathrm{us})}$ is the maximum shear modulus under unsaturated conditions, ζ and ξ are fitting parameters. The fitting parameter ξ equals to 0.5 and 1 for the soils classified as SP and SW, respectively. The fitting parameter ζ is strongly related to the coefficient of uniformity C_{U}. The value of ζ decreases from 0.035 to 0.025 as C_{U} increases up to 2. More details of the relationship between ζ and C_{U} can be found in Oh and Vanapalli (2014).

2.3 The behavior of axially loaded piles in saturated and unsaturated soils

2.3.1 Axially loaded piles in saturated soils

Practical and economic factors are usually considered in the design of pile foundations. In addition, analysis should be undertaken to ensure that pile can fulfill its functions under various working loading conditions. Determination of the reliable ultimate bearing capacity of the pile is required in the analysis of pile foundations, which has always been a challenge to geotechnical engineers. In the last several decades, four main approaches have been developed and widely used for investigating the behavior of pile foundations: namely, (i) static pile load tests; (ii) dynamic methods; (iii) static analysis (e.g., total and effective stress approach); and (iv) direct or indirect use of results from in-situ tests. The pile load test is considered the most accurate method for determining the ultimate bearing capacity of the piles under working loading conditions (Birid 2017). However, both static and dynamic pile load tests are expensive and time-consuming. Due to this reason, many researchers focused on proposing methods extending static analysis (i.e., theoretical methods) for estimating the pile load capacity. The theoretical static analysis utilizes the shear strength parameters with simplified assumptions which provide reasonable agreements with full scale tests. However, the in-situ tests play a prominent role in the design of pile foundations as they provide reliable information. In the following sections, published studies from literature related to determining the pile end-bearing capacity and friction capacity using static analysis and in-situ tests will be reviewed.

2.3.1.1 Static analysis by utilizing soil shear strength

The ultimate bearing capacity, Q_{u}, of a pile under axial loading is the sum of the end bearing capacity Q_{b}, and the shaft carrying capacity Q_{s} given by:

$$Q_{\mathrm{u}} = Q_{\mathrm{s}} + Q_{\mathrm{b}} = q_{\mathrm{f}} A_{\mathrm{s}} + q_{\mathrm{b}} A_{\mathrm{p}} \tag{2.6}$$

where q_f is the unit pile shaft carrying capacity, A_s is the side area of the pile, q_b is unit end bear capacity and A_p is the total area of pile end. This equation assumes that the maximum pile shaft carrying capacity and maximum end-bearing capacity are mobilized at the same time (API 2011). The shaft carrying capacity is typically mobilized at a small vertical displacement of 0.5% to 2% of the pile diameter, which is less than that of 5 to 10% of the pile diameter when the end bearing capacity is mobilized (Fleming et al. 1992). Therefore, the difference between the mobilization of the shaft carrying capacity and end bearing capacity should be considered in pile settlement and load sharing analysis.

The soil shear strength parameters considering the interaction between the pile and surrounding soils is used in the theoretical static analysis. The installation of piles influences the surrounding soil properties. However, it is difficult to predict the changes in soil properties. Therefore, the bearing capacity of piles is typically estimated based on the initial strength and deformation characteristics of the soil. The effect of changed soil properties is reflected in the non-dimensional bearing capacity factors and mobilized shaft carrying capacity (Prakash and Sharma 1990).

The pile shaft carrying capacity can be considered as a function of cohesion and friction angle of the pile-soil interface. The commonly used semi-empirical methods to estimate the shaft load carrying capacity of single piles are the α method (Skempton 1959), β method (Burland 1973), and λ method (Vijayvergiya and Focht 1972), in which the parameters α, β, λ are usually obtained from empirical correlations.

The α method is used to determine the shaft carrying capacity of piles placed in saturated cohesive soils based on the total stress approach (TSA). This method relates the average shaft adhesion to the mean undrained shear strength by an empirical coefficient α. Some studies have shown much evidence to support this relationship (Tomlinson 1957, McCarthy 1977, Sladen 1992). The unit shaft carrying capacity q_f can be calculated by the equation:

$$q_f = c_{ad} = \alpha c_u \tag{2.7}$$

where c_{ad} is the average adhesion between the clay and the pile shaft, and c_u is the undrained shear strength of the clay within the depth of penetration of the pile in clay. Some researchers have studied the relationship between the parameter α and c_u (Peck 1958, Kerisel 1965, Sowers 1979, McCarthy 1977, Dennis and Olson 1983,). α can also be calculated using the following equation (API 2011):

$$\alpha = 0.5\psi^{-0.5} \quad \text{if } \psi \le 1$$

$$\alpha = 0.5\psi^{-0.25} \quad \text{if } \psi > 1$$

where $\psi = c_u/\sigma_v'$, σ_v' is the effective overburden pressure.

Burland (1973) proposed β method to calculate shaft carrying capacity by extending the effective stress approach (ESA). The TSA is only suitable for clay, while ESA can be used for all types of soil. The excess porewater pressures that arise from the pile installation between soil adjacent to the shaft are assumed to be completely dissipated before loading. The shaft carrying capacity q_f is calculated by:

$$q_f = K_0 \sigma_v' \tan\delta' \tag{2.8}$$

where K_0 is the earth pressure coefficient and δ' is the effective friction angle of the pile-soil interface. For bored piles, the angle δ' is commonly assumed to be equal to the angle of shearing resistance of the surrounding soil, ϕ', for practical purposes. The empirical factor β and the general expression of pile shaft carrying capacity Q_s is in the form of the following equation:

$$\beta = \frac{q_f}{\sigma_v'} = K_0 \tan\delta' \tag{2.9a}$$

$$Q_s = \beta \sigma_v' \pi D L \tag{2.9b}$$

where D is the pile diameter and L is the length of the pile, β is the Burland-Bjerrum coefficient which is related to the fundamental effective stress parameters K and δ'. Burland

(1973) and Meyerhof (1976) suggested an expression to estimate β value in clay: β=(1-sinϕ')tanϕ'(OCR)$^{0.5}$, where OCR is the over consolidation ratio. The CFEM (1992) recommends a β value of 0.25 to 0.30 for clay and 0.30 to 0.90 for sand. The Hong Kong Geotechnical Engineering Office (HKGEO 2005) suggested β ranging from 0.1 to 0.4 for driven piles in saprolite soils and 0.1 to 0.6 for bored piles. For piles in sands, β ranges from 0.29 to 0.56 for soils from medium dense to very dense conditions according to API (2011). Rollins et al. (2005) conducted uplift load tests on many piles in sedimentary soils and measured the shaft resistance. Figure 2.2 shows the back-calculated β values from these tension tests. It is evident that the β coefficient is largest near the ground surface and reduces with depth.

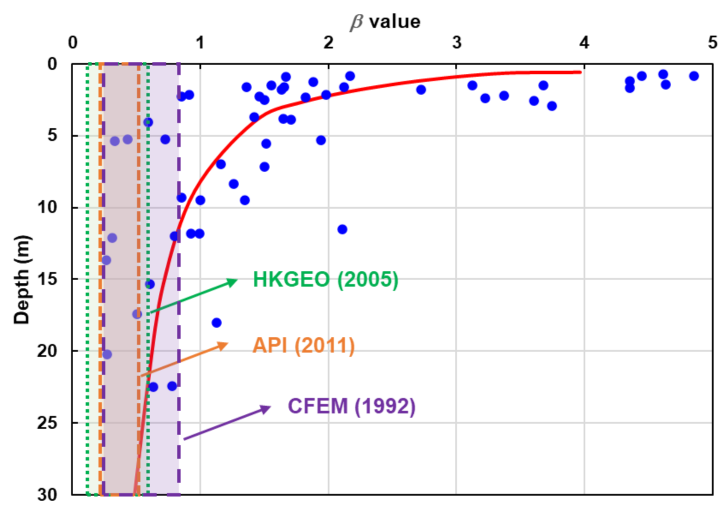

Figure 2.2 Back-calculated β values from tension tests by Rollins et al. (2005) and range values indicated for sand by CFEM (1992) and API (2011), and for saprolites by the HKGEO (2005) (modified after Fellenius et al. 2007)

Vijayvergiya and Focht (1972) developed λ method to predict pile shaft carrying capacity, which combines both TSA and ESA. This method assumes that the unit shaft carrying capacity has a relationship with both vertical effective stress and undrained shear strength. q_f can be estimated by the following equation:

$$q_f = \lambda\left(\sigma'_{v(avg)} + 2c_u\right) \quad (2.10)$$

where $\sigma'_{v(avg)}$ is the mean effective stress along the pile shaft, and λ is the frictional capacity coefficient which is a function of the entire embedded depth of the pile.

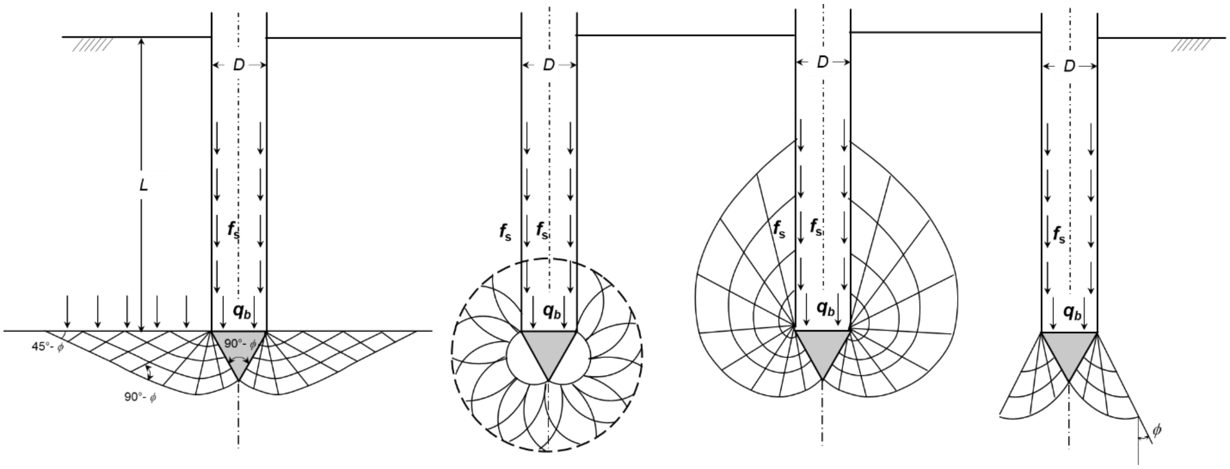

Figure 2.3 Assumed failure patterns around the pile tip by (a) Prandtl (1920), Reissner (1924), Caquot (1934), Buisman (1935), Terzaghi (1943); (b) Bishop et al. (1945), Skempton et al. (1953), Yasufuku and Hyde (1995); (c) De Beer (1945), Jáky (1948), Meyerhof (1951), Janbu (1976); (d) Berezantzev and Yaroshenko (1962), Vesić (1963)

Theoretical approaches that have been developed for determining the bearing capacity of shallow foundations can be extended with modifications for estimating the end-bearing capacity of pile foundations (Terzaghi 1943, Meyerhof 1951, Vesić 1967). Figure 2.3 shows several typical possible failure patterns around the pile base assumed by different researchers. The end-bearing capacity can be represented by the following general form:

$$Q_b = A_p\left(cN_c + qN_q + \tfrac{1}{2}\gamma D N_\gamma\right) \quad (2.11)$$

where A_p is the pile base area, c is soil cohesion, q is vertical effective stress at the level of pile base, γ is the unit weight of soil beneath the pile, D is pile diameter, and N_c, N_q, N_γ are non-dimensional bearing capacity factors that are functions of soil friction angle. In pile foundations, the contribution arising from the third term can be neglected since the length/diameter (D/B) ratio of piles is much larger than that of shallow foundations (Bowles 1996). For cohesionless soil, the cohesion is negligible (i.e., $c' = 0$). Therefore, Equation 2.11 will take the form qN_q. Table 2.2 presents values of N_q proposed by different researchers. There can be a relatively large difference in predicting N_q using different assumed failure surfaces.

Table 2.2 Bearing capacity factors for piles in cohesionless soils (modified after Coyle and Castello 1981)

References	Approximate N_q values for various friction angles, ϕ (°)				
	25	30	35	40	45
Terzaghi (1943)	12.7	22.5	41.4	81.3	173.3
De Beer (1945)	59	155	380	1150	4000
Skempton et al.(1953)	46	66	110	220	570
Caquot and Kerisel (1956)	26	55	140	350	1050
Berezantzev and Yaroshenko (1962)	16	33	75	186	–
Hansen (1961)	23	46	115	350	1650
Vesić (1963)	15	28	58	130	315
Meyerhof (1976)					
Driven piles	12	25	52	120	230
Drilled piles	5	12	26	60	115

2.3.1.2 *In-situ* test-based methods (direct or indirect)

In-situ tests such as the standard penetration tests (SPT) and the cone penetrometer tests (CPT) have been widely used and played a prominent role in estimating the bearing capacity of piles because they are rapid testing techniques (Shooshpasha et al. 2013). The SPT technique provides representative soil samples along with the SPT N values. The test procedure is simple, quick, and relatively inexpensive. The SPT-based method includes two main approaches: namely, direct and indirect methods. Direct methods apply N values in determining pile shaft and end bearing capacity with some modification factors. For indirect methods, empirical relationships have been developed between N value and soil parameters such as the angle of internal friction (Suzuki et al. 1993, Hatanaka and Uchida 1996), undrained shear strength (Hara et al. 1974, Sivrikaya and Toğrol 2006, Kalantary et al. 2009) and shear wave velocity (Hara et al. 1974, Wei et al. 1996, Hasancebi and Ulusay 2007, Maheshwari et al. 2010, Chatterjee and Choudhury 2013). However, the quality of test results is affected by many factors, including the actual energy delivered to the head of the drill rod, dynamic properties of the drill rod, drilling equipment and sampler driving characteristics (Schmertmann 1978, Kovacs and Salomone 1982). A correction factor is usually needed since the actual energy delivered to the head of the drill rod varies from 50% to 80% of the theoretical free energy (Seed and De Alba 1986).

The CPT is a simple, quick, and relatively economical technique that provides continuous readings of various soil properties that include cone tip resistance (q_c) and sleeve friction (f_s). As shown in Figure 2.4, there are also two main approaches for predicting the ultimate bearing capacity of piles from CPT data: namely, direct methods and indirect methods (Abu-Farsakh and Titi 2004, Mayne 2007). During the last several decades, direct CPT methods have been developed for evaluating the bearing capacity of full-scale piles from CPT parameters based on scale relationships between the cone penetrometer and a single pile (e.g., Schmertmann 1978, Karlsrud et al. 2005, Schneider et al. 2008). These direct CPT methods are determined empirically from diverse datasets of piles installed in specific regions with different geologies (Abu-Farsakh and Titi 2004, Niazi and Mayne 2013). In addition to these methods, the piezocone penetration test (CPTu) method was also developed providing additional readings of pore water pressure at the cone shoulder (u_2). The corrected cone tip resistance (q_t) is obtained after correction for pore pressure at the shoulder and adjustment to effective stress (Almeida et al. 1996, Eslami and Fellenius 1997, Van Dijk and Kolk 2011). Table 2.3 summarizes direct CPT, CPTu and SPT- based methods that have been employed for predicting the bearing capacity of piles.

Table 2.3 Direct CPT, CPTu and SPT methods for estimating the bearing capacity of piles

	Unit end-bearing capacity, q_b	**Unit shaft carrying capacity, q_f**
CPT-based methods		
Schmertmann (1978) method	$q_b = (q_{c1} + q_{c2}) / 2 \leq 15$ MPa (in sands) and 10 MPa (in silty sands) q_{c1}: the minimum average q_c of zones ranging from 0.7D to 4D below the pile tip (D is the pile diameter) q_{c2}: the average minimum q_c of zones up to 8D above the pile tip	In clay: $q_f = k_c f_s \leq 120$ kPa k_c = 0.2-1.25 depends on the pile types In sand: $Q_s = k\left[\sum_{d=0}^{8D} \frac{d}{8D} f_s A_s + \sum_{d=8D}^{L} f_s A_s\right]$ k depends on the L/D ratio (L is the pile embedded length)
Dutch method (de Ruiter and Beringen 1979)	In clay: $q_b = N_c s_u \leq 15$ MPa, $s_u = q_{ca}/N_k$ N_c: bearing capacity factor q_{ca}: arithmetic average of q_c in a specified zone/soil layer N_k: cone factor ranges between 15 and 20 depending on local experience In sand: similar to Schmertmann (1978)	In clay: $q_f = \alpha s_{u\,(side)} \leq 120$ kPa; $s_{u(side)} = q_{c(side)}/ N_k$; N_k =15-20; α = 1 for normally consolidated (NC) clay and 0.5 for overconsolidated (OC) clay In sand: q_f = min [f_s, $q_{c(side)}$/300 for compression, $q_{c(side)}$/400 for tension, 120 kPa]
LCPC method (Bustamante and Gianeselli 1982)	$q_b = k_b\, q_{eq\,(tip)}$ q_{eq}: equivalent average of q_c values of zones ranging from 1.5D above to 1.5D below pile tip For non-displacement pile: k_b = 0.375 for clay and silt, k_b = 0.15 for sand and gravel. For displacement pile: k_b = 0.6 for clay and silt; k_b = 0.375 for sand and gravel	$q_f = q_{eq\,(side)} / k_s$ k_s = 30 –150 depends on the soil type, pile type and installation procedure
CPTu-based methods		
Unicone method (Eslami and Fellenius 1997)	$q_b = C_t\, q_{eg}$ C_t: the toe correction coefficient. C_t is generally taken as 1; for D > 0.4 m, C_t =1/(3D) q_{eg}: the geometric average q_c values over the zone of 4D below the tip to a height of 4D to 8D above the toe after	$q_f = C_s\, q_E$ C_s: shaft correlation coefficient depends on the soil type q_E: the corrected cone resistance after correction for pore pressure on the shoulder and adjustment to effective stress

	correction for pore pressure on the shoulder and adjustment to effective stress	
NGI-BRE method (Almeida et al. 1996; Powell et al. 2001)	$q_b = q_{t(net),avg} / k_2$ $k_2 = N_{kt} / 9$; N_{kt} = 15 for soft and firm intact clay; N_{kt} =25 to 35 for fissured to hard clay	$q_f = q_{t(net)} / k_1$ $k_1 = 10.5 + 13.3 \log[q_{(tnet)}/\sigma_{v0}']$ $q_{t(net)} = q_t - \sigma_{v0}'$ $q_{t(net),avg}$ = average $q_{t(net)}$ value over 1.5D below the pile tip
Furgo V-K method (Van Dijk and Kolk 2010)	$q_b = 0.7 q_{t(net),avg}$	$q_f = k_{s(z)} \cdot q_{t(net),z}$ $k_{s(z)} = 0.16(h/\mathrm{uL}) - 0.3[Q_{t(z)}]^{-0.4} < 0.08$ uL=1.0 m; $Q_{t(z)} = q_{t(net),z} / \sigma_{v0}'$ at z z: depth below ground surface h = distance between pile tip and z
SPT method		
Meyerhof (1976)	$q_b = 0.4 N_1 C_N$ N_1: N value at the pile base C_N: correction factor	$q_f = n_s N_s$ n_s = 2 for driven piles
Shioi and Fukui (1982)	$q_b = n_b N_b$ n_b = 0.15 (clay), 0.2 (silt), 0.3 (sand)	$q_f = n_s N_s$ n_s = 10 for clay, n_s =2 for sand
Bazaraa and Kurkur (1986)	$q_b = n_b N_b$ $n_b = 0.06 \sim 0.02$	$q_f = n_s N_s$ $n_s = 2 \sim 4$

The indirect CPT-based method requires a two-step procedure (e.g., Jamiolkowski et al. 2003, Mayne et al. 2010). The CPT parameters are first utilized to estimate the soil properties such as the unit weight, friction angle and undrained shear strength. The q_b and f_p can then be evaluated using the semi-empirical and theoretical methods based on these input soil parameters. Table 2.4 presents a listing of relationships for evaluating the soil parameters using CPT data, which includes unit weight (γ), internal angle of friction (ϕ'), Relative density (D_r), overconsolidation ratio (OCR) and lateral stress coefficient (k_0).

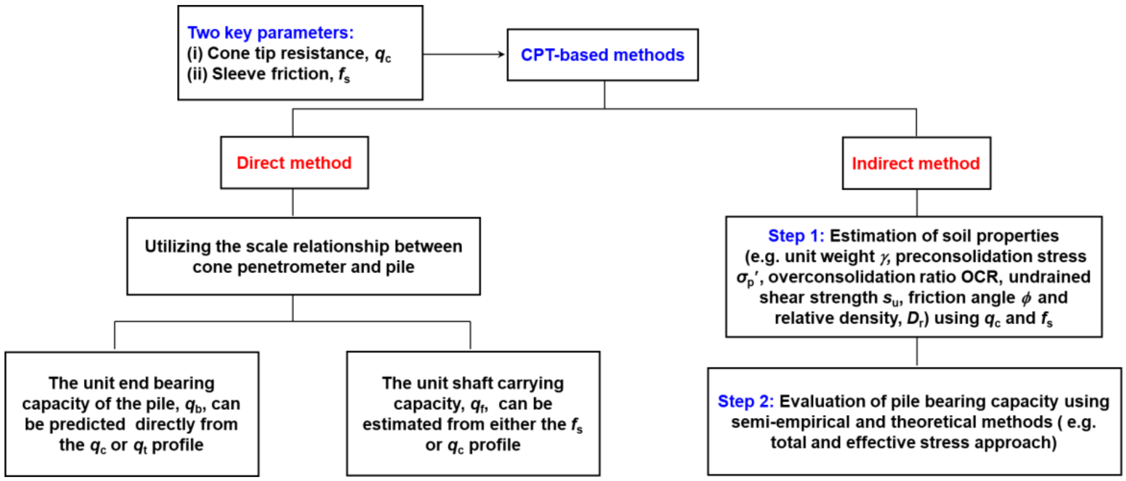

Figure 2.4 The methodology used to estimate the pile shaft and end bearing capacity from the CPT methods

2.3.1.3 Static pile load tests

Static pile load tests are considered the most accurate method for estimating the load-displacement behavior of pile foundations. The ultimate bearing capacity can be obtained through the plotted load-displacement curve from tests and the allowable bearing capacity can then be calculated. The ultimate failure load for piles is defined as the load when the pile plunges or rapid displacement occurs under sustained loads. Some criteria define the failure load as and when the pile settlement exceeds 10 % of the pile diameter or 1.5 inches (38 mm). However, these criteria do not consider the effect of elastic shortening of piles, which is substantial for long piles. The settlement limits relate to the superstructure that is to be supported by the piles, but not to the pile bearing capacity (Fellenius 2005). Various standards have been developed for defining the failure load from the load-displacement curve (Davisson 1972, Hansen 1963, Chin 1970, Mazurkiewicz 1972, Van Der Veen 1953, De Beer 1968, Fuller and Hoy 1970, Butler and Hoy 1977, Decourt 1999).

Davisson (1972) suggested that the ultimate load is the load when the settlement exceeds the elastic compression of the pile by 0.15 inches (i.e., 4 mm) plus a factor equal to $D/120$ (D = diameter of the pile), as shown in Figure 2.5. This method assumes that the pile capacity is reached at a certain settlement and this settlement can be predicted by compensating for the stiffness of the pile. This method is commonly used worldwide since it provides the least estimation of axial bearing capacity from the load-displacement curve and no extrapolation is required.

Table 2.4 Relationships for evaluating soil properties from CPT data

Property	Relationship	Eq No.	Reference
Internal angle of friction ϕ'(°)	$\phi' = \arctan\left\{\frac{1}{2.68}\left[\log\left(\frac{q_c}{\sigma_{v'}}\right)+0.29\right]\right\}$	(2.12)	Robertson and Campanella (1983)
	$\phi' = 17.6 + 11\log\frac{q_c}{\sqrt{100\sigma_v'}}$	(2.13)	Kulhawy and Mayne (1990)
Unit weight, γ (kN/m^3)	$\gamma = 11.46 + 0.33\log[z(\text{m})] + 3.1\log[f_s(\text{kPa})] + 0.7\log[q_t(\text{kPa})]$	(2.14)	Mayne et al. (2010)
Relative density, D_r (%)	$D_r = 100\left(\frac{q_c}{\sqrt{100\sigma_v'}\cdot 300\cdot OCR^{0.2}}\right)^{0.5}$	(2.15)	Kulhawy and Mayne (1990)
	$D_r = 100\left[0.268\ln\left(\frac{q_c}{\sqrt{100\sigma_v'}}\right)-0.675\right]$	(2.16)	Jamiolkowski et al. (2001)
OCR	$OCR = c_{OCR}\left(\frac{q_t-\sigma_v'}{\sigma_v'}\right)$; c_{OCR} = 0.2 to 0.3	(2.17)	Kulhawy and Mayne (1990)
	$OCR = \left[\frac{0.192\left(\frac{q_t}{\sigma_{atm}}\right)^{0.22}}{(1-\sin\phi')\cdot\left(\frac{\sigma_v'}{\sigma_{atm}}\right)}\right]^{\left(\frac{1}{\sin\phi'-0.27}\right)}$; σ_{atm} = 100 kPa	(2.18)	Mayne (2005)
Lateral stress coefficient k_0	$k_0 = (1-\sin\phi')\cdot OCR^{\sin\phi'}$	(2.19)	Kulhawy and Mayne (1990)

Hansen (1963) proposed an 80% criterion defining the pile capacity as the load that equals to 4 times the settlement as obtained for 80% of that load. This method assumes the relationship between load versus displacement as hyperbolic. The failure criterion agrees well with the plunging failure of the pile. However, the method of interpolation is not suitable for tests that have unloading conditions or where the plunging failure is not reached (Prakash and Sharma 1990). A simple relation was developed for estimating the ultimate load by Fellenius (2001) according to Hansen's 80%-criterion:

$$Q_u = \frac{1}{2\sqrt{C_1 C_2}} \tag{2.20a}$$

$$\Delta_u = \frac{C_1}{C_2} \tag{2.20b}$$

where Q_u = capacity or ultimate load, Δ_u = settlement at the ultimate load, C_1 = slope of the straight line and C_2 = y-intercept of the straight line.

Butler and Hoy (1977) assumed the ultimate load-carrying capacity to be the value at the intersection of the initial tangents to the load versus settlement curve and the tangent to or the extension to the final portion of the curve, as shown in Figure 2.5.

2.3.2 Axially loaded piles in unsaturated soils

In recent years, several studies focused on the load-displacement behavior of single piles and pile groups in unsaturated soils considering the influence of matric suction. For example, experimental studies were undertaken to understand the influence of matric suction (Douthitt et al. 1998, Uchaipichat 2012, Vanapalli and Taylan 2012, Fattah et al. 2014, Akrouch et al. 2016, Vanapalli et al. 2018, Al Khazaali and Vanapalli 2019). Theoretical approaches were proposed to interpret the bearing capacity and settlement behavior of piles in unsaturated soils (Vanapalli and Taylan 2012, Vanapalli et al. 2018). In addition, numerical techniques are also widely used because they are quick and economical (Georgiadis et al. 2003, Al-Khazaali et al. 2016, Han et al. 2016, Chung and Yang 2017).

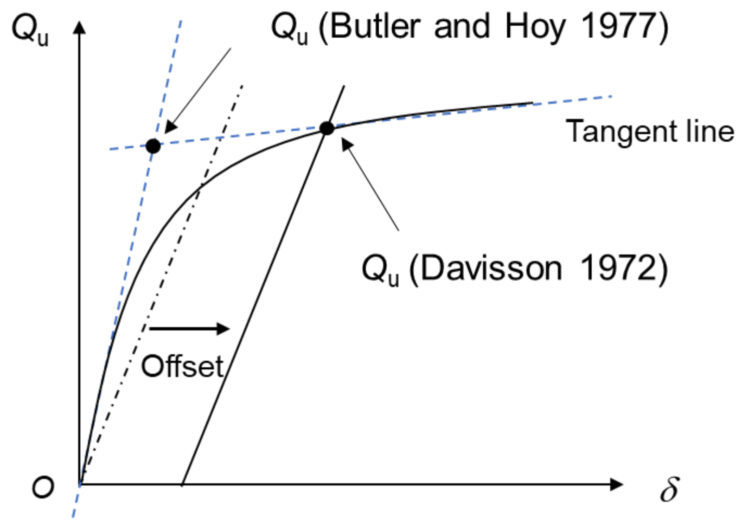

Figure 2.5 The Davisson offset limit method and Butler and Hoy's double tangent method

2.3.2.1 Theoretical approaches

Vanapalli and Mohamed (2007) proposed an approach for predicting the bearing capacity of surface shallow foundations with respect to matric suction, which is consistent with the conventional approach used for saturated soils. In this approach, the effective cohesion, c' term is replaced with total cohesion, c_a for determining the variation of bearing capacity of unsaturated soils taking account the influence of matric suction. The same equation can be also used for predicting the variation of total cohesion, c_a with respect to matric suction:

$$c_a = c' + (u_a - u_w)_b \left(1 - S^{\psi_{BC}}\right) \tan\phi' + (u_a - u_w)_{AVR} S^{\psi_{BC}} \tan\phi' \tag{2.21}$$

where ψ_{BC} = fitting parameter with respect to bearing capacity (ψ_{BC} =1 for nonplastic soil). A relationship between ψ_{BC} and plasticity, I_p was developed that can be used for fine-grained soils:

$$\psi_{BC} = 1.0 + 0.34 I_p - 0.003 I_p^{\ 2} \tag{2.22}$$

Vanapalli et al. (2018) extended this approach to predict the end-bearing capacity $Q_{p(us)}$ of single piles in unsaturated soils. Three conventional methods originally proposed by Terzaghi (1943), Hansen (1970) and Janbu (1976) for estimating the end-bearing capacity of piles in saturated soils were used in extending this approach.

Table 2.5 Modified model for predicting the pile end-bearing capacity in unsaturated soils by Vanapalli et al. (2018)

Methods	Eq. No.	Bearing capacity equations	Remarks
Modified Terzaghi (1943) method	(2.23)	$q_b = \begin{bmatrix} c' + (u_a - u_w)_b (1 - S^{\psi}) \tan\phi' + \\ (u_a - u_w)_{AVR} S^{\psi} \tan\phi' \end{bmatrix} N_c s_c + q' N_q + \tfrac{1}{2}\gamma D N_\gamma s_\gamma$ where $N_c = (N_q - 1)\cot\phi$, $N_q = \dfrac{e^{2(0.75\pi - \phi'/2)\tan\phi'}}{2\cos^2(45° + \phi'/2)}$, $N_\gamma = \dfrac{\tan\phi'}{2}\left(\dfrac{K_{py}}{\cos^2\phi'} - 1\right)$	q': vertical effective stress at pile base D: pile diameter N_c, N_q, N_γ: bearing capacity factors s_c, s_γ: shape factors (s_c = 1.3 and s_γ = 0.6 for round pile foundation) K_{py}: passive pressure coefficient
Modified Hansen (1970) method	(2.24)	$q_b = \begin{bmatrix} c' + (u_a - u_w)_b (1 - S^{\psi}) \tan\phi' + \\ (u_a - u_w)_{AVR} S^{\psi} \tan\phi' \end{bmatrix} N_c' d_c + \eta q' N_q' d_q + \tfrac{1}{2}\gamma D N_\gamma'$ where $N_c' = (N_q' - 1)\cot\phi'$, $N_q' = e^{\pi\tan\phi'}\tan^2(45° + \phi'/2)$, $N_c = (N_q - 1)\cot\phi'$, $N_\gamma' = 1.5(N_q' - 1)\tan\phi'$ $\dfrac{L}{D} > 1 \quad \begin{cases} d_c = 1 + 0.4\tan^{-1}(L/D) \\ d_q = 1 + 2\tan\phi'(1 - \sin\phi')\tan^{-1}(L/D) \end{cases}$	$N_c´$, $N_q´$, $N_\gamma´$: bearing capacity factors η =1.0 for all except the Vésic (1975) bearing capacity factors d_c, d_q: depth factors L: pile embedded depth
Modified Janbu (1976) method	(2.25)	$q_b = \begin{bmatrix} c' + (u_a - u_w)_b (1 - S^{\psi}) \tan\phi' + \\ (u_a - u_w)_{AVR} S^{\psi} \tan\phi' \end{bmatrix} N_c^* + q' N_q^* + \tfrac{1}{2}\gamma D N_\gamma^*$ where $N_c^* = (N_q^* - 1)\cot\phi'$, $N_q^* = \left(\tan\phi' + \sqrt{1 + \tan^2\phi'}\right)^2 e^{(2\theta\tan\phi')}$ $N_\gamma^* = 1.5(N_q' - 1)\tan\phi'$	N_c*, N_q*, N_γ*:bearing capacity factor which determined by θ for different types of soils, θ varies from 60° in soft compressible to 105° in dense soil sand.

Table 2.5 summarizes the equations of these three modified methods. ψ_{BC} value equal to unity for soils with no plasticity is used in this study as the soils investigated are

predominantly coarse-grained soils. More details of this relationship are available in Vanapalli et al. (2018).

Vanapalli and Taylan (2012) modified three conventional semi-empirical approaches (i.e., α method proposed by Skempton (1959), β method proposed by Burland (1973), λ method by Focht and Vijayvergiya (1972) for saturated soils to predict the variation of the shaft carrying capacity of pile foundations in unsaturated fine-grained soils.

- **Modified α method**

Oh and Vanapalli (2009) proposed an equation for estimating the variation of the undrained shear strength, $c_{u(unsat)}$ for unsaturated fine-grained soils:

$$c_{u(unnsat)} = c_{u(sat)}\left[1+\frac{(u_a - u_w)}{(P_a/100)}(S^v)/\mu\right] \tag{2.26}$$

where v and μ are fitting parameters. v is 2 for fine grained soil and μ is related to the plasticity index, I_p:

$$\mu = 9,\ 8.0 \le I_p(\%) \le 15.5$$

$$\mu = 2.1088e^{0.0903(I_P)},\ 15.5 < I_p(\%) \le 60.0$$

where e is Euler's number. The above relationship was derived from six sets of unconfined compression test results (e.g., Chen 1984, Ridley 1993, Babu et al. 2005). This approach has been used by several investigators in recent years (Vanapalli and Taylan 2012, Han et al. 2016, Yanamandra and Oh 2021) and is valuable for use in geotechnical design practice.

The α method was originally proposed by Skempton (1959) to determine the shaft carrying capacity of piles placed in saturated cohesive soils extending the total stress approach (TSA) (i.e., ϕ =0 concept). Extending the same philosophy, the shaft carrying capacity of pile Q_f under undrained loading conditions in UFG soils can be estimated using Equation 2.27.

$$Q_{\mathrm{f(us)}} = q_{\mathrm{f}} \times A_{\mathrm{s}} = \alpha c_{\mathrm{u}} \pi DL$$
$$= \alpha c_{\mathrm{un(sat)}} \left(1 + \frac{(u_{\mathrm{a}} - u_{\mathrm{w}})}{P_a / 101.3} S^{\upsilon} / \mu \right) \pi DL \tag{2.27}$$

- **Modified β method**

The ultimate shaft capacity of a single pile in unsaturated soils $Q_{\mathrm{f(us)}}$ arises from the contribution of matric suction $Q_{(\mathrm{ua}-\mathrm{uw})}$ and conventional shaft resistance Q_{f} under saturated conditions. $Q_{\mathrm{f(us)}}$ can be written as:

$$Q_{\mathrm{f(us)}} = Q_f + Q_{(u_{\mathrm{a}} - u_{\mathrm{w}})} = \left[c'_{\mathrm{a}} + \beta(\sigma'_z) + (u_{\mathrm{a}} - u_{\mathrm{w}})(S^{\kappa})(\tan\delta') \right] \pi DL \tag{2.28a}$$

$$Q_{\mathrm{f(us)}} = Q_f + Q_{(u_{\mathrm{a}} - u_{\mathrm{w}})} = \left[c'_{\mathrm{a}} + \beta(\sigma'_z) + (u_{\mathrm{a}} - u_{\mathrm{w}}) \frac{(S - S_{\mathrm{r}})}{(1 - S_{\mathrm{r}})} (\tan\delta') \right] \pi DL \tag{2.28b}$$

where S_{r} is the residual degree of saturation. The fitting parameter κ can be obtained from the relationships proposed by Vanapalli et al. (2000). For bored piles, the pile-soil interface angle δ' is commonly assumed to be equal to the angle of shearing resistance of the surrounding soil, ϕ', for practical purposes.

- **Modified λ method**

The λ method originally proposed by Vijayvergiya and Focht (1972) was modified to estimate the shaft carrying capacity of single pile $Q_{\mathrm{f(us)}}$ with respect to matric suction:

$$Q_{\mathrm{f(us)}} = \lambda \left[\sigma'_{\mathrm{v(avg)}} + 2c_{\mathrm{un(sat)}} \left(1 + \frac{(u_{\mathrm{a}} - u_{\mathrm{w}})}{P_a / 101.3} S^{\upsilon} / \mu \right) \right] \pi DL \tag{2.29}$$

All the modified approaches (i.e., α method, β method, and λ method) provide a smooth transition of pile shaft carrying capacity from unsaturated to saturated soil conditions. In other words, these equations (i.e., Equations 2.27, 2.28 and 2.29) take the form of conventional equations used for saturated soils, when matric suction equals value of zero.

2.3.2.2 Experimental studies

Vanapalli and Taylan (2012) have conducted a series of single model pile tests to study the contribution of matric suction on the pile carrying shaft capacity in unsaturated fine-grained soils under undrained and drained loading conditions. The schematic of the model pile test is shown in Figure 2.6. The soil was placed in a 300 mm depth and 300 mm diameter cylinder tank. It was compacted statically under 350 kPa stress using a specially designed compaction plate. The soil samples were compacted at four different initial water contents: (i) w = 13% (i.e., as-compacted condition, referred as ASCOMP-13%), (ii) w = 16% (ASCOMP-16%), (iii) w = 18% (ASCOMP-18%), and (iv) w = 13% in fully saturated condition (SAT-13%). Axis-translation technique with a modified null pressure plate (Power et al. 2008) was used to measure the matric suction of soil samples. Model piles with 20 mm diameter were installed to a depth of 200 mm after the borehole drilling was done. A 20 mm depth gap under the base of the pile was set up to eliminate the end-bearing capacity while loading the model pile. Model piles were subjected to a strain rate of 0.0120 mm/min loading to simulate drained loading conditions. This loading rate is consistent with the tests performed by Gan et al. (1988) and Vanapalli et al. (1996) on the same soil under drained conditions. A relatively faster loading rate of 1.4 mm/min was controlled to simulate undrained loading conditions. Table 2.6 shows the comparison between the measured and estimated undrained shear strength of Indian Head Till. The determination of α values obtained from the correlation charts (Sowers 1979) and back-calculated from experimental results are also summarized in Table 2.6. The coefficient, β = 0.3 was used for both the saturated and unsaturated soils based on the value of the soil-pile interface friction angle. A value of λ = 0.32 was used in the study. The results highlighted a significant increase in shaft carrying capacity due to the influence of matric suction. The results calculated by the modified α, β and λ methods also provide a good agreement with those measured results in model pile tests.

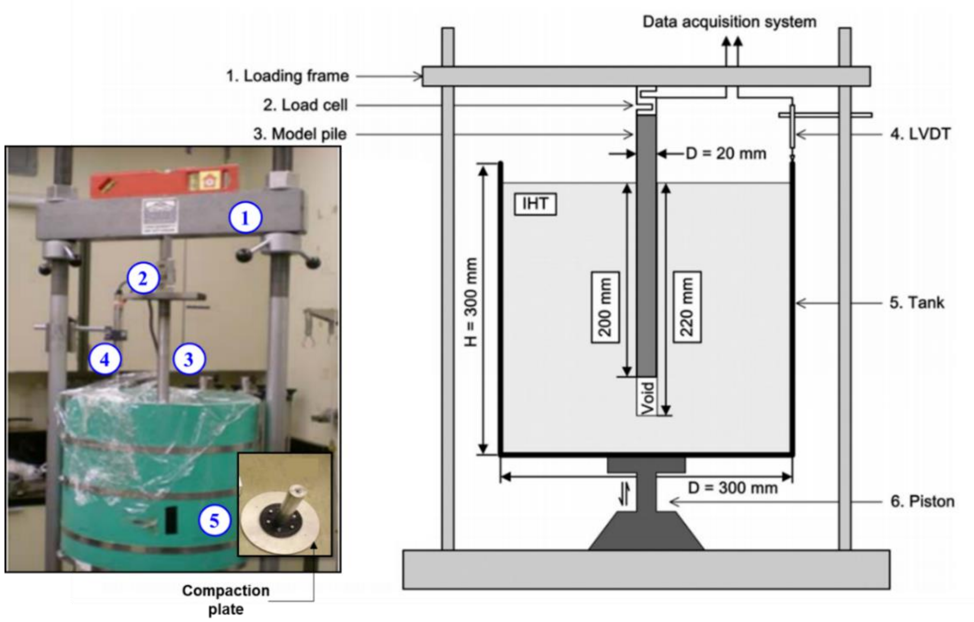

Figure 2.6 Test setup for single model pile loading test (Modified after Han et al. 2016)

Table 2.6 Comparison between the measured and estimated undrained shear strength

Sample	Matric suction (kPa)	S (%)	Measured c_u (kPa)	Estimated c_u (kPa)	α from (Sowers 1979)	Back-calculated α
SAT-13%	0	100	11.5	11.5	0.9	0.71
ASCOMP-18%	55	83	58	60	0.82	0.7
ASCOMP-16%	110	65	68	71	0.67	0.57
ASCOMP-13%	205	44	80	62	0.75	0.79

Chung and Yang (2017) conducted a small-scale model pile test in unsaturated clayey soil. The soil specimens were compacted to two water content of 15 and 21% with a dry density of 16.64 kN/m^3. The model pile with a diameter of 16 mm was embedded 300 mm into unsaturated soils. The pile head was subjected to stepwise increasing axial loads. The load-displacement curve from the experiments showed that when the water content increases, the ultimate bearing capacity of the single pile decreases significantly.

Vanapalli et al. (2018) carried out experimental studies to investigate the load versus displacement behavior of single piles in unsaturated coarse-grained soil (i.e., Unimin Sand). The details of the test program are presented in Figure 2.7(a). The soil container was 300 mm in diameter, 700 mm in height and 8 mm in thickness. The model pile used in the tests were stainless steel piles with three different diameters (i.e., 38.30, 31.75, and 19.25 mm) with a length of 350 mm. Two different matric suction distribution profiles were achieved by setting one water level at 450 mm deep and the other at 650 mm deep from the soil surface in the compacted sand (Figure 2.7(b)). The water level was raised from the bottom of the sand to slightly above the soil surface to achieve saturated soil conditions. For convenience, the average matric suction values of 2 kPa, and 4 kPa were used to represent the water levels at 450 mm and 650 mm deep from the soil surface, respectively. A vertical load was applied to the top of the model pile at a rate of 0.7 mm/min to ensure a drained loading condition.

Figure 2.8 shows a good agreement with less than 10% deviation between the measured end-bearing capacity values and those calculated by the modified Terzaghi (1943), Hansen (1970), and Janbu (1976) methods. Relatively high R square values for all cases were obtained. Among the three methods, the modified Terzaghi (1943) method provides results that are closer to the measured values compared to the other two modified methods.

Fattah et al. (2020) have conducted a series of model pile tests in saturated and unsaturated expansive soils. The expansive soil used in the experiment consists of 70% bentonite and 30 % sand. Three soil samples were compacted to three initial degrees of saturation at 70, 87 and 91%. A compression machine with a strain-controlled system was used to apply axial loads to the model piles. The results indicated that the sharing ratio (i.e., the ratio of ultimate shaft carrying capacity obtained from pullout test to the total bearing capacity obtained from compression tests) reduces as the degree of saturation decreases.

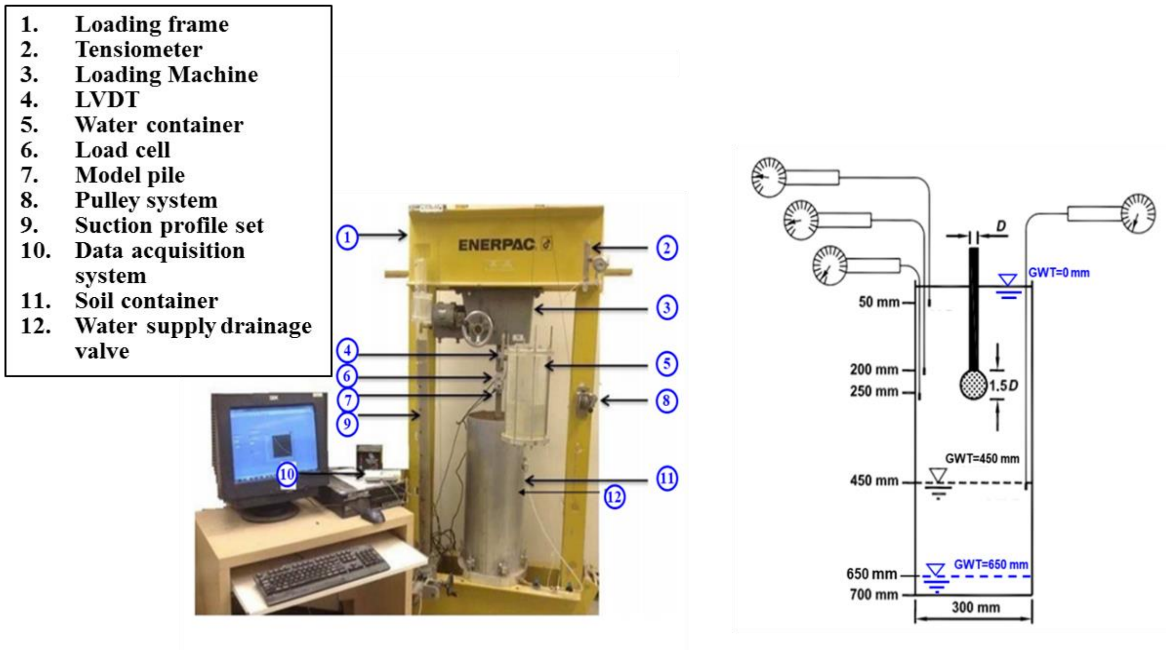

(a) (b)

Figure 2.7 Details of test program: (a) Details of the test setup for determining the load carrying for the model pile (b) Cross-sectional schematic of the testing program with the water level at 450 mm and 650 mm from the soil surface (Modified after Vanapalli et al. 2018)

Few experimental studies were conducted to investigate the behavior of pile groups in unsaturated soils. Al Khazaali and Vanapalli (2019) performed model pile tests to study the behavior of single model piles and 2 × 2 pile groups in saturated and unsaturated sands. Model piles of 38.1 mm diameter and 300 mm embedded length with smooth and rough shafts with three different pile center-to-center spacing (i.e., 3*D*, 4*D*, and 5*D*) for the pile group, were used in the tests, to investigate the influence of matric suction, the roughness of soil-shaft interface, dilation, and group effects.

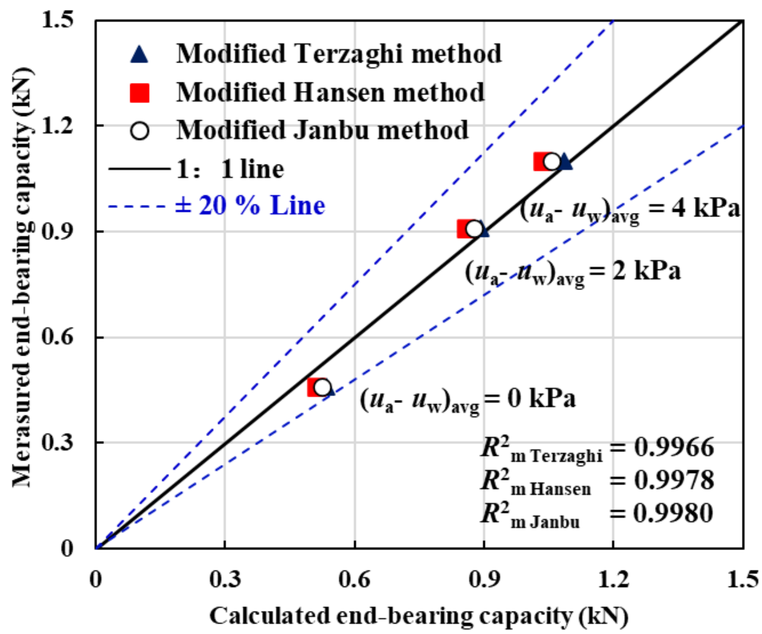

Figure 2.8 Comparison between measured end-bearing capacity values and those estimated using the three modified end-bearing capacity equations (modified after Vanapalli et al. 2018)

The test setup and preparation for pile groups performed in modified UOBCE are shown in Figure 2.9. First, a square pit was dug in the middle of the soil container in Figure 2.9(c). The model pile or pile group was then placed in the prepared pit. The sand surrounding the pile was manually compacted to optimum moisture content while model piles or pile group was supported by a wooden frame in Figure 14b. The water supply/drainage valve connected to the soil container was used to control the saturation and desaturation procedures in the sand. The load of 0.5 mm/s rates was applied at the top of the model pile or pile groups to simulate a drained loading condition. The results of the tests showed that the bearing capacity of both single piles and pile groups increased significantly due to the contribution of matric suction to the shear strength and stiffness of unsaturated soils. The ultimate bearing capacity increases linearly in the BEZ until suction reached AEV, then increases nonlinearly in the TEZ and reduces in the RZS. Al-Omari et al. (2019) have carried out model tests of pile groups in unsaturated soils. Model piles 200 mm in length with 6 configurations (i.e., single, 2 × 1, 3 × 1, 2 × 2, 3 × 2 and 3 × 3) were constructed in saturated soils and unsaturated clay. Three soil samples with different dry densities and degrees of saturation were prepared. The results showed that the ultimate load capacity of the pile group increases as the dry unit weight increases. Significant increases in ultimate load-carrying capacity were observed when the soil moves from saturated to unsaturated soil conditions.

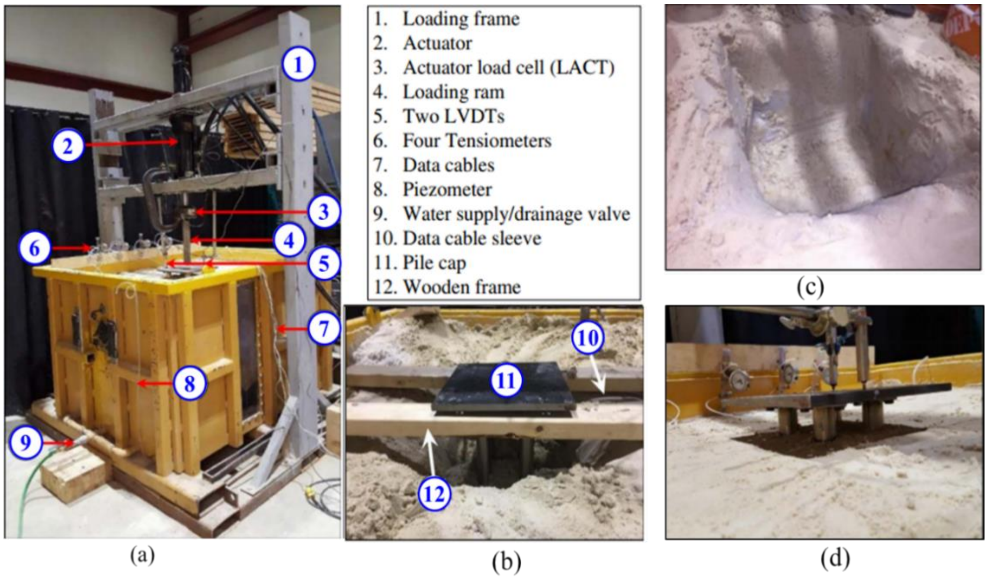

Figure 2.9 Test setup for model pile group test (Modified after Al-Khazaali and Vanapalli 2019)

2.3.2.3 Numerical simulations

In the early stage of FEA applications to piles in unsaturated soils, Georgiadis et al. (2003) developed a total stress constitutive model to investigate the influence of the degree of saturation on pile behavior. Their model incorporates an equation for the yield and plastic potential surfaces and well reproduces the collapse and wetting characteristics of unsaturated soils. FEA was performed using the proposed model to simulate the behavior of single piles in unsaturated soils. The studies showed that the ultimate bearing capacity of single piles increases with an increase in the GWT depth. The FEA using unsaturated soil mechanics provides more consistent results with the field data compared to conventional analysis using saturated soil mechanics.

Noor et al. (2013) investigated the influence of inundation of collapse soils on the negative skin friction of pile shafts. Numerical models were performed in PLAXIS to simulate a single pile passing through the collapsible soil layer. The soil suction was estimated using unsaturated soil mechanics and the SWCC. The change in some soil properties such as the modulus of elasticity and void ratio, and irrecoverable volume change during inundation were considered in the FEA. The predictions from numerical models were used to develop an analytical model, which provides the guidelines for the design of single piles in collapsed soils under inundation effects.

Al-Khazaali et al. (2016) and Han et al. (2016) used PLAXIS to simulate the $P-\delta$ behaviour of single piles in unsaturated sands and clayey soils, respectively. The influence of matric suction on the shear strength, elastic modulus and shear strength of the pile-soil interface was considered in the FEA. They both concluded that the bearing capacity and slope of the $P-\delta$ curve of the model pile increases largely with increasing matric suction.

Chung and Yang (2017) performed FEM analysis of single piles in unsaturated clayey soils under vertical loads using PLAXIS. Prior to performing the numerical simulation, several tests were conducted to determine the parameters used in the FEA. For example, matric suction was measured using the contact filter method. An interface direct shear test was conducted to determine the interface strength reduction factor ($R_{\text{interface}}$) and interface friction angle (δ). The numerical results showed good agreement with the measured data from pile load tests.

2.4 The behavior of laterally loaded piles

2.4.1 Laterally loaded piles in saturated soils

Significant research has been published in the literature for analyzing the behavior of laterally loaded piles, which can be generally classified into four categories: (i) Subgrade reaction method; (ii) Ultimate state method; (iii) Continuum method and (iv) Numerical method. The details of these four methods will be introduced in the following sections.

2.4.1.1 Subgrade reaction (Winkler) method

The behavior of a laterally loaded pile is commonly analyzed by extending the subgrade reaction method, which is also referred to as the Winkler spring method. Winkler's (1867) method is considered the oldest and most well-known method for interpreting the behavior of laterally loaded piles. The pile is simplified as a beam while the surrounding soil is represented by a series of nonlinear springs placed along the length of the pile in Figure 2.10.

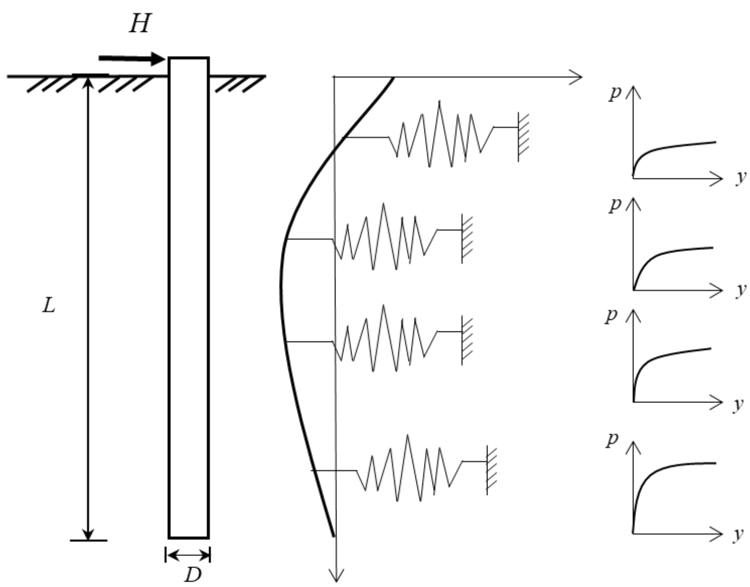

Figure 2.10 *p-y* models for the analysis of laterally loaded pile (modified after Reese 1997)

The nonlinear behavior of soil can be represented by load-displacement characteristics, which is also known as the *p-y* curve, where p is the lateral soil resistance pile (FL^{-1}) and y is the lateral deflection (L). Figure 2.11(a) presents a typical *p-y* curve. The soil resistance increases nonlinearly at a decreasing rate until it reaches the ultimate lateral soil resistance (p_u). The initial stiffness k_i is an important parameter that influences the load versus lateral deflection behavior of the pile in the elastic zone. The lateral soil resistance (p) per unit length prior to reaching p_u can be expressed as:

$$p = k_h y \tag{2.30}$$

where k_h is defined as the modulus of horizontal subgrade reaction. Figure 2.11 (b) shows the decay of k_h (FL^{-2}) due to the lateral deflection. k_h stays constant within a small deflection, then it starts to decrease nonlinearly with an increase in the lateral deflection of the pile. For cohesive soils, the modulus of horizontal subgrade reaction (k_{hc}) does not change with an increase in depth (Terzaghi, 1955); however, the modulus of horizontal subgrade reaction for cohesionless soils (k_{hq}) increases linearly with the depth z, that is:

$$k_{hq} = n_h z \tag{2.31}$$

where n_h is constant horizontal subgrade reaction (FL^{-3}).

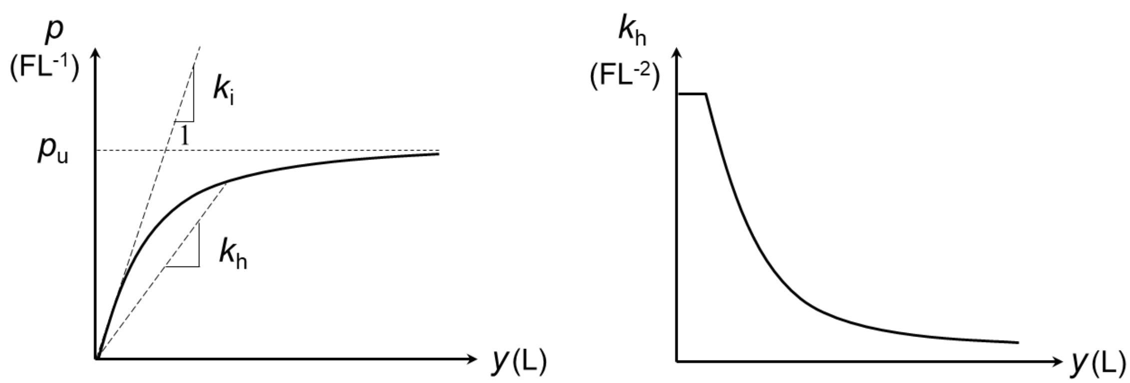

(a) (b)

Figure 2.11 (a) A typical *p-y* curve; (b) Degradation of horizontal subgrade reaction modulus (modified after Reese and Van Impe, 2000)

The *p*-*y* curves have been developed by many researchers based on either field tests or analytical derivations for different types of soils: clay (e.g., Matlock 1970, Reese et.al 1975, Murff and Hamilton 1993), sand (e.g., Reese et al. 1974, Rollins et al. 2005, Suleiman et al. 2014), rock (e.g., Reese 1997, Gabr et al. 2002). Several classic *p*-*y* curve models for soft clay, stiff clay and sand, respectively are succinctly reviewed in the following.

Matlock (1970) has proposed *p*-*y* relations of laterally loaded piles through pile tests in soft clay under static and cyclic loading. The relationship between soil resistance *p* and deflection *y* for the static loading is expressed as

$$\frac{p}{p_{\mathrm{u}}} = 0.5\left(\frac{y}{y_{50}}\right)^{\frac{1}{3}} \tag{2.32}$$

where p_{u} is the ultimate soil resistance per unit length of the pile. y_{50} is the deflection at one-half ultimate soil resistance given by

$$y_{50} = 2.5\varepsilon_{50} d \tag{2.33}$$

where ε_{50} is the strain at one-half the maximum difference in principal stresses (σ_1- σ_3). As shown in Figure 2.12, *p* remains constant beyond the deflection $8y_{50}$. p_{u} is determined as the smaller value of the following two equations:

$$p_{\mathrm{u}} = \left(3 + \frac{\gamma' z}{c_{\mathrm{u}}} + J\frac{z}{d}\right)c_{\mathrm{u}} d \tag{2.34}$$

$$p_{\mathrm{u}} = 9c_{\mathrm{u}} d \tag{2.35}$$

where c_{u} is the undrained shear strength at depth *z*, γ' is the submerged unit weight, *d* is the diameter of the foundation, and *J* is the coefficient with values ranging from 0.25 to 2.5 that are required to be determined from the experiment. A value of $J = 0.5$ is satisfactory for common use (Matlock 1970).

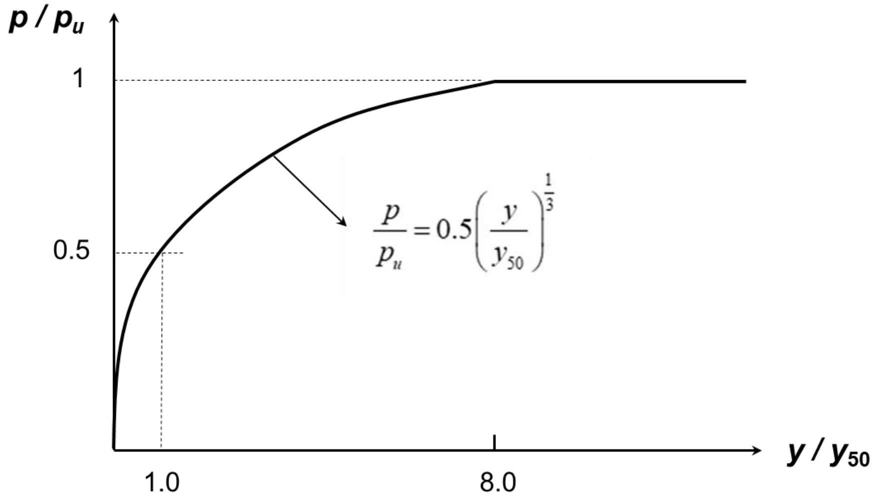

Figure 2.12 *p-y* curve for soft clay under static loading (Modified after Matlock 1970)

Reese et al. (1975) have proposed procedures for developing *p-y* curves for stiff clay below the water based on the results from a full-scale field lateral load test. The shape of the *p-y* curve under static loading conditions for stiff clay is shown in Figure 2.13. Gazioglu and O'Neill (1984) indicated that there are uncertainties in the *p-y* model by Reese et al. (1975) for submerged stiff clay. The influence of softening of the near-surface soil layer could be significant since it was derived from the tests performed in expansive soils that may have imbibed water. Stevens and Audibert (1979) compared the *p-y* models proposed by Matlock (1970) and Reese et al. (1975) through the results from lateral load tests and suggested some modifications for the determination of parameters N_p and y_{50}. Gabr et al. (1994) have developed a procedure for the development of a hyperbolic *p-y* curve based on the modulus of subgrade reaction from dilatometer tests (DMT) taking account of the influence of pile-installation on the soil adjacent to the pile. Khalili-Tehrani et al. (2014) have carried out three full-scale lateral load tests to provide the load-deflection behavior of reinforced concrete drilled piles. A robust procedure, CES, was introduced for obtaining stable *p-y* curves from the measured data. The accuracy of the CES procedure was assessed by comparing the experimental *p-y* curves with API *p-y* curves.

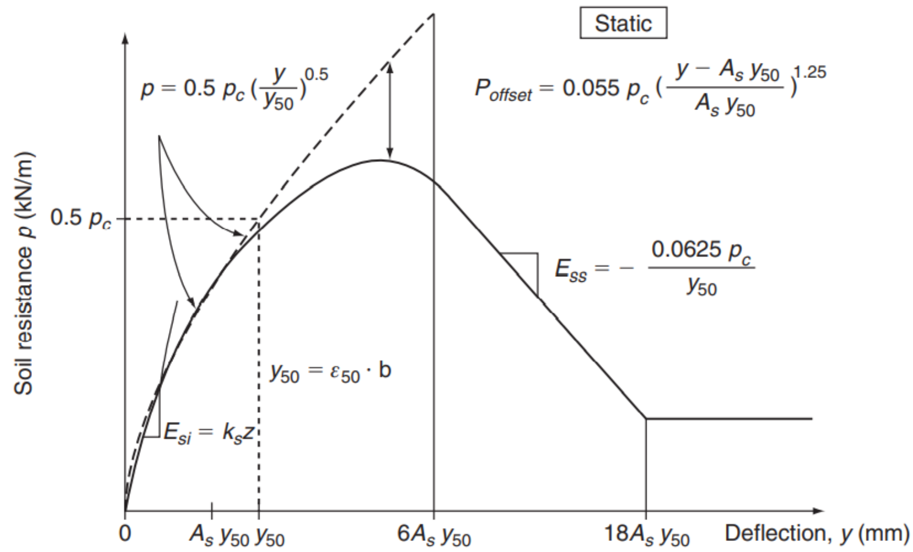

Figure 2.13 Characteristic shape of *p-y* curves in stiff clay below the water table (Reese and Van Impe 2000)

Reese et al. (1974) proposed a semi-empirical *p-y* curve for sandy soils based on the data from two field tests on 24-inch (i.e., 600mm) diameter steel piles at Mustang Island. Long and Vanneste (1994) investigated the effects of cyclic lateral loads on the pile in sand. The results of 34 cyclic lateral load tests were analyzed and the lateral response of a pile was modelled by degrading the soil resistance as a function of cyclic loading characteristics, soil properties and pile installation method. Zhang et al. (1999) conducted centrifuge tests for single battered piles embedded in dry sands. Modified nonlinear *p-y* curves were developed for battered piles at five different angles in both medium-dense and loose sands. Sørensen et al. (2010) have extended the *p-y* curve method for the design of laterally loaded offshore monopiles. The effect of large pile diameter on the initial stiffness of the *p-y* curve was investigated by numerical simulations. API (2011) and DNV (2014) recommended the *p-y* curve for laterally loaded piles in the sand by the following equation:

$$p = Ap_u \tanh\left(\frac{kz}{Ap_u} y\right) \tag{2.36}$$

where k is the initial modulus of subgrade reaction and z is the depth. A is a nondimensional factor depending on cyclic or static loading conditions given by:

$$A = 0.9 \qquad \text{(for cyclic loading)}$$

$$A = \left(3.0 - 0.8\frac{z}{D}\right) \geq 0.9 \qquad \text{(for static loading)}$$

Kallehave et al. (2012) have found that the current API *p*-*y* formulation underestimates the soil stiffness of sand for large-diameter monopiles. They introduced an approximate method by modifying the initial slope of the *p*-*y* curves, and the modified *p*-*y* curves were benchmarked against full-scale measurements from three wind turbines.

The *p*-*y* curve method is widely used for simulating the nonlinear behavior of the soil around the pile. Due to its simplicity and practicality, the *p*-*y* method was included in design code API (2011) as well as computational programs such as COM624P (Reese 1984) and LPILE (Reese et al. 1989). However, the subgrade reaction method also has its limitations. The modulus of horizontal subgrade reaction, k, is not only influenced by the soil properties, but also by the pile stiffness and loading conditions. Due this reason, determination of a rigorous value for k is complex. In addition, the continuous feature of the soil medium is not considered in the subgrade reaction method. For this reason, this method is not suitable for analyzing pile groups since the interaction effects between neighbouring piles can not be quantified (Randolph 1981).

2.4.1.2 Ultimate limit state method

The ultimate limit state method is used to estimate the maximum lateral load that piles can carry. The analysis of laterally loaded piles placed in cohesive soil is typically based on a total stress approach considering undrained loading conditions. The ultimate lateral soil resistance p_u in cohesive soils is generally written in the following form:

$$p_u = N_p c_u d \tag{2.37}$$

where c_u is the undrained shear strength of the soil, d is the pile diameter, and N_p is the lateral bearing capacity factor. N_p increases from the ground surface up to a critical depth and then remains constant. Many studies have been focused on the determination of N_p value, as summarized in Table 2.7.

Table 2.7 Variation of the N_p value from literature (modified after Su et al. 2018)

Authors	N_{p0} at z = 0	N_{pmax}
Hansen (1961)	2.57	8.14
Broms (1964a)	0	9
Matlock (1970)	3	9
Reese et al. (1975)	2	11
Sullivan (1977)	2	9
Stevens and Audibert (1979)	4.83	12
Randolph and Houlsby (1984)	2	9.14 (smooth)
	3.57	11.94 (rough)
API RP 2A (1987)	0	9

Some theoretical methods have been proposed for predicting the ultimate soil resistance, p_u, for laterally loaded piles in cohesionless soils. For example, Hansen (1961) developed an equation for laterally loaded short piles in a c-ϕ soil based on earth pressure theory. The proposed theory was then validated using lateral load tests of 26 wooden model piles, which presents accurate predictions of the ultimate lateral load of rigid piles. Broms (1964b) has derived models for predicting the distribution of ultimate soil resistance and bending moment of piles in cohesionless soils. Unlike Hansen's equation, which is only suitable for short rigid piles, Brom's equations account for both short and long piles under lateral loads. Several published equations for estimating the ultimate soil resistance in cohesionless soils are listed in Table 2.8.

Figure 2.14(a), (b) and (c) shows the lateral soil resistance distribution along the pile length in cohesionless soils assumed by some researchers using theoretical methods (Hansen 1961, Broms 1964b, Petrasovits and Awad 1972). However, several investigators have measured the actual profile of soil pressure along the pile length using pressure transducers (Radhakrishna and Adams 1973, Chari and Meyerhof 1983, Joo 1985, Prasad and Chari 1999, Nasr 2014, Lin et al. 2015) and found that the measured soil pressure distribution is different from those presented in Figure 2.14(a), (b) and (c). Prasad and Chari (1999) suggested that the soil pressure increases with the depth up to 0.6 z_c (where z_c is the depth of rotation point) based on experimental results, the pressure then decreases to zero and increases in the opposite direction, as shown in Figure 2.14(d). A modified method was proposed to predict the ultimate lateral load capacity of rigid piles based on the soil pressure distribution. Fan and Long (2005) have assessed existing analytical methods for predicting the ultimate soil resistance of laterally loaded piles in sand using a FE program (PILE3D). The results showed that the dilatancy of sands has a significant influence on the ultimate soil resistance, while it is generally ignored in the theoretical methods. In addition, Hansen's (1961) method provides more reasonable predictions of p_u than the API (1987) and Broms (1964b) method.

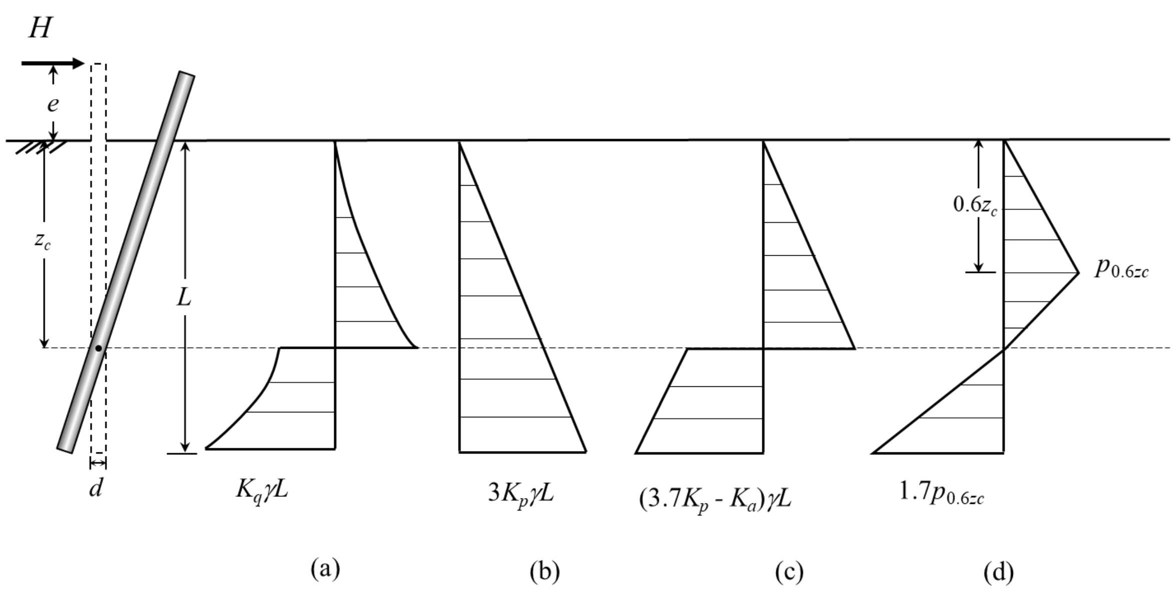

Figure 2.14 Profile of lateral soil pressure along pile length in cohesionless soils (a) Hansen (1961); (b) Broms (1964b); (c) Petrasovits & Awad (1972); (d) Meyerhof et al. (1981) and (e) Prasad & Chari (1999) (modified after Zhang and Grismala 2005)

Table 2.8 Published methods for predicting the p_u on laterally loaded piles in cohesionless soil

Methods	Equations	Description
Hansen (1961)	$p_{\mathrm{u}} = K_{\mathrm{q}} \gamma z d$	where K_q is Hansen earth pressure coefficient which is a function of ϕ'
Broms (1964b)	$p_{\mathrm{u}} = 3K_{\mathrm{p}} \gamma z d$	where K_p is the coefficient of passive earth pressure
Petrasovits and Awad (1972)	$p_{\mathrm{u}} = \left(3.7K_{\mathrm{p}} - K_{\mathrm{a}}\right) \gamma z d$	where K_a is the coefficient of active earth pressure
Reese et al. (1974)	$p_{\mathrm{st}} = \gamma z \begin{bmatrix} \dfrac{K_0 z \tan\phi \sin\beta}{\tan(\beta-\phi)\cos\alpha} + \dfrac{\tan\beta}{\tan(\beta-\phi)}(d + z\tan\beta\tan\alpha) \\ + K_0 z \tan\beta(\tan\phi\sin\beta - \tan\alpha) - K_a d \end{bmatrix}$ $p_{\mathrm{sd}} = K_{\mathrm{a}} d\gamma z\left(\tan^8\beta - 1\right) + K_0 d\gamma z \tan\phi \tan^4\beta$ $p_{\mathrm{u}} = A_{\mathrm{s}} \cdot \min(p_{\mathrm{st}}, p_{\mathrm{sd}})$	where A_s is a function of z/d; $\alpha = \dfrac{\phi'}{2}; \beta = 45° + \dfrac{\phi'}{2}$; K_0 is the at rest earth pressure coefficient
API RP2A (1987)	$p_{\mathrm{us}} = \left(C_1 z + C_2 d\right)\gamma z;\ p_{\mathrm{ud}} = C_3 d\gamma z$ $p_{\mathrm{u}} = \min(p_{\mathrm{us}}, p_{\mathrm{ud}})$	where p_{us} is resistance at shallow depths, p_{ud} is resistance at deeper depth; C_1, C_2, C_3 are coefficients that are functions of ϕ'
Fleming et al. (1992)	$p_{\mathrm{u}} = K_{\mathrm{p}}^{2} \gamma' z d$	

2.4.1.3 Continuum method

While the soil is assumed as a series of springs in the subgrade reaction method, the soil is replaced by an elastic continuum in the continuous approach. Poulos (1971a, b) was one of the pioneering investigators who has proposed appropriate solutions for laterally loaded piles using the boundary element method (BEM). The pile was represented by a thin strip in an ideal linear elastic medium and was divided into n segments along the length. The horizontal displacement at each segment can be solved using Mindlin's (1936) equation.

Further developments for modelling the pile and soil continuum (Banerjee and Davies 1978, Kuhlemeyer 1979, Randolph 1981, Davies and Budhu 1986, Verruijt and Kooijman1989, Ng and Zhang 2001, Klar and Frydman 2002) were based on the finite element method

(FEM), finite difference method (FDM) and BEM. Banerjee and Davies (1978) performed an elastic analysis of the behavior of single piles under axial and lateral loads in two-layered soils. They provided solutions for point load acting at the interface of a two-layered elastic half-space system using BEM. The results using their method provide reasonable predictions compared with the experimental data. Randolph (1981) has proposed algebraic expressions for predicting the behavior of laterally loaded flexible piles using the FEM. The soil stiffness is assumed to increase linearly with depth. The effect of variations of Poisson's ratio, ν, on the lateral deformation of a pile can be represented by introducing a parameter G^* given by

$$G^* = G\left(1 + 3\nu / 4\right) \tag{2.38}$$

where G is the shear modulus. The parameter G^* was used to avoid the necessity of including separate solutions for different Poisson's ratio values (Randolph 1981). The characteristic modulus, G_c, is introduced as the average of G^* over the critical length of the pile. This enables the horizontal displacement of the pile at the ground surface to be solved from a single pair of expressions. In addition, expressions are proposed to quantify the effect of interaction between adjacent piles in pile groups.

Considering the soil surrounding the pile as a continuum, Sun (1994) has proposed the modified Vlasov model, which was originally proposed by Vlasov and Leontiev (1966), for the analysis of laterally loaded piles using variational calculus. A step-by-step computing procedure was presented for predicting the lateral response of single piles embedded in a homogeneous elastic medium. Guo and Lee (2001) suggested that Sun (1994)'s two-parameter model may not provide reliable results for Poisson's ratio over 0.3. They used simple expressions and proposed a new load transfer model that overcomes the disadvantages of the two-parameter model. Moreover, Basu and Salgado (2007, 2008) extended Sun (1994)'s model and developed analytical solutions for single piles with circular and rectangular cross sections in a multilayer elastic continuum. Their approach considers the 3D interaction of the pile-soil system and the solutions that can be quickly obtained using computer programs.

2.4.1.4 Numerical method

Many studies have been published in the literature that use numerical methods for analyzing the behavior of laterally loaded piles (Brown and Shie 1991, Fan and Long 2005, Yang and Liang 2006, Chik et al. 2009, Ahmadi and Ahmari 2009, Kim and Jeong 2011, Khodair and Abdel-Mohti 2014, Tzivakos and Kavvadas 2014, Kampitsis et al. 2015, Yu et al. 2015, Russo 2016, Murphy et al. 2018, Zdravković et al. 2020). One of the advantages of numerical models is their flexibility in implementing constitutive models and boundary conditions. The numerical modelling approach can provide rigorous predictions considering the nonlinear behavior of the soil and the pile-soil interface. Both stresses and deformation can be obtained easily through numerical models. However, substantial computational power is needed. Also, the accuracy of the results depends on the adopted constitutive soil models and the calibration of these models (Brødbæk et al. 2009).

Brown and Shie (1991) performed a series of 3D FE models of laterally loaded piles. The pile was modelled using linear elastic solid elements, while the soil was modelled as a simple elastic-plastic material obeying the Von Mises criterion. Parametric studies were conducted numerically to investigate the influence of pile head fixity, pile-soil interface friction and sloping ground on the *p*-*y* curves derived from the model. Ahmadi and Ahmari (2009) established 3D FE models to study the behavior of laterally loaded piles in clay. The measurements from two case studies, one performed in Lake Austin and reported by Matlock (1970) and the other in stiff clay and reported by Reese and Welch (1975), were compared with the numerical predictions. Moreover, the results from a sensitivity analysis showed that the optimum dimension of the soil domain is 40 times the pile diameter. Kim and Jeong (2011) presented a nonlinear 3D FE modelling technique to obtain the lateral load-transfer curve using PLAXIS 3D Foundation. The simulation technique was validated by the measurements from full-scale field lateral load tests performed in marine clay in Korea. Khodair and Abdel-Mohti (2014) have investigated the response of single piles under axial and lateral loads using a FD software LPILE and two FE software ABAQUS and SAP2000. The results showed that the bending moment obtained from ABAQUS is slightly higher than that from LPILE. This is because ABAQUS considers soil continuum, while LPILE is based on the discrete features of the soil. In both LPILE and SAP2000, the soil is represented as a series of nonlinear springs. It was found that the bending moment and lateral displacement in SPA2000 using more springs shows better agreement with that in LPILE. Murphy et al. (2018) proposed a 3D FEM approach for modelling the behavior of laterally loaded monopiles. The hardening soil (HS) model was adopted to simulate the behavior of the soil stiffness. Cone Penetration Test (CPT) data was used to calibrate the HS parameters in the numerical model. Their approach provides useful information for optimizing the design of monotonic piles.

2.4.2 Laterally loaded piles in unsaturated soils

There is limited research that has been devoted to studying the response of laterally loaded piles in unsaturated soils from experimental and numerical studies (Helmers 1997, Mokwa et al. 2000, Choi et al. 2013, Stacul et al. 2017, Mahmood et al. 2018, Lalicata et al. 2019).

A series of field tests on laterally loaded piles were performed by Helmers (1997) at five sites in Virginia, where the foundations soils are unsaturated silts and clays. They recommended multiplying the theoretical values for soil resistance by a modification factor, *M*, with a value of 0.85 to improve the reliability of Hansen's (1961) theory. Mokwa et al. (2000) proposed an approach for estimating the load versus settlement curves for unsaturated soils based on the results from Helmers' (1997) field tests. An average value of the stress-strain coefficient *A* times ε_{50} of 0.014 was suggested for the *p*-*y* formulation by Evans and Duncan (1982), which was back-calculated using the load-deflection curves from field measurements.

Choi et al. (2013) have conducted four field tests on single piles subjected to lateral loading in weathered granite soil. The existing analysis methods including theoretical methods (i.e., Hansen's (1961), Broms' (1964b), Poulos' (1971a) methods) and numerical methods using software LPILE, FAD and ABAQUS were applied to the results to compare with the field measurements. It was found that the results using ABAQUS give the most accurate predictions among all the methods. Analyses using LPILE and FAD underpredict the lateral load capacity of the pile in weathered granite soil. Also, Broms' (1964b) and Poulos' (1971a) methods tend to provide conservative lateral load capacity.

Stacul et al. (2017) developed a hybrid BEM *p-y* curve approach for single piles considering the nonlinear behavior of soil. The Modified-Kovacs model was used to simulate the effect of matric suction by increasing the stress state and the stiffness of shallow soil layers. Lalicata et al. (2019) conducted a series of centrifuge tests of laterally loaded piles embedded in saturated and unsaturated silty soils. Two different GWTs, one at the ground surface, and the other one at 7 m deep were set up to investigate the influence of the degree of saturation on the lateral response of piles. They reported a significant increase in soil stiffness and ultimate lateral resistance in unsaturated soils. The effect of the degree of saturation is stronger on looser soil due to an increase in capillary forces in the soil structure.

2.5 Summary

There is a strong relationship between the shear strength and bearing capacity of saturated soils. Several pioneers who contributed to geotechnical engineering have exploited this relationship and developed approaches for determining the bearing capacity of pile foundations. Unsaturated soils, due to the presence of air-water interphase, have more complex hydraulic and mechanical properties than saturated soils. Due to this reason, many researchers have focused on developing simple approaches extending the conventional saturated soil mechanics principles considering the contribution of matric suction. In this chapter, a comprehensive review of the literature about the shear strength of unsaturated soils (*SSUS*) and the variation of *SSUS* using SWCC and saturated shear strength parameters is first presented.

The theoretical background for interpreting the bearing capacity of a single pile under vertical loads in saturated soils is then reviewed. Some empirical methods and theoretical formulations for estimating the shaft carrying capacity and end-bearing capacity of single piles are presented. In recent years, more and more studies have been focused on the load-displacement behavior of single piles and pile groups in unsaturated soils. The studies on axially loaded piles in unsaturated soils that focus on the influence of matric suction are summarized based on experimental studies, theoretical approaches, and numerical simulations. More studies on different unsaturated soils that include large-scale field tests are necessary to better understand the strengths and limitations of the proposed modified approaches for use in the design of foundations in unsaturated soils.

The behavior of laterally loaded piles in saturated soils has been well-studied by several researchers. Four categories of methods (i.e., subgrade reaction method, ultimate limit state method, continuum method and numerical method) for analyzing the behavior of laterally loaded piles in saturated soils are reviewed and discussed. These methods primarily focus on the behavior of laterally loaded piles in saturated cohesive ($c_u \neq 0$, $\phi_u = 0$) and cohesionless soils ($c' = 0$, $\phi' \neq 0$). Then, both experimental and numerical studies on the response of laterally loaded piles in unsaturated soils are summarized. Currently, the understanding of laterally loaded piles in unsaturated soils is still limited for geotechnical engineers to reliably use them in geotechnical engineering practice. Due to this reason, there is a need for developing simple models for the rational design of the laterally loaded piles in unsaturated soils considering the influence of matric suction. Such models are likely to be well received for use in conventional engineering practice applications. For this reason, the focus of the research in this thesis has been undertaken in this direction.

CHAPTER 3

PREDICTION OF THE NONLINEAR BEHAVIOR OF LATERALLY LOADED PILES IN UNSATURATED SOILS

3.1 Introduction [2]

Pile foundations are widely used substructures to carry axial and lateral loads from the superstructure safely to the soil adjacent to the pile and or/ below significantly limiting the settlements. The design of pile foundations for supporting high-rise buildings, long-span bridges, transmission lines, and offshore structures is governed in many scenarios by lateral loads (e.g., Matlock and Reese, 1962; Broms, 1965). The natural groundwater table (GWT) is often at a greater depth below the natural ground surface due to the influence of environmental factors such as the rainfall infiltration, evaporation, and plant transpiration, particularly in semi-arid and arid regions. However, the current practice for design of pile foundations is typically based on principles of saturated soil mechanics. Both the ultimate bearing capacity of pile foundations and their settlement behavior may not be reliably estimated extending saturated soil mechanics for soils that are in a state of unsaturated condition because of ignoring the contribution arising from matric suction. Some researchers have investigated the behavior of piles placed in unsaturated soils under vertical loading based on model tests and numerical simulations (e.g., Mohamedzein et al., 1999; Georgiadis et al., 2003; Vanapalli and Taylan, 2012; Liu and Vanapalli, 2019).

Significant research has been published in the literature for analyzing the behavior of laterally loaded piles, which can be classified into three categories; (i) subgrade reaction method (Matlock, 1970; Reese et al., 1974; Reese, 1997; Rollins et al., 2005; Suleiman et al., 2014), (ii) continuum method (Douglas and Davis, 1964; Poulos, 1971; Randolph, 1981; Guo and Lee, 2001; Colasanti and Horvath, 2010), and (iii) numerical methods such as the

[2] The contents presented in this chapter are published as a journal article: **Cheng, X**., & Vanapalli, S. K. (2021). Prediction of the nonlinear behavior of laterally loaded piles in unsaturated soils. *Computers and Geotechnics*, 140, 104480.

finite element methods (FEM) and boundary element methods (BEM) (Brown and Shie, 1991; Yang and Liang, 2006; Kampitsis et al., 2015; Russo, 2016). However, these methods primarily focus on the behavior of laterally loaded piles in saturated cohesive ($c_u \neq 0$, $\phi_u = 0$) and cohesionless soils ($c' = 0$, $\phi' \neq 0$). Limited research has been undertaken to investigate the lateral response of piles in unsaturated soils. For example, Mokwa et al. (2000) proposed an approach for estimating the load versus settlement curves for unsaturated soils based on the results of five full-scale load tests. They recommended multiplying the theoretical values for soil resistance by a modification factor, M, with a value of 0.85 to improve the reliability of Hansen's (1961) theory. Stacul et al. (2017) developed a hybrid BEM p-y curve approach for single piles to simulate the effect of matric suction by increasing the stress state and the stiffness of shallow soil-layers using the Modified-Kovacs model. Lalicata et al. (2019) conducted a series of centrifuge tests to investigate the influence of degree of saturation on the behavior of laterally loaded piles. They reported a significant increase of soil stiffness and ultimate lateral resistance in unsaturated soils. Currently, there is limited understanding of laterally loaded piles in unsaturated soils for reliably extending it to conventional engineering practice applications using simple approaches.

The main objective of the study presented in this Chapter is to propose both an analytical method and a numerical technique for predicting the lateral response of single piles embedded in unsaturated soils that are subjected to lateral loads. First, a nonlinear analytical method is proposed to predict the load versus displacement curve of laterally loaded rigid piles in unsaturated soils. Considering the variation of lateral soil resistance along the pile length under three different but distinct states (i.e., pre-tip yield state, post-tip yield state and ultimate limiting state), the lateral load corresponding to lateral displacement at ground surface is derived based on force and moment equilibrium equations. The details of determining the parameters required in the equations are also described. The published data from seven field studies are used in the validation of the proposed method. Secondly, 3D finite element analysis (FEA) is performed to simulate the behavior of laterally loaded piles in unsaturated soils with the aid of ABAQUS software. The conventional Mohr-Coulomb approach used in ABAQUS does not have the capability for taking account of the nonlinear shear strength and modulus of elasticity of unsaturated soils. However, ABAQUS, has valuable tools such as the user-subroutines that can be incorporated using constitutive relationships to solve complex nonlinear problems. Exploiting this feature, a numerical technique based on a user-defined subroutine (USDFLD: user subroutine to redefine field variables at a material point) is developed exclusively to incorporate the nonlinear behavior of shear strength and modulus of elasticity with respect to matric suction to predict the load versus displacement curves. This approach is validated using two laboratory tests published from the literature: one in unsaturated silty soil and the other in unsaturated sandy soil. Lastly, the results between the proposed analytical method and the FEA are also compared and discussed for an example problem of a single pile with varying GWTs. Good agreements are found between the predictions using the proposed analytical method and the numerical technique. The studies presented in this Chapter are useful for the practicing geotechnical engineers to rationally design the laterally loaded piles in unsaturated soils taking account the influence of matric suction.

3.2 Background

3.2.1 Ultimate lateral resistance in pure cohesive and cohesionless soil

The behavior of a laterally loaded pile is commonly analyzed extending the subgrade reaction, which is also referred to as the Winkler spring method. The pile is simplified as an elastic beam while the surrounding soil is represented by a series of nonlinear springs placed along the length of the pile (Winkler, 1867; Biot, 1937). The nonlinear behavior of the soil is commonly represented by load-displacement characteristics, which is also known as *p-y* curve. The nonlinear *p-y* curve and the decay of the modulus of horizontal subgrade reaction has been introduced in Chapter 2. The analysis of laterally loaded pile placed in cohesive soils ($c_u \neq 0$, $\phi_u = 0$) is typically based on a total stress approach under undrained loading conditions. The p_u in cohesive soils is estimated using the equation below:

$$p_{\mathrm{u}} = N_{\mathrm{p}} c_{\mathrm{u}} d \tag{3.1}$$

where c_u is the undrained shear strength of the soil, d is the pile diameter, and N_p is lateral bearing capacity factor. N_p value was suggested equal to a value of 9, according to Broms (1964a) and API RP 2A (1987).

Broms (1964b) studies suggest that the limiting force on the pile is proportional to the transversal dimension of the pile in cohesionless soil ($c' = 0$, $\phi' \neq 0$). The general form for p_u in cohesionless soils is:

$$p_u = K_q \gamma z d \tag{3.2}$$

where K_q is the lateral earth pressure coefficient for cohesionless soil, z is the depth and γ is unit weight of the soil. More details of K_q used in this study are discussed in the later sections.

Guo et al. (2008) reported that the distribution of soil resistance typically has three distinct states for a rigid pile under increasing lateral load in cohesionless soils: (i) Prior to tip-yield state (tip-yield state refers to the lateral force per unit length at the pile tip just before reaching the limiting state); (ii) Post-tip yield state (lateral load and rotation angle continue increasing after yielding occurs at the pile tip in this state); (iii) Yield at rotation point state (with infinite increase in lateral load, the response of the whole pile achieves limiting state). The distribution of lateral soil resistance on the pile, which is depicted using solid lines, is mobilized along the p_u profile shown by two dashed lines (see Figure 3.1). In this study, along similar lines, three states were assumed for the lateral response of rigid piles in unsaturated soils.

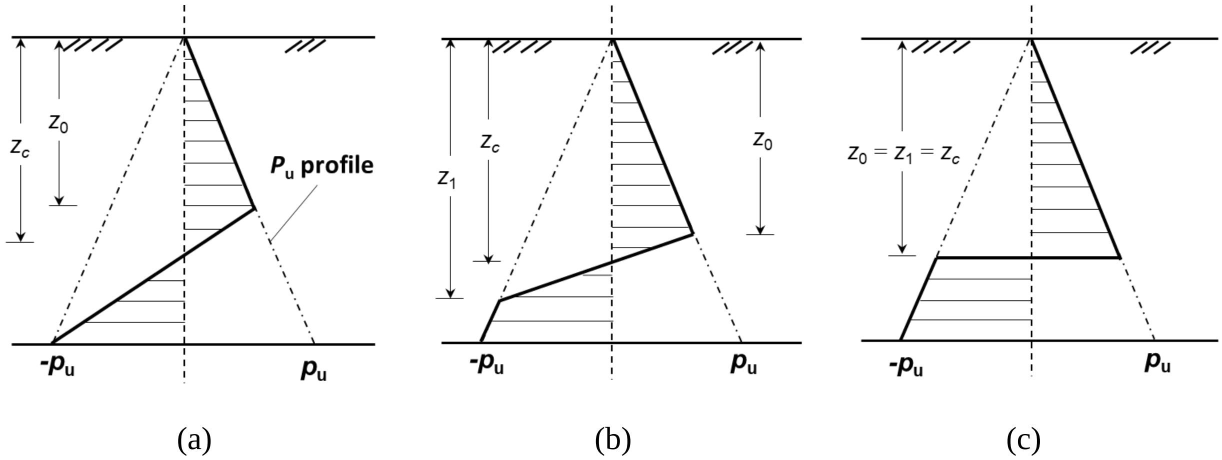

Figure 3.1 Profile of lateral soil resistance for (a) Tip-yield state (b) Post-tip yield state (c) Yield at rotation point state (modified after Guo et al. 2008)

3.2.2 The nonlinear shear strength behavior of unsaturated soil

An unsaturated soil is a multiphase continuum system comprised of soil particles, water, and air. The presence of an air-water interface generates surface tension within the soil skeleton that is strongly related to the matric suction that contributes to improving the mechanical behavior of unsaturated soils. Figure 3.2 shows a short rigid pile embedded in an unsaturated soil that is subjected to the influence of a lateral load. The soil above the GWT has negative pore water pressures, whose distribution varies due to the influence of environment factors. The relationship between the mass of water in the soil and the soil suction is defined as Soil-Water Characteristic Curve (SWCC). The terms, soil-water retention curve and soil moisture curve are also used in the literature for defining this relationship. The SWCC can be divided into three distinct zones of saturation (i.e., boundary effect zone, transition zone and residual zone) which are influenced by different ranges of soil suction values (Vanapalli et al., 1996). In the boundary effect zone, the soil is typically in a state of saturated condition. The soil behavior in this zone can be interpreted based on saturated soil mechanics. The shear strength contribution due to matric suction (ϕ^b) in this zone is equal to the angle of internal friction (ϕ'). When air enters the largest pores of the soil, the soil suction is referred to as the air-entry value (AEV). The soil desaturates rapidly with a further increase in matric suction beyond the AEV. ϕ^b is less than

ϕ' in the transition zone. In the residual zone, there are relatively small changes in the degree of saturation despite greater increase in the matric suction value. The shear strength may increase, decrease, or remain constant depending on the soil types and the amount of drainage in soil pores (Vanapalli, 2009). Similar conceptual behavior can also be extended for explaining the modulus of elasticity of unsaturated soils.

The determination of unsaturated soil properties from experimental studies can be costly and time-consuming. Therefore, many researchers have proposed semi-empirical methods for predicting the nonlinear shear strength of unsaturated soils using the information of SWCC and saturated shear strength parameters (for example, Vanapalli et al., 1996; Lee et al., 2003; Tekinsoy et al., 2004; Guan et al., 2010).

Vanapalli et al. (1996) provided the following semi-empirical models for predicting the variation of shear strength of unsaturated soil considering the influence of matric suction:

$$\tau_{unsat} = c' + (\sigma_{\mathrm{n}} - u_{\mathrm{a}})\tan\phi' + (u_{\mathrm{a}} - u_{\mathrm{w}})\left[\frac{(\theta - \theta_{\mathrm{r}})}{(\theta_{\mathrm{s}} - \theta_{\mathrm{r}})}\tan\phi'\right] \tag{3.3}$$

$$\tau_{unsat} = c' + (\sigma_{\mathrm{n}} - u_{\mathrm{a}})\tan\phi' + (u_{\mathrm{a}} - u_{\mathrm{w}})S^{\kappa}\tan\phi' \tag{3.4}$$

where c' and ϕ' are the effective shear strength parameters, $(\sigma_{\mathrm{n}} - u_{\mathrm{a}})$ is net normal stress, $(u_{\mathrm{a}} - u_{\mathrm{w}})$ is matric suction, θ is volumetric water content, θ_s, θ_r is saturated and residual volumetric water content respectively, S is the degree of saturation and κ is a fitting parameter that related to the plasticity index, I_{P} (Garven and Vanapalli, 2006). Equations 3.3 and 3.4 can provide reasonable predictions of the shear strength in the boundary effect zone and transition zone. However, some recent studies showed that the shear strength might be overestimated at high suctions, especially for clayey soils since these equations do not account for contributions arising from capillary water and absorptive water (Sheng et al., 2011, Zhou et al., 2016). Experimental studies performed by several researchers suggested that the slope of shear strength and net normal stress relationship are approximately the same, which means that the internal friction angle ϕ' is not influenced by matric suction (Ho and Fredlund, 1982; Fredlund and Rahardjo, 1993; Vanapalli et al., 1996). Due to this reason, the contribution of matric suction towards shear strength can be incorporated as apparent cohesion (c_a) using Equations 3.3 and 3.4 respectively (e.g., Oh and Vanapalli, 2011):

$$c_{\mathrm{a}} = c' + \left(u_{\mathrm{a}} - u_{\mathrm{w}}\right)\left[\frac{\left(\theta - \theta_{\mathrm{r}}\right)}{\left(\theta_{\mathrm{s}} - \theta_{\mathrm{r}}\right)}\tan\phi'\right] \tag{3.5a}$$

$$c_{\mathrm{a}} = c' + \left(u_{\mathrm{a}} - u_{\mathrm{w}}\right)S^{\kappa}\tan\phi' \tag{3.5b}$$

Equations 3.5a and 3.5b were employed in this study to derive necessary equations.

As shown in Figure 3.2, z_c is the depth of the center of rotation. For rigid pile, the lateral displacement of pile y at the depth z has a linear relationship with the displacement at the ground surface y_0 given by:

$$y = \frac{z_{\mathrm{c}} - z}{z_{\mathrm{c}}}\,y_0 \tag{3.6}$$

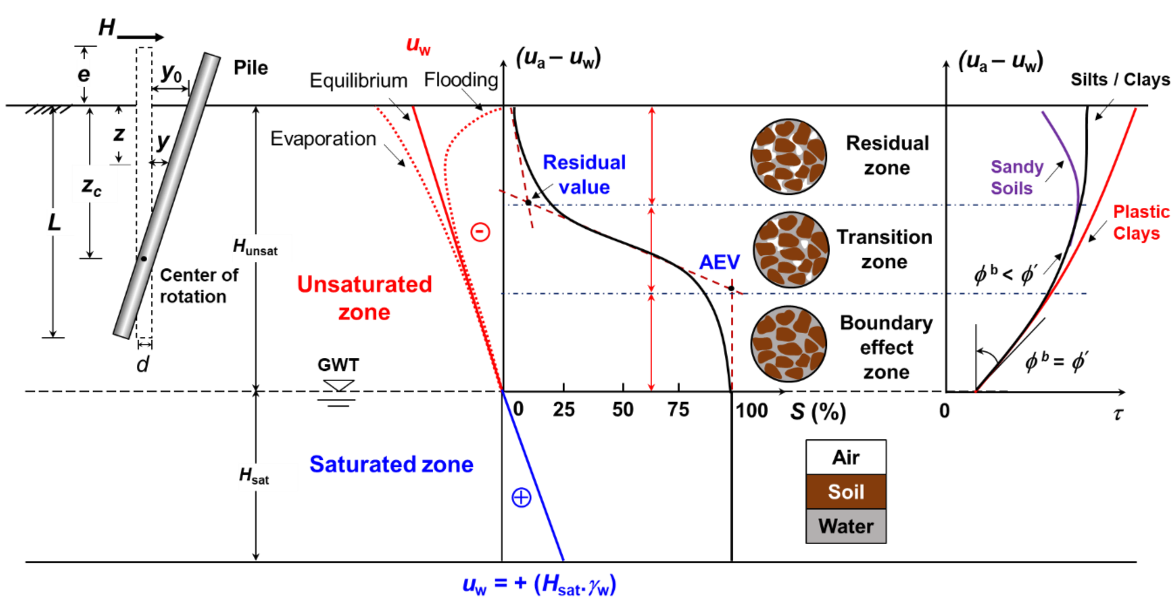

Figure 3.2 A laterally loaded rigid pile in a typical unsaturated soil

3.3 Proposed method for ultimate lateral resistance in unsaturated soils

In this study, an analytical method is proposed to estimate the ultimate lateral resistance for a short rigid pile that is homogeneous and isotropic in an unsaturated soil. The characteristic length of the soil–pile system, T, is defined as:

$$T = \sqrt[5]{\frac{E_{\mathrm{p}} I_{\mathrm{p}}}{n_{\mathrm{h}}}} \tag{3.7}$$

where E_{p} is modulus of elasticity of pile, I_{p} is moment of inertia of the pile section. $E_{\mathrm{p}}I_{\mathrm{p}}$ is the flexural stiffness of pile. n_{h} has been defined in Equation 2.31. The pile is considered long if its length $\geq 4T$. However, if pile length $\leq 2T$, it can be considered a short rigid pile (Davisson and Robinson, 1965; Tomlinson and Woodward, 2007; IS 2911, 2010).

In many scenarios, the entire rigid pile is embedded in unsaturated soils. The ultimate soil resistance p_{u} of a pile embedded in unsaturated soils arises from cohesion and friction components of shear strength that are influenced by matric suction and are respectively, p_{uc} and p_{uq}.

$$p_{\mathrm{u}} = p_{\mathrm{uc}} + p_{\mathrm{uq}} \tag{3.8}$$

p_{uq} can be expressed as Equation 3.2. p_{uc} under drained loading conditions can be written in a similar form that is consistent with undrained conditions (i.e., Equation 3.1):

$$p_{\mathrm{uc}} = K_c c_{\mathrm{a}} d \tag{3.9}$$

where K_c is the lateral earth pressure coefficient for cohesion component, c_a is the average apparent cohesion of unsaturated soil that has been defined in Equations 3.5a and 3.5b considering the influence of matric suction.

As discussed earlier, prior to the lateral soil resistance p reaches p_{u}, p is proportional to the lateral deflection y at any depth. The lateral soil resistance in unsaturated soils is defined as:

$$p = k_{\mathrm{h}} y = \left(k_{\mathrm{hc}} + k_{\mathrm{hq}}\right) y \tag{3.10}$$

where k_{hc} and k_{hq} are the modulus of horizontal subgrade reaction for cohesion component and friction component, respectively.

The distribution of lateral soil resistance along the pile varies in pre-tip yield state, post-tip yield state and ultimate limiting state. The details of predicting the load-displacement behavior of piles for three different states are described in the following sections.

3.3.1 Pre-tip yield state

Assume a single rigid pile with an embedded length L is subjected to a lateral load H with eccentricity e. The rotation point is at the depth of z_c and the lateral displacement is zero at the rotation point. The lateral displacement at the ground surface y_0 increases as H increases. Figure 3.3(a) and (b) show the profile of soil resistance along the pile for the cohesion and friction components, respectively. In this state, H and y_0 are relatively low. The lateral soil resistance on the upper part of the pile from the ground surface to a depth of z_0 starts to achieve the ultimate state as the pile rotates. At depth from 0 to z_0, p follows the p_u profile. In Figure 3.3(c), p_u at any depth of z are the sum of these two components, which can be written as:

$$p_{0\sim z_0} = p_{\mathrm{u}} = \left(K_{\mathrm{c}} c_{\mathrm{a}} + K_{\mathrm{q}} \gamma z\right) d \qquad \left(0 \le z \le z_0\right) \tag{3.11}$$

where $p_{0\sim z0}$ is lateral soil resistance at the depth from 0 to z_0.

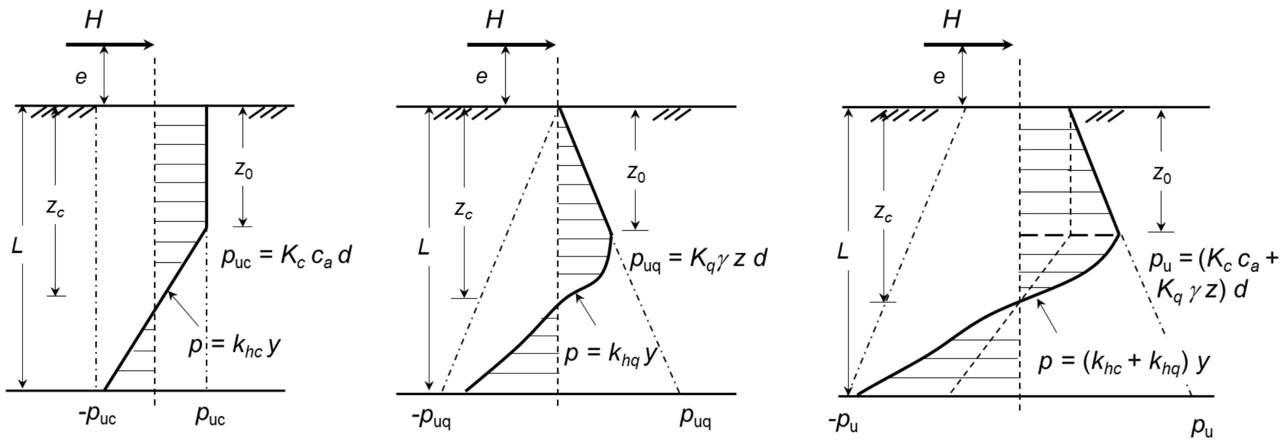

(a) (b) (c)

Figure 3.3 Profile of lateral soil resistance in pre-tip yield state for (a) cohesion component (b) friction component (c) unsaturated soils

There is no soil yielding in the remainder part of the pile from depth of z_0 to L (i.e., prior to the pile tip reaching its limiting state). From Figure 3.3(b), k_{hq} is proportional to the depth z and y is a linear function of z; thus, the distribution of p on the remainder part of the pile is a nonlinear curve. The lateral resistance of unsaturated soils from depth of z_0 to L can be expressed by combining Equations 2.31 and 3.10:

$$p_{0\sim z_0} = p_{\mathrm{u}} = \left(K_{\mathrm{c}} c_{\mathrm{a}} + K_{\mathrm{q}} \gamma z\right) d \qquad \left(z_0 \le z \le L\right) \tag{3.12}$$

Therefore, force and moment limit equilibrium equations can be given by:

$$\begin{cases} H - \int_{z_0}^{0} p_{\mathrm{u}} dz - \int_{z0}^{L} p dz = 0 \\ He + \int_{z_0}^{0} p_{\mathrm{u}} z dz + \int_{z0}^{L} p z dz = 0 \end{cases} \tag{3.13}$$

Substituting Equations 3.6, 3.10,3.11 and 3.12 into Equation 3.13, we have:

$$H - \left(K_{\mathrm{c}} c_{\mathrm{a}} z_0 + \frac{1}{2} K_{\mathrm{q}} \gamma z_0^{\,2}\right) d + \frac{y_0}{z_{\mathrm{c}}} \left[k_{\mathrm{hc}} z_{\mathrm{c}} \left(z_0 - L\right) + \frac{1}{2} \left(n_{\mathrm{h}} z_{\mathrm{c}} - k_{\mathrm{hc}}\right) \left(z_0^{\,2} - L^2\right) - \frac{1}{3} n_{\mathrm{h}} \left(z_0^{\,3} - L^3\right) \right] = 0 \tag{3.14}$$

$$He + \left(\frac{1}{2}K_c c_a z_0^{\ 2} + \frac{1}{3}K_q \gamma z_0^{\ 3}\right)d - \frac{y_0}{z_c}\left[\frac{1}{2}k_{hc} z_c \left(z_0^{\ 2} - L^2\right) + \frac{1}{3}\left(n_h z_c - k_{hc}\right)\left(z_0^{\ 3} - L^3\right) - \frac{1}{4}n_h \left(z_0^{\ 4} - L^4\right)\right] = 0 \quad (3.15)$$

At depth $z = z_0$, we have $p_u = p$. Thus, the relationship between z_0 and z_c can be obtained by:

$$(K_c c_a + K_q \gamma z_0)d = \left(k_{hc} + n_h z_0\right)\frac{z_c - z_0}{z_c} y_0 \quad (3.16)$$

If the value of y_0 is determined, three unknown variables z_0, z_c and H can be solved by combining Equations 3.14 – 3.16. In other words, using these equations, the relationship between lateral load H and displacement y_0 can be plotted.

When the lateral soil resistance at the pile tip reaches the ultimate value p_u, yielding occurs at the pile tip. Therefore, if p at the pile tip does not exceed p_u, y_0 satisfies the following equation which is obtained by substituting $z = L$ into Equations 3.11 and 3.12:

$$-\left(k_{hc} + n_h L\right)\frac{z_c - L}{z_c} y_0 \le (K_c c_a + K_q \gamma L)d \quad (3.17)$$

The equations for pre-tip yield state are suitable for this situation. After the pile tip yields, the distribution of soil resistance will transfer to post-tip yield state.

3.3.2 Post-tip yield state

As the lateral load H and lateral displacement y_0 continue to increase after the pile tip yields, the limiting soil pressure is mobilized not only on the upper part of the pile (from the depth of 0 to z_0) but also on the lower part from the pile tip up to the depth of z_1. Figure 3.4(a) and (b) show the profile of lateral soil resistance for cohesion and friction component, respectively. Then, p at any depth of z from 0 to z_0 for unsaturated soils, as shown in Figure 3.4(c), can be written as:

$$p_{0\sim z_0} = p_{\mathrm{u}} = \left(K_{\mathrm{c}}c_{\mathrm{a}} + K_{\mathrm{q}}\gamma z\right)d \qquad \left(0 \le z \le z_0\right) \tag{3.18}$$

At depth of z from z_1 to L, the lateral soil resistance is the negative value of p_u:

$$p_{z_1\sim L} = -p_{\mathrm{u}} = -\left(K_{\mathrm{c}}c_{\mathrm{a}} + K_{\mathrm{q}}\gamma z\right)d \qquad \left(z_1 \le z \le L\right) \tag{3.19}$$

Since there is no yielding in the soil from depth of z_0 to z_1, p in this zone is:

$$p_{z_0\sim z_1} = \left(k_{\mathrm{hc}} + n_{\mathrm{h}}z\right)y \qquad \left(z_0 \le z \le z_1\right) \tag{3.20}$$

Therefore, force and moment limit equilibrium equations can be expressed as:

$$\begin{aligned} &H - \left\{K_{\mathrm{c}}c_{\mathrm{a}}\left(L - z_0 - z_1\right) + \frac{1}{2}K_{\mathrm{q}}\gamma\left(L^2 - z_0{}^2 - z_1{}^2\right)\right\}d \\ &+ \frac{y_0}{z_{\mathrm{c}}}\left[k_{\mathrm{hc}}z_{\mathrm{c}}\left(z_0 - z_1\right) + \frac{1}{2}\left(n_{\mathrm{h}}z_{\mathrm{c}} - k_{\mathrm{hc}}\right)\left(z_0{}^2 - z_1{}^2\right) - \frac{1}{3}n_{\mathrm{h}}\left(z_0{}^3 - z_1{}^3\right)\right] = 0 \end{aligned} \tag{3.21}$$

$$\begin{aligned} &He + \left\{\frac{1}{2}K_{\mathrm{c}}c_{\mathrm{a}}\left(z_0{}^2 + z_1{}^2 - L^2\right) + \frac{1}{3}K_{\mathrm{q}}\gamma\left(z_0{}^3 + z_1{}^3 - L^3\right)\right\}d \\ &- \frac{y_0}{z_{\mathrm{c}}}\left[\frac{1}{2}k_{\mathrm{hc}}z_{\mathrm{c}}\left(z_0{}^2 - z_1{}^2\right) + \frac{1}{3}\left(n_{\mathrm{h}}z_{\mathrm{c}} - k_{\mathrm{hc}}\right)\left(z_0{}^3 - z_1{}^3\right) - \frac{1}{4}n_{\mathrm{h}}\left(z_0{}^4 - z_1{}^4\right)\right] = 0 \end{aligned} \tag{3.22}$$

As shown in Figure 3.4, at $z = z_0$, we have $p_{\mathrm{u}} = p$. The relationship between z_0 and z_{c} can be given by:

$$(k_{\mathrm{c}}c_{\mathrm{a}} + k_{\mathrm{q}}\gamma z_0)d = \left(k_{\mathrm{hc}} + n_{\mathrm{h}}z_0\right)\frac{y_0\left(z_{\mathrm{c}} - z_0\right)}{z_{\mathrm{c}}} \tag{3.23}$$

At $z = z_1$, p is equal to $-p_{\mathrm{u}}$. The relationship between z_1 and z_{c} can be written as:

$$\left(k_{\mathrm{hc}} + n_{\mathrm{h}}L\right)\frac{y_0\left(z_{\mathrm{c}} - z_1\right)}{z_{\mathrm{c}}} = -(k_{\mathrm{c}}c_{\mathrm{a}} + k_{\mathrm{q}}\gamma z_1)d \tag{3.24}$$

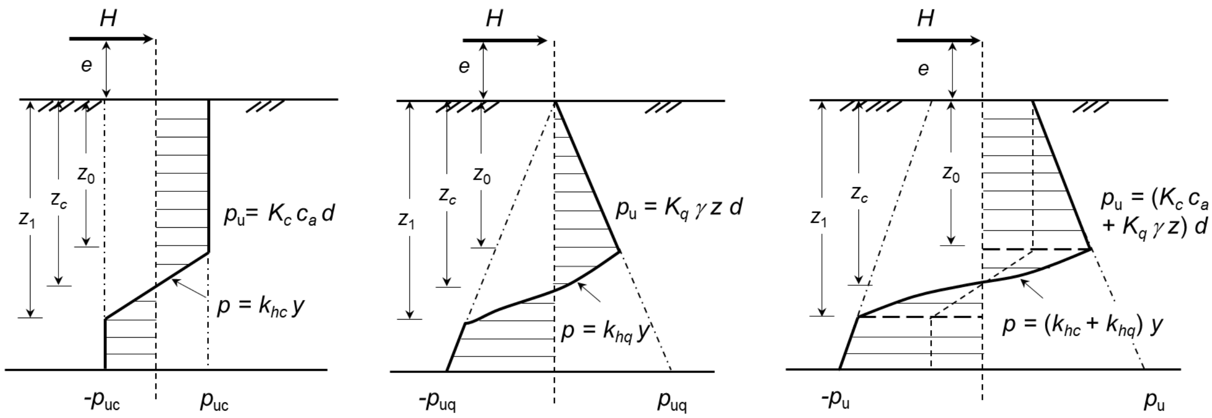

(a) (b) (c)

Figure 3.4 Profile of lateral soil resistance in post-tip yield state for (a) cohesion component (b) friction component (c) unsaturated soils

If the value of y_0 is determined, four unknown variables z_0, z_1, z_c and H can be solved with the aid of Equation 3.21 thru 3.24. In addition, the lateral load versus displacement curve can also be obtained.

3.3.3 Ultimate limiting state

z_0 and z_1 tend to approach to the same value as z_c due to significantly large increases in the lateral displacement at the pile head. As shown in Figure 3.5, the limiting force will be fully mobilized on the entire pile in this state. However, this state is practically unreachable; yet it can provide a useful upper bound for lateral load and bending moment. Thus, from the depth of 0 to z_c, p equals to p_u and from the depth of z_c to L, p equal to - p_u. Therefore, force and moment limit equilibrium equations can be expressed as:

$$\begin{cases} H_{\lim} + K_c c_a d\left(L - 2z_c\right) + \dfrac{1}{2} K_q \gamma d\left(L^2 - 2z_c^{\ 2}\right) = 0 \\ H_{\lim} e + \dfrac{1}{2} K_c c_a d\left(2z_c^{\ 2} - L^2\right) + \dfrac{1}{3} K_q \gamma d\left(2z_c^{\ 3} - L^3\right) = 0 \end{cases} \tag{3.25}$$

The unknown variables z_c and limiting load $H_{\lim}$ can be obtained by solving Equation 3.25.

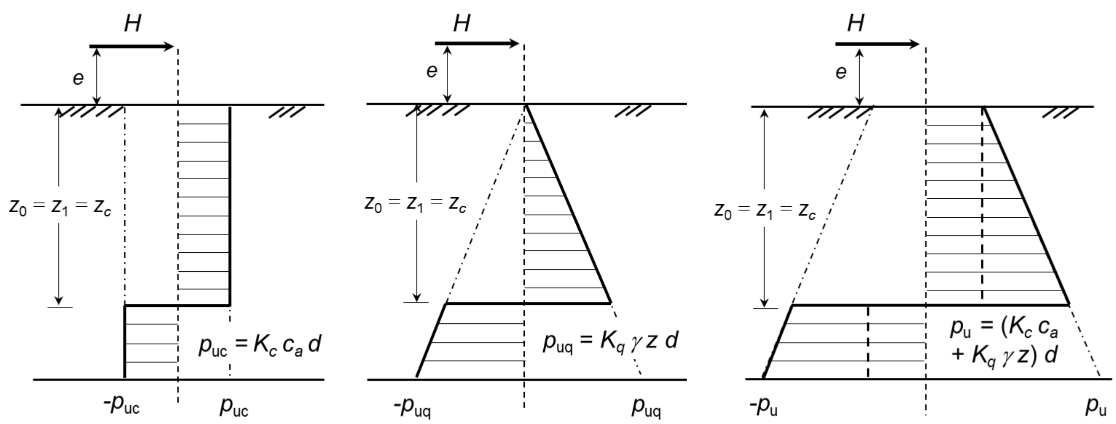

Figure 3.5 Profile of lateral soil resistance in ultimate limiting state for (a) cohesion component (b) friction component (c) unsaturated soils

Figure 3.6 shows a flow chart of the proposed analytical method. y_0 starts from a relatively small value and continues increasing following a loop until it reaches a specific upper limit of the displacement (y_s) as designated by users. A MATLAB program was developed to provide solutions for all the equations.

3.3.4 Determination of lateral earth pressure parameters

3.3.4.1 The lateral earth pressure coefficient for friction component K_q

Table 2.8 in Chapter 2 summarizes the published methods from the literature for predicting the p_u on laterally loaded piles in cohesionless soils. To determine the coefficient K_q for this study, a simple FE model was established to simulate an example case using ABAQUS. The ultimate soil resistance at given depths from the FE model are compared with the results calculated using the published equations listed in Table 2.8. It is assumed that a single pile with a length of 600 mm and a diameter of 60 mm is embedded in a saturated Unimin Sand under lateral loading. The internal friction angle of the soil, ϕ' is 35.3°. The saturated and dry unit weight is 20.4 kN/m^3 and 16.05 kN/m^3, respectively (Vanapalli et al., 2018). In the numerical model, the single pile was modelled as a linear-elastic material. The elastic modulus of pile is 20 GPa and the Poisson's ratio is 0.15 (Potts and Zdravković, 2001). The sand was modelled as an elastic perfectly plastic material extending Mohr–Coulomb constitutive model. The Poisson ratio of the soil is 0.334 and the void ratio is 0.55. The saturated elastic modulus of the sand is 2000 kPa (Al-Khazaali et al., 2016). The dilation angle was considered 10% of ϕ' according to DS 415 (1984). The pile-soil interface friction angle (δ) was assumed $2/3\phi'$ (Potyondy, 1961). Both Fan and Long (2005) and Kim and Jeong (2011) have reported that the lateral soil resistance can be obtained from the soil elements closest to the pile.

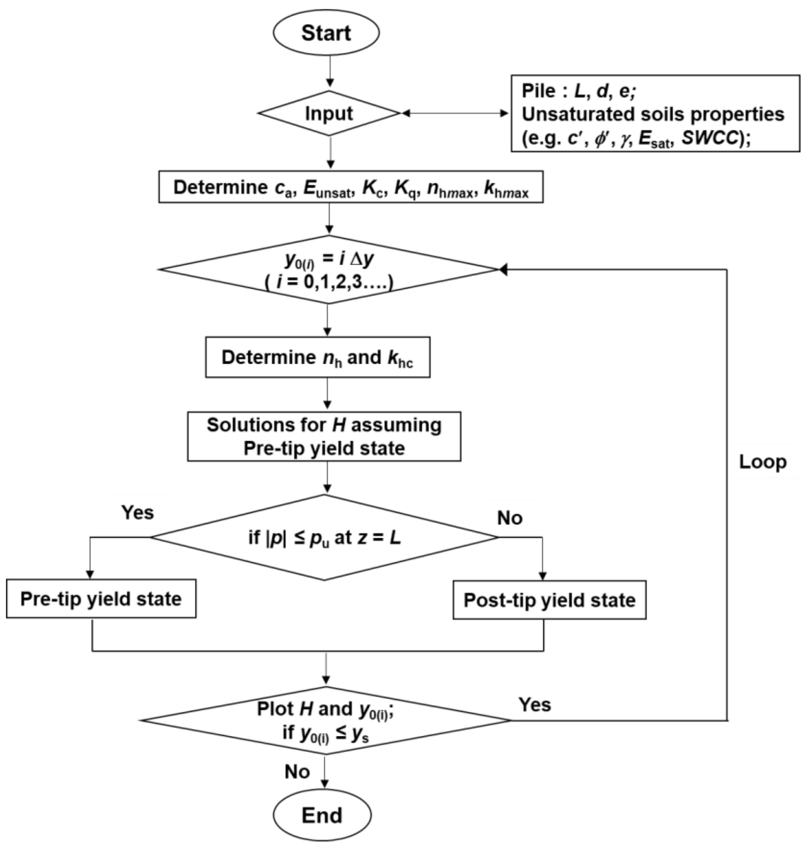

Figure 3.6 Flow chart of the proposed method

Figure 3.7 shows a pile-soil system with a lateral load applied in the *x*-direction and positions of Gauss points in a soil element. The stresses σ_{xx} and σ_{xy} at Gauss points in the soil elements closest to the pile, which are shown on the circumference with short dashes in Figure 3.7, were first selected from ABAQUS. The *x*-component stress at each Gauss point, T_x, was calculated by the component of stresses σ_{xx} and σ_{xy} in the *x* direction:

$$T_x = \sigma_{xx} n_x + \sigma_{xy} n_y \tag{3.26}$$

where n_x and n_y are components of unit normal along the x-, and y- directions, respectively. n_x and n_y are given by:

$$n_x = \cos\theta_x = \frac{x_g}{\sqrt{{x_g}^2 + {y_g}^2}}, n_y = \cos\theta_y = \frac{y_g}{\sqrt{{x_g}^2 + {y_g}^2}} \tag{3.27}$$

The total soil resistance, p_x, can be estimated by integrating the x-component stress over the circumference of the closest Gauss points in the soil elements surrounding the pile. Therefore, p_x can be obtained by:

$$p_x = \int T_x \mathrm{d}L \tag{3.28}$$

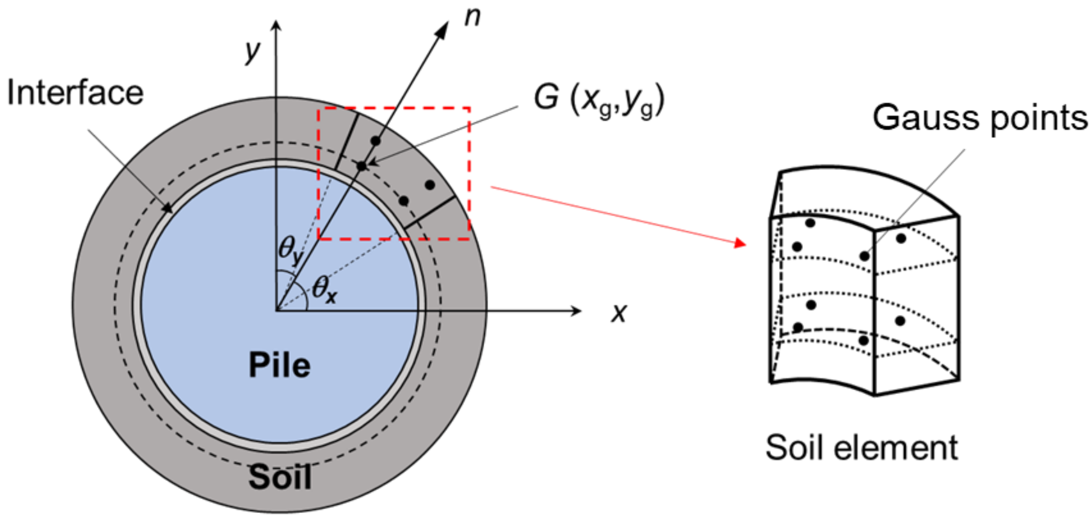

Figure 3.7 A pile-soil system with a lateral load applied in the *x*-direction and the positions of Gauss points

The ultimate soil resistance versus depth using the published methods and FEA is shown in Figure 3.8. The ultimate soil resistance increases linearly using Broms (1964b), Petrasovits and Awad (1972) and Fleming et al. (1992) methods. The ultimate soil resistance estimated using both Hansen (1961) and API (1987) methods is less than that using other methods near the ground surface and then become larger at a greater depth. The

FEA predictions are typically larger than the results using the above theoretical methods. This is because the ultimate soil resistance of laterally loaded piles increases with soil dilatancy that was considered in the FEA. However, theoretical methods ignore the volume change characteristics of sands when subjected to shearing. Figure 3.8 shows that FEA predictions are closer to Fleming et al. (1992) method. Due to its simplicity, the equation proposed by Fleming et al. (1992) has been used in this study to provide reasonable results for predicting p_u, that is:

$$K_q = K_p^{\,2} \tag{3.29}$$

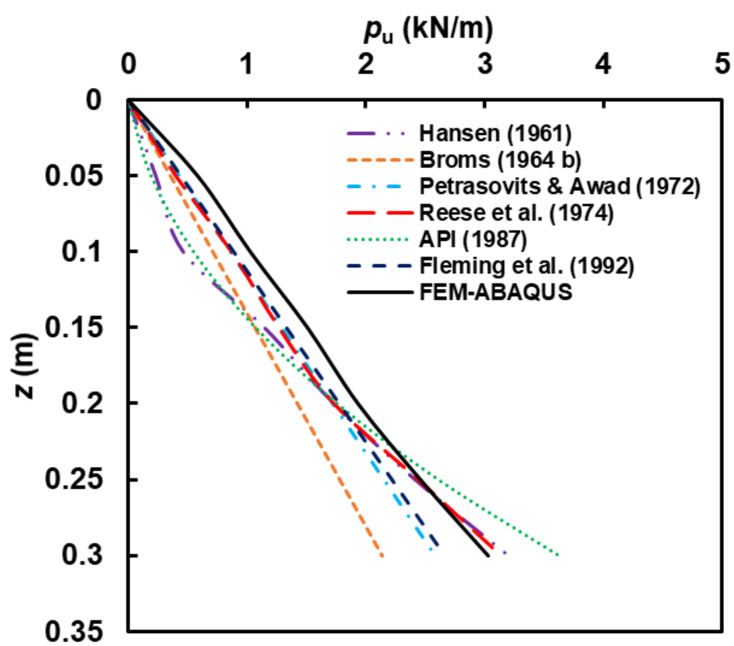

Figure 3.8 Comparisons of the ultimate soil resistance versus depth calculated using published methods and using FEA in ABAQUS

3.3.4.2 The lateral earth pressure coefficient for cohesion component K_c

Evans and Duncan (1982) proposed an equation for predicting the ultimate soil resistance for c-ϕ soils by introducing a dimensionless modifying factor C_p to account for 3D effect of the passive wedge in front of the pile. Cecconi et al. (2019) proposed a simple profile of ultimate soil resistance extending Broms (1964b) theory to soils possessing both cohesion and friction. They reported that the 3D effect factor can be applied to the shear strength. Extending this concept, for a plane-strain (2D) problem, the net limit pressure for a perfectly smooth pile embedded in pure cohesionless soil is the difference between the passive pressure in front of the pile (σ_{hp}) and the active pressure behind the pile (σ_{ha}):

$$p_{u(2D)} / d = \sigma_{hp} - \sigma_{ha} = \left(K_{\mathrm{p}} - K_{\mathrm{a}}\right)\gamma z \tag{3.30}$$

where K_{a} is the coefficient of active earth pressure. The p_{u} for cohesionless soil in this study is expressed as:

$$p_{u(3D)} / d = K_{\mathrm{p}}^{\ 2}\gamma z \tag{3.31}$$

Then, the 3D-effect factor α is the following ratio (i.e., $p_{\mathrm{u(3D)}} / p_{\mathrm{u(2D)}}$):

$$\alpha = \frac{K_{\mathrm{p}}^{\ 2}}{K_{\mathrm{p}} - K_{\mathrm{a}}} \tag{3.32}$$

For unsaturated soil ($c_{\mathrm{a}} \neq 0$, $\phi \neq 0$), a cohesion term can be added into Equation 3.30 (2D problem), which takes the form:

$$p_{u(2D)} / d = \sigma_{hp} - \sigma_{ha} = 2c\left(\sqrt{K_{\mathrm{p}}} + \sqrt{K_{\mathrm{a}}}\right) + \left(K_{\mathrm{p}} - K_{\mathrm{a}}\right)\gamma z \tag{3.33}$$

The same 3D-effect factor α can be applied to both cohesion and friction terms of shear strength in the 3D problem, to obtain the relationship:

$$p_{u(3D)} / d = \alpha 2c\left(\sqrt{K_{\mathrm{p}}} + \sqrt{K_{\mathrm{a}}}\right) + \alpha\left(K_{\mathrm{p}} - K_{\mathrm{a}}\right)\gamma z \tag{3.34}$$

Combining Equations 3.32 and 3.34, the lateral earth pressure coefficient for cohesion component K_c can be derived as:

$$K_c = \frac{2K_p^{\ 2}}{\sqrt{K_p} - \sqrt{K_a}} \tag{3.35}$$

3.3.4.3 The modulus of horizontal subgrade reaction n_h and k_{hc}

The modulus of horizontal subgrade reaction k_{hq} for sands is a nonlinear function of lateral deflection of piles that decreases with an increase in lateral deflection. Several researchers have studied the degradation of k_{hq} with shear strain γ around the pile for laterally loaded piles (Blaney and O'Neil, 1986; Prakash and Kumar, 1996; Miwindo, 1992). Prakash and Kumar (1996) proposed an equation to represent the relationship between k_{hq} and shear strain γ in sands. k_{hq} is proportional to the depth z ($k_{hq} = n_h z$), then the constant horizontal reaction subgrade n_h can be expressed as:

$$\frac{n_h}{n_{h\max}} = 0.052\gamma^{-0.48} \tag{3.36}$$

where n_{hmax} is maximum value of n_h at a strain of $\gamma \leq 0.002$. Mwindo (1992) reported that γ is related to the lateral displacement y_0 at the ground surface. The average shear strain around pile γ can be expressed as:

$$\gamma = \frac{1+\nu}{2.5B} y_0 \tag{3.37}$$

where B is the diameter of pile and ν is the Poisson's ratio. Reese and Van Impe (2000) recommended the variation of n_{hmax} for sands above and below GWT based on the relative density D_r (%), as summarized in Table 3.1. Table 3.1 also provides the relationship between the corrected SPT N-values, relative densities and friction angles of soils (Skempton, 1986).

The modulus of elasticity of unsaturated soil is significantly influenced by matric suction (Vanapalli and Mohamed, 2007). Oh et al. (2009) proposed a semi-empirical model for predicting the variation of elastic modulus of unsaturated soils (E_{unsat}) taking into account the influence of matric suction. Their method requires the information of SWCC along with two fitting parameters α and β for predicting E_{unsat}:

$$E_{\text{unsat}} = E_{\text{sat}} \left[1 + \alpha \frac{(u_{\text{a}} - u_{\text{w}})}{(P_a / 101.3)} (S^{\beta}) \right] \tag{3.38}$$

where E_{sat} is modulus of elasticity of soil under saturated conditions, and P_a is atmosphere pressure (101.3 kPa). The fitting parameter α is related to plasticity index for fine-grained soils. The value of α for coarse-grained soil ranges from 0.5 to 2.5 depending on the footing size. The fitting parameter β equal to 1 for coarse-grained soils and 2 for fine-grained soils.

Table 3.1 Recommended values of n_h for sandy soil

$N_{1(60)}$	D_r (%)	ϕ' (°)	Soil compactness	n_{hmax} (MN/m^3) (above the GWT)	n_{hmax} (MN/m^3) (below the GWT)
0-3	0-15	<29	Very loose	-	-
3-8	15-35	29-30	Loose	6.8	5.4
8-25	35-65	30-36	Medium	24.4	16.3
25-42	65-85	36-41	Dense	61	34
42-58	85-100	>41	Very dense	-	-

The water content near ground surface varies due to the influence of environmental factors such as the rainfall, evaporation, and evapotranspiration. The matric suction profile variations associated with these factors can be estimated by numerical techniques using constitutive relationships for unsaturated soils. There are commercial software packages such as SIGMA/W and VADOSE/W that can be used for simulating the physical processes of evaporation and infiltration in unsaturated soils and predicting the changes in suction profile in response to environmental variations. The input data typically includes initial soil conditions, climatic parameters (e.g., recorded rainfall data, GWT location and surface runoff data) and soil properties (e.g., SWCC, permeability functions and thermal conductivity functions). Adem and Vanapalli (2013) provide more details of such an approach.

The matric suction also can be measured directly in the field using instruments such as tensiometers in coarse-grained soils with low suctions or using thermal conductivity sensors or filter paper method in fine-grained soils. However, such approaches can be cumbersome and time consuming. For this reason, it is reasonable to assume negative pore water pressures of linear or nonlinear variation above the GWT based on supporting results from limited field studies. Since the pore-air pressure component of matric suction is generally atmospheric in the field, the matric suction, (u_a - u_w), is equal to negative porewater pressures.

Alternatively, the information of variation of degree of saturation and volumetric water content above the GWT can be obtained from simple tests collecting soil samples or using Time Domain Reflectometry (TDR), respectively. Since SWCC is defined as a relationship between volumetric water content or degree of saturation and matric suction, information of matric suction can be derived from the SWCC measured using an undisturbed soil sample collected from the field once measured degree of saturation or volumetric water content is gathered from the field.

Any of the above techniques can be used for gathering the suction profile and degree of saturation. Using the gathered information, the variation of elastic modulus of unsaturated soils (E_{unsat}) with respect to the depth can be predicted using Equation 3.38.

Many researchers have reported that some factors such as the pile flexural stiffness and diameter have an influence on the modulus of horizontal subgrade reaction k_{hc} (Glick, 1948; Yoshida and Yoshinaka, 1972; Zhang, 2009; Phanikanth et al., 2013). Therefore, the equation proposed by Glick (1948) was modified by replacing E_s with E_{unsat} for unsaturated soil (Equation 3.38) and used in this study to predict the value of k_{hcmax}.

$$k_{\mathrm{hc\,max}} = \frac{8\pi(1-\nu)E_{\mathrm{sat}}\left[1+\alpha\frac{(u_{\mathrm{a}}-u_{\mathrm{w}})}{(P_a/101.3)}(S^{\beta})\right]}{C_1(1+\nu)(3-4\nu)\left[2\ln\left(\frac{2L}{d}\right)-0.443\right]} \tag{3.39}$$

where k_{hcmax} is the maximum modulus of horizontal subgrade reaction (i.e. the initial straight-line portion of the *p-y* curve), constant C_1 is equal to 1.13 and ν is the Poisson's ratio. k_{hc} degrades with an increase in the lateral deflection y_0. If k_{hcmax} is known, k_{hc} at any given y_0 can be determined considering the nonlinearity of k_{hc}. The following equation proposed by Zhang and Ahmari (2013) can be used for the estimation of k_{hc}:

$$\frac{k_{\mathrm{hc}}}{k_{\mathrm{hcmax}}} = 0.058\left(\frac{y_0}{B}\right)^{-0.5} \tag{3.40}$$

3.4 Validation for the proposed analytical model

In this section, the proposed analytical method is validated providing comparisons with the results of four and three field studies published by Truong (2017) and Choi et al. (2013), respectively.

3.4.1 Field tests conducted by Truong (2017)

Field load tests were carried out by Truong (2017) to investigate the behavior of laterally loaded piles in unsaturated residual soil at Bullsbrook site, which is 45 km Northeast of Perth in Western Australia. The residual soil is a material resulting from the weathering and decomposition of parent rocks. Many of residual soils are unsaturated and their shear strength properties are characterized by both cohesion and friction components. Table 3.2 provides the summary of soil properties and shear strength parameters for two unit of samples; namely, Unit B1 that extends from 0.5 m to 1 m and Unit B2 that lies below. Four steel pipe piles with an outer diameter of 127 mm, wall thickness of 19 mm and length of 2 m were used in the field tests. After pile installation, the top 0.5 m of the soil layer was excavated to the upper level of Unit B1. Cone Penetration Tests (CPTs) were performed within the test area of each pile that was labelled P1, P2, P3 and P4. The average values of corrected tip resistance (q_t), normalized cone resistance (Q_t), friction ratio (F_r), and soil behavior type (I_c) from depths between 0.5 m to 2 m are presented in Table 3.2. According to the CPT-based soil behavior type chart from Robertson (2016), the tested residual soil is classified as a dense dilative sandy clay or clayey sand. The elastic modulus of the residual soil (E_s) can be estimated using the Robertson and Cabal's (2015) equation:

$$
\begin{aligned}
E_s &= \alpha_E \left(q_t - \sigma_{v0}\right) \\
\alpha_E &= 0.015 \times \left[10^{(0.55 I_c + 1.68)}\right]
\end{aligned}
\tag{3.41}
$$

where σ_{v0} is in-situ total vertical stress. The mean values for degree of saturation and matric suction of the residual soil are 0.53 and 97 kPa, respectively. The calculated average apparent cohesion is 38 kPa using Equation 3.5b. The coefficient K_c and K_q was estimated as 19.45 and 13.61 based on friction angle using Equations 3.35 and 3.29 respectively. The Poisson's ratio of the foundation soils was assumed 0.33 based on the type of soil. The values of k_{hcmax} and k_{hc} at any given depth were calculated using Equations 3.39 and 3.40 respectively. Based on the relative density and friction angle of the soil, the values of n_{hmax} for all four cases were determined to be 45 MN/m^3 using Table 3.1.

Table 3.2 Summary of pile and soil properties from field load tests

Pile and CPT parameters	L (m)	e (m)	$q_{t,avg}$ (MPa)	Q_t	F_r (%)	I_c	E_s (MPa)	k_{hcmax} (MN/m^3)	n_{hmax} (MN/m^3)
P1	1.39	0.26	6.5	529.6	5.5	2.1	66.3	77.79	45
P2	1.41	0.26	8	652.1	4.6	2.0	71.6	83.55	45
P3	1.35	0.21	8	652.1	3.3	1.9	59.8	70.89	45
P4	1.48	0.25	6.25	509.2	4.6	2.0	58.8	67.50	45
Soil	Clay (%)	Silt (%)	Sand (%)	Gravel (%)	w (%)	S (%)	c' (kPa)	ϕ' (°)	γ_{bulk} (kN/m^3)
Unit B1	28	20	43	9	13	43	5	35	16.7
Unit B2	20	22	49	9	16	63	5	35	18.3

The values of n_h corresponding to displacement y_0 can be estimated using Equations 3.36 and 3.37. Figure 3.9 shows lateral load versus deflection curves for P1-P4 cases. The predictions using the proposed analytical method is consistent with the field test data.

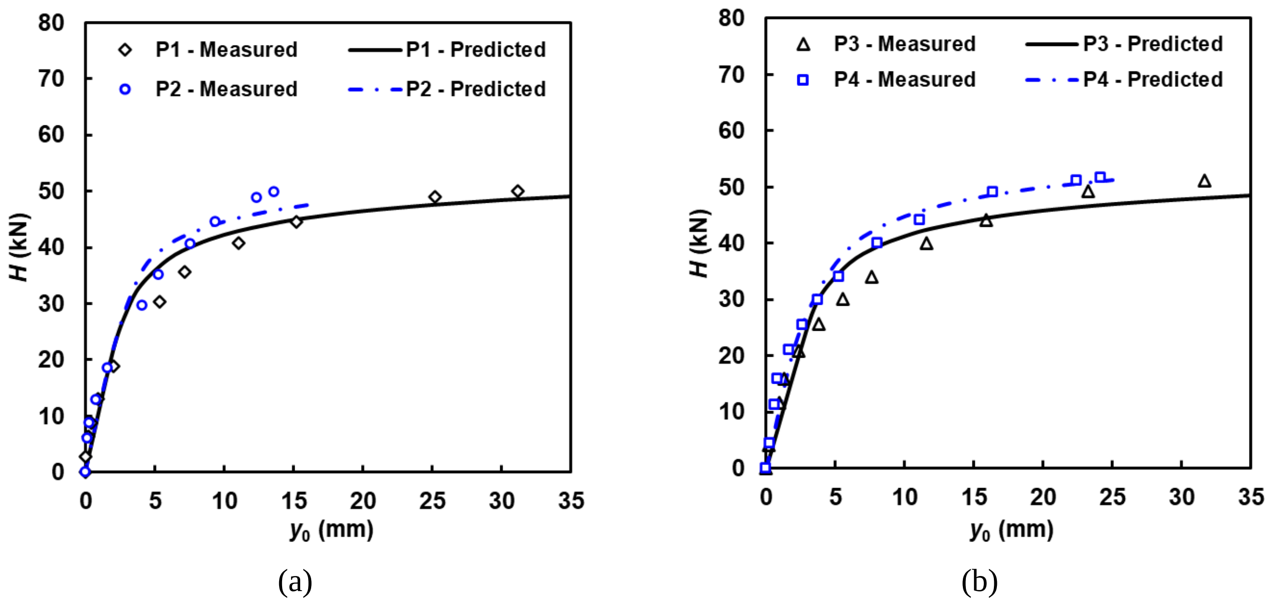

Figure 3.9 Comparisons of lateral load-deflection curves between predicted results by using proposed analytical method and the measured data by Truong (2017)

3.4.2 Field tests conducted by Choi et al. (2013)

Choi et al. (2013) have conducted three field tests on single piles subjected to lateral loading in unsaturated soils. The site for the rigid bored pile tests is in Iksan city, South Korea, that is predominantly comprised of weathered granite soil. Table 3.3 summarizes the details of three pile load tests. A 2 m thick silty clay above the weathered granite soil was removed before the field tests started. The groundwater table was 8 m deep from the ground surface. The relative density of the soil varied from 30% to 35% and the unit weight was 18 kN/m^3. The cohesion of granite soil varies from 0 to 35 kPa with an average value of 20 kPa. The natural water content was 24.9 % and the void ratio was 0.85. The internal friction angle of soil was 30°. The coefficient K_c and K_q was estimated as 15.59 and 9 using Equations 3.35 and 3.29, respectively. The elastic modulus of soil was 30 MPa and Poisson ratio was 0.3. The value of the coefficient k_{hc} can be determined based on pile lengths and diameters using Equations 3.39 and 3.40. Since the soil is loose to medium dense, n_{hmax} can be estimated to fall in range from 12 to 18 MN/m^3 based on the information summarized in Table 3.1. n_h corresponding to displacement y_0 can be found using Equations 3.35 and 3.37. The lateral load versus deflection curves of 3 cases are presented in Figure 3.10. There are good comparisons between the predicted results and the measured data. For case 3, the upper bound curve using the cohesion of 35 kPa and lower bound curve using the cohesion of 20 kPa were presented in Figure 3.10. The predicted results closely matched with the measured data when an average cohesion value of 30 kPa was used.

Table 3.3 Soil properties and other details of the model pile tests

Case No.	L (m)	d (m)	e (m)	c'(kPa)	ϕ'(°)	γ_{total} (kN/m^3)	L/d	e/d
1	1.2	0.4	2	20	30	18	3	5
2	2.4	0.4	2	20	30	18	6	5
3	2.4	0.4	0.15	20-35	30	18	6	0.375

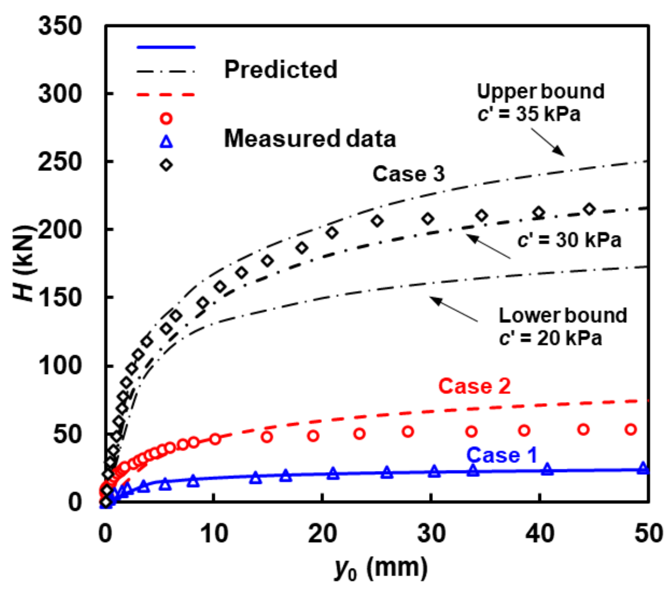

Figure 3.10 Comparisons of lateral load-deflection curves between predicted results using proposed analytical method and the measured data by Choi et al. (2013)

3.5 The proposed numerical approach and its validation

FEA was performed to simulate the behavior of single piles subjected to lateral loading in unsaturated soils in ABAQUS. As detailed in earlier sections of this Chapter, modified Mohr-Coulomb model and modified stiffness have been used in ABAQUS to interpret the nonlinear shear strength and modulus of elasticity behavior of unsaturated soils respectively taking account of matric suction. This is achieved through the USDFLD using appropriate constitutive models (i.e., Equations 3.4 and 3.5b). The USDFLD allows the user to define field variables at every integration point of an element and calculate the material properties taking account of the influence of field variables. The material properties of the unsaturated soil can be defined as functions of field variables such as pore water pressure or degree of saturation in a material point. In other words, the contribution of matric suction towards cohesion at any point can be incorporated into apparent cohesion via the USDFLD. The input parameters for the numerical model only include the shear strength parameters of the saturated soil, saturated modulus of elasticity and the SWCC.

To validate the proposed numerical method, the results of two pile model tests under lateral loading, one in unsaturated silty soil by Lalicata et al. (2019) and the other in unsaturated sandy soil by Mahmood et al. (2018), were simulated using the proposed numerical method.

Lalicata et al. (2019) conducted a series of centrifuge tests to investigate the behavior of laterally loaded piles in saturated and unsaturated soils. The study was performed in a rigid cylindrical container at 100 *g* (*g* is the gravity acceleration) using the IFSTTAR centrifuge facilities in Nantes. These results simulated for the prototype single pile with diameter of 1.2 m that was embedded 15 m into a silty soil named B-grade kaolin. The parameters used in the FEA are summarized in Table 3.4. The soil consists of approximately 90% fine silt and 10 % clay that was compacted at a water content of 15% to achieve an initial void ratio e_{ini} of 0.93. A horizontal load was applied at 3.5 m above the soil surface. As shown in Figure 3.11, the SWCC of B-grade kaolin obtained from the experiment was fitted by the Fredlund and Xing's (1994) equation:

$$S = \left[C(\psi)\right]\left[\frac{1}{\ln\left(e+\left(\frac{\psi}{a}\right)^{n}\right)}\right]^{m} \tag{3.42}$$

where $C(\psi)$ is the correction function, ψ is matric suction, e is Euler's number, and the SWCC fitting parameters are a = 26.556, n = 1.308, m = 0.51.

Table 3.4 The material parameters used in the FEA

	Pile			Soil					
	γ (kN/m^3)	E (MPa)	ν	γ_d (kN/m^3)	γ_{sat} (kN/m^3)	c' (kPa)	ϕ' (°)	e_{ini}	ν
Lalicata et al. (2019)	27	39000	0.2	15.3	26.1	5	22	0.93	0.25
Mahmood et al. (2018)	24	20000	0.2	15.45	19.53	0	38	0.58	0.3

The saturated coefficient of permeability k_{sat} of B-grade kaolin was 4×10^{-9}m/s. Since there is no information of the effective cohesion, c' and modulus of elasticity of soil in saturated conditions, values of 5 kPa and 8 MPa were respectively used in the FEA that provide a reasonable load versus displacement behavior compared to the measured data. The average E_{unsat} along with pile depth was estimated as 17.2 MPa at GWT = 7 m using Equation 3.38. Figure 3.12(a) summarizes the load versus lateral deflection curves of the pile in saturated and unsaturated soil conditions.

Mahmood et al. (2018) performed a series of laboratory tests on laterally loaded piles in unsaturated sandy soils. The model pile with 16 mm in diameter and 600 mm in length was embedded 500 mm into the soil. The soil properties are presented in Table 3.4. The unsaturated soil conditions were achieved by lowering the water levels to predetermined depth values using a water supply valve. Static lateral loads at different levels (i.e., 20, 40, 60, 80, 120 N) were applied on the head of pile. The measured SWCC was fitted using

Equation 3.42 assuming the fitting parameters a = 7.822, n = 1.285, m = 1.278, as shown in Figure 3.11. The dilation angle of sandy soil φ' was estimated as 3.8° (i.e., 10% of ϕ'). The saturated elastic modulus of the sandy soil was estimated to be 10 MPa. Since sand is non-plastic soil, the fitting parameter $\alpha = 0.5$ and $\beta = 1$ were used. Therefore, the average values of E_{unsat} along with pile depth for GWT at 350 mm and 500 mm deep were estimated as 14.87 MPa and 19.3 MPa, respectively using Equation 3.38. Good comparisons were found between the measured and predicted results for different water levels in Figure 3.12(b). Thus, the proposed numerical method has a reasonable level of accuracy and reliability for capturing the laterally loaded pile behavior taking account of the influence of matric suction.

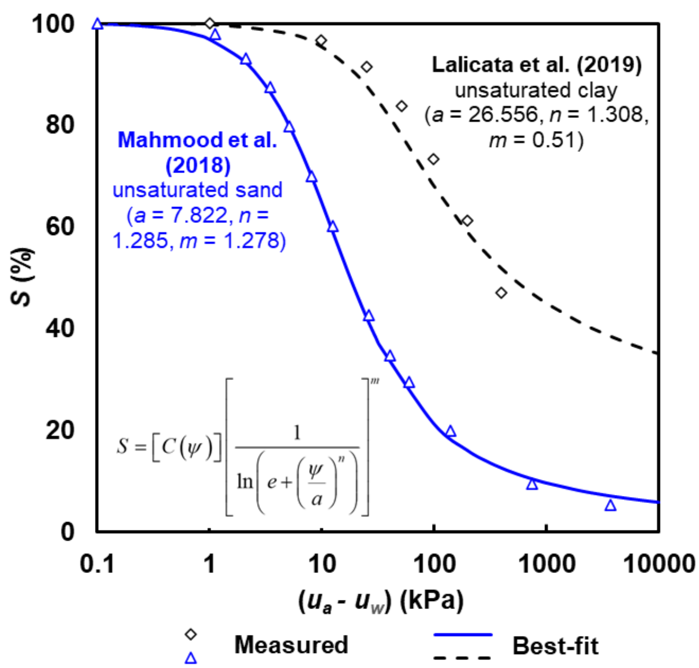

Figure 3.11 Measured SWCC and fitting curves for the two investigated soils

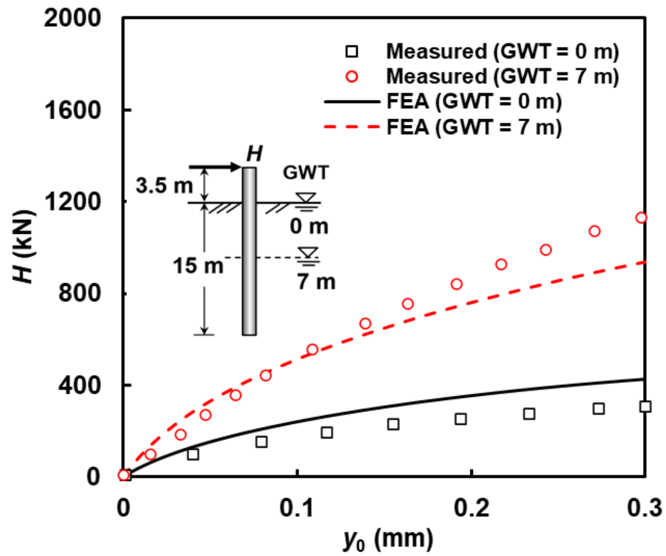

(a)

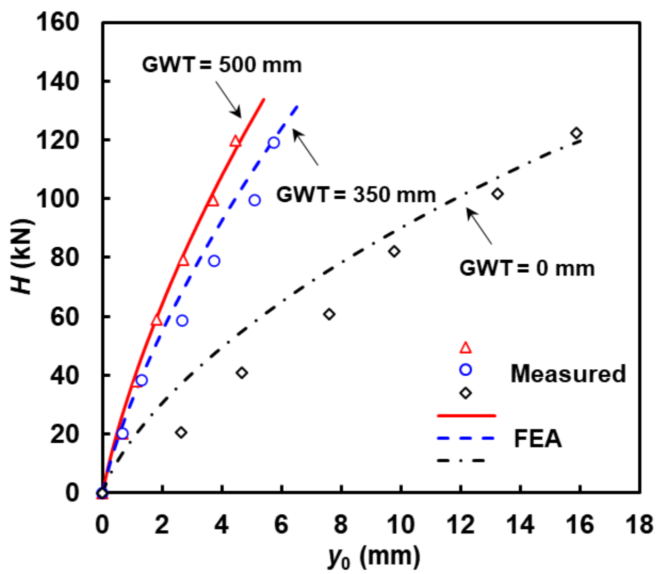

(b)

Figure 3.12 Comparisons between the numerical results and measured data by (a) Lalicata et al. (2019) (b) Mahmood et al. (2018)

3.6 Numerical modeling analysis

This part of the study has been undertaken for two reasons: (i) to provide information of using the proposed numerical approach for preliminary studies and (ii) to provide comparisons between the FEA and the analytical method.

3.6.1 Numerical model description of laterally loaded piles in Indian Head till

In this section, example problems of laterally loaded piles in Indian Head till (IHT) using 3D FE models are described considering various scenarios. Two different piles of 0.4 m in diameter and embedded lengths of 2 and 3 m subjected to loading with two eccentricities e = 0.5 and 1.5 m, respectively were placed in soils which GWTs depths varied (i.e., 0 m, 2 m, 4 m and 6 m). The details of pile parameters used in the FEA are summarized in Table 3.5.

Table 3.5 Model parameters used for piles in the FEA

No.	Pile embedded length, L (m)	Pile diameter, d (m)	Loading eccentricity, e (m)	L/d	e/d
1	2	0.4	0.5	5	1.25
2	2	0.4	1.5	5	3.75
3	3	0.4	0.5	7.5	1.25

IHT is a glacial till that is widely distributed in Indian Head, Saskatchewan, Canada. The soil has 28% sand, 42 % silt and 30 % clay with a liquid limit (w_L) and plastic index (I_P) values of 32.5 % and 15.5 %, respectively. The soil properties of IHT are summarized in Table 3.6. Han et al. (2016) previously measured the drying path SWCC of IHT using a modified null pressure plate. The measured SWCC data was fitted by Fredlund and Xing (1994) equation (i.e., Equation 3.42) which yielded the fitting parameters a = 12.23, n = 1.55, m = 0.54. Figure 3.13 shows the measured and best-fit SWCC of IHT. With the aid of the SWCC, water content or degree of saturation can be estimated for different values of matric suction. Therefore, the shear strength of unsaturated soils can also be estimated using Equation 3.4. The IHT is assumed to be in a state of hydrostatic conditions, so pore water pressure is linearly distributed above the GWT (i.e., $u_w = -\gamma_w \cdot h_{unsat}$, where h_{unsat} is the height above the GWT).

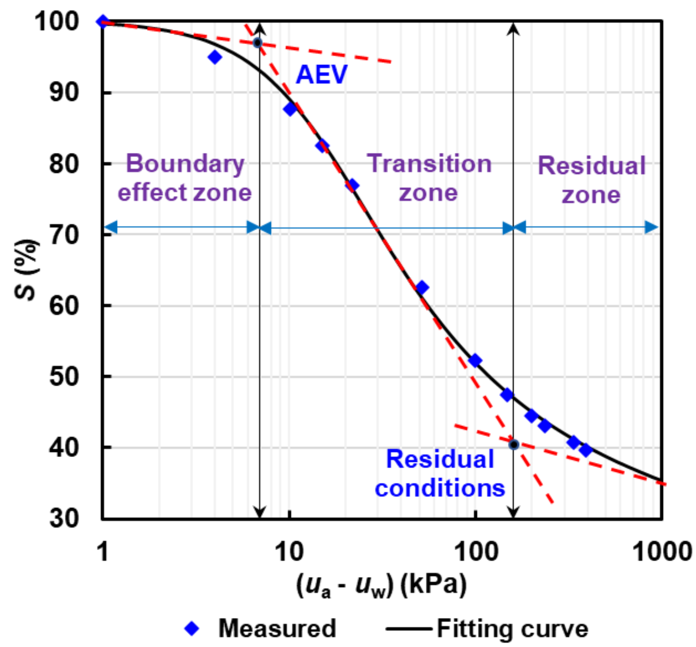

Figure 3.13 The measured and best-fit SWCC of IHT (modified after Han et al., 2016)

Considering the symmetry of the pile-soil system, half of the 3D pile and soil domain was established. Figure 3.14 shows the geometry of the three-dimensional model. The size of the pile-soil domain is 25 d × 12.5 d × (L+10 d), where L is the pile embedded length, d is the pile diameter. The single pile was modelled as a linear-elastic material using eight-node linear brick elements (C3D8). The pile modulus of elasticity E_p is 20 GPa and the Possion's ratio ν is 0.15. The IHT was modelled as a linear-elastic, perfectly plastic material with a Mohr-Coulomb constitutive model using eight-node stress–pore-pressure coupled brick elements (C3D8P). The USDFLD provides access to the solutions from previous increment and updates the field variables for the current increment during the operation process. The SWCC of IHT was imported into ABAQUS by adding "Sorption" material properties with a range of degrees of saturation and corresponding matric suction values. The unsaturated modulus of elasticity, E_{unsat} was determined using Equation 3.38. For the convenience of achieving geostatic equilibrium, average value of E_{unsat} along with pile depth is defined as a uniform elastic modulus of soil. The fitting parameter α and β were estimated as 1/10 and 2 for IHT soil, respectively. For a typical case of L = 2 m pile, the values of E_{unsat} for GWT at 2, 4, 6 m were 11.84, 17.25 and 20.14 MPa, respectively. The hydraulic conductivity of unsaturated soils assumed to vary with the degree of saturation according to Brooks and Corey (1964):

$$k = k_{sat} S^{\lambda} \tag{3.43}$$

where the saturated permeability k_{sat} of IHT was 5×10^{-5}m/s. The parameter λ was estimated as 2. The pore water pressure of all the nodes at GWT surface was set to zero.

Table 3.6 Soil Properties of IHT

w_L (%)	I_P (%)	γ_{sat} (kN/m^3)	γ_d (kN/m^3)	c' (kPa)	ϕ' (°)	E_{sat} (kPa)	USCS
32.5	15.5	20	16.7	9	23	7000	CL

The dilation angle of IHT was assumed as zero. The coefficient of earth pressure K_0 was equal to 0.61 according to empirical relationship (i.e., K_0 = 1-sinϕ' by Jaky, 1944). A surface-to-surface contact algorithm was used to simulate small sliding and gapping at the pile-soil interface. The pile-soil interface friction angle (δ') was assumed 15.3°, that is equal to 2/3ϕ'. The displacements at the bottom of the model and in the direction perpendicular to the symmetry planes were fixed. The local meshes adjacent to the pile were refined to improve the computational accuracy. For a typical case of pile length L, diameter, d and eccentricity e, with values of 2, 0.4 and 0.5 m respectively, the pile and soil cylinder were discretized with 96 C3D8 elements and 4400 C3D8P elements respectively. A lateral load was applied on the pile top surface in the x direction, as shown in Figure 3.14.

3.6.2 The comparison between FEA and analytical method

Figure 3.15 shows the comparisons of the FEA and the analytical method as load versus lateral deflection curves for varying GWTs of a typical case (i.e., L = 2 m, d = 0.4 m, e = 0.5 m pile). The average matric suction along the pile length was used in calculating the proposed analytical method. The average apparent cohesion was calculated using Equation 3.5b which yielded values of 12.48 kPa, 17.8 kPa and 21.9 kPa for the soil at GWT = 2, 4 and 6 m, respectively. The coefficient K_c and K_q was estimated as 12.28 and 5.21 based on the friction angle, using Equations 3.35 and 3.29, respectively. The value of the coefficient k_{hc} was determined based on the unsaturated modulus of elasticity and pile slenderness ratio using Equations 3.39 and 3.40. Since the soil was loose, n_{hmax} was estimated as 2 MN/m^3 based on the information summarized in Table 3.1. n_h corresponding to displacement y_0 can be obtained using Equations 3.36 and 3.37. The difference between the results using numerical modeling and the analytical method is less than 12% suggesting that the comparison between the results from these two proposed methods is satisfactory. The GWT has a significant influence on the lateral response of piles. As the GWT moves deeper from the soil surface, a considerable increase in lateral load can be observed compared to saturated conditions (i.e., GWT = 0 m). The load-carrying capacity of a laterally loaded pile can be defined as the value at the intersection of the initial tangents to the load versus displacement curve and the tangent to or the extension to the final portion of the curve (Prakash and Sharma, 1990). The locations of load-carrying capacity (H_u) for four GWTs are indicated in Figure 3.15. The value of H_u for GWT depth of 2 m is 25.9 kPa, which is 1.59 times that of saturated conditions (16.2 kPa), while the H_u for GWT depth of 4 and 6 m is 2.26 and 2.83 times higher, respectively. This is because the average matric suction of the soil increases as GWT locates at a greater depth. The soil stiffness and shear strength in unsaturated soils increases with matric suction, thereby leading to higher lateral soil resistance than that in saturated soils that are typically associated with lower stiffness and shear strength.

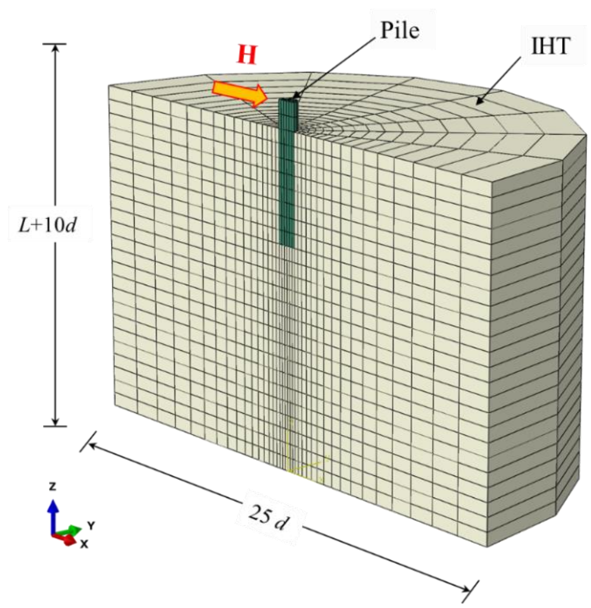

Figure 3.14 Geometry of the 3D FE model

H_u can be determined by double tangent method for various scenarios of GWT as discussed earlier (see Figure 3.15). H_u arises when the deflection is typically between 8 to 15 mm, which is 2 % to 3.75 % of pile diameter. Figure 3.16 shows the comparison of load versus lateral deflection curves at GWT depth of 4 m between predictions using FEA and analytical method with varying pile embedded lengths and load eccentricities as shown in Table 3.5. The average cohesion of the soil at GWT = 4 m is 17.8 kPa and 16.6 kPa for L = 2 m and 3 m pile, respectively. It can be observed that the predictions using proposed analytical methods are in reasonable agreement with the FEA results. The differences between these two methods may be due to the use of average matric suction in the analytical method, while the matric suction is simulated as linearly distribution above the GWT in the numerical model.

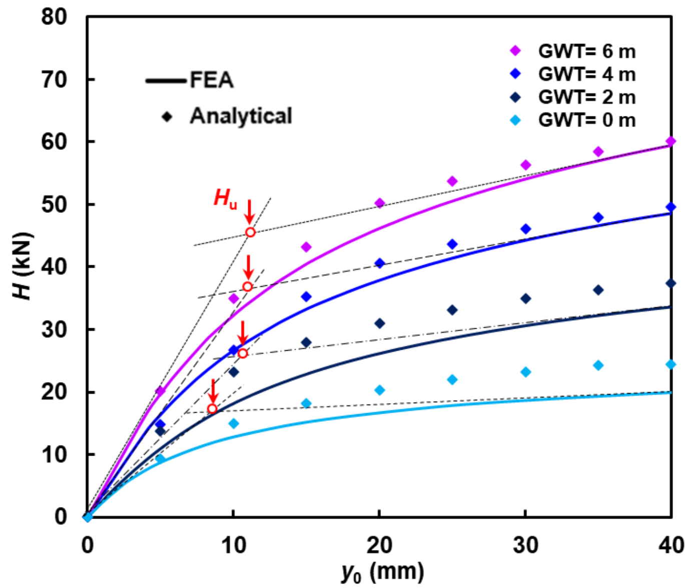

Figure 3.15 Comparisons between the FEA and the analytical methods in IHT with varying GWTs

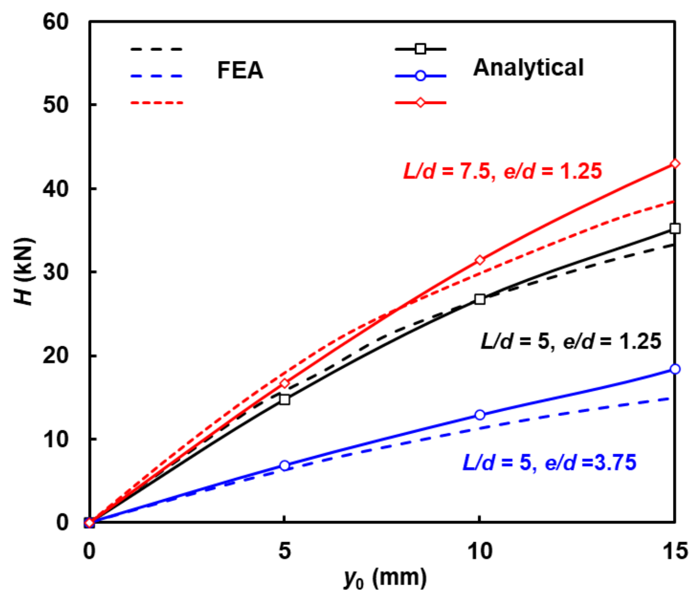

Figure 3.16 Load versus lateral deflection curve at GWT = 4 m with varying *L* and *e*

3.7 Summary and conclusions

In this Chapter, a nonlinear analytical method has been proposed for estimating the load versus displacement curve of laterally rigid piles in unsaturated soils. Taking account of the variation of lateral soil resistance along the pile length at three different states (pre-tip yield state, post-tip yield state and ultimate limiting state), the lateral load corresponding to lateral displacement at ground surface were derived. The lateral earth pressure coefficient for cohesion component K_c required in the solutions was derived considering the 3D effect factor for drained loading. Good comparisons were achieved between the results of this method and published data of seven field pile tests in unsaturated soils (see Figure 3.9 and 3.10). In addition, a series of 3D FE analyses were performed using a numerical technique that was developed to simulate the behavior of laterally loaded piles in unsaturated soils. The developed numerical technique was implemented as USDFLD into ABAQUS for modeling the variation of load-displacement curves considering the influence of matric suction in the shear strength and the elastic modulus of unsaturated soils. The required information for modeling includes only the shear strength parameters of the saturated soil, saturated modulus of elasticity and the SWCC. The proposed numerical method was validated using two experimental studies from literature (see Figure 3.12 (a) and (b)). In both cases, the comparisons between numerical results and measured data are satisfactory. Compared with the analytical method developed only for short rigid pile, the numerical method can be used for pile with varying lengths or stiffness, including short, intermediate, and long piles or non-rigid piles. In addition, the results between the proposed analytical method and the FEA were compared using an example problem in an unsaturated soil with varying GWTs for two different piles. Good agreement was also found between the predictions using the proposed analytical method and the numerical technique. The studies presented in this paper are simple and promising for the geotechnical engineers to use in practice for the design laterally loaded piles in unsaturated soils.

CHAPTER 4

PREDICTION OF THE END-BEARING CAPACITY OF AXIALLY LOADED PILES IN SATURATED AND UNSATURATED SOILS BASED ON THE STRESS CHARACTERISTICS METHOD

4.1 Introduction [3]

The design of pile foundations in unsaturated soils is typically based on the principles of saturated soil mechanics in conventional engineering practice. However, the presence of the air-water interface that generates due to surface tension effects within the soil skeleton has a significant influence on the mechanical behavior of unsaturated soils. Extending the conventional soil mechanics approach to unsaturated soils leads to unreliable estimations of the pile behavior due to ignoring the influence of matric suction. A significant vadose zone layer (i.e., unsaturated soil zone) that is above the ground water table is widely observed in semi-arid and arid regions due to the cumulative influence of environmental activities such as rainfall infiltration, evaporation, and plant transpiration. In these regions, in many scenarios, the entire or a portion of the pile is in unsaturated zone throughout its design life. In recent years, several studies focused on investigating the ultimate bearing capacity of single piles suggest that the matric suction contributes to an increase in the bearing capacity by 2 to 5 times in coarse-grained soils (Vanapalli et al. 2018) and 2 to 6 times in fine-grained soils (Vanapalli and Taylan 2012, Pujiastuti et al. 2022).

The axial bearing capacity of driven piles in unsaturated soils is significantly influenced by the pile-soil interface and the soil properties surrounding the pile. Various approaches are available to consider the effect of degree of saturation, water table depth and matric suction on the bearing capacity of single piles in unsaturated soils. For example, several

[3] The contents presented in this chapter are published as a journal article: **Cheng, X.,** & Vanapalli, S. K. (2023). Prediction of the end-bearing capacity of axially loaded piles in saturated and unsaturated soils based on the stress characteristics method. *International Journal of Geomechanics*, 23(7), 04023104.

investigators have undertaken laboratory and field investigations to interpret pile shaft-carrying capacity and end-bearing capacity using the shear strength parameters of the saturated soil and the Soil Water Characteristics Curve (SWCC) (Douthitt et al.1998, Uchaipichat 2012, Vanapalli and Taylan 2012, Fattah et al. 2014, Akrouch et al. 2016, Vanapalli et al. 2018). Numerical techniques have also been increasingly used due to the advantages associated with obtaining quick results at a relatively low cost (Georgiadis et al. 2003, Han et al. 2016, Chung and Yang 2017, Cheng et al. 2021). Limited efforts have been undertaken to study the response of driven piles in unsaturated soils under axial loading. Mahmoudabadi and Ravichandran (2019) proposed a framework that incorporates the climate parameters into computing the axial capacity and settlement of driven piles. However, studies relating to the determination of the end-bearing capacity of driven piles taking account the influence of matric suction and the pile-soil interface roughness are limited.

The ultimate bearing capacity, Q_u, of a pile under axial loading is typically estimated as the sum of the end-bearing capacity Q_b, and the shaft carrying capacity Q_s as given below:

$$Q_u = Q_s + Q_b = f_s A_s + q_b A_b \tag{4.1}$$

where f_s is the unit pile shaft carrying capacity, A_s is the surface area of the pile, q_b is the unit end-bearing capacity and A_b is the area of the pile tip.

Four different methods are widely used for determining or estimating the bearing capacity of pile foundations assuming saturated soil conditions; namely, static pile load tests (Vesić 1970, Altaee et al. 1992, Paik et al. 2003, Karlsrud et al. 2014, Yang et al. 2015), dynamic methods (Hery 1983, Rausche et al. 1985, Fellenius 2006); static analysis (e.g., total and effective stress approach) (Skempton 1959, Vesić 1963, Burland 1973, Vijayvergiya and Focht 1972), and direct or indirect use of results from in situ tests (Nottingham 1975, Schmertmann 1978, Bustamante and Gianeselli 1982, Eslami and Fellenius 1997, Lehane et al. 2005, Jardine et al. 2005). Both static and dynamic pile load tests are expensive and time-consuming. Due to this reason, several researchers focused on proposing methods extending static analysis (i.e., theoretical methods) for estimating the pile load capacity. In recent years, cone penetration tests (CPT) have been widely used to estimate pile capacity because they are low cost in-situ tests with several similarities to static pile load tests (Hong et al. 2010, Alkroosh and Nikraz 2012).

The stress characteristics method (SCM) is a valuable tool for providing rigorous solutions to plasticity problems in soil mechanics by solving the limit equilibrium equations together using yield equations (Sokolovskii 1960, Harr 1966, Martin 2004). The SCM that is also referred to as the slip line theory has been widely used to solve a variety of problems, especially for shallow foundations and retaining walls (Martin 2005, Bolton and Lau 1993, Kumar and Chitikela, 2002, Santhoshkumar and Ghosh 2021). Some researchers used SCM to investigate the behavior of piles in saturated soils (Gui 2006, Veiskarami et al. 2011, Valikhah et al. 2019). To the best of the authors knowledge, no studies have been undertaken in the literature to investigate the response of piles in unsaturated soils using the SCM. For this reason, in this Chapter, a general framework has been developed for the prediction of the end-bearing capacity of axially loaded piles in both coarse- and fine-grained saturated and unsaturated soils based on the SCM. The families of hyperbolic differential equations associated with the SCM for an axisymmetric problem were solved by the iterative finite difference method. MATLAB code has been developed as a part of this Chapter that can provide solutions for the finite difference equations extending iterative technique for implementing this procedure. The proposed method was validated using the measured results for eleven driven pile load tests in saturated soils and two in unsaturated soils. Comparisons between the predictions made by the proposed method and several published theoretical methods (i.e., direct CPT methods and static analysis approach) and measured data, suggest reasonable predictions. In addition, finite element analysis (FEA) was performed to simulate the procedure of pile penetration in unsaturated soils and the pile load test using commercial software ABAQUS. The Arbitrary Lagrangian-Eulerian (ALE) adaptive mesh technique was employed in the FEA to alleviate the large-deformation problem that is typically associated with the convergence difficulties. The ultimate bearing capacity derived from the FEA as well as the computed results using the proposed analytical method were compared against the measurements from a model pile test conducted by Kong et al. (2005). The proposed generalized framework extending the SCM is a useful tool for predicting the end-bearing capacity of piles in saturated soils extending conventional soil mechanics and in unsaturated soils considering the influence of matric suction.

4.2 Methodology

4.2.1 The nonlinearity of shear strength and bearing capacity of unsaturated soils

Vanapalli et al. (1996) proposed a semi-empirical model to predict the nonlinear shear strength of unsaturated soils, τ_{unsat}, using the saturated shear strength parameters (c' and ϕ') and the SWCC. In this model, the SWCC information is typically expressed as a relationship between either degree of saturation or volumetric water content versus suction:

$$\tau_{\mathrm{unsat}} = c' + (\sigma_{\mathrm{n}} - u_{\mathrm{a}})\tan\phi' + (u_{\mathrm{a}} - u_{\mathrm{w}})\left[\frac{(S - S_{\mathrm{r}})}{(1 - S_{\mathrm{r}})}\tan\phi'\right] \tag{4.2a}$$

$$\tau_{\mathrm{unsat}} = c' + (\sigma_{\mathrm{n}} - u_{\mathrm{a}})\tan\phi' + (u_{\mathrm{a}} - u_{\mathrm{w}})\left[\frac{(\theta - \theta_{\mathrm{r}})}{(\theta_{\mathrm{s}} - \theta_{\mathrm{r}})}\tan\phi'\right] \tag{4.2b}$$

where $(\sigma_{\mathrm{n}} - u_{\mathrm{a}})$ is net normal stress in which σ_n is the normal stress and u_{a} is the atmospheric pressure, u_{w} is pore water pressure, $(u_{\mathrm{a}} - u_{\mathrm{w}})$ is matric suction, S is the degree of saturation, S_{r} is the residual degree of saturation, θ is volumetric water content, θ_{s} and θ_{r} is saturated and residual volumetric water content, respectively. The contribution of matric suction towards the bearing capacity of unsaturated soils can be expressed as a form of total cohesion, c_{t}, which is calculated by taking into account the contribution of matric suction, as given below:

$$c_{\mathrm{t}} = c' + (u_{\mathrm{a}} - u_{\mathrm{w}})_{\mathrm{b}}\left(1 - S^{\psi}\right)\tan\phi' + (u_{\mathrm{a}} - u_{\mathrm{w}})_{\mathrm{AVR}} S^{\psi}\tan\phi' \tag{4.3}$$

where $(u_{\mathrm{a}} - u_{\mathrm{w}})_{\mathrm{b}}$ is the air-entry value (AEV), $(u_{\mathrm{a}} - u_{\mathrm{w}})_{\mathrm{AVR}}$ is the average matric suction within the influence zone and ψ is the fitting parameter with respect to bearing capacity. ψ

equal to unity for soils with no plasticity is used in this Chapter as the soils investigated are predominantly coarse-grained soils.

4.2.2 Modified stress characteristic method considering the influence of matric suction

A single pile is considered in this study with an embedded length, L and diameter, D. Only half of the section is considered because of the axis symmetry of the pile foundation. It is assumed that the shaft resistance of the pile has been fully mobilized so that the estimation of pile end-bearing capacity is separate from that of shaft resistance. It is also assumed that the soil mass is rigid-plastic, obeys the Mohr-Coulomb failure criterion (i.e., $\tau_f = c_t + (\sigma_n - u_a)\tan\phi'$) and associate flow rule. Figure 4.1 shows the definition of various stress variables and the Mohr circle for unsaturated soils under failure characteristics. In the coordinate system shown in Figure 4.1(a), r and z are the radial and vertical coordinates, respectively. φ is the angle between the net major principal stress direction $(\sigma_1 - u_a)$ and the positive z axis. The counter-clockwise rotation with respect to the positive z-axis is considered positive in this analysis.

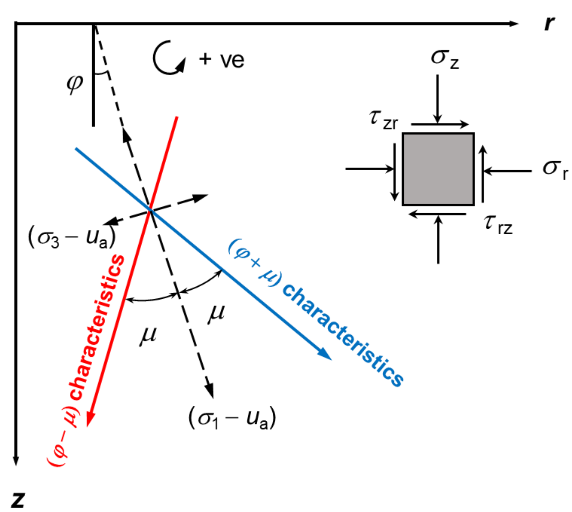

(a)

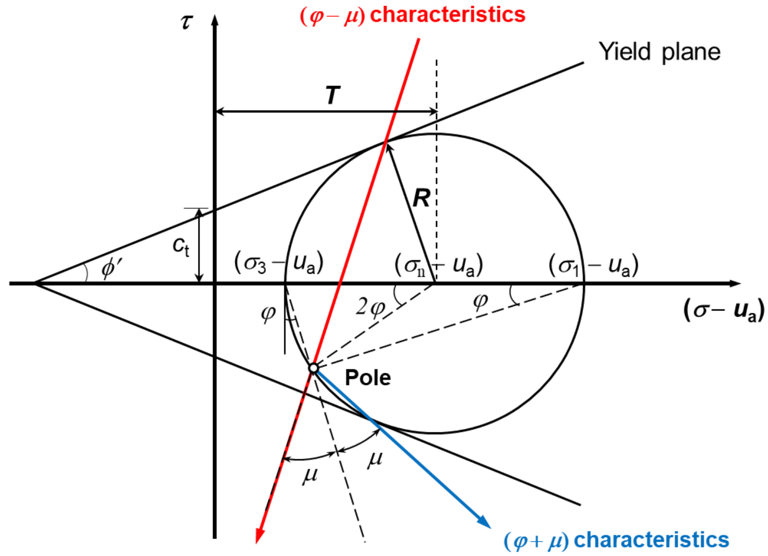

(b)

Figure 4.1 (a) Sign conventions and notations (b) Mohr circle for unsaturated soils at failure condition

The stress components shown in Figure 4.1(a) (i.e., σ_r, σ_z, τ_{rz}) are expressed in terms of two variables; namely, T and R as follows:

$$\begin{aligned}\sigma_r &= T - R\cos 2\varphi \\ \sigma_z &= T + R\cos 2\varphi \\ \tau_{rz} &= R\sin 2\varphi\end{aligned} \tag{4.4}$$

where σ_r and σ_z are normal stresses in the r and z axis, respectively, τ_{rz} is shear stress, T represents net mean stress and R represents the radius of Mohr circle as shown in Figure 4.1(b). The expression of T and R can be written as:

$$\begin{aligned}T &= \left(\sigma_n - u_a\right) \\ R &= \left(\sigma_n - u_a\right)\sin\phi' + c_t\cos\phi'\end{aligned} \tag{4.5}$$

where $(\sigma_n - u_a)$ is net mean stress, ϕ' is the internal friction angle and c_t is the total cohesion of unsaturated soil that has been defined in Equation 4.3 incorporating the influence of matric suction. Pore air pressure can be assumed to be equal to atmospheric pressure in the field (i.e., $u_a = 0$); due to this reason, the net mean stress ($\sigma_n - u_a$) is equal to the total mean stress σ. The friction angle ϕ' is constant since the influence of matric suction on ϕ' is negligible in conventional soils (Vanapalli et al. 1996). Total cohesion c_t can be constant or vary with depth depending on the soil profile. For the axis-symmetric case, the static equilibrium equations can be written as:

$$\begin{cases} \frac{\partial \sigma_r}{\partial r} + \frac{\partial \tau_{rz}}{\partial z} + \frac{(\sigma_r - \sigma_\theta)}{r} = 0 \\ \frac{\partial \tau_{rz}}{\partial r} + \frac{\partial \sigma_z}{\partial z} + \frac{\tau_{rz}}{r} = \gamma \end{cases} \tag{4.6}$$

where γ is the unit weight of the soil and σ_θ is the circumferential stress component. The Haar and von Karman (1909) hypothesis states that σ_θ is equal to either major or the minor principal stress. Following Cox et al. (1961) and Bolton and Lau (1993), the value of σ_θ is equal to the net minor principal stress σ_3 in this study (i.e., as small as possible). Combining the equilibrium equations (i.e., Equations 4.4 and 4.5) and yield equations (i.e., Equation 4.6) and following the stress characteristics method, the ordinary coupled differential equations along the ($\varphi + \mu$) characteristics are given below:

$$\frac{\mathrm{d}r}{\mathrm{d}z} = \tan(\varphi + \mu) \quad \text{where} \quad \mu = \left(\frac{\pi}{4} - \frac{\phi'}{2}\right) \tag{4.7}$$

$$\mathrm{d}\sigma + \frac{2R}{\cos\phi'}\mathrm{d}\varphi = \left(b_r - b_z \tan\phi' - \frac{\partial c_t}{\partial z}\right)\mathrm{d}r + \left(b_z + b_r \tan\phi'\right)\mathrm{d}z \tag{4.8}$$

Along similar lines, the differential equations for the ($\varphi - \mu$) characteristics are given as follows:

$$\frac{\mathrm{d}r}{\mathrm{d}z} = \tan(\varphi - \mu) \tag{4.9}$$

$$\mathrm{d}\sigma - \frac{2R}{\cos\phi'}\mathrm{d}\varphi = \left(b_r + b_z \tan\phi' + \frac{\partial c_t}{\partial z}\right)\mathrm{d}r + \left(b_z - b_r \tan\phi'\right)\mathrm{d}z \tag{4.10}$$

where μ denotes the angle between the direction of σ_1 and the direction of two families of characteristics as shown in Figure 4.1. The variables b_r and b_z are expressed as follows:

$$\begin{cases} b_r = \dfrac{R(\cos 2\varphi - 1)}{r} \\ b_z = \gamma - \dfrac{R\sin 2\varphi}{r} \end{cases} \tag{4.11}$$

Four unknown variables (i.e., spatial variables r and z, field variables σ and φ) can be obtained by solving Equations 4.7 to 4.11 from imposed boundary conditions. As shown in Figure 4.2, a new Point C lies on the intersection of the $(\varphi+\mu)$ characteristics line from Point A with the $(\varphi-\mu)$ characteristics line from Point B. The variables for the new point C (r_C, z_C, σ_C, φ_C) can be obtained, if four variables are known for two points A (r_A, z_A, σ_A, φ_A) and B (r_B, z_B, σ_B, φ_B). The finite difference forms of governing equations of the stress characteristics method can be summarized as below:

For the $(\varphi+\mu)$ characteristics:

$$\frac{r_C - r_A}{z_C - z_A} = \tan\left(\varphi_{AC} + \mu\right) \tag{4.12}$$

$$\begin{aligned} &\sigma_C - \sigma_A + \frac{R_A + R_C}{\cos\phi'}(\varphi_C - \varphi_A) = \left(b_{r,AC} - b_{z,AC}\tan\phi' - \frac{\partial c_t}{\partial z}\right)(r_C - r_A) \\ &+\left(b_{z,AC} + b_{r,AC}\tan\phi'\right)(z_C - z_A) \end{aligned} \tag{4.13}$$

For the $(\varphi-\mu)$ characteristics:

$$\frac{r_C - r_B}{z_C - z_B} = \tan\left(\varphi_{BC} - \mu\right) \tag{4.14}$$

$$\sigma_C - \sigma_B - \frac{R_B + R_C}{\cos\phi'}(\varphi_C - \varphi_B) = \left(b_{r,BC} + b_{z,BC}\tan\phi' + \frac{\partial c_t}{\partial z}\right)(r_C - r_B) + \left(b_{z,BC} - b_{r,BC}\tan\phi'\right)(z_C - z_B) \tag{4.15}$$

σ_C and φ_C are initially approximated to ($\sigma_A+\sigma_B-\sigma_C'$) and ($\varphi_A+\varphi_B-\varphi_C'$), respectively. σ_C' and φ_C' are the known solutions of Point C' which locates diagonally opposite to Point C in the current cell of the mesh. σ_{AC} is initially set to $(\sigma_A+\sigma_C)/2$ and σ_{BC} is set to $(\sigma_B+\sigma_C)/2$. φ_{AC} is initially set to $(\varphi_A+\varphi_C)/2$ and φ_{BC} is set to $(\varphi_B+\varphi_C)/2$. Then, r_C and z_C are obtained from Equations 4.12 and 4.14. Substituting these values into Equations 4.13 and 4.15 results in σ_C and φ_C becoming known. The proportion changes in the stress parameter σ_C and φ_C are computed to check the convergency at the end of iteration. This process is repeated until the until acceptable convergence is achieved for both σ and φ. The allowable error in this study is set to 10^{-5}. A MATLAB code was developed to provide solutions for the finite difference equations and implement the iterative procedure. The computational procedure for the analysis is shown in the form of a flow chart in Figure 4.3.

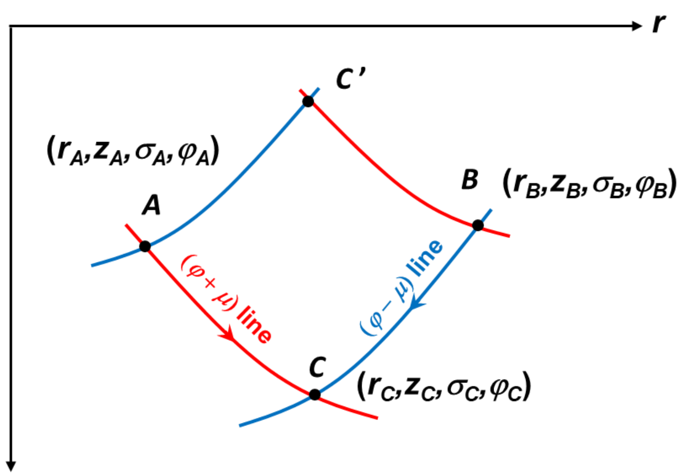

Figure 4.2 Computation of a new point *C* from two known points *A* and *B*

4.2.3 Boundary conditions

Figure 4.4 shows the failure zone and failure surface pattern around the pile tip suggested by Meyerhof (1951) and De Beer (1963). When a pile is driven into the soil, a logarithmic spiral shaped failure surface is assumed to generate below the pile base that extends all the way back to the pile shaft. The height and depth of the spiral surface increase as the soil friction angle increases and can vary between 4 to 9*D* above the pile tip (Altaee et al. 1992, Shariatmadari et al. 2008) and 1.5 to 4*D* below the pile tip (Janbu 1976, Bowles 1988), respectively.

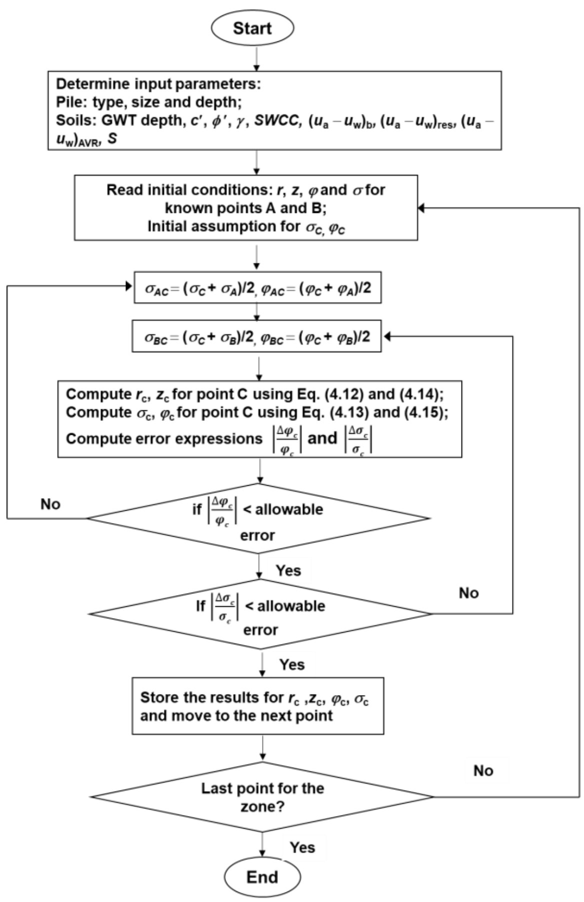

Figure 4.3 Flow chart for explaining the iterative procedure to compute stress field

Figure 4.5(a) illustrates a complete mesh of the characteristic lines near the pile base for the right half of a pile foundation. There are three different zones generated during the plastic flow of the soil due to ultimate load: namely, passive zone, radial shear zone and plane shear zone. The detailed procedures for obtaining these variables for different zones can be found in the literature (e.g., Sokolovskii 1960, Graham 1968, Gui 2006).

In this study, the k_0 state (i.e., no horizontal displacements near the pile shaft) were assumed since the state of soil adjacent to the pile shaft shows better agreement with the experimental results (Veiskarami et al. 2011). In the passive zone, variable z at any point on the pile shaft surface OA is known, and the corresponding r and φ equal to zero. The variable σ along OA using Mohr circle relations (i.e., Equations 4.4 and 4.5) can be written as:

$$\sigma = \frac{\sigma_h + c_t \cos\phi' \cos 2\varphi}{1 - \sin\phi' \cos 2\varphi} \tag{4.16}$$

where σ_h is the horizontal soil pressure.

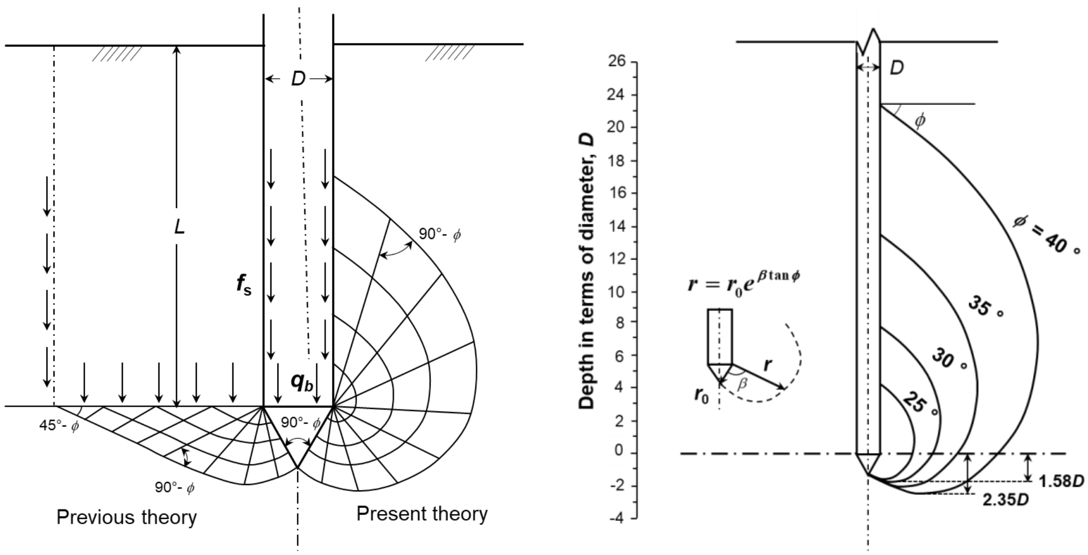

(a) (b)

Figure 4.4 The logarithmic spiral failure surface around the pile tip by (a) Meyerhof (1951) (b) De Beer (1963)

The remainder points in the passive zone can be obtained subsequently from the boundary conditions of OA, and then OB becomes the known boundary conditions for the radial fan zone. In the radial shear zone, the singular point O can be regarded as a degenerate $(\varphi - \mu)$ characteristic with the same r and z but varying σ and φ. The relationship between σ and φ is given by:

$$\mathrm{d}\sigma + \frac{2R}{\sin 2\mu}\mathrm{d}\varphi = 0 \tag{4.17}$$

Following Meyerhof (1951) and Randolph et al. (1994), a conical wedge with a base angle of (45°+$\phi'/2$) is assumed beneath the pile base. The angle of plane shear zone depends on the roughness of the conical wedge. The following relationship can be derived for the interface on the conical surface OD:

$$\varphi_{\mathrm{D}} = \frac{\pi}{2} + \frac{1}{2}\left[\delta - \arcsin\left(\frac{\sin\delta}{\sin\phi'}\right)\right] \tag{4.18}$$

where φ_{D} is the inclination of major principal stress at the conical surface OD, δ is the friction angle of pile-soil interface. Lastly, the unit end-bearing capacity, q_{b}, can be calculated by integrating the vertical pressure, q_{f}, along the conical surface beneath the pile base as follows:

$$q_{\mathrm{b}} = \frac{4}{\pi D^2}\int_0^{D/2} 2\pi r \cdot q_{\mathrm{f}}\,\mathrm{d}r \tag{4.19}$$

$$q_{\mathrm{f}} = \sigma_z + \tau_{rz}\frac{\mathrm{d}z}{\mathrm{d}r} - \gamma z \tag{4.20}$$

where the normal stress σ_{r} and shear stress τ_{rz} at each point along surface OD were obtained from Equations 4.4 and 4.5.

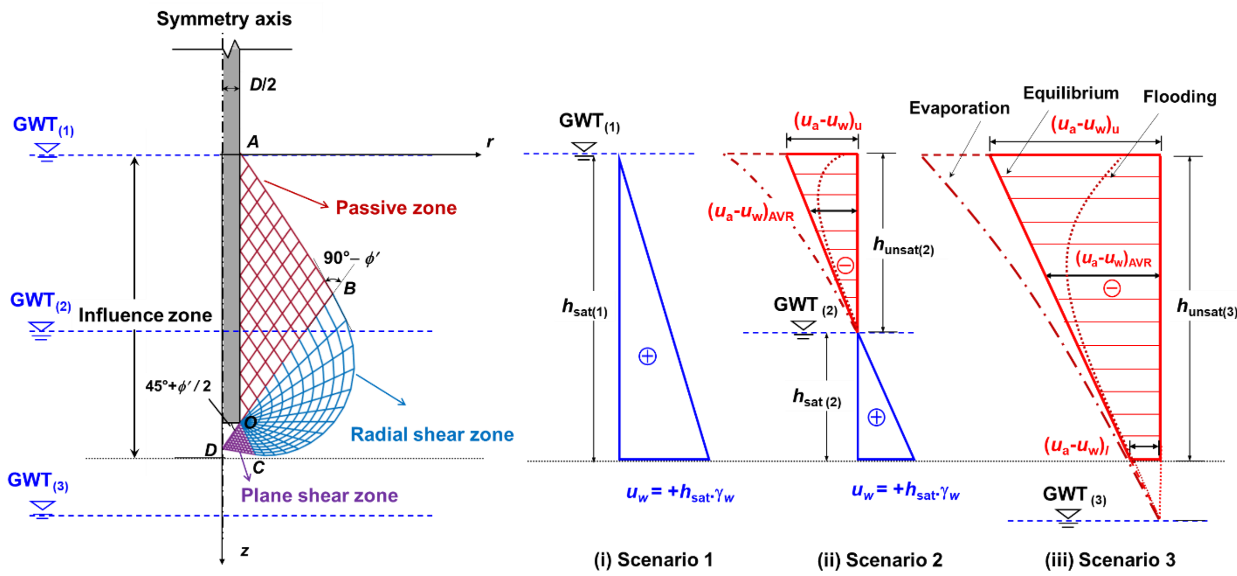

(a) (b)

Figure 4.5 (a) Mesh of the characteristic lines around the pile base and (b) Pore water pressure profile for three different scenarios

4.2.4 Computation procedures for different scenarios of GWTs

The term $\partial c_t/\partial z$ in Equations 4.8 and 4.10 depends on the distribution of soil suction profile along the depth. In this study, $\partial c_t/\partial z$ is equal to zero as the concept of average (i.e., representative) matric suction at the centroid of the influence zone near the pile tip is used in Equation 4.3 to compute c_t for the sake of simplicity. Many researchers (e.g., Oh and Vanapalli 2011, Vahedifard and Robinson 2016, Vanapalli et al. 2018, Zhang et al. 2020) suggest that using the average value as representative matric suction can provide reliable estimations of bearing capacity of foundations in unsaturated soils.

The contribution of matric suction towards the end-bearing capacity of single piles changes as the GWT depth varies. As illustrated in Figure 4.5(b), in this study, three different scenarios with varying depths of GWTs located above, within and below the influence zone were considered. The influence zone was assumed to be around 6–8*D* above the pile base and 0.7–4*D* below the pile base, which is consistent with Schmertmann (1978) and de

Ruiter and Beringen (1979). The pore-water pressure profile along the depth under the three different conditions is shown in Figure 4.5(b). The matric suction is linearly distributed under hydrostatic conditions (i.e., $(u_a - u_w) = -\gamma_w h_{unsat}$, where γ_w is the unit weight of water and h_{unsat} is the height above the GWT). In some circumstances, the matric suction profile becomes nonlinear under different moisture flux boundary conditions due to the influence of environmental factors.

For Scenario 1, the GWT is located above the influence zone around the pile tip. The soil in the influence zone is saturated and $(u_a - u_w)_{AVR}$ is zero. Total cohesion, (c_t) for computing the end-bearing capacity of piles in saturated soils is equal to the effective cohesion, (c'). For Scenario 3 where the GWT is located below the influence zone of the pile tip, the entire influence zone is in a state of unsaturated condition. $(u_a - u_w)_{AVR}$ is taken as the centroid of matric suction between the upper and lower limit of the matric suction, $(u_a - u_w)_u$ and $(u_a - u_w)_l$, respectively. Total cohesion (c_t) is computed by adding the apparent cohesion to effective cohesion c' considering the contribution of matric suction (i.e., Equation 4.3).

For Scenario 2, where the GWT is located within the influence zone, the average soil unit weight should be modified considering the influence of matric suction as follows:

$$\bar{\gamma} = \gamma' + (\gamma - \gamma')\frac{h_{unsat}}{h_z} \tag{4.21}$$

where $\bar{\gamma}$ is the modified average unit weight, γ' is the effective unit weight and h_z is the length of the influence zone. The remainder of the calculations will be the same as discussed for Scenario 3.

4.3 Validation and comparisons

4.3.1 Case studies in saturated soils (Scenario 1)

The end-bearing capacity of driven piles in saturated soils has been computed for 11 pile load tests. All the information related to the soil description from the site investigation, including CPT records for undertaking rigorous analyses using the proposed approach are summarized in Table 4.1. In these pile load tests, piles are driven into dense sands to transfer large loads from the topsoil to a stronger stratum below. The internal friction angle ϕ' is obtained from CPT records using the following relationship provided by Kulhawy and Mayne (1990) was used for certain soils that did not provide the information for ϕ':

$$\phi'\left(\text{degrees}\right)=17.6+11\log\frac{q_c}{\sqrt{100\sigma'_{\mathrm{v}}}} \tag{4.22}$$

where q_{c} is cone tip resistance. The square-shaped piles can be simulated by idealizing them as circular piles with equivalent cross-sectional areas to achieve the same shaft and base load (Poulos and Davis 1968). The predictions of pile end-bearing capacity were made using the proposed approach for Scenario 1. Comparisons between the measured and predicted end-bearing capacity of piles in saturated soils are shown in Figure 4.6. The predictions are in good agreement with the field measurements with a high coefficient of correlations (R^2) value.

4.3.2 Case studies in unsaturated soils (Scenario 2 and 3)

The predictions using the proposed approach are compared against the measurements for two pile load tests in unsaturated soils reported by Beringen et al. (1980) (for Scenario 2) and Fellenius et al. (2007) (for Scenario 3), respectively. The details of pile and soil properties for these two sites are summarized in Table 4.2.

Table 4.1. Summary of the pile load tests information used in the present study

Pile					Soil				
No.	Pile No.	*L* (m)	*B or D* (mm)[a]	Material and shape[b]	$q_{c,avg}$[c]	ϕ' (°)	Soil type at pile tip	Measured Q_b (kN)	**References**
1	J2	9.1	320	S, C	–	34	Sand	296	Tavenas (1970)
2	J3	12.2	320	S, C	–	34	Sand	356	Tavenas (1970)
3	J4	15.2	320	S, C	–	34	Sand	372	Tavenas (1970)
4	J5	18.3	320	S, C	–	34	Sand	372	Tavenas (1970)
5	A	8.0	280	C, C	3.0	30	Sand	60	Gregersen et al. (1973)
6	D/A	16.0	280	C, C	4.5	31	Sand	110	Gregersen et al. (1973)
7	FHW ASF	9.2	273	S, P	4.0	32	Sand	355	O'Neill (1988)
8	UBC3	16.8	324	S, P	2.0	31	Sand	315	Campanella et al. (1989)
9	TWN TP6	34.3	609	S, C	9.5	33	Sand	1650	Yen et al. (1989)
10	BGH D1	11.0	285	C, S	3.2	34	Sand	360	Altaee et al. (1992)
11	P1	16.8	610	C, S	6.0	35	Sand	689	Pando et al. (2003)

[a] Exterior width of square piles or the diameter of circular piles
[b] Material from which pile was made: S = steel; C= concrete. Pile shape: S = square; C = circular; P = pipe
[c] Average value of cone tip resistance (q_c) in the influence zone near the pile tip (Pile load tests reported by Tavenas (1970) have no information of average q_c value)

Table 4.2 The pile and soil properties in pile load tests for Scenario 2 and 3

	Pile		***Soil***						
	L (m)	*D* (mm)	Soil type	GWT (m)	γ (kN/m^3)	*w* (%)	c' (kPa)	ϕ'(°) tip	$q_{c,avg}$ (MPa)
Scenario 2									
Beringen et al. (1980)	5.25	356	Very dense sand	3.2	20	15-20	0	42	20
Scenario 3									
Fellenius et al. (2007)	6	350	Silty sand	11	18	16.2-22.5	2.0	36	5.1

The end-bearing capacity information was not available for the case studies summarized in Scenario 2 and 3 (see Table 4.2). For this reason, the total bearing capacity was computed and compared with the measured data information that was available. The total bearing capacity was obtained as the sum of pile shaft carrying and end-bearing capacity. The end-bearing capacity, q_b, was calculated using the proposed approach while the shaft carrying capacity, f_p, was obtained using the method proposed by Vanapalli and Taylan (2012), the equation of which is given below:

$$Q_{s(us)} = \left[c' + \beta(\sigma_v') + (u_a - u_w)(S^\kappa)(\tan\phi')\right]\pi DL \tag{4.23}$$

where β is the Burland-Bjerrum coefficient and σ_v' is vertical effective stress at the middle of the pile shaft. The coefficient β equals to $K\tan\delta$, where K is the lateral earth pressure coefficient and δ is the friction angle of the pile-soil interface. The value of K depends on various factors such as the method of pile installation, soil type, and the material of the pile, and can be related to the earth pressure coefficient at rest, K_0. Table 4.3 presents recommended values for the ratios K/K_0 and δ/ϕ. For both pile case studies, K is determined as $1.5K_0$ and δ/ϕ is 0.7 based on pile and soil type.

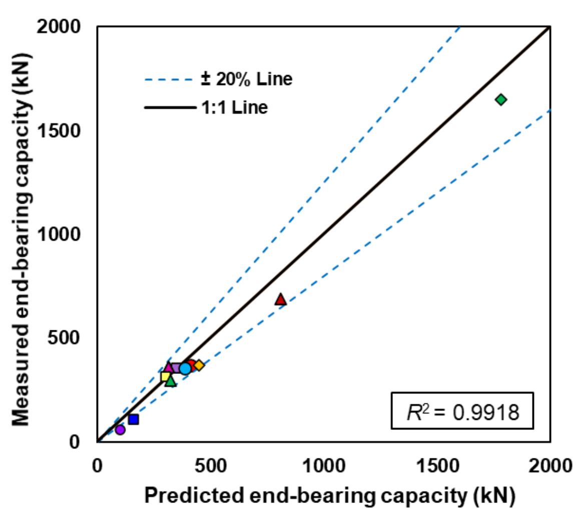

Figure 4.6 Comparisons between the predicted and measured end-bearing capacity for the case studies in saturated soils

Beringen et al. (1980) performed a series of pile load tests at Hoogzand/Oostermeer in the Netherlands to study the design of offshore pile foundations. The tested pile is 356 mm in diameter and 5.25 m in length. The upper 2 m of sand consists of different proportions of sand, silt and clay but is predominantly sand. Underneath is a layer of very dense and overconsolidated sand at a depth of between 2.5 m to 10 m. The saturated and unsaturated unit weights were 20 kN/m^3 and 21 kN/m^3, respectively. Since the GWT is located at a depth of 3.2 m, which is within the influence zone, the soil unit weight was modified as 20.3 kN/m^3 using Equation 4.21. The water content in the influence zone ranges from 15% to 20% and the void ratio varies between 0.5 to 0.55. Prediction models for the SWCC are desirable in engineering practice where time and/or resources are limited and the actual SWCC is not available. The van Genuchten (1980) equation is widely used for predicting the effective degree of saturation, S_e as a function of matric suction. The relationship can be expressed in terms of the degree of saturation or volumetric water content as given below:

$$S_e = \frac{S - S_\mathrm{r}}{1 - S_\mathrm{r}} = \frac{\theta - \theta_\mathrm{r}}{\theta_\mathrm{s} - \theta_\mathrm{r}} = \left[\frac{1}{1 + \left(\alpha \left| u_\mathrm{a} - u_\mathrm{w} \right| \right)^n} \right]^{(1-1/n)} \tag{4.24}$$

where α and n are fitting parameters. The recommended values of α and n given by Wösten et al. (1999) and Carsel and Parrish (1988) based on soil classifications are utilized in this study to predict the SWCC of unsaturated soils, as presented in Table 4.4. The van Genuchten (1980) model parameters α and n recommended by Wösten et al. (1999) for coarse soil were determined as 0.0383 and 1.1377, respectively, based on the soil classification information. The values of α = 0.075, n = 1.89 recommended by Carsel and Parrish (1988) for sandy loam were used for predicting the SWCC. These two predicted SWCCs are presented in Figure 4.7. '*This study* ^{a}' and '*This study* ^{b}' in Figure 4.8 represent the computed results using recommended α and n values by Wösten et al. (1999) and Carsel and Parrish (1988), respectively.

Table 4.3 Recommended values of K and δ

Reference	Recommended values of K and δ	Pile or soil type
Kulhawy (1984)	$K/K_0 = 0.7\text{-}1.2$	Smooth steel pipe piles, H piles or concrete piles (Small-displacement piles)
	$K/K_0 = 1.0\text{-}2.0$	Smooth steel pipe piles, H piles or concrete piles (Large-displacement piles)
Das (2004)	$K/K_0 = 1.0\text{-}1.4$	Small-displacement piles
	$K/K_0 = 1.0\text{-}1.8$	Large-displacement piles
Yang et al. (2006)	$K/K_0 = 1.2\text{-}1.5$	Driven steel pile, alluvium and completely decomposed granite
Kulhawy (1984)	$\delta/\phi = 0.5\text{-}0.7$	Smooth steel pipe piles or H-piles
	$\delta/\phi = 0.8\text{-}1.0$	Smooth concrete piles
Yang et al. (2006)	$\delta/\phi = 0.7\text{-}0.9$	Driven steel pile, alluvium and completely decomposed granite

Table 4.4 van-Genuchten parameters for two SWCC models

SWCC model	Soil texture	θ_r	θ_s	α (L^{-1})	n (dimensionless)
SWCC-A (Wösten et al. 1999)	Coarse (Clay < 18% and sand > 65%)	0.025	0.403	0.0383	1.3774
	Medium (18% < clay < 35% and 15% < sand or clay < 18% and 15% < sand < 65%)	0.010	0.439	0.0314	1.1804
	Medium Fine (Clay < 35% and sand < 15%)	0.010	0.430	0.0083	1.2539
	Fine (35% < clay < 60%)	0.010	0.520	0.0367	1.1012
	Very fine (60% < clay)	0.010	0.614	0.0265	1.1033
SWCC-B (Carsel and Parrish 1988)	Clay	0.068	0.38	0.008	1.09
	Clay loam	0.095	0.41	0.019	1.31
	Loam	0.078	0.43	0.036	1.56
	Loamy sand	0.057	0.41	0.124	2.28
	Silt	0.034	0.46	0.016	1.37
	Silt loam	0.067	0.45	0.020	1.41
	Silty clay	0.070	0.36	0.005	1.09
	Silty clay loam	0.089	0.43	0.010	1.23
	Sand	0.045	0.43	0.145	2.68
	Sandy clay	0.100	0.38	0.027	1.23
	Sandy clay loam	0.100	0.39	0.059	1.48
	Sandy loam	0.065	0.41	0.075	1.89

To validate the proposed approach, further comparisons with other methods (i.e., semi-empirical approaches and direct CPT methods) have been made. Table 4.5 presents three semi-empirical approaches proposed by Vanapalli et al. (2018) that have been commonly referenced for predicting the pile end-bearing capacity in unsaturated soils. In addition, direct CPT methods have been widely used during the last several decades for evaluating the bearing capacity of full-scale piles from CPT parameters (i.e., cone tip resistance q_c and sleeve friction f_s) based on scale relationships between the cone penetrometer and a single pile (e.g., Schmertmann 1978, Karlsrud et al. 2005, Schneider et al. 2008). Four well-known direct CPT methods that provide design equations for evaluating both q_b and f_p are summarized in Table 4.5.

Figure 4.8(a) shows the comparisons of total bearing capacity using all different methods with measured data. The measured total ultimate load is 1950 kN whereas the computed values using two SWCC models in the proposed approach are 1815.6 kN and 1895 kN, respectively, which are slightly lower than the actual value. The difference between the field measurement and the predictions is approximately 6.8% and 2.8%, respectively. The modified Janbu method, as well as the direct use of CPT methods, suggested by Schmertmann (1978) and de Ruiter and Beringen (1979) also show good agreement with measured values.

Fellenius et al. (2007) reported static load test results for a square pile with a width of 350 mm embedded to a length of 6 m driven in residual soils. The soil at the site is a weathered granite that is subject to high mean annual precipitation. The grain-size analysis shows that the soil consists of 10% clay, 30% silt, 40% sand and 20% gravel, which are classified as “sand and silt with some gravel and some clay”. The ground water table was located at a depth of 11 m. The water content of the soil varies from 16.2% to 22.5% and the degree of saturation ranges from 56 % to 86%. A CPTu profile was carried out and the pore water pressure measurement (i.e., u_2 profile) within 8 m depth from the natural ground surface shows a negative value of 10 to 20 kPa (i.e., matric suction), indicating that the soil is unsaturated. The average cone resistance $q_{c,avg}$ in the influence zone is 5.1 MPa. The effective cohesion is estimated as 2 kPa according to Ortiz et al. (1986).

Table 4.5 Summary of different methods for estimating the bearing capacity of piles

Method	Reference	Unit end-bearing capacity	Unit shaft carrying capacity	Average zone of q_c
Static analysis	Vanapalli et al. (2018)[a]	Modified Terzaghi (1943): $q_b = c_t N_c s_c + q' N_q + \frac{1}{2}\gamma D N_\gamma s_\gamma$ Modified Hansen (1970): $q_b = c_t N'_c d_c + \eta q' N'_q d_q + \frac{1}{2}\gamma D N'_\gamma$ Modified Janbu (1976): $q_b = c_t N^*_c + q' N^*_q + \frac{1}{2}\gamma D N^*_\gamma$	Same with Vanapalli and Taylan (2012): $Q_s = \begin{bmatrix} c' + \beta(\sigma'_v) + \\ (u_a - u_w)(S^\kappa)(\tan\phi') \end{bmatrix} \pi DL$	–
Direct CPT	Schmertmann (1978)[b]	$q_b = (q_{c1} + q_{c2})/2 \leq 15$ MPa (in sands) and 10 MPa (in silty sands)	In *sand*: $Q_s = \alpha_{sand} \begin{bmatrix} \sum_{d=0}^{8D} \frac{d}{8D} f_s A_s + \\ \sum_{d=8D}^{L} f_s A_s \end{bmatrix}$	8*D* above & 0.7*D* to 4*D* below
	Dutch method (de Ruiter and Beringen 1979)[c]	In *sand*: similar to Schmertmann (1978)	In *sand*: q_f = min [f_s, q_{ca}/300 for compression, q_{ca}/400 for tension, 120 kPa]	Same with Schmertmann (1978)
	LCPC method (Bustamante and Gianeselli 1982)[d]	$q_b = k_b\, q_{eq\,(tip)}$	$q_f = q_{eq\,(side)} / k_s$	1.5*D* above &1.5*D* below
	Unicone method (Eslami and Fellenius 1997) [e]	$q_b = C_t\, q_{eg}$	$q_f = C_s\, q_E$	2*D* or 8*D* above & 4*D* below

Note: [a]q' = vertical effective stress at pile base; N_c, N_q, N_γ, N_c', N_q', N_γ', N_c*, N_q* and N_γ*: bearing capacity factors; s_c, s_γ = shape factors (s_c = 1.3 and s_γ = 0.6 for round pile foundation); η = 1.0 for all except the Vésic (1975) bearing capacity factors; d_c, d_q = depth factors [b]q_{c1}= the minimum average q_c of zones 0.7*D* to 4*D* below the pile tip; q_{c2} = the average minimum q_c of zones 8*D* above the pile tip; α_{sand} depends on the *L*/*D* ratio; [b]q_{ca}= the arithmetic average of q_c in the influence zone; [c]q_{eq}= equivalent average of q_c values; k_b = 0.375 for sand and gravel; k_s = 30–150 depends on the soil type, pile type and installation procedure [e]C_t = the toe correction coefficient (generally taken as 1, for D > 0.4 m, C_t =1/(3*D*)); q_{eg} = the geometric average q_c values after correction for pore pressure on shoulder and adjustment to effective stress; C_s = shaft correlation coefficient; q_E: the corrected cone resistance

Fellenius et al. (2007) suggest that the dominant soil type is silty clay to silty sand according to the CPTU-based soil classifications. The van Genuchten (1980) parameters α and n recommended by Wösten et al. (1999) for medium soil were determined as 0.0314 and 1.1804 respectively. α = 0.010, n = 1.23 recommended by Carsel and Parrish (1988) for silty clay loam were used. Figure 4.8(b) shows the comparisons between predictions using other methods and the proposed approach with two different SWCC prediction models. The measured pile-head load-displacement curve is superimposed in Figure 4.8(b). The ultimate limit load is 1312 kN while the computed values using the two SWCC models are 1329 kN and 1096 kN, respectively, with a difference of approximately 1.2 % and 16.5%.

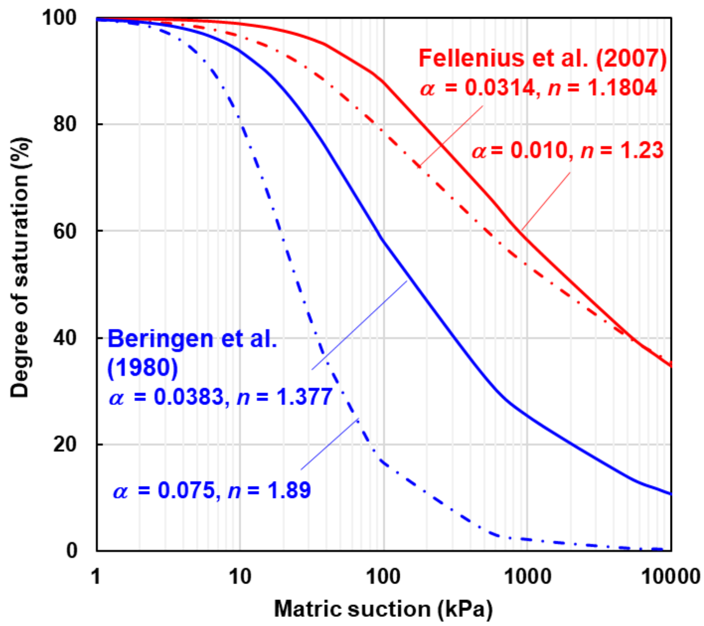

Figure 4.7 The predicted SWCCs using different van Genuchten (1980) parameters for Scenario 2 and 3

The modified Terzaghi's method provides conservative estimates for most of the cases because the assumption of Terzaghi (1943)'s failure pattern arises only from the soil below the base of the foundation which is not consistent with the actual soil movement. The modified Janbu's (1976) method assumes a reliable failure surface around the pile base that is shown in Figure 4.4(a); hence it provides better agreement with the measured values. Among four direct CPT methods, the method presented by Schmertmann (1978) provided the most consistent predictions with the measured pile bearing capacity. As reported by Fellenius (2007) and Niazi and Mayne (2013), CPT methods are empirically derived for specific piles tested in certain geomaterials, and therefore they need to be calibrated for their use in soils of different regions that likely have different geological histories. The empirical correlations between CPT and pile static load tests depend largely on the specific stress histories at the site that are influenced by the soil formation and geology. Due to this reason, the CPT methods are sensitive and provide results that may agree or disagree with the measured data compared to static pile tests.

The predictions for three different scenarios based on the available information suggest that the proposed approach can reasonably estimate the end-bearing capacity with relatively good agreement with measured results. CPT methods can capture the actual behavior of soil including the contribution arising from matric suction. In addition, one of the key advantages of the proposed analytical method is that it can predict the pile bearing capacity considering environmental factors such as rainfall, evaporation, or evapotranspiration. The matric suction profile variations affected by these factors can be employed in the program so that the change in ultimate bearing capacity can be predicted using the proposed method.

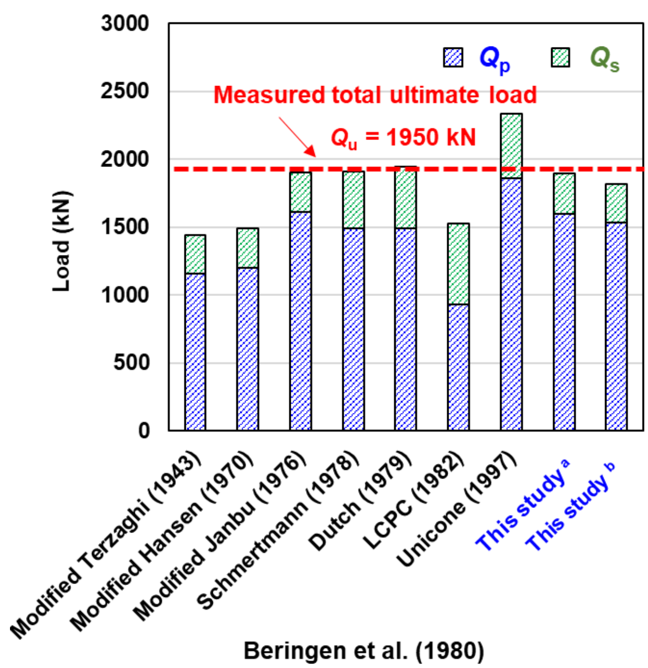

(a)

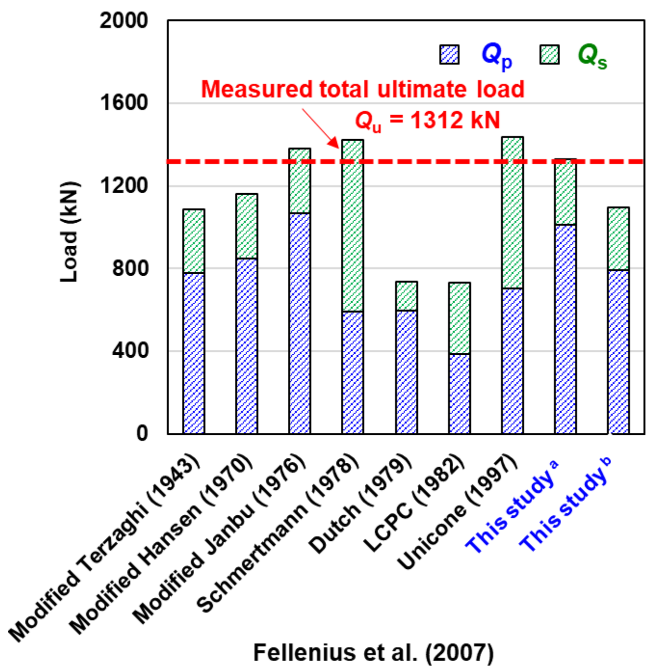

(b)

Figure 4.8 Comparisons between measured and computed pile bearing capacity using different methods for (a) Scenario 2 and (b) Scenario 3

4.4 Finite element model

In recent years, with the rapid growth of computational techniques, numerical analyses based on the finite element (FE) methods have been extensively used for simulating the behavior of pile foundations considering the nonlinear response of soils. Therefore, in this study, finite element analysis (FEA) was undertaken to model a pile load test reported by Kong et al. (2005) using FE software ABAQUS. Kong et al. (2005) conducted a model pile load test in unsaturated sands with different dry density conditions under various matric suction values. The gassy sand, which contains some clay particles, is collected from 50 m deep stratum in Hangzhou Bay Bridge site, China. The SWCC for two fine sand samples is presented in Figure 4.9. During the test, a stainless-steel pile with a length of 30 mm and an outside diameter of 18 mm is first penetrated 180 mm depth of gassy sand. Then the static load test is performed to investigate the ultimate bearing capacity of pile foundations after the installation of the pile. These two stages of pile loading were simulated with the aid of ABAQUS and the influence of matric suction was considered in the numerical model.

The measured results from Kong et al. (2005) were compared with the numerical predictions as well as results from the proposed analytical method.

A 2*D* axisymmetric model around the central line of the pile is established considering the axisymmetric geometry of the pile-soil system and loading conditions. Since pile penetration is a dynamic process, ABAQUS/Explicit solver was utilized for this stage due to the distinct advantages of improving calculation time. The following pile load test is a static loading process; for this reason, it was calculated with ABAQUS/Standard (i.e., implicit solver). In ABAQUS, it is not possible to incorporate both the implicit and explicit solvers from a single analysis (Dassault Systèmes Simulia 2016). Therefore, in this study, two models were established to separate dynamic and static analysis. In the first model, dynamic analysis was performed using ABAQUS/Explicit to simulate pile penetration. Then, the model results of soil elements such as deformed soil mesh, and its associated stress and strain state at the end of the analysis were imported to the second model as the initial state so that the static analysis can continue using ABAQUS/Standard solver.

Since the elastic modulus of the pile is significantly greater than that of soil, the pile is modelled as a rigid body in the FEA. The whole pile region is defined as a rigid body using rigid body constraints; this facilitates in constraining the motion of the whole pile to the motion of a reference point. The reference point (RP) on the top of the pile is shown in Figure 4.10. Sheng et al. (2005) found that a pile with a flat end or a cone angle larger than 90° can hardly be driven into soil in the finite element modelling using ABAQUS, due to massive element distortion and convergence difficulties. They also concluded that if the cone angle is less than 60˚, the analysis requires relatively small-time steps that can significantly increase analysis time. Therefore, the pile tip is conical with a cone angle of 60˚ in the current numerical analysis which is consistent with the approach used by Sheng et al. (2005) and Rooz and Hamidi (2019). The soil is modelled as a linear-elastic, perfectly plastic material based on Mohr-Coulomb constitutive model. The soil properties of two fine sand samples that are used in the FEA model are summarized in Table 4.6. The Poisson's ratio is assumed to be 0.3 for sand. Using Equation 4.3, the total cohesion for three different soil samples of sand #1 with uniform matric suction at 20, 50 and 100 kPa are calculated as 9.5, 16.2 and 25.4 kPa, respectively. Similarly, the computed total cohesion for soil samples of sand #2 with matric suction at 20, 50 and 100 kPa are 10.8, 18.7 and 30.8 kPa, respectively. The elasticity of modulus of both sands with (u_a - u_w) = 0 (i.e., saturated), 50 and 100 kPa are 7000, 14286 and 10811 kPa, respectively, which are derived from the deviator stress versus axial strain curves of triaxial tests under various matric suction (Kong et al. 2005). Since the deviator stress versus strain curve for sand with (u_a - u_w) = 20 kPa is not provided, it is estimated to be 9914 kPa using linear interpolation method. Figure 4.10 shows the geometry and mesh of the axisymmetric model. Four-node quadrilateral axisymmetric elements (CAX4) were used to model both pile and soil.

Table 4.6 The soil parameters of gassy fine sand used in the FEA model

Soil	Dry density, γ_d (g/cm^3)	Matric suction (kPa)	SWCC		Effective cohesion, c' (kPa)	Internal friction angle, ϕ' (°)	Total cohesion, c_a (kPa)	Modulus of elasticity, E_s (kPa)
			AEV (kPa)	Residual suction values (kPa)				
Fine sand #1	1.50	20	2.5	15.0	2.0	34.5	9.5	9914
		50					16.2	14286
		100					25.4	10811
Fine sand #2	1.63	20	3.0	20.0	2.0	34.5	10.8	9914
		50					18.7	14286
		100					30.8	10811

Unlike the numerical simulation of bored piles, the pile penetration progress involves large stress and strain change and severe distortion of soil elements. Several researchers highlighted challenges associated with large deformations (Wang et al. 2015, Abu-Farsakh et al. 2015). The standard Lagrangian approach, which is typically used in ABAQUS, often leads to contact problems, mesh distortions and terminating the analysis when the process undergoes large deformations. Therefore, an Arbitrary Lagrangian-Eulerian (ALE) adaptive mesh technique was applied to the soil elements adjacent to the driven pile to encounter convergence difficulties. The ALE adaptive mesh method allows the mesh to deform independently of the material but the mesh topology (i.e., number of elements and nodes and their connectivity) is maintained. Subsequently, the solution variables can be remapped from the old mesh to the new mesh. The ALE adaptive mesh method can generate a smoother mesh at regular intervals to reduce element distortion and maintaining a high-quality mesh even under excessive deformation. This method has been commonly used to simulate the penetration of conically tipped piles in ABAQUS (Zhang et al. 2013, Wang et al. 2015, Yang et al. 2020). Figure 4.10 shows the region of the ALE adaptive mesh domain. The soil elements near the pile were subjected to ALE adaptive mesh control. The default remeshing frequency, which refers to how often the mesh is adapted, was set to once every 5 increments as a typical adaptive mesh without Eulerian boundaries requires adaptive meshing every 5–100 increments (Dassault Systèmes Simulia 2016). The default number of mesh sweeps was set to 1. During every sweep, the nodes are relocated based on the current locations of adjacent nodes to reduce element distortion.

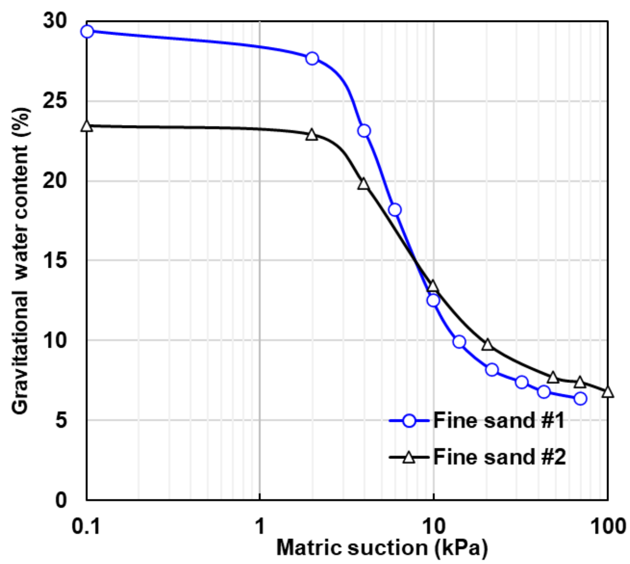

Figure 4.9 SWCC of two soil samples from gassy sand (modified after Kong et al. 2005)

Numerical analyses were performed in three main steps. In the first step, before the initiation of pile driving process, the pile is initially placed right above the soil surface. A small opening is made on the soil below the pile tip to facilitate the computational penetration of the pile upon driving (Mabsout and Tassoulas 1994), as shown in Figure 4.10. Gravitational stresses are applied to both pile and soil to obtain a geostatic equilibrium initial state. In the second step, the prescribed boundary conditions were released and the interaction between pile and soil are activated. A prescribed vertical displacement of 180 mm was applied on the pile head to simulate the pile penetration at a constant loading velocity. The pile-soil interface was modelled by a surface-to-surface contact model, where the pile was regarded as the master surface and the soil as the slave surface. The contact between pile and soil surfaces is governed by kinematic constraints in the normal and tangential directions. In the last step, the model results including deformed mesh and its associated stress state of soil from the second step were imported at the beginning of this step. The static load test was then simulated by applying an additional displacement on the pile head until failure. The total pile resistance is taken as the vertical component of the total reaction force on the pile.

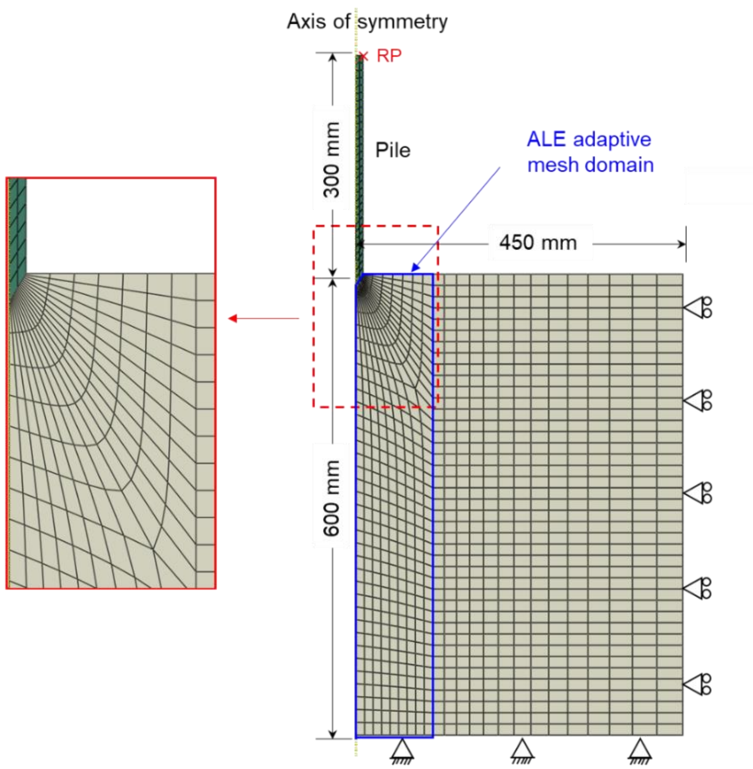

Figure 4.10 Axisymmetric model and ALE mesh domain for the simulation of pile penetration

4.4 Results and Discussions

The soil around the pile was pushed downwards and sideways during the pile penetration, which can be clearly seen from the deformed mesh in Figure 4.11(a). It can also be seen that due to the implementation of the ALE technique, the soil elements around the pile are not severely distorted even though the deformation and displacement in the pile-soil interface are large. The soil elements directly under the pile cone are compressed. The soil zone adjacent to the pile shaft is under the plastic state. As shown in Figure 4.11(a) and (b), the plastic zone enlarges and moves downwards as the pile is driven to a greater soil depth. Figure 4.11(c) shows the computed stress contour at the end of pile penetration. The radial stress (S11) is high near the pile cone and reaches a maximum value of 1109 kPa at the intersection of the pile shaft and cone. It is observed that the shape of radial stress distribution around the pile tip has a logarithmic spiral failure surface as assumed in the proposed analytical method. The vertical stress (S22) has its maximum value of 684.1 kPa at the same crossing point as the maximum S11. Compared with the radial stress bulb, the vertical stress concentration bulb below the pile cone is larger in the vertical direction (extends to 4*D*), and smaller in the radial direction (extends to 1.8*D*). The maximum shear stress (S12) is 430.4 kPa, which is mostly concentrated at the pile cone. The stress concentration occurring near the cone shoulder is due to the inclined surface of the cone and the interface friction.

Figure 4.12 shows the comparisons between the FEA predictions and measurements reported by Kong et al. (2005) for two kinds of fine sands with matric suction at 20 kPa. The load versus displacement curves derived from the FEA are in good agreement with the experimental data for both sands. This agreement validates the feasibility of using the ALE technique and incorporating the effect of matric suction in modelling the driven piles in unsaturated soils.

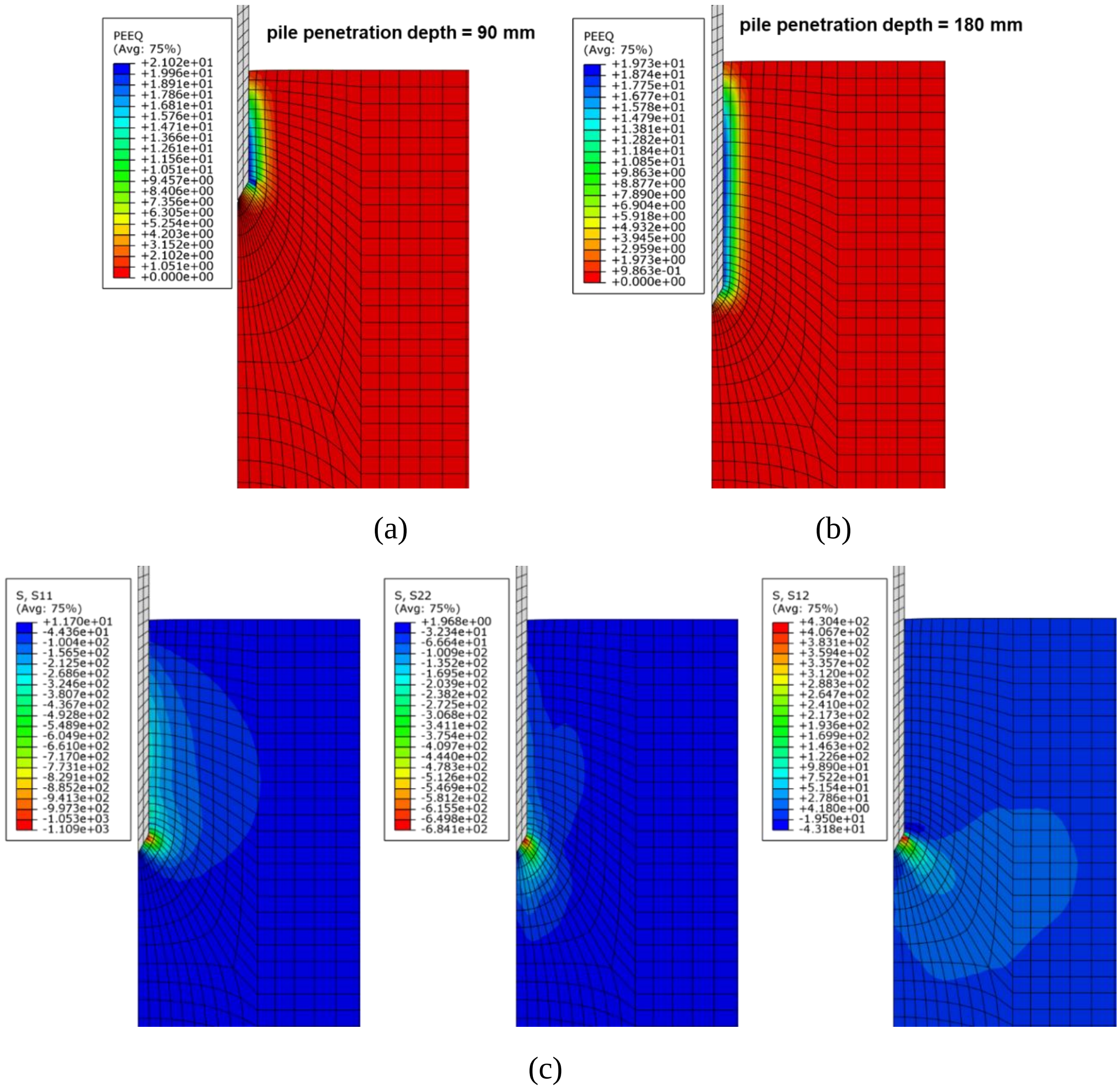

Figure 4.11 Typical stress contours at the end of pile penetration for fine sand#1 with (u_a-u_w) = 50kPa (a) PEEQ at Pile penetration depth = 90 mm (b) PEEQ at Pile penetration depth = 180 mm (c) stress contours (PEEQ: equivalent plastic strain; S11: radial stress; S22: vertical stress; S33: circumferential stress)

The ultimate bearing capacity computed from the proposed analytical method is also compared against the measurements from Kong et al. (2005). The coefficients K = 1.2K_0 and $\delta = 0.7\phi$ are used in Equation 4.23 for computing the shaft carrying capacity of the pile. The total bearing capacity is obtained by summing the end-bearing and shaft carrying capacity. Table 4.7 presents the ultimate bearing capacity of piles in unsaturated gassy sands with matric suction at 20, 50 and 100 kPa using both FEA and analytical methods.

From Figure 4.13, all the predictions from both methods are within the 20% deviation line compared with the measurements. The FEA predictions are consistent with the measured data with a high coefficient of correlations (R^2) value of 0.9966. A few predictions from the proposed method overestimate the ultimate bearing capacity due to the errors caused by the separation of computing the end-bearing and shaft capacity.

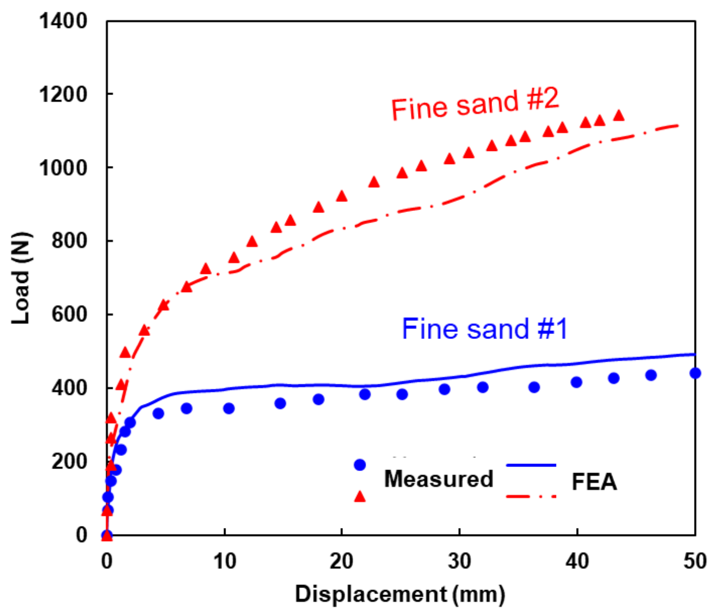

Figure 4.12 Comparisons between the FEA results and measured data from Kong et al. (2005) for soil with (u_a - u_w) = 20 kPa

Table 4.7 The ultimate bearing capacity of piles in gassy sand using different methods

	Fine sand#1					Fine sand#2				
Matric suction (kPa)	Measured Q_u (N)	FEA Q_u (N)	Proposed method			Measured Q_u (N)	FEA Q_u (N)	Proposed method		
			Q_b (N)	Q_s (N)	Q_u (N)			Q_b (N)	Q_s (N)	Q_u(N)
20	304	332	263	99.8	362.8	495	565	398.9	100.2	499.1
50	378	453	311.6	168	479.6	727	791	512.2	188.7	700.9
100	555	612	450.2	262.6	712.8	1054	1178	662.9	315.8	978.7

The results from this study suggest that the FEA can provide results that are close to the measured values than the proposed analytical method. This can be attributed to the advantage of taking account of the friction angle dependency and considering different soil shear strength values for different stress level, in the FEA in comparison to the proposed method. Another advantage of the FEA lies in its ability to generate output data, such as load-displacement behavior and stress distribution along the pile under different displacements, whereas the proposed analytical method restricted to providing only the end-bearing capacity of the pile. However, simulating a driven pile using FE approaches can contribute to convergence problems both in dynamic and static analyses. Solving large deformation geotechnical problems can be challenging especially when dealing with more complex soil-structure interactions such as the driven piles behavior. The proposed analytical method, on the other hand, provides geotechnical engineers with relatively quick and reasonable and reliable estimations of the bearing capacity for a driven pile embedded in unsaturated soils. It only requires input parameters that include pile (i.e., length, diameter, and material), soil properties (i.e., saturated shear strength parameters c', $\phi'$and unit weight γ) and the SWCC. This method is promising for use in conventional geotechnical engineering practice for the design of pile foundations both in saturated and unsaturated soils.

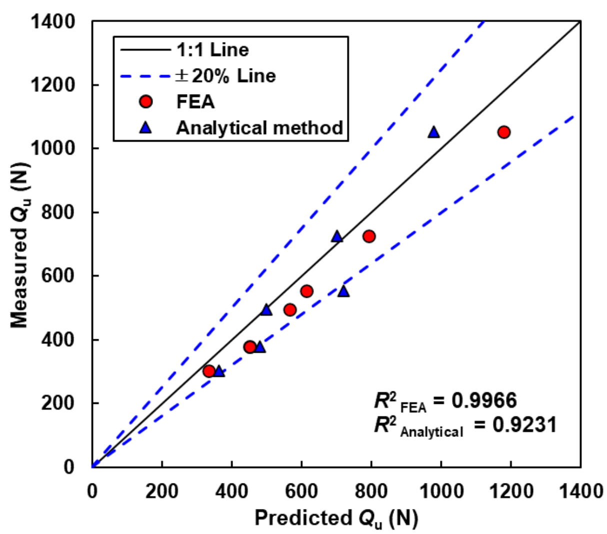

Figure 4.13 The predicted and measured ultimate bearing capacity of piles in unsaturated soils

4.5 Conclusions

In this study, a generalized analytical approach has been developed for determining the end-bearing capacity of driven piles for both saturated and unsaturated soils based on the stress characteristics method (SCM) which is also referred to as slip line theory. The novel contribution of this study includes the development of a rational approach for the interpretation and prediction of the end bearing capacity of driven piles extending the principles of unsaturated soil mechanics. The finite-difference forms of the governing equations of the SCM were solved with the aid of a MATLAB program that was developed with a feature of providing graphical output to visualize the results. Eleven case studies of driven piles in saturated soils and two in unsaturated soils were examined. The comparisons showed that the proposed method that is based on the SCM, and the principles of unsaturated soil mechanics provide reasonable predictions. Lastly, numerical analysis was undertaken to simulate a model test of driven piles in unsaturated sand reported by Kong et al. (2005). Both dynamic and static analysis was involved in the numerical analysis to simulate the pile driving and the following pile loading. ALE adaptive mesh technique was applied to prevent severe distortion of soil elements due to the large deformation between the pile and soil interface during the pile penetration. Both FEA predictions and computed ultimate bearing capacity of piles using the proposed approach are in good agreement with the measured data. The advantages of the proposed analytical method providing relatively quick and reliable estimations of the bearing capacity for a driven pile embedded in unsaturated soils are highlighted.

This study highlights the need for considering the influence of matric suction for the reliable design of pile foundations in unsaturated soils. The proposed SCM approach presented in this paper is robust yet simple. The required information only includes pile properties, the shear strength parameters of the saturated soil and the SWCC. Hence, the proposed approach is of significant interest for practicing engineers for implementing the rational design of driven piles extending the mechanics of saturated and unsaturated soils.

CHAPTER 5

NONLINEAR ANALYSIS OF LOAD-DISPLACEMENT BEHAVIOR OF SINGLE PILE AND PILE GROUPS IN UNSATURATED SOILS

5.1 Introduction[4]

Many regions in the world are experiencing drying trends because of global warming effects, especially in Africa, southeast of the United States, eastern Australia and Eurasia (Dai 2013, Ma and Yang 2017, Deng et al. 2020). The arid and semi-arid regions of the world cover 1.9 × 10^7 km^2 and 2.3× 10^7 km^2, respectively that account for 13 and 15 % of the Earth's land surface and represent the most common habitat on earth after oceans (Huang et al. 2016, Mares 2017, Meslier and DiRuggiero 2019). The natural groundwater table (GWT) is typically at a great depth in semi-arid and arid regions and the soils above it are in a state of unsaturated condition. Unsaturated soils are tri-phase materials comprised of solids (i.e., soil particles), liquid (i.e., water) and gas (i.e., air). The air-water interface has a significant impact on the behavior of unsaturated soils since it generates capillary tension within the soil skeleton that is strongly related to the soil suction that contributes towards improving the mechanical behavior of unsaturated soils (Fredlund and Rahardjo, 1993). Therefore, the hydraulic and mechanical properties of unsaturated soils are complex in comparison to saturated soils.

Conventional pile foundations are typically long slender axial columns that have been used for centuries to support structures such as high-rise buildings, bridges, and transmission towers. In the current foundation engineering practice, pile foundations in some scenarios are used as single piles to transmit loads from the superstructure to deeper strata. However, in many scenarios they are installed in groups to carry larger loads and alleviate settlement

[4] The contents presented in this chapter are from a manuscript that has been submitted to an international journal for review: **Cheng, X.**, & Vanapalli, S. K. Nonlinear analysis of load-displacement behavior of single pile and pile groups in unsaturated soils (*Under peer review with an international journal*)

problems. The analysis of the load-displacement response of pile groups is a three-dimensional problem. It is quite challenging to estimate the nonlinear behavior of pile groups under axial loading. Several researchers proposed theoretical methods to investigate the behavior of single piles and pile groups. One of the widely used methods, load transfer method (LTM), is based on the load-displacement relationship at the pile head extending the Winkler model (Coyle and Reese 1966). In their method, the soil was assumed as a linear-elastic material and employed the concentric cylinder model to describe the attenuation of shear stress with a radial distance from the pile. These idealizations have been used to establish linearly elastic springs for axially loaded piles which are widely used in practice. Following the same approach, a variety of linear or nonlinear load transfer models were developed, such as the linear-elastic model (Randolph and Wroth 1978, Verbrugge 1981, Chow 1986), the elastic-perfectly plastic model (Bagulin et al. 1982, Matyas and Santamarina 1994), the power law model (Vardanega et al. 2012), the hyperbolic model (Kraft et al. 1981, Hirayama 1990, Zhu and Chang 2002, Zhang et al. 2010), and the trilinear model (Frank and Zhao 1982, Frank 1985, Liu et al. 2004). The LTM for single piles has also been extended to analyze the nonlinear responses of pile groups considering the group effects (Chow 1986, Lee and Xiao 2001, Wang et al. 2012, Zhang and Zhang 2012, Comodromos et al. 2016). The applicability of these theoretical methods for pile groups has been well-established from case studies and numerical results over the last two decades. In addition, some rigorous computer-based methods have been developed by researchers, such as the boundary element method (BEM) which is based on elastic continuum theory to model the elastic behavior of soils (e.g., Banerjee and Davis 1978, Mendonca and De Paiva 2003, Ai and Han 2009, Leung et al. 2010), and the finite element method (FEM) in which not only the nonlinear behavior of soil can be considered, but also the processes of pile construction can be simulated (e.g., Pressley and Poulos 1986, Comodromos et al. 2009, Ladhane and Sawant 2016). However, previous studies have mainly focused on dry or saturated soils. The current design codes for pile foundations assume the soil is saturated ignoring the contribution of matric suction in unsaturated soils. Such approaches can lead to unreliable estimations both with respect to load carrying capacity and settlement behavior.

In recent years, several researchers developed tools for the design of pile foundations in unsaturated soils. Several studies that focused on investigating the behavior of piles in unsaturated soils have highlighted the need for considering the influence of matric suction. For example, matric suction has been found to contribute towards an increase in the ultimate bearing capacity of single piles by 2-5 times in unsaturated coarse-grained soils (Vanapalli et al. 2018) and 2-6 times in fine-grained soils (Vanapalli and Taylan 2012, Fattah et al. 2014, Pujiastuti et al. 2022). There are limited experimental studies that were conducted to investigate the load-displacement behavior of pile groups in unsaturated soils (Al-Khazaali and Vanapalli 2019, Al-Omari et al. 2019, Pujiastuti et al. 2022). The results from pile load tests suggest that the ultimate bearing capacity of pile groups increases significantly due to the contribution of matric suction towards the shear strength and stiffness of unsaturated soils. Those studies provide insight into the pile-soil interaction and the matric suction contribution in unsaturated soils. However, the load transfer mechanism of pile foundations embedded in unsaturated soils has not been fully investigated in the literature. Therefore, more rigorous methods are necessary for the rational design of pile foundations in unsaturated soils which requires a better understanding of the principles of unsaturated soil mechanics combined with the load transfer mechanisms.

The focus of this study is directed to investigate the influence of unsaturated conditions on the performance of single piles and pile groups under axial loadings. A modified load transfer method (MLTM) is first proposed to predict the load-displacement response of single piles considering the nonlinear shear strength and modulus of elasticity of unsaturated soils with respect to matric suction. The nonlinear relationship between the pile shaft shear stress and pile-soil relative displacement along the pile shaft is described by a hyperbolic function, while the pile base resistance and displacement at the pile base follow a bilinear model. The proposed analytical approach was then extended for the analysis of pile groups considering the interaction effects between individual piles in a group. Iterative procedures for obtaining the solutions to load-displacement curves of both single pile and pile groups are developed using MATLAB. The proposed approach was validated against two single pile tests in the field on one instrumented bored pile in Piedmont residual soil in Atlanta and another in the residual soil in Portugal. A model pile group test from the literature was also used to validate the proposed approach for the analysis of pile groups. In addition, 3D FEA is performed to simulate the behavior of pile groups in unsaturated soils using ABAQUS software. The conventional Mohr-Coulomb model used in ABAQUS does not have the capability for taking account of the nonlinear shear strength of unsaturated soils. Thus, a user-defined subroutine (USDFLD: user subroutine to redefine field variables at a material point) that can be incorporated into constitutive relationships is written and implemented to model the nonlinear mechanical behavior of unsaturated soils with respect to matric suction. Good comparisons were observed between both the analytical method and numerical analysis with the experimental data. The proposed methods can provide valuable insight into implementing the unsaturated soil mechanics into the rigorous design of both single piles and pile groups in unsaturated soils.

5.2 Background

The LTM describes the pile shaft and base resistance mobilization as functions of axial pile-soil relative displacement (Frank et al. 1991). The pile is divided into several segments of equal lengths for extending the LTM (Figure 5.1(a)). The nonlinear interaction between a pile segment and surrounding soil can be replaced by a series of independent Winkler springs, which are distributed along the pile shaft and at the pile tip to represent the mobilization of the pile shaft shearing (*t-z* curve) and end bearing (*q-z* curve), respectively. Using the *t-z* curve or *q-z* curve, the nonlinear relationship between the pile shaft shear stress or end bearing resistance and relative axial displacement can be described mathematically.

The relationship between shaft shear stress and pile-soil relative displacement is commonly described as a hyperbolic function (Wong and Teh 1995, Kim et al. 1999, Basarkar and Dewaikar 2006, Zhang et al. 2010). Several researchers from their studies (Desai and Drumm 1985, Zong-ze et al. 1995, Zhang and Zhang 2009), have suggested using a hyperbolic model to reasonably capture the soil shearing behavior on the pile-soil interface. As shown in Figure 5.1(b), at a given depth z, the shear stress on the pile-soil interface increases nonlinearly at a decreasing rate with the increase in the pile-soil relative displacement. When the pile-soil relative displacement at a given depth z, $w(z)$, reaches a limiting displacement w_u, the shear stress $\tau(z)$ achieves the ultimate shear stress τ_u. Here, a hyperbolic function-based load transfer model is employed to describe the relationship between the pile shaft resistance and relative displacement, which can be written as follows:

$$\tau(z)=\begin{cases}\dfrac{w(z)}{\dfrac{1}{K_{\mathrm{si}}}+R_{\mathrm{sf}}\dfrac{w(z)}{\tau_{\mathrm{u}}}} & w(z)\le w_{\mathrm{u}}\\ \tau_{\mathrm{u}} & w(z)>w_{\mathrm{u}}\end{cases} \tag{5.1}$$

where $w(z)$ is the pile-soil relative displacement due to the applied axial load, $\tau(z)$ is unit shaft shear stress at depth z, R_{sf} is a failure ratio ($R_{sf} = \tau_u/\tau_f$, τ_f is the shear stress at which $w(z)$ is infinity). R_{sf} is found to be in the range of 0.8 to 0.95 as recommended by Clough and Duncan (1971). K_{si} represents the initial shear stiffness (i.e., the initial tangent of the t-z curve), which can be obtained from the equation suggested by Wong and Teh (1995) as follows:

$$K_{\mathrm{si}}=\frac{G_0}{r_0\ln\left(\dfrac{r_{\mathrm{m}}}{r_0}\right)} \tag{5.2}$$

where G_0 is the maximum shear modulus which refers to the shear modulus at a small strain (typically <0.001%), r_0 is the pile radius and r_m is the maximum radius at which the shear stress of soil induced by the pile becomes negligible. Empirically, r_m has been found to be related to the embedded length of pile, L, and Poisson's ratio, υ (Randolph and Wroth 1978):

$$r_{\mathrm{m}}=2.5\rho_{\mathrm{m}}(1-\upsilon)L \tag{5.3}$$

where ρ_m is a non-homogeneity factor (= ratio of G_0 at pile mid-depth to G_0 at the pile tip).

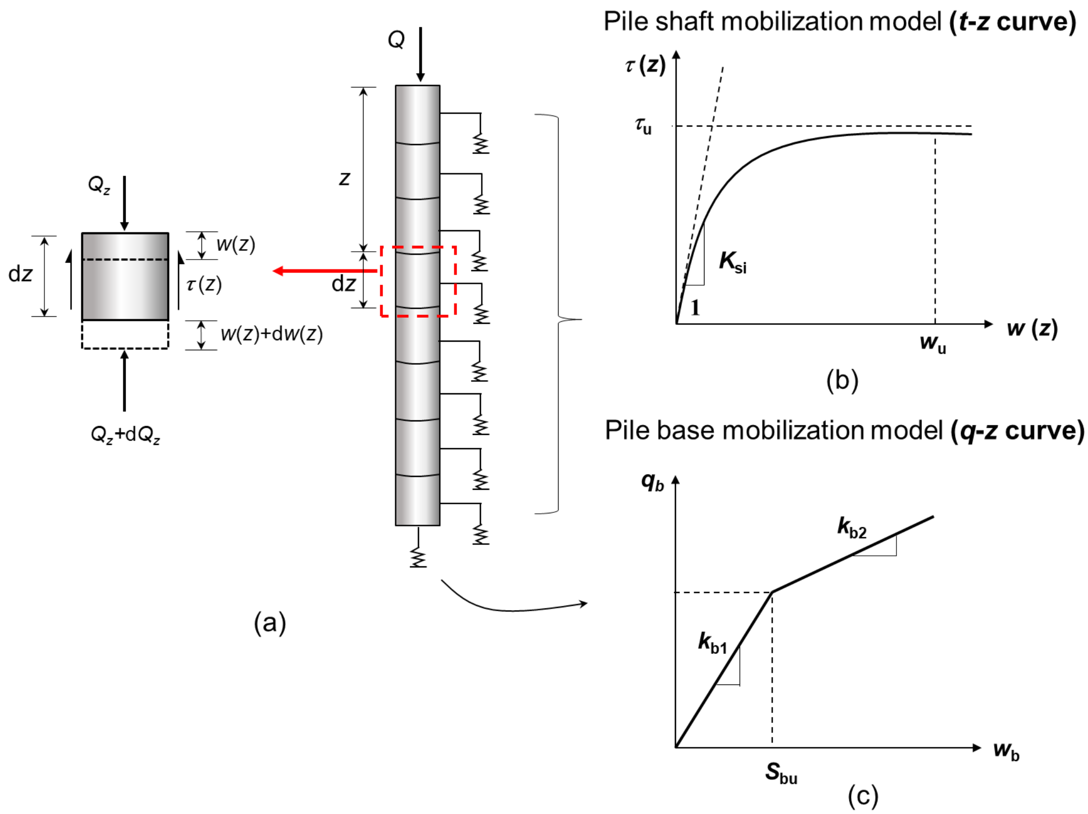

Figure 5.1 Schematic of LTM for an axially loaded pile

The relationship between the pile base resistance and the pile base displacement is characterized by a bilinear model, as shown in Figure 5.1(c). The bilinear relationship between the displacement at the pile base, w_b, and the mobilized unit base resistance, q_b, is expressed as

$$q_{\mathrm{b}} = \begin{cases} k_{\mathrm{b1}} w_{\mathrm{b}}, & w_{\mathrm{b}} \le S_{\mathrm{bu}} \\ k_{\mathrm{b1}} S_{\mathrm{bu}} + k_{\mathrm{b2}} \left(w_{\mathrm{b}} - S_{\mathrm{bu}} \right), & w_{\mathrm{b}} > S_{\mathrm{bu}} \end{cases} \tag{5.4}$$

where k_{b1} and k_{b2} are the compressive rigidity of the pile-base soil in the first and second stage of the pile loading, respectively; and S_{bu} is the pile base settlment related to the limit shear stress in the first stage. Three required parameters k_{b1}, k_{b2} and S_{bu} can be determined experimentally or back-calculated from field load tests. The variation of k_{b1} can be conveniently esimtated using the following equation as suggested by Randolph and Wroth (1978):

$$k_{\mathrm{b1}} = \frac{4G_{\mathrm{b}}}{\pi r_0 \left(1-\upsilon_{\mathrm{b}}\right)} \tag{5.5}$$

where G_{b} is the average shear modulus of the soils in the range from pile base to $8r_0$ below the pile base, υ_{b} is Possion's ratio of the soil in the range from pile base to $8r_0$ below the pile base. The value of k_{b2} can be predicted using the equation proposed by Zhang et al. (2010):

$$k_{\mathrm{b2}} = \frac{\Delta P_{\mathrm{t}}}{\left(\Delta w_t - \dfrac{\Delta P_{\mathrm{t}} L}{E_{\mathrm{p}} A_{\mathrm{p}}}\right)} = \frac{k_{\mathrm{t}}}{1-\dfrac{k_{\mathrm{t}} L}{E_{\mathrm{p}} A_{\mathrm{p}}}} \tag{5.6}$$

where ΔP_{t} is the increased load at the pile head when w_{b} is larger than the limiting pile base settlement of the first stage of q_{b} versus w_{b} curve (i.e., S_{bu}), Δw_{t} is the increased settlement at the pile head induced by ΔP_{t}, L is the pile length, E_{p} is the modulus of elasticity of pile, A_{p} is the cross-section area of the pile and k_{t} is the ratio of the load increment to the settlement increment at the pile head, $k_{\mathrm{t}} = \Delta P_{\mathrm{t}}/\Delta w_{\mathrm{t}}$. Both hyperbolic and bilinear models are reliable and relatively simple. Hence, these two models are used to predict the behavior of single piles and pile groups in unsaturated soils.

5.3 The proposed MLTM for single piles in unsaturated soils

5.3.1 Influence of matric suction on soil properties

The shear strength and modulus of elasticity of unsaturated soils are two key parameters governing the bearing capacity and settlement of pile foundations in unsaturated soils, respectively. Experimental studies demonstrate an increase in shear strength and elastic modulus of unsaturated soils as soil suction increases (Gan and Fredlund 1988, Escario and Sáez 1986, Nam et al. 2011). Therefore, the mechanical properties of unsaturated soil vary with respect to matric suction profile along the depth. The matric suction is significantly influenced by the change in water content in the soil. Typical distributions of matric suction above the GWT can be categorized into three cases (i.e., uniform, linear and nonlinear distribution profiles) based on the influence of environmental conditions (e.g., water infiltration, evaporation and evapotranspiration), as shown in Figure 5.2(a).

The Soil Water Characteristic curve (SWCC) is a useful tool to describe the relationship between the water storage capacity within the voids of soil and different values of matric suction. The air-entry value (AEV) and residual suction, $(u_a - u_w)_r$ are two key points of SWCC as illustrated in Figure 5.2(b). AEV is the suction value at which air enters the largest soil pore and initiates the soil desaturation. The relationship between shear strength and matric suction up to AEV is linear; however, it becomes non-linear for suction values greater than the AEV (Gan et al. 1988, Vanapalli et al. 1996). The residual suction is the value beyond which the water phase is discontinuous and an increase in matric suction has a marginal influence on the degree of saturation.

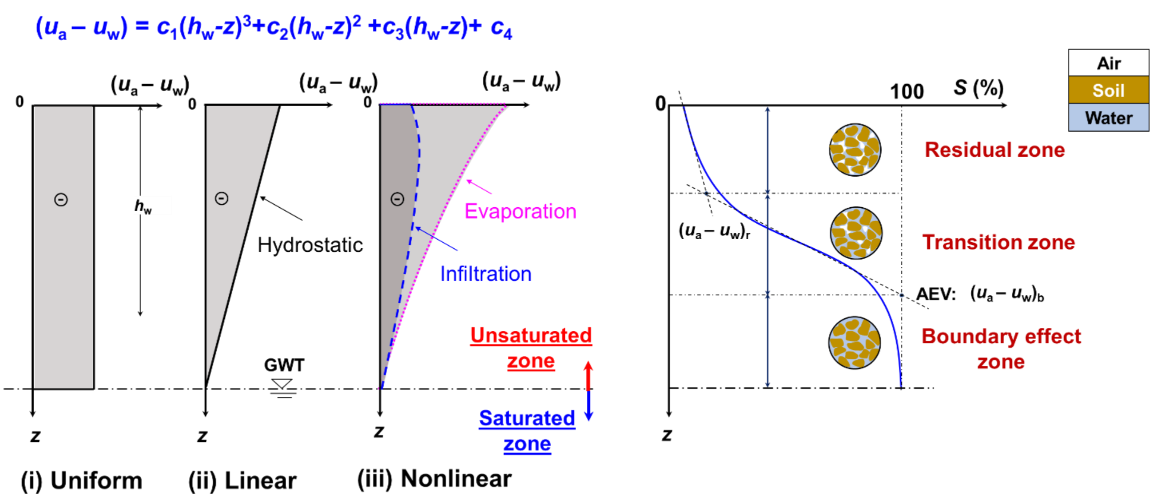

(a) (b)

Figure 5.2 (a) Matric suction profile (b) SWCC

5.3.2 The computation process of proposed MLTM

Figure 5.3 illustrates the computation process of the proposed MLTM. The details will be elaborated in the following.

5.3.2.1 Step 1: Input parameters

First, the input information related to the soil and pile properties is gathered. The input parameters include pile properties such as pile length, diameter, material and elastic modulus, soil properties include conventional soil properties (e.g., unit weight, void ratio, specific gravity and saturated shear strength parameters), matric suction profile and SWCC. The variation of matric suction along the pile length can be written in the following general form (Figure 5.2(a))

$$\left(u_{\mathrm{a}}-u_{\mathrm{w}}\right)=c_1(h_{\mathrm{w}}-z)^3+c_2\left(h_{\mathrm{w}}-z\right)^2+c_3\left(h_{\mathrm{w}}-z\right)+c_4 \tag{5.7}$$

where h_{w} is the height of GWT, and c_1, c_2, c_3 and c_4 are curve-fitting constants. For special cases such as the uniform matric suction that is a constant with depth, $c_1 = c_2 = c_3 = 0$, $c_4 = (u_{\mathrm{a}} - u_{\mathrm{w}})_{\mathrm{avg}}$, where $(u_{\mathrm{a}} - u_{\mathrm{w}})_{\mathrm{avg}}$ is the average matric suction along the depth; For linearly distributed matric suction under hydrostatic conditions, $c_1 = c_2 = c_4 = 0$, $c_3 = \gamma_{\mathrm{w}}$, where γ_{w} is the unit weight of water.

The degree of saturation, S, can be expressed as a function of matric suction, $(u_{\mathrm{a}} - u_{\mathrm{w}})$ via the SWCC (Figure 5.2(b)). Equation 5.8 proposed by Fredlund and Xing (1994) is used in this study to predict S based on the matric suction profile:

$$S=C\left(\varphi\right)\left[\frac{1}{\ln\left[e+\left(\frac{\varphi}{a}\right)^n\right]}\right]^m \tag{5.8}$$

where $C(\varphi)$ is correction factor, φ is soil suction, e is Euler's number and a, n, m are fitting parameters.

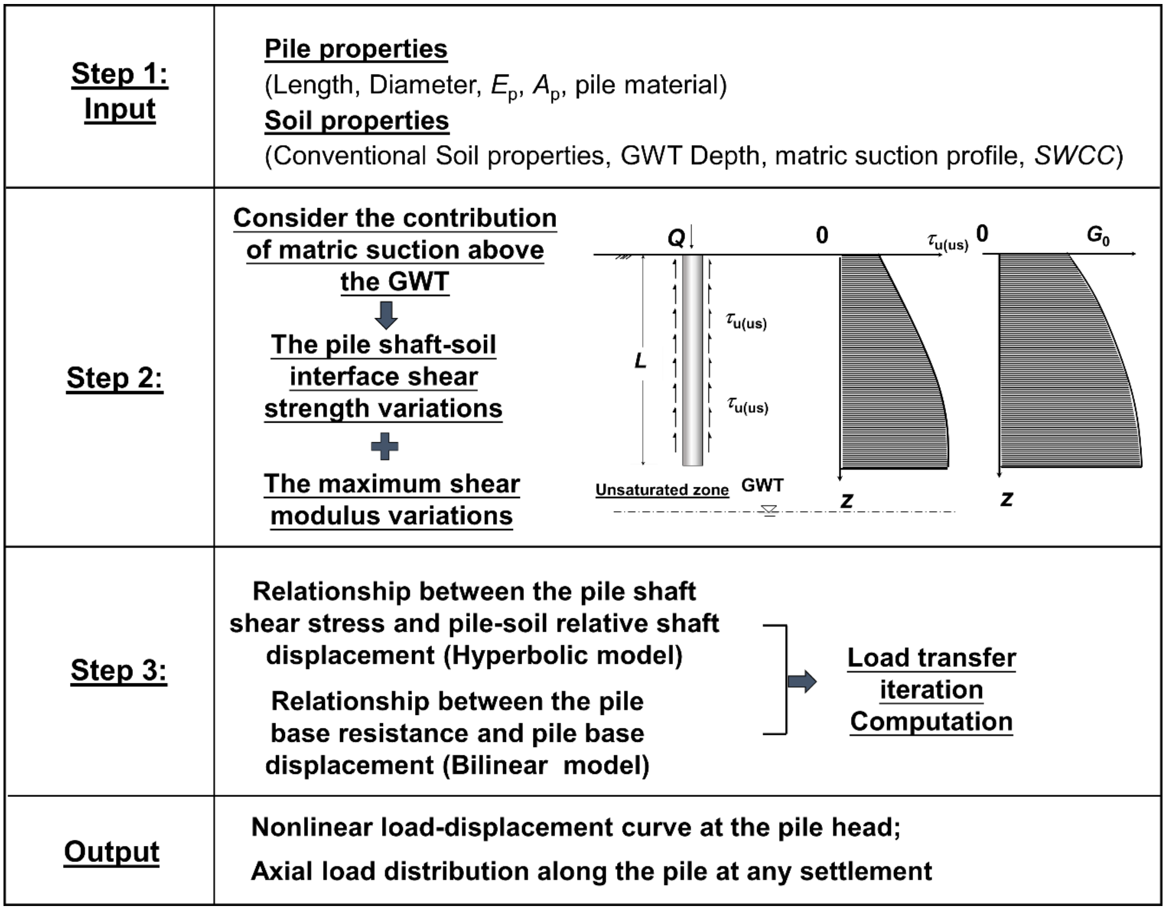

Figure 5.3 The computation process of the proposed MLTM

5.3.2.2 Step 2

The ultimate shaft shear stress for saturated soils under drained conditions, τ_u, can be determined utilizing the soil effective shear strength parameters based on Coulomb's friction law:

$$\tau_u = K\sigma'_z \tan\delta' = K_0\left(\frac{K}{K_0}\right)\sigma'_z \tan\left[\phi'\left(\frac{\delta'}{\phi'}\right)\right] \tag{5.9}$$

where K is lateral earth pressure coefficient (the ratio of mobilized horizontal effective stress σ'_h to vertical effective stress σ'_z), δ' is the effective friction angle of the pile-soil interface, ϕ' is effective internal friction angle of soil and K_0 is at rest earth pressure coefficient. The coefficient K is influenced by various factors including soil type and properties, pile type and stiffness, pile installation method, and can be related to K_0. The value of δ' is typically less than ϕ'; however, for bored piles with rough surfaces, δ' can be assumed as $1.0\phi'$. Table 5.1 summarizes the recommended values of K/K_0 and δ'/ϕ' for different pile and soil types.

Table 5.1 Recommended K/K_0 and δ'/ϕ' for different pile and soil types

Reference	Values	Pile and soil conditions
Tomlinson and Woodward (2007)	K/K_0 = 1.0–2.0	Driven piles, large displacement
	K/K_0 = 0.75–1.25	Driven piles, small displacement
	K/K_0 = 0.7–1.0	Bored piles and cast-in-place piles
	K/K_0 = 0.5-0.7	Jetted piles
Yang et al. (2006)	K/K_0 = 1.2-1.5	Driven steel pile, alluvium, and completely decomposed granite
Kulhawy and Mayne (1990)	δ'/ϕ' = 0.5–0.7	Smooth steel pile piles or H piles
	δ'/ϕ' = 1.0	Rough concrete piles
	δ'/ϕ' = 0.8–1.0	Smooth concrete piles
Tomlinson and Woodward (2007)	δ'/ϕ' = 1.0	Cast-in-place concrete piles, sand
	δ'/ϕ' = 0.8–1.0	Precast concrete, sand
	δ'/ϕ' = 0.8–0.9	Timber piles

Several empirical or semi-empirical models have been proposed in the literature for predicting the shear strength of unsaturated soils, τ_{unsat}, using the information of saturated shear strength parameters and the SWCC (e.g., Vanapalli et al. 1996, Khalili and Khabbaz 1998, Rassam and Cook 2002). Equations 5.10a and 5.10b are two semi-empirical models proposed by Vanapalli et al. (1996) to predict the nonlinear variation of τ_{unsat} with respect to $(u_a - u_w)$ in terms of volumetric water content, θ, or degree of saturation, S, which can be derived from the SWCC:

$$\tau_{\mathrm{unsat}} = c' + (\sigma_{\mathrm{n}} - u_{\mathrm{a}})\tan\phi' + (u_{\mathrm{a}} - u_{\mathrm{w}})\left(\frac{\theta - \theta_{\mathrm{r}}}{\theta_{\mathrm{s}} - \theta_{\mathrm{r}}}\right)\tan\phi' \tag{5.10a}$$

$$\tau_{\mathrm{unsat}} = c' + (\sigma_{\mathrm{n}} - u_{\mathrm{a}})\tan\phi' + (u_{\mathrm{a}} - u_{\mathrm{w}})S^{\kappa}\tan\phi' \tag{5.10b}$$

where c' is effective cohesion, ϕ' is effective internal friction angle, $(\sigma_{\mathrm{n}} - u_{\mathrm{a}})$ is net normal stress in which σ_{n} is the normal stress and u_{a} is the atmospheric pressure, u_{w} is pore water pressure, $(u_{\mathrm{a}} - u_{\mathrm{w}})$ is matric suction, θ_{s} and θ_{r} is saturated and residual volumetric water content, respectively. Equation 5.10a requires the residual water content that can be identified from the SWCC. Equation 5.10b requires a fitting parameter κ that is related to the plasticity index, I_{p} (Garven and Vanapalli 2006). κ equals to 1 for predicting the variation of shear strength of unsaturated sandy soils (i.e., I_{p} = 0). The third term in Equation 5.10a and 5.10b (i.e., $(u_{\mathrm{a}} - u_{\mathrm{w}})[(\theta - \theta_{\mathrm{r}})/(\theta_{\mathrm{s}} - \theta_{\mathrm{r}})]\tan\phi'$ or $(u_{\mathrm{a}} - u_{\mathrm{w}})S^{\kappa}\tan\phi'$), represents the contribution of matric suction towards the shear strength.

Matric suction has also been found to have a significant influence on the interface behavior between unsaturated soils and different construction materials (Sharma et al. 2007, Hamid and Miller 2009, Hossain and Yin 2010). Hamid and Miller (2009) performed a series of interface direct shear tests between unsaturated silt and steel (smooth and rough surfaces). They suggested the following equation for determining the ultimate shear stress of unsaturated soil-structure interface, which is similar in form to Equation 5.10a

$$\tau_{\mathrm{u(us)}} = c' + (\sigma_{\mathrm{n}} - u_{\mathrm{a}})\tan\delta' + (u_{\mathrm{a}} - u_{\mathrm{w}})\left(\frac{\theta - \theta_{\mathrm{r}}}{\theta_{\mathrm{s}} - \theta_{\mathrm{r}}}\right)\tan\delta' \tag{5.11}$$

Incorporating the contribution of $(u_{\mathrm{a}} - u_{\mathrm{w}})$ and combining Equations 5.9, 5.10a, 5.10b and 5.11, the ultimate shaft shear stress can be calculated as follows using the information of matric suction profile and SWCC.

$$\tau_{\mathrm{u(us)}} = c' + K\sigma_z' \tan\delta' + \left(u_\mathrm{a} - u_\mathrm{w}\right)\frac{\left(\theta - \theta_\mathrm{r}\right)}{\left(\theta_\mathrm{s} - \theta_\mathrm{r}\right)}\tan\delta' \tag{5.12a}$$

$$\tau_{\mathrm{u(us)}} = c' + K\sigma_z' \tan\delta' + \left(u_\mathrm{a} - u_\mathrm{w}\right)S^{\kappa}\tan\delta' \tag{5.12b}$$

Assume a single pile is divided into n segments and the length of segment j is ΔL_j. The average ultimate shear stress for a segment at depth z can be calculated using Equation 5.13

$$\tau_{\mathrm{u},j} = \frac{\int_0^{\Delta L_j} \tau_{\mathrm{u(us)}}(z)\mathrm{d}z}{\Delta L_j} \tag{5.13}$$

The maximum shear modulus of unsaturated soils $G_{0\mathrm{(us)}}$ can be determined from both laboratory tests and seismic field tests (e.g., Kawaguchi et al. 2001, Lee and Santamarina 2005). Empirical or semi-empirical equations have also been proposed for estimating $G_{0\mathrm{(us)}}$ in unsaturated soils considering the water content and matric suction (e.g., Mancuso et al. 2002, Mendoza and Colmenares 2006, Sawangsuriya et al. 2009, Lu and Kaya 2014). Oh and Vanapalli (2014) proposed a similar model for predicting the variation of $G_{0\mathrm{(us)}}$ with respect to $(u_\mathrm{a} - u_\mathrm{w})$ in unsaturated sandy soils using the saturated maximum shear modulus, $G_{0\mathrm{(sat)}}$ and SWCC

$$G_{0\mathrm{(us)}} = G_{0\mathrm{(sat)}}\left[1 + \zeta\frac{\left(u_\mathrm{a} - u_\mathrm{w}\right)}{\left(P_\mathrm{a}/101.3\right)}\left(S^{\xi}\right)\right] \tag{5.14}$$

where ζ and ξ are fitting parameters. The fitting parameter ξ equals to 0.5 and 1 for the soils classified as SP and SW, respectively. The fitting parameter ζ is strongly related to the coefficient of uniformity C_U. The value of ζ decreases from 0.035 to 0.025 as C_U increases up to 2. More details of the relationship between ζ and C_U can be found in Oh and Vanapalli (2014).

5.3.3 Step 3 and output

In the Step 3, the values of $\tau_{u,j}$ and $G_{0(us)}$ derived from Equations 5.13 and 5.14 respectively, can be introduced into Equation 5.1. The hyperbolic model along the pile shaft can be extended for load displacement analysis of piles in unsaturated soil considering the influence of matric suction. One of the key parameters to be determined in the pile base bilinear model is the pile base settlement related to the limit shear stress, S_{bu}. The value of S_{bu} is influenced by various factors that include the soil properties, pile type, loading method and environmental factors. Therefore, for the sake of simplicity, it is recommended to determine it experimentally or through back-analysis of field load test results (Liu and Vanapalli 2019).

After all the required parameters for both hyperbolic and bilinear model are determined, the load transfer iteration computation can be performed. The detailed step-by-step computational procedures are summarized in the Appendix. The output results include the nonlinear load-displacement curve at the pile head, axial load distribution along the pile at any settlement.

5.4 MLTM for group piles in unsaturated soils

5.4.1 Interaction between pile shafts

The proposed MLTM for single piles in unsaturated soils is extended for the analysis of pile groups considering the interaction effects between individual piles. The interaction between a pair of identical adjacent piles, *i* and *j* is shown in Figure 5.4. The center-to-center pile spacing is denoted as r_{ij}. The shaft displacement of pile *i*, $w_{i,z}$, can be regarded as the sum of the displacement due to its own loading, $w_{ii,z}$ and the additional displacement induced by the adjacent pile *j*. $w_{ii,z}$ can be obtained using the proposed approach for single piles (i.e., Equation 5.1). The additional displacement induced by the adjacent pile *j* can be further regarded as two components. The first component is the displacement induced by the loading of pile *j*, $w_{ij,z}$. The second component, $w'_{ij,z}$, is the negative displacement caused by the reinforcement effect of pile *j*, which is in the opposite direction to the pile group movement. Caputo and Viggiani (1994) reported a case history of pile load tests on two identical adjacent piles and concluded that the load versus displacement relationship for the loaded pile is highly nonlinear, whereas the displacement of load-free piles increases linearly as the applied load increases on the loaded pile (see Figure 5.4). Therefore, the interaction effect between a pair of identical piles can be considered as linearly elastic (Lee and Xiao 2001, Leung et al. 2010, Wang et al. 2012).

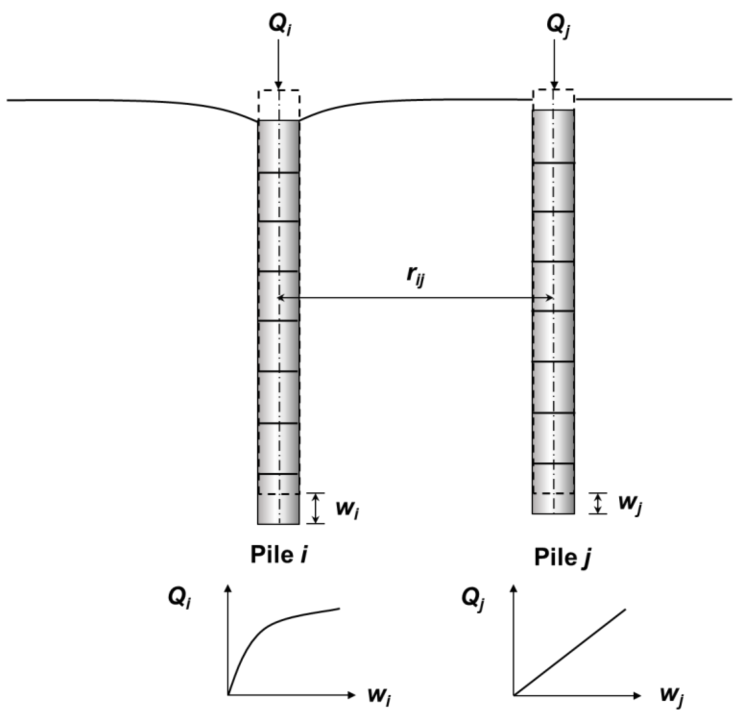

Figure 5.4 Illustration of the interaction effect between two adjacent piles reported by Caputo and Viggiani (1994)

The additional elastic displacement at a given depth z for pile i, $w_{ij,z}$, induced by the shear stress of adjacent pile j, $\tau_{j,z}$, can be calculated extending the elastic theory proposed by Randolph and Wroth (1978).

$$w_{ij,z} = \frac{r_0}{G_0} \tau_{j,z} \ln\left(\frac{r_m}{r_{ij}}\right) \tag{5.15}$$

In order to obtain simplified solutions, Lee and Xiao (2001) assumed that the shaft shear stress on each individual pile at a given depth z is identical (i.e., $\tau_{i,z} = \tau_{j,z}$ for j =1 to n, $j \neq i$). They verified that the difference between the methods with or without extending this assumption is quite small using the results from field pile-group tests reported by O'Neil (1981). Zhang et al. (2010) and Li et al. (2020) also reported that this assumption provides relatively accurate results and can be considered reliable. For this reason, in this study, the shear stresses for all piles in an m-pile group is assumed to be identical for the sake of developing a simpler solution and reducing the computational time. Equation 5.15 can be written in an incremental form as

$$\Delta w_{ij,z} = \frac{1}{K_{sij,z}} \Delta \tau_{i,z} \tag{5.16}$$

where $K_{sij,z}$ is the initial shear stiffness of the soils around pile i due to the shear stress, $\tau_{j,z}$. $K_{sij,z}$ can be derived from Equations 5.15 and 5.16:

$$\frac{1}{K_{sij,z}} = \frac{r_0}{G_0} \ln\left(\frac{r_{\mathrm{m}}}{r_{ij}}\right) \tag{5.17}$$

The shaft shear stress on the pile i, $\tau_{i,z}$, spreads to pile j and induces a shear stress on pile j that is denoted as $\tau'_{ij,z}$, which can be expressed as

$$\tau'_{ij,z} = \frac{\tau_{i,z}}{r_{ij}} r_0 \tag{5.18}$$

Due to the shear stress $\tau'_{ij,z}$ applied on pile j, the surrounding soil of pile j tends to move upwards and $\tau'_{ij,z}$ can be regarded as negative skin friction that pulls pile j down. Accordingly, pile j generates a counter shear stress that is the same value as $\tau'_{ij,z}$ in the opposite direction. The effect of $\tau'_{ij,z}$ on pile j may reduce the elastic displacement of pile i. This is referred to as the reinforcement effect. The vertical displacement of pile i due to the reinforcement effect, namely, $w'_{ij,z}$, can be expressed using Equation 5.19 below.

$$w'_{ij,z} = \frac{\tau'_{ij,z} r_0}{G_0} \ln\left(\frac{r_{\mathrm{m}}}{r_{ij}}\right) = \frac{\tau_{i,z} r_0^{\,2}}{G_0 r_{ij}} \ln\left(\frac{r_{\mathrm{m}}}{r_{ij}}\right) \tag{5.19}$$

The initial shear stiffness of the soils around pile i, $K'_{sij,z}$, induced by the shear stress $\tau'_{ij,z}$ is given by

$$\frac{1}{K'_{sij,z}} = \frac{r_0^{\,2}}{G_0 r_{ij}} \tau_{i,z} \ln\left(\frac{r_{\mathrm{m}}}{r_{ij}}\right) \tag{5.20}$$

For a group of m piles, the overall shaft displacement of pile i at depth z due to its own load and loads from other piles can be expressed as

$$w_{i,z} = w_{ii,z} + \sum_{j=1,\, j\neq i}^{m} w_{ij,z} - \sum_{j=1,\, j\neq i}^{m} w'_{ij,z} \tag{5.21}$$

Assuming the *t-z* curve for an individual pile i in a group also follows the hyperbolic relationship which is similar to that for single piles from Equation 5.1, the relationship between shaft shear stress and pile-soil relative displacement for pile i can be expressed as

$$\tau_{i,z} = \frac{w_{i,z}}{\dfrac{1}{K_{si,z}} + R_{\mathrm{sf}} \dfrac{w_{i,z}}{\tau_{\mathrm{u(us)},z}}} \tag{5.22}$$

where $\tau_{\mathrm{u(us)},z}$ is the ultimate shear stress at depth z and $K_{si,z}$ represents the generalized equivalent initial stiffness of *t-z* curve for pile i, the value of which can be obtained by substituting Equations 5.2, 5.17 and 5.20 into Equation 5.23

$$\frac{1}{K_{si,z}} = \frac{1}{K_{sii,z}} + \sum_{j=1,\, j\neq i}^{m} \frac{1}{K_{sij,z}} - \sum_{j=1,\, j\neq i}^{m} \frac{1}{K'_{sij,z}} \tag{5.23}$$

where $K_{sii,z}$ represents the initial shear stiffness of the soils around pile i induced by its own loading.

5.4.2 Interaction between pile bases

In this study, the interaction between the pile shafts and pile bases is considered uncoupled (Lee and Xiao 2001, Wang et al. 2012). The overall pile base displacement for pile i, $w_{i,\mathrm{b}}$, is composed of two parts. One part is the nonlinear displacement due to its own loading, $w_{ii,\mathrm{b}}$, and the other one is the additional displacement caused by loadings of other piles in the group, $w_{ij,\mathrm{b}}$. For a group of m-piles, the interaction effects on the pile base displacement can be considered following the principle of superposition. Then, $w_{i,\mathrm{b}}$ can be written as

$$w_{i,\mathrm{b}} = w_{ii,\mathrm{b}} + \sum_{j=1,\, j\neq i}^{m} w_{ij,\mathrm{b}} \tag{5.24}$$

where $w_{ii,\mathrm{b}}$ can be derived from Equation 5.4:

$$w_{ii,\mathrm{b}} = \begin{cases} \dfrac{1}{k_{\mathrm{b}1}} q_{i,\mathrm{b}} & w_{\mathrm{b}} \leq S_{\mathrm{bu}} \\ \dfrac{1}{k_{\mathrm{b}2}} q_{i,\mathrm{b}} + \left(1 - \dfrac{k_{\mathrm{b}1}}{k_{\mathrm{b}2}}\right) S_{\mathrm{bu}} & w_{\mathrm{b}} > S_{\mathrm{bu}} \end{cases} \tag{5.25}$$

Following the assumption of treating the pile base as a rigid punch on the surface of a soil medium, the load at some distance of the pile base appears as a point load. The interaction between pile bases can be expressed using the solution reported by Randolph and Wroth (1978):

$$w_{ij,\mathrm{b}} = \frac{q_{j,\mathrm{b}}\left(1-\upsilon_{\mathrm{b}}\right)}{2\pi r_{ij} G_{\mathrm{b}}} \tag{5.26}$$

where $q_{j,\mathrm{b}}$ is the unit base resistance of pile j. For the same reason as that used for the shaft shear stress, it is assumed that the unit pile base resistance for all the piles in an m-pile group are identical (i.e., $q_{i,\mathrm{b}} = q_{j,\mathrm{b}}$,for j =1 to n, $j \neq i$). Equation 5.26 can be written in an incremental form as

$$\Delta w_{ij,\mathrm{b}} = \frac{1}{K_{ij,\mathrm{b}}} \Delta q_{i,\mathrm{b}} \tag{5.27}$$

where $K_{ij,\mathrm{b}}$ is the initial shear stiffness of the soils at the base of pile i induced by adjacent piles. $K_{ij,\mathrm{b}}$ can be derived from Equations 5.26 and 5.17:

$$\frac{1}{K_{ij,b}} = \frac{(1-\upsilon_\mathrm{b})}{2\pi r_{ij} G_\mathrm{b}} \tag{5.28}$$

The relationship between the displacement at the pile base, and the mobilized unit base resistance, $q_{i,\mathrm{b}}$, for an individual pile i in a group can be also described by a bilinear function similar to single piles. Such a relationship is summarized below.

$$q_{i,\mathrm{b}} = \begin{cases} \bar{a}\, w_{ii,\mathrm{b}} & w_{ii,\mathrm{b}} \leq S_\mathrm{bu} \\ \bar{b} w_{ii,\mathrm{b}} + \bar{b}\left(\frac{k_\mathrm{b1}}{k_\mathrm{b2}} - 1\right) S_\mathrm{bu} & w_{ii,\mathrm{b}} > S_\mathrm{bu} \end{cases} \tag{5.29}$$

$$\text{where } \bar{a} = \frac{1}{\frac{1}{k_{b1}} + \sum_{j=1, j\neq i}^{m} \frac{1}{K_{ij,b}}}, \bar{b} = \frac{1}{\frac{1}{k_{b2}} + \sum_{j=1, j\neq i}^{m} \frac{1}{K_{ij,b}}} \tag{5.30}$$

The load-displacement curve of pile groups can then be calculated using MATLAB. The detailed computational procedures are summarized in the following.

5.4.3 Algorithm for load-displacement analysis of single piles and pile groups

The procedures for calculating the load-displacement curve of single piles and pile groups in unsaturated soils are similar. However, the procedure used for pile group is complex since it also must account for the interaction effect between piles in a group. Both procedures require to call a function namely *FINDQWS*, which is written for obtaining output of the load and displacement at the head of an individual pile. The only input parameter for this function is pile base displacement. The detailed computational procedure is described as follows:

1. A pile with length of L is divided into n segments and numbered from the pile head to base (Figure 5.5(a)). The corresponding pile base load, $Q_{b,n}$ for a given pile can be calculated taking account of the base displacement. For single piles, $Q_{b,n}$ is determined using Equations 5.4-5.6. For an individual pile i in a group, $Q_{b,n}$ is obtained using Equations 5.29 and 5.30.

2. For the first trial, assume the average shear stress around segment n, τ_n, as a certain percentage of the average ultimate shear stress $\tau_{u,n}$ (for example, set $\tau_n = 0.3\tau_{u,n}$). Based on the input soil parameters, $\tau_{u,n}$ can be calculated using Equation 5.13.

3. The pile-soil relative displacement at the middle point of segment n, $w_{m,n}$. is calculated. For single piles, $w_{m,n}$ can be derived from Equation 5.1. For an individual pile i in a group, $w_{m,n}$ is calculated using Equations 5.22 and 5.23.

4. The load at the top of the segment n, $Q_{t,n}$, can be computed as:

$$Q_{t,n} = Q_{b,n} + C \cdot \tau_n \cdot \Delta L \tag{5.31}$$

where C is the circumferential area and ΔL is the length of the segment.

5. The elastic deformation of the pile segment n can be calculated using:

$$s_n = \frac{Q_{m,n}}{E_p A_p}\left(\frac{\Delta L}{2}\right) \tag{5.32}$$

where E_p is the elastic modulus of the pile, A_p is the area of the pile base, and the average axial load of the segment, $Q_{m,n}$ equals to $(Q_{t,n} + Q_{b,n})/2$.

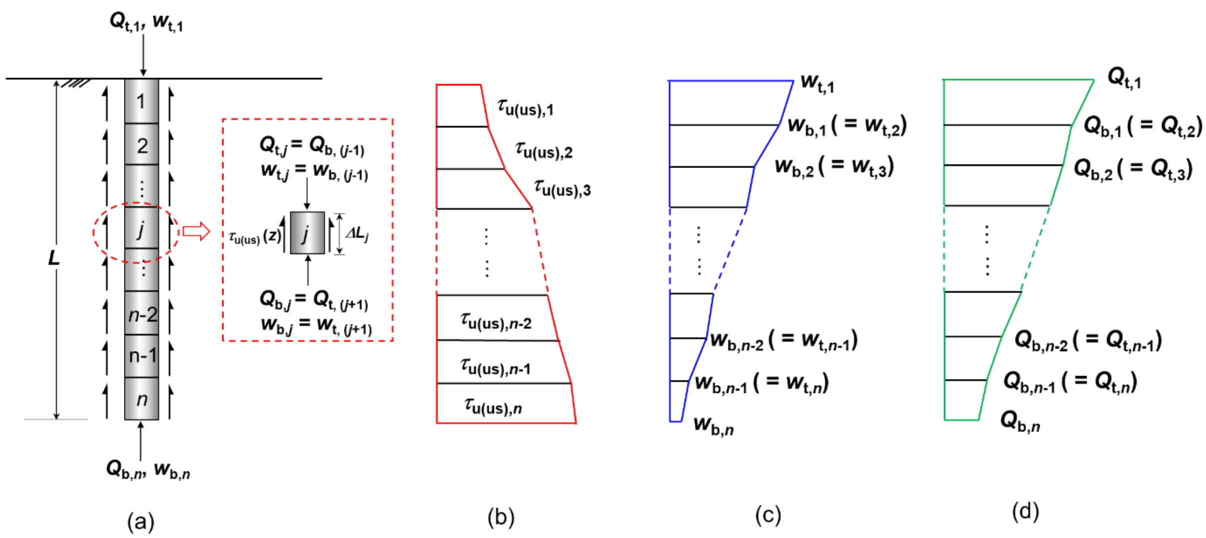

Figure 5.5 Schematic diagram of load transfer model

6. The new displacement at the middle point of the pile segment n, $w'_{m,n}$, can then be determined using the following equation:

$$w'_{\mathrm{m},n} = w_{\mathrm{b},n} + s_n \tag{5.33}$$

7. Check the convergence. If the deviation between the new computed displacement $w'_{m,n}$ and $w_{m,n}$ exceeds the allowable error, ε (e.g., 10^{-5}), Steps 2-6 will be repeated with a different assumed value of average shear stress τ_n. If $w_{m,n}$ is less than $w'_{m,n}$, increase τ_n by a very small amount and apply it in Step 2. Otherwise, if $w_{m,n}$ is larger than $w'_{m,n}$, decrease τ_n by a very small amount and apply it in Step 2.

8. If $w'_{m,n}$ and $w_{m,n}$ agrees within the allowable tolerance, move on to the next segment (n – 1). The top axial force of the segment will be the bottom axial force of the next segment (n – 1) as shown in Figure 5.5(c) and (d). Similarly, the top displacement of the segment n, $w_{t,n}$ will become the bottom displacement of the next segment (n – 1), which can be obtained as follows:

$$Q_{b,n-1} = Q_{t,n} \tag{5.34}$$

$$w_{b,n-1} = w_{t,n} = 2w_{m,n} - w_{b,n} \tag{5.35}$$

9. Repeat steps 2-8 from pile segment n until the load and displacement at the top of segment 1 (i.e., $Q_{t,1}$ and $w_{t,1}$) are obtained. The values of $Q_{t,1}$ and $w_{t,1}$ are recorded for developing the load-displacement curve. Figure 5.6 illustrates the flow chart for function *FINDQWS*.

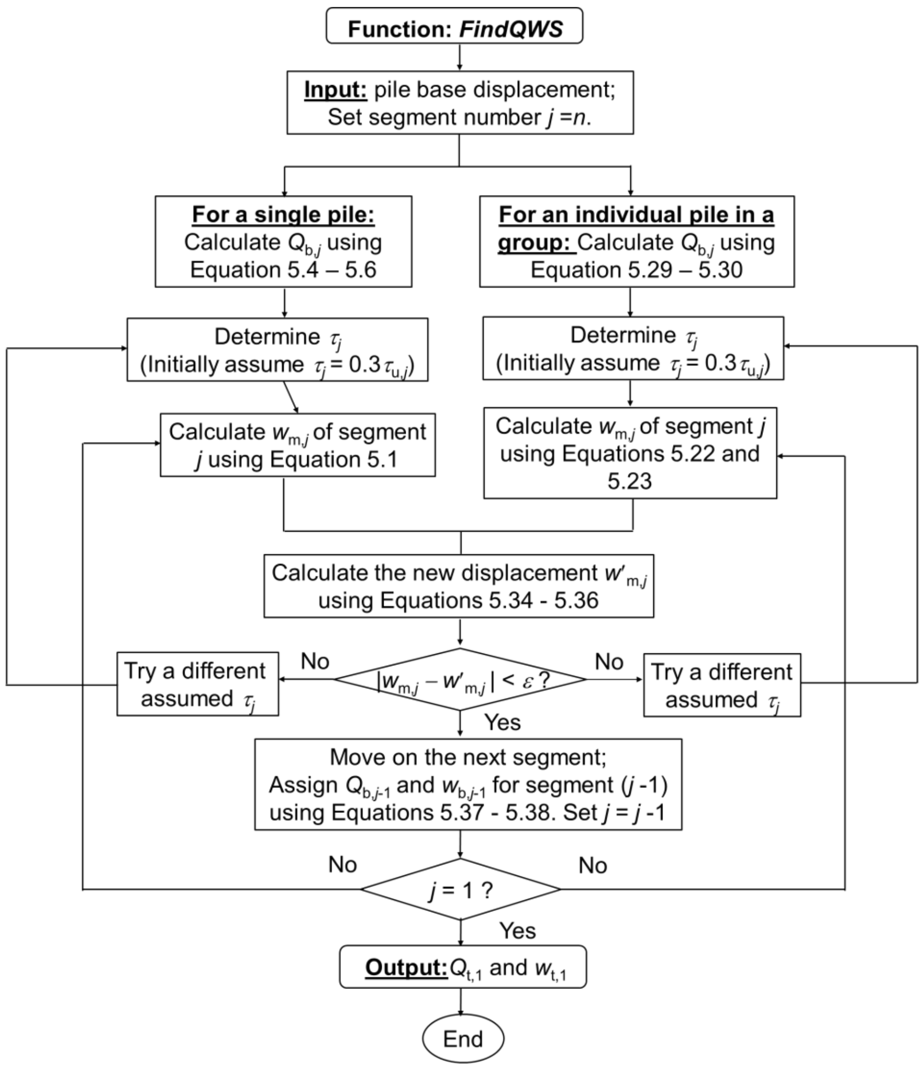

Figure 5.6 Computational flow chart for function *FINDQWS*

The algorithm for predicting the load-displacement curve of single piles in unsaturated soils is summarized below:

1. Input parameters.

2. Assume a small pile base displacement of segment n, $w_{b,n}$.

3. Call function *FINDQWS* using the assumed $w_{b,n}$ to obtain the load and displacement at the pile head, $Q_{t,1}$ and $w_{t,1}$.

4. Assume a different pile base displacement $w_{b,n}$. Repeat step 3 until the whole range of load- displacement curve of the pile is obtained.

For pile groups with perfectly rigid pile caps in unsaturated soils, the load versus displacement curve can be calculated using a bisection method. The detailed procedure is described below:

1. For a group of m piles with perfectly rigid pile cap, the displacement at the top of each pile is assumed to be identical and a specific value of pile cap displacement, $w_{cap,}$ is given.

2. Assume a small pile base displacement for pile i, $w_{ib,n}$.

3. Call function *FINDQWS* using the given $w_{ib,n}$ to obtain the load and displacement at the pile head, $Q_{it,1}$ and $w_{it,1}$.

4. Assume a large pile base displacement for pile i, $w'_{ib,n}$.

5. Call function *FINDQWS* using the given $w'_{ib,n}$ to obtain the load and displacement at the pile head, $Q'_{it,1}$ and $w'_{it,1}$.

6. Then, the average displacement at the pile head $w_{it,1(avg)}$ can be calculated (i.e., $w_{it,1(avg)} = (w_{it,1}+w'_{it,1})/2$). If the difference between $w_{it,1(avg)}$ and the assumed pile cap displacement w_{cap} exceeds the allowable error, check if the value of $(w_{it,1(avg)} - w_{cap})\cdot(w_{it,1(avg)} - w'_{it,1})$ is greater than zero. If so, replace $w'_{it,1}$ with $w_{it,1(avg)}$. Otherwise, replace $w_{it,1}$ with $w_{it,1(avg)}$. Repeat Steps 2-5 until $w_{it,1(avg)}$ and w_{cap} agree within the allowable tolerance.

10. Repeat steps 2-6 for all the piles in the group (i =1 to m). The axial load of the pile cap, Q_{cap} is the sum of the load on the top of each pile, that is

$$Q_{cap} = \sum_{i=1}^{m} Q_{it,1} \tag{5.36}$$

11. Assume a different pile cap displacement w_{cap} and repeat steps 2-10 until the whole range of load-displacement is obtained.

On the other hand, for the case of a pile group with a perfectly flexible pile cap, a similar computational procedure can be used to predict the load-displacement curve. The load on the top of each pile is assumed to be identical and a specific value of pile load, Q_{cap}, will be given. The computational flow chart for analyzing the behavior of single piles and pile groups is presented in Figure 5.7.

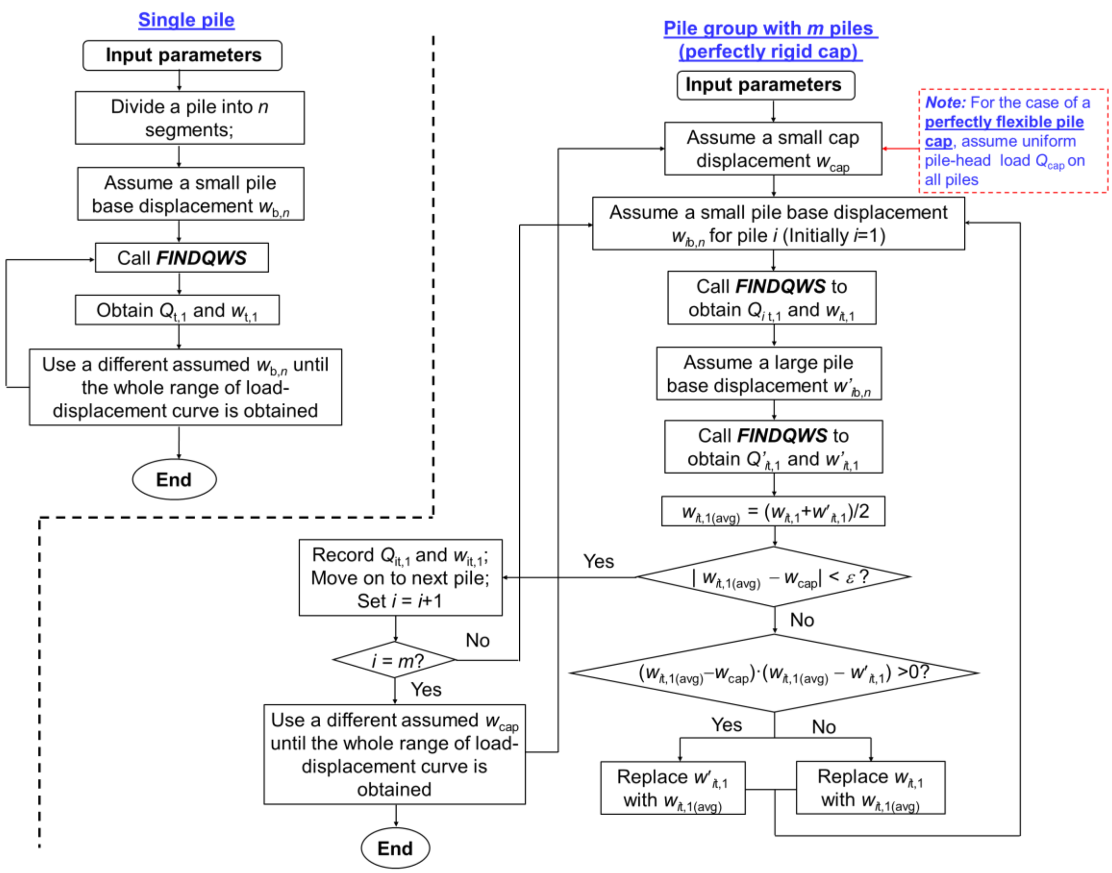

Figure 5.7 Flow chart for analyzing the response of single piles and pile groups

5.5 Validation-Single pile

Three pile load tests in unsaturated soils including two performed on single piles and one on pile group from the literature are used to validate the reliability of the proposed method for predicting the load-displacement curve of single piles and pile groups.

5.5.1 Single pile load tests in Piedmont residual soils

A static load test was performed on a bored pile in Piedmont residual soils at the Georgia Institute of Technology, Atlanta (Mayne and Harris 1993). The Piedmont soils are primarily the product of in-place weathering of gneisses, granites and schists. The soil strata have an 18.5 m layer of residual, silty silica sand overlying partially weathered rock. The residual soils in Piedmont consist of around 70% sand and less than 10 % clay fractions. The GWT is located 17 m below the ground level. The tested pile is 16.8 m in length and 0.76 m in diameter. The pile is divided into 17 segments of 1 m thickness for the first 16 segments and 0.8 m thick for the 17th layer. The degree of saturation, S, for each layer is obtained using the water content w, void ratio e and specific gravity G_s (i.e., $S = wG_s/e$, where G_s=2.67). The corresponding matric suction for each layer is derived from the SWCC, which can be predicted using van Genuchten's (1980) fitting equation. Based on the soil classification information, the fitting parameters α and n for van Genuchten (1980) were determined as 0.0383 and 1.3774, respectively, according to Wösten et al. (1999) for coarse soil. The small-strain shear modulus $G_{0(us)}$ for each layer is provided by Harris and Mayne (1994) as summarized in Table 5.2. The effective cohesion is determined as 0 kPa from the consolidated undrained triaxial tests. The at rest lateral earth pressure coefficient K_0, was taken as 1–sinϕ'. According to Table 5.1, for bored piles, the values for K/K_0 of 0.70, 0.80 and 0.90 were used for the whole deposit. The values for R_{sf} of 0.85,0.90 and 0.95 were assumed in Equation 5.1. The elastic modulus for the steel pile is determined as 210 GPa. δ' is determined as 1.0ϕ' for bored piles. The average ultimate shear stress for each layer at depth z, $\tau_{u,z}$, can be calculated using Equation 5.13. Using the back-analysis of the test pile base results from Mayne and Harris (1993), the values of parameters k_{b1}, k_{b2} and S_{bu} in Equation 5.4 are determined as 46,735 (kN/m), 12,654 (kN/m) and 21.25 (mm), respectively. The soil properties and input parameters for MLTM along the pile shaft are summarized in Table 5.2.

Table 5.2 Soil properties and input parameters for MLTM along the pile shaft

ΔH (m)	z (m)	w (%)	e	S (%)	$(u_a - u_w)$ (kPa)	ϕ' (°)	σ'_{v0} (kPa)	$\tau_{u,z}$ (kPa) K/K_0 = 0.7	$\tau_{u,z}$ (kPa) K/K_0 = 0.8	$\tau_{u,z}$ (kPa) K/K_0 = 0.9	$G_{0(us)}$ (MPa)
1	0.5	19.1	0.7	72.85	45.93	34	8.25	24.29	24.53	24.78	7
1	1.5	19.1	0.7	72.85	45.93	34	24.75	27.72	28.46	29.19	21
1	2.5	19.1	0.7	72.85	45.93	34	41.25	31.16	32.38	33.61	36
1	3.5	19.5	0.7	74.38	42.33	34	57.75	33.26	34.97	36.69	50
1	4.5	19.8	0.73	72.42	47.00	34	74.25	38.41	40.62	42.83	64
1	5.5	19.8	0.73	72.42	47.00	37	90.75	44.71	47.43	50.15	78
1	6.5	19.5	0.73	71.32	49.79	33	107.25	45.26	48.43	51.61	93
1	7.5	18	0.74	64.95	69.24	31	123.75	52.26	55.87	59.47	107
1	8.5	19.2	0.71	72.20	47.54	31	140.25	49.23	53.32	57.41	121
1	9.5	18.8	0.76	66.05	65.43	33	156.75	60.51	65.15	69.78	136
1	10.5	18.4	0.83	59.19	93.32	34	173.25	68.60	73.75	78.91	150
1	11.5	16.2	0.73	59.25	93.01	35	189.75	72.70	78.36	84.03	164
1	12.5	17.3	0.74	62.42	78.87	37	206.25	78.19	84.38	90.56	178
1	13.5	18.1	0.69	70.04	53.24	35	222.75	72.67	79.32	85.97	193
1	14.5	16.5	0.67	65.75	66.42	38	239.25	84.41	91.60	98.78	207
1	15.5	14.7	0.67	58.58	96.36	36	255.75	87.23	94.89	102.55	221
0.8	16.4	14.7	0.67	58.58	96.36	36	270.6	94.93	103.04	111.14	236

Following the proposed calculation procedure, the response of a single pile in unsaturated Piedmont soils can be calculated. Figure 5.8(a) and 5.8(b) show comparisons of load-displacement curves at the pile head between the measured results and calculated values using different K/K_0 and R_{sf} values. The computed results are generally consistent with the measured axial load along the pile shaft at different loading levels. The calculated load-displacement curve using $K/K_0 = 0.7$ and $R_{sf} = 0.95$ closely matches with the measured results. It can be observed that the pile displacement decreases with an increase in the ratio K/K_0 at the same loading level. On the other hand, the influence of the hyperbolic curve fitting coefficient R_{sf} on the pile behavior is insignificant and hence has negligible influence in practical applications.

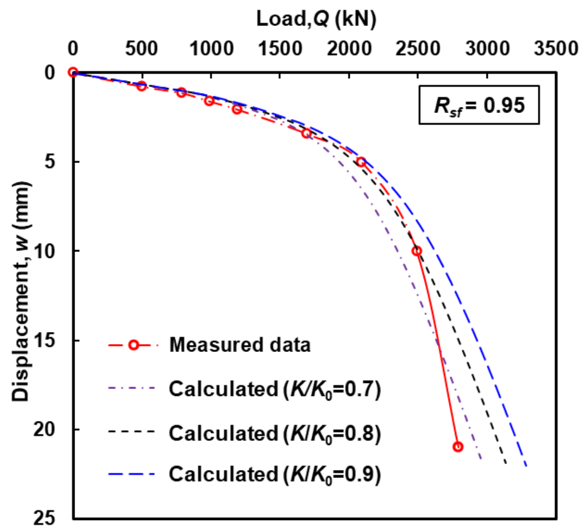

(a)

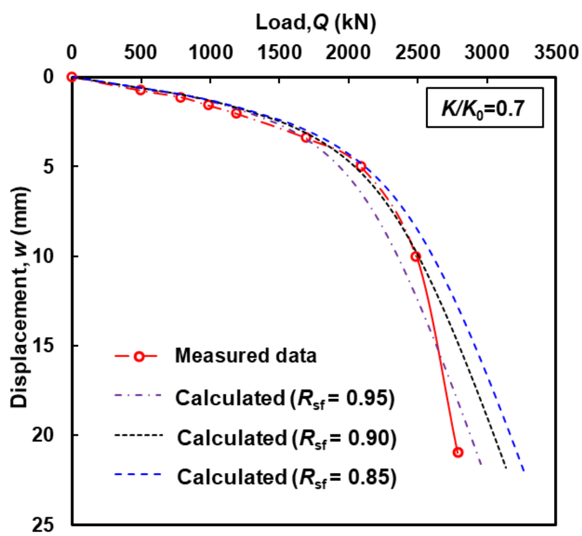

(b)

Figure 5.8 Comparisons between the measured and predicted load-displacement curve at the pile head

5.5.2 Single pile load tests by Fellenius et al. (2007)

Fellenius et al. (2007) performed static piles load tests on the campus of the Faculty of Engineering of the University of Porto, Porto, Portugal. The soil in the north-western region of Portugal is dominantly residual saprolitic soil, the thickness of which can sometimes attain more than 20 m, with more common values of 5 to 10 m. The GWT is at 10-12 m depth. Grain size analysis shows that the residual soil consists of around 40 % sand size, 20% gravel size, 30% silt size and 10% clay size. Based on CPTU-based soil classifications, the dominant soil can be classified as "silty clay to silty sand". The total unit weight is 18 kN/m^3. The natural water content ranges from 16.2 % to 22.5% and the degree of saturation is between 56% to 86%. The effective cohesion is 4.5 kPa and the internal friction angle is 36˚. The tested bored pile is 6 m in embedded length with 600 mm in diameter, and an elastic modulus of 20 GPa. Table 5.3 summarizes some key properties used as input parameters of MLTM along the pile shaft. The soil is divided into 12 layers with a 0.5 m-thickness of each layer. The values of ($u_a - u_w$) along the depth are obtained based on the U2 pore-pressure measurements. The negative pore water pressure (i.e., matric suction) above an 8 m depth is about 5 to 25 kPa. The degree of saturation is back-calculated using the SWCC and measured matric suction profile. The fitting parameters α and n were determined as 0.0383 and 1.3774 using van Genuchten (1980) SWCC model, respectively (Wösten et al. 1999). The average horizontal stress index, K_D, given by da Fonseca et al. (2007) along the pile length is 6.647. The at-rest coefficient K_0 was calculated as 1.04 using the following correlation between K_0 and K_D (Marchetti 1980).

$$\begin{cases} OCR = \left(0.5K_D\right)^{1.56} \\ K_0 = \left(1-\sin\phi'\right)OCR^{\left(\sin\phi'\right)} \end{cases} \tag{5.37}$$

where OCR is the overconsolidation ratio. Based on site conditions, the values for K/K_0 of 0.80, 0.90 and 1.0 and R_{sf} of 0.85,0.90 and 0.95 were adopted for the entire deposit. The interface friction angle δ is determined as 1.0ϕ' for bored piles. The average ultimate shear stress for each layer at depth z, $\tau_{u,z}$, was calculated using Equation 5.13. The values of the parameters k_{b1}, k_{b2} and S_{bu} are derived by the back-analysis of field load test results, which are determined as 31,782 (kN/m), 4,492 (kN/m) and 2.95 (mm), respectively. The small-strain shear modulus $G_{0(us)}$ is obtained from CH shear waves by da Fonseca et al. (2007).

Based on the proposed algorithm, the load-displacement curves at the pile head were calculated and shown in Figure 5.9. Different values of K/K_0 and R_{sf} were adopted and compared with the measured data. From Figure 5.9(a) and 5.9(b), it can be observed that at the same pile head displacement, the pile head load increases slightly with an increase in K/K_0 and decrease in R_{sf}. The comparison reveals good agreement between the computed results and measured data using the values of K/K_0 =1.0 and R_{sf} = 0.90.

Table 5.3 Input parameters of modified LTM along the pile shaft

ΔH (m)	z (m)	w (%)	E	S (%)	(u_a-u_w) (kPa)	ϕ' (°)	σ'_{v0} (kPa)	$\tau_{u,z}$ (kPa) K/K_0 = 0.8	$\tau_{u,z}$ (kPa) K/K_0 = 0.9	$\tau_{u,z}$ (kPa) K/K_0 = 1.0	$G_{0(us)}$ (MPa)
0.5	0.25	19.1	0.7	94.20	9.25	36	4.5	13.57	13.91	14.25	101.50
0.5	0.75	19.1	0.7	97.70	4.50	36	13.5	15.90	16.92	17.95	115.32
0.5	1.25	19.1	0.7	97.80	4.34	36	22.5	21.26	22.97	24.67	129.15
0.5	1.75	19.5	0.7	95.21	8.00	36	31.5	29.18	31.57	33.96	130.31
0.5	2.25	19.8	0.73	86.57	20.00	36	40.5	41.69	44.77	47.84	131.48
0.5	2.75	19.8	0.73	93.73	10.00	36	49.5	41.39	45.15	48.91	134.92
0.5	3.25	19.5	0.73	95.24	7.96	36	58.5	45.56	50.00	54.45	136.08
0.5	3.75	18	0.74	87.93	18.00	36	67.5	57.02	62.15	67.27	138.38
0.5	4.25	19.2	0.71	87.93	18.00	36	76.5	62.49	68.30	74.11	142.95
0.5	4.75	18.8	0.76	85.26	22.00	36	85.5	70.08	76.58	83.07	145.24
0.5	5.25	18.4	0.83	85.91	21.00	36	94.5	75.03	82.21	89.39	149.81
0.5	5.75	16.2	0.73	83.37	25.00	36	103.5	82.54	90.40	98.26	152.10

The results summarized for the above two cases suggest that the proposed MLTM for predicting the response of single piles in unsaturated soils is reliable.

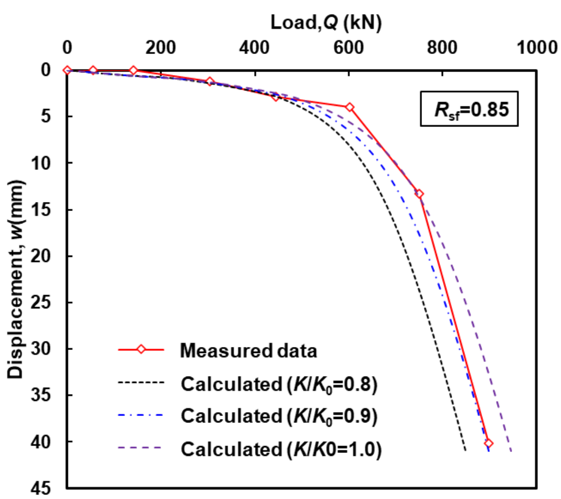

(a)

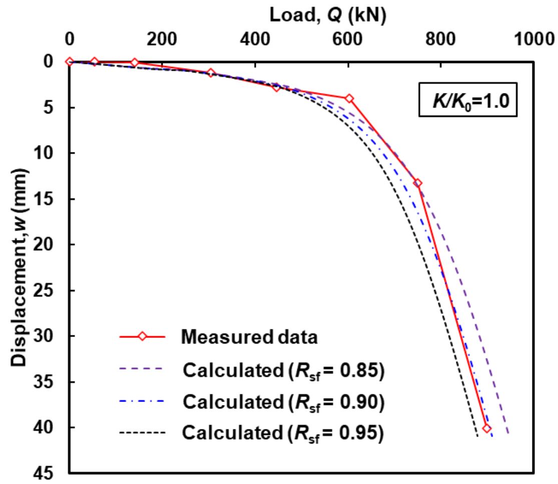

(b)

Figure 5.9 Comparisons between the measured and calculated load-displacement curves

5.6 Validation-Pile group

5.6.1 Model pile tests conducted by Al Khazaali and Vanapalli (2019)

Al Khazaali and Vanapalli (2019) have performed a series of model pile tests in saturated and unsaturated sands to study the influence of various saturation conditions on the behavior of pile groups by varying the GWT depths at 0 (i.e., ground surface), 300, 400 and 550 mm. In this study, the measured response of pile groups with two different pile center-to-center spacings, *s* (i.e., 3*D* and 5*D*) were used to validate the proposed method. For both field cases of single piles, the local *q-z* curves are measured in the literature, and they were used to calibrate the proposed bilinear model at the pile base. However, for the model pile group test, the *q-z* curve is not available; thus, a 3D numerical technique is developed which utilizes the commercial finite-element software ABAQUS. Besides, numerical modeling predictions are also compared with measurements. The detailed calculation using both methods are described as following.

5.6.2 Calculation using proposed approach

The soil properties of Unimin Sand are summarized in Table 5.4. As presented in Figure 5.10, a best-fit analysis was performed for the measured drying path of SWCC using Equation 5.8 with values of $a = 16.673$, $n = 4.341$, $m = 177.27$. The SWCC can be divided into three zones as boundary effect zone, transition zone and residual zone and they are separated by AEV and $(u_a - u_w)_r$ (see Figure 5.10). The AEV and residual suction value, $(u_a - u_w)_r$ were determined as 3.8 and 7.8 kPa, respectively. This is obtained graphically from the matric suction values corresponding to the intersection of two linear tangent lines in SWCC (Vanapalli et al. 1998). With the aid of the SWCC, degree of saturation or water content information can be obtained for various soil suction values.

Table 5.4 Basic soil properties of Unimin 7030 Sand (from Al-Khazaali and Vanapalli et al. 2019)

Soil Property	Value
Specific gravity, G_s	2.65
Maximum dry unit weight, $\gamma_{d(max)}$ (kN/m^3)	16.3-16.7
Total unit weight, γ (kN/m^3)	18.6
Saturated unit weight, γ_{sat} (kN/m^3)	20.4
Average void ratio, e	0.606
Range of relative density, D_r (%)	60-70
Effective cohesion, c' (kPa)	0
Internal friction angle, ϕ'(°)	35.3
Pile-soil interface friction angle for smooth shaft surface, δ'(°)	24

The matric suction profile for different GWT conditions in the soil container were measured using tensiometers at different depths: 150mm, 300 mm, 450 mm and 600 mm as shown in Figure 5.11. Best-fitted analyses are undertaken using Equation 5.7 to estimate the nonlinear relationship between the matric suction and depth. The curve-fitting constants c_1, c_2, c_3 and c_4 in Equation 5.7 are determined as 4.17, -28.08, -1.05 and 2.73 for GWT = 300 mm, -170.7, 60.45, -8, and 4.45 for GWT = 400 mm and -121.7, 64.7, -9.8 and 6.15 for GWT = 550 mm, respectively (see Figure 5.11).

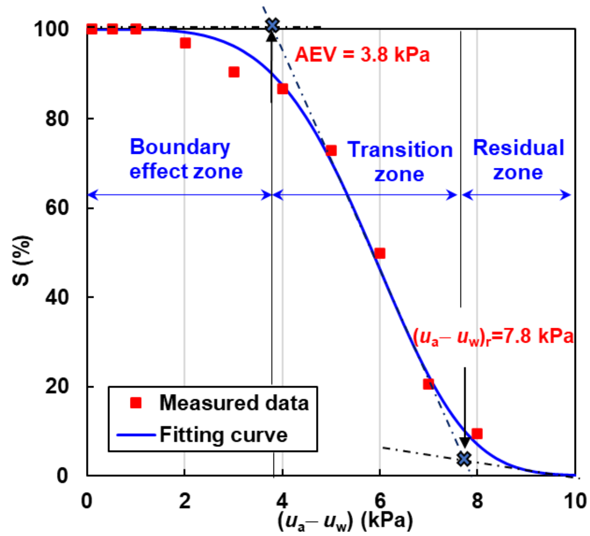

Figure 5.10 SWCC of Unimin sand (modified from Vanapalli et al. 2018)

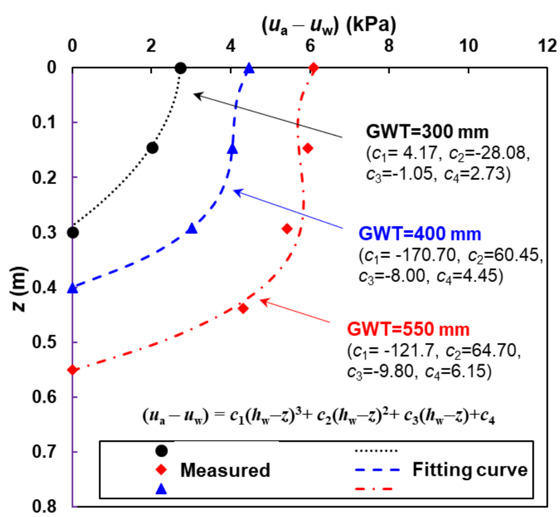

Figure 5.11 Matric suction profile for different GWT conditions

The modulus of pile and pile cap are both determined as 210 GPa. The Poisson's ratio, υ, is 0.334. The modulus of elasticity of the soil under saturated conditions, E_{sat}, is assumed to be 4000 kPa. Experimental studies performed on unsaturated soils suggest a strong dependence of elastic modulus on both matric suction and volumetric water content values (Fredlund et al. 1975, Edil et al. 1981, Costa et al. 2003, Sawangsuriya et al. 2009). The modulus of elasticity of unsaturated soil, E_{unsat}, can be calculated using a semi-empirical model proposed by Oh et al. (2009)

$$E_{\mathrm{unsat}} = E_{\mathrm{sat}}\left[1+\alpha\frac{(u_{\mathrm{a}}-u_{\mathrm{w}})}{(P_{\mathrm{a}}/101.3)}\left(S^{\beta}\right)\right] \tag{5.38}$$

where P_{a} is atmospheric pressure (101.3kPa), and α and β are two fitting parameters. Since Unimin sand is a non-plastic soil, both fitting parameters α and β equal to unity. The maximum shear modulus ($G_{0(\mathrm{us})}$) of the soil along the depth can then be estimated using the relationship between shear modulus and elastic modulus. The friction angle of pile-soil interface δ' is given as 24°. The at rest lateral earth pressure coefficient K_0 equals to 0.42. The values for K/K_0 and R_{sf} is assumed to be 1.0 and 0.90, respectively. It is noted that the parameters k_{b1}, k_{b2} and S_{bu} are back calculated by the load-displacement curve at the pile base obtained from numerical modelling analysis.

Table 5.5 Input parameters of MLTM along the pile shaft for different GWT scenarios

<table>
<tr><th rowspan="4">Layer No.</th><th rowspan="4">ΔH (m)</th><th rowspan="4">z (m)</th><th rowspan="4">σ'_{v0} (kPa)</th><th colspan="6">GWT = 0 mm</th><th colspan="6">GWT = 300 mm</th><th colspan="6">GWT = 400 mm</th><th colspan="6">GWT = 550 mm</th></tr>
<tr><th colspan="2">k_{b1}</th><th colspan="2">k_{b2}</th><th colspan="2">S_{bu}</th><th colspan="2">k_{b1}</th><th colspan="2">k_{b2}</th><th colspan="2">S_{bu}</th><th colspan="2">k_{b1}</th><th colspan="2">k_{b2}</th><th colspan="2">S_{bu}</th><th colspan="2">k_{b1}</th><th colspan="2">k_{b2}</th><th colspan="2">S_{bu}</th></tr>
<tr><td colspan="2">126</td><td colspan="2">71.4</td><td colspan="2">0.01</td><td colspan="2">152</td><td colspan="2">124</td><td colspan="2">0.01</td><td colspan="2">177</td><td colspan="2">152</td><td colspan="2">0.01</td><td colspan="2">246</td><td colspan="2">169</td><td colspan="2">0.005</td></tr>
<tr><th colspan="3">$\tau_{u,z}$ (kPa)</th><th colspan="3">$G_{0(us)}$ (MPa)</th><th colspan="3">$\tau_{u,z}$ (kPa)</th><th colspan="3">$G_{0(us)}$ (MPa)</th><th colspan="3">$\tau_{u,z}$ (kPa)</th><th colspan="3">$G_{0(us)}$ (MPa)</th><th colspan="3">$\tau_{u,z}$ (kPa)</th><th colspan="3">$G_{0(us)}$ (MPa)</th></tr>
<tr><td>1</td><td>0.03</td><td>0.015</td><td>0.279</td><td colspan="3">0.05</td><td colspan="3">1.58</td><td colspan="3">1.34</td><td colspan="3">5.35</td><td colspan="3">1.88</td><td colspan="3">6.12</td><td colspan="3">1.46</td><td colspan="3">5.71</td></tr>
<tr><td>2</td><td>0.03</td><td>0.045</td><td>0.837</td><td colspan="3">0.16</td><td colspan="3">1.58</td><td colspan="3">1.41</td><td colspan="3">5.21</td><td colspan="3">1.98</td><td colspan="3">6.21</td><td colspan="3">1.67</td><td colspan="3">6.01</td></tr>
<tr><td>3</td><td>0.03</td><td>0.075</td><td>1.395</td><td colspan="3">0.26</td><td colspan="3">1.58</td><td colspan="3">1.45</td><td colspan="3">4.99</td><td colspan="3">2.09</td><td colspan="3">6.24</td><td colspan="3">1.84</td><td colspan="3">6.16</td></tr>
<tr><td>4</td><td>0.03</td><td>0.105</td><td>1.953</td><td colspan="3">0.36</td><td colspan="3">1.58</td><td colspan="3">1.47</td><td colspan="3">4.68</td><td colspan="3">2.20</td><td colspan="3">6.25</td><td colspan="3">1.97</td><td colspan="3">6.21</td></tr>
<tr><td>5</td><td>0.03</td><td>0.135</td><td>2.511</td><td colspan="3">0.47</td><td colspan="3">1.58</td><td colspan="3">1.52</td><td colspan="3">4.50</td><td colspan="3">2.31</td><td colspan="3">6.26</td><td colspan="3">2.09</td><td colspan="3">6.19</td></tr>
<tr><td>6</td><td>0.03</td><td>0.165</td><td>3.069</td><td colspan="3">0.57</td><td colspan="3">1.58</td><td colspan="3">1.53</td><td colspan="3">4.16</td><td colspan="3">2.42</td><td colspan="3">6.27</td><td colspan="3">2.18</td><td colspan="3">6.13</td></tr>
<tr><td>7</td><td>0.03</td><td>0.195</td><td>3.627</td><td colspan="3">0.68</td><td colspan="3">1.58</td><td colspan="3">1.47</td><td colspan="3">3.64</td><td colspan="3">2.52</td><td colspan="3">6.28</td><td colspan="3">2.28</td><td colspan="3">6.06</td></tr>
<tr><td>8</td><td>0.03</td><td>0.225</td><td>4.185</td><td colspan="3">0.78</td><td colspan="3">1.58</td><td colspan="3">1.39</td><td colspan="3">3.04</td><td colspan="3">2.60</td><td colspan="3">6.27</td><td colspan="3">2.46</td><td colspan="3">6.24</td></tr>
<tr><td>9</td><td>0.03</td><td>0.255</td><td>4.743</td><td colspan="3">0.88</td><td colspan="3">1.58</td><td colspan="3">1.28</td><td colspan="3">2.35</td><td colspan="3">2.65</td><td colspan="3">6.20</td><td colspan="3">2.68</td><td colspan="3">6.56</td></tr>
<tr><td>10</td><td>0.03</td><td>0.285</td><td>5.301</td><td colspan="3">0.99</td><td colspan="3">1.58</td><td colspan="3">1.14</td><td colspan="3">1.58</td><td colspan="3">2.59</td><td colspan="3">5.72</td><td colspan="3">2.83</td><td colspan="3">6.66</td></tr>
</table>

Note: The units for k_{b1}, k_{b2} and S_{bu} are kN/m, kN/m and m, respectively.

Table 5.5 shows the values of some key input parameters of MLTM for different GWT scenarios. For each pile in a 2×2 symmetric pile group that consists of 4 individual piles, center-to-center pile spacings, s, from other three piles, r_{ij1}, r_{ij2} and r_{ij3}, are s, s and $\sqrt{2}s$, respectively. Following the proposed calculation procedure for the case of a perfectly rigid pile cap, the load-displacement behavior of the pile group can be calculated.

5.6.3 Finite element analysis (FEA)

Three-dimensional numerical analyses of a 2 × 2 pile group using ABAQUS were undertaken to investigate the effects of varying GWT depths and interaction between piles in a group using the pile load tests conducted by Al Khazaali and Vanapalli (2019). Both the pile group and pile cap were modelled as a linear-elastic material using eight-node linear brick elements (C3D8), with Young's modulus of E_p = 210 GPa. The density and Poisson's ratio of piles were 7850 kg/m^3 and 0.3, respectively. The unsaturated soil was modelled as a linear elastic perfectly plastic material obeying the Mohr-Coulomb criterion using eight-node stress–pore-pressure coupled brick elements (C3D8P). Since experimental studies indicated that the internal friction angle ϕ' is not influenced by matric suction (e.g., Ho and Fredlund 1982, Fredlund and Rahardjo 1993, Vanapalli et al. 1996), the contribution of matric suction towards shear strength can be incorporated as apparent cohesion (c_a) based on Equations 5.10a and 5.10b, respectively (e.g., Oh and Vanapalli, 2011)

$$c_a = c' + (u_a - u_w)\left[\frac{(\theta - \theta_r)}{(\theta_s - \theta_r)}\tan\phi'\right] \tag{5.39a}$$

$$c_a = c' + (u_a - u_w) S^{\kappa} \tan\phi' \tag{5.39b}$$

The variation of c_a along the depth (Figure 5.12(a)) was introduced to the ABAQUS by implementing a user subroutine USDFLD so that the nonlinear shear strength of unsaturated soil can be interpreted in the numerical models. The USDFLD allows the user to define field variables (i.e., pore water pressure or degree of saturation) and calculate the corresponding material properties of unsaturated soils in every material point. More details on how USDFLD is incorporated in ABAQUS to simulate the mechanical behavior of unsaturated soils are available in Cheng and Vanapalli (2021). The variation of E_{unsat} with respect to depths for different GWTs scenarios is shown in Figure 5.12(b). For the sake of simplicity, an average value of E_{unsat} from the pile head to 1.5 times the diameter below the pile base was used as a uniform elastic modulus of soil in the model. The SWCC of Unimin sand was imported into ABAQUS by adding "Sorption" material properties with a range of matric suction and corresponding degrees of saturation values. The saturated permeability k_{sat} of Unimin sand is assumed as 1×10^{-4} m/s. The pore water pressure of all the nodes at GWT surface was set to zero. The dilation angle for sand was calculated as 10% of the effective angle of internal friction ϕ' (Bolton 1986).

The pile-soil interaction is simulated by defining tangential and normal contact behavior, where the surface of pile components was defined as "Master surface" and the soil components as "Slave surface". The tangential contact between surfaces pile and unsaturated soil using a coefficient of friction of 0.44 (i.e., tan δ').

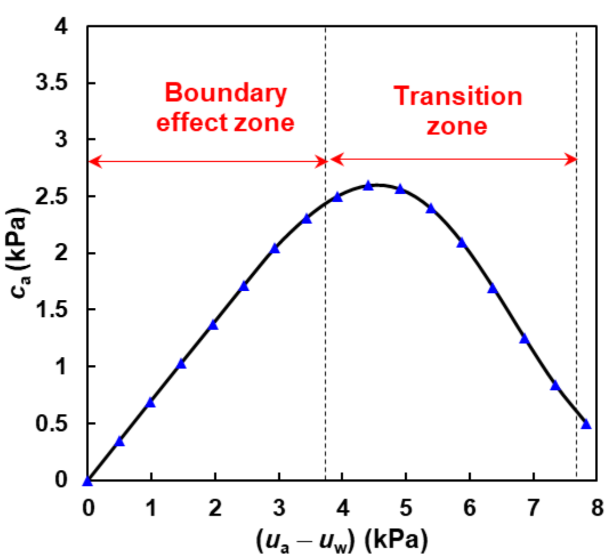

(a)

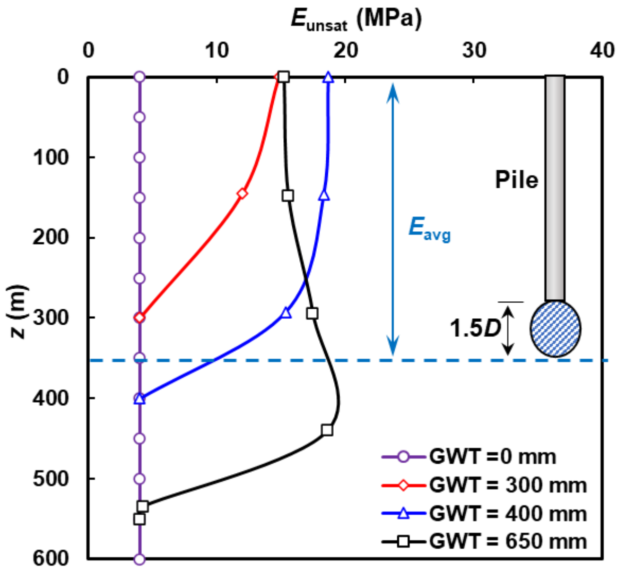

(b)

Figure 5.12(a) The variation of c_a with respect to (u_a – u_w) (b) The variation of E_{unsat} with respect to depths for different GWTs scenarios

For boundary conditions, the displacements at the bottom of soil mesh and in the direction perpendicular to the symmetry planes were fixed. Figure 5.13 shows the 3D FE meshes and dimensions of the pile-soil system. The meshes for the pile group and surrounding soils were refined to analyze the interactions between piles and soils better.

For a 2×2 pile group which consists of 4 piles with 38 mm in diameter and 300 mm in length, the pile and soil system were discretized with 640 C3D8 elements and 11160 C3D8P elements, respectively. There were two steps in the FE analyses: (1) the geostatic step. The holes for placing or casting the pile group are pre-excavated to minimize the pile installation effect. A gravity load is applied to the soil body to replicate the in-situ stress state of a soil under gravity prior to the pile installation. (2) In the loading step, the pile group and pile cap were placed in the pre-excavated hole and each pile head was tied with the pile cap. A prescribed vertical displacement was then applied on the top of the pile cap in the z direction, as shown in Figure 5.13(a).

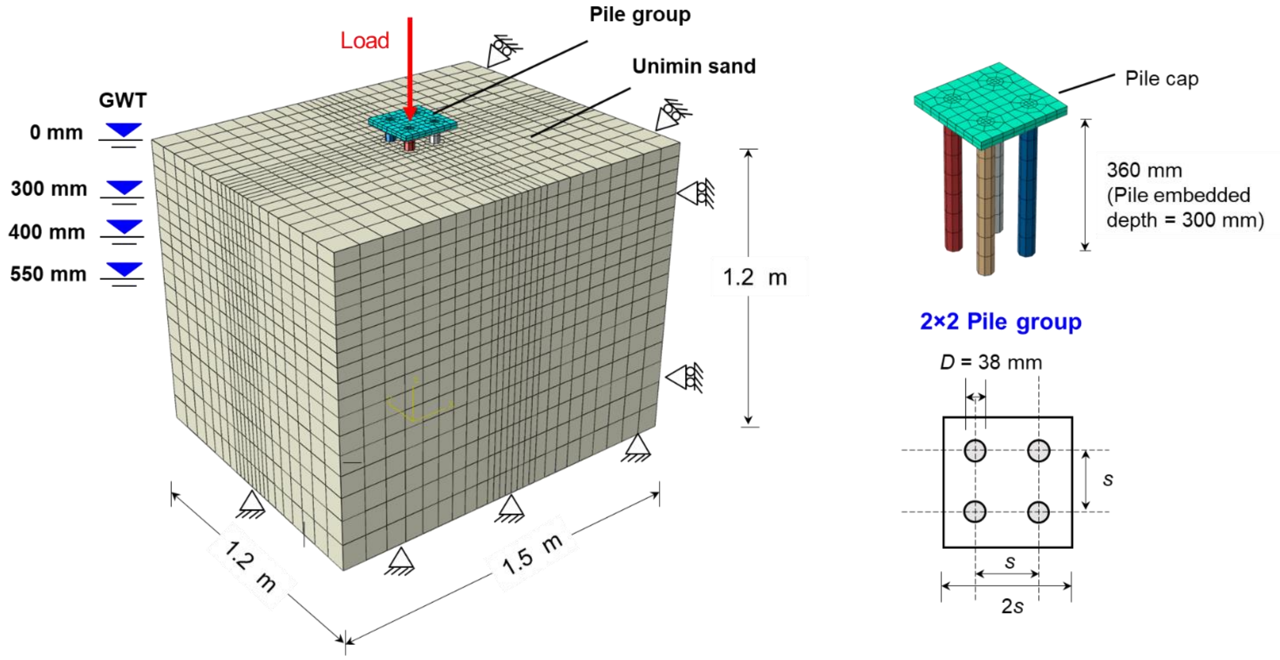

(a) (b)

Figure 5.13 (a) Geometry and meshes of a 2×2 pile group-soil system (b) Schematic plan view

5.6.4 Comparisons with measured results

As shown in Figure 5.14 and Figure 5.15, the measured load-displacement curves of 2×2 pile group for different GWT scenarios and pile center-to-center spacings (i.e. s=3*D* and 5*D*) were compared with the numerical predictions as well as results from the proposed analytical method. It can be observed that the pile group capacity increases with the lowering of the water table. Lowering the water table will develop matric suction. The matric suction applies tensile stresses on the soil particles and their packets. This is mainly because higher matric suction contributes to an increase in soil stiffness and shear strength of unsaturated soils, thereby leading to higher bearing capacity.

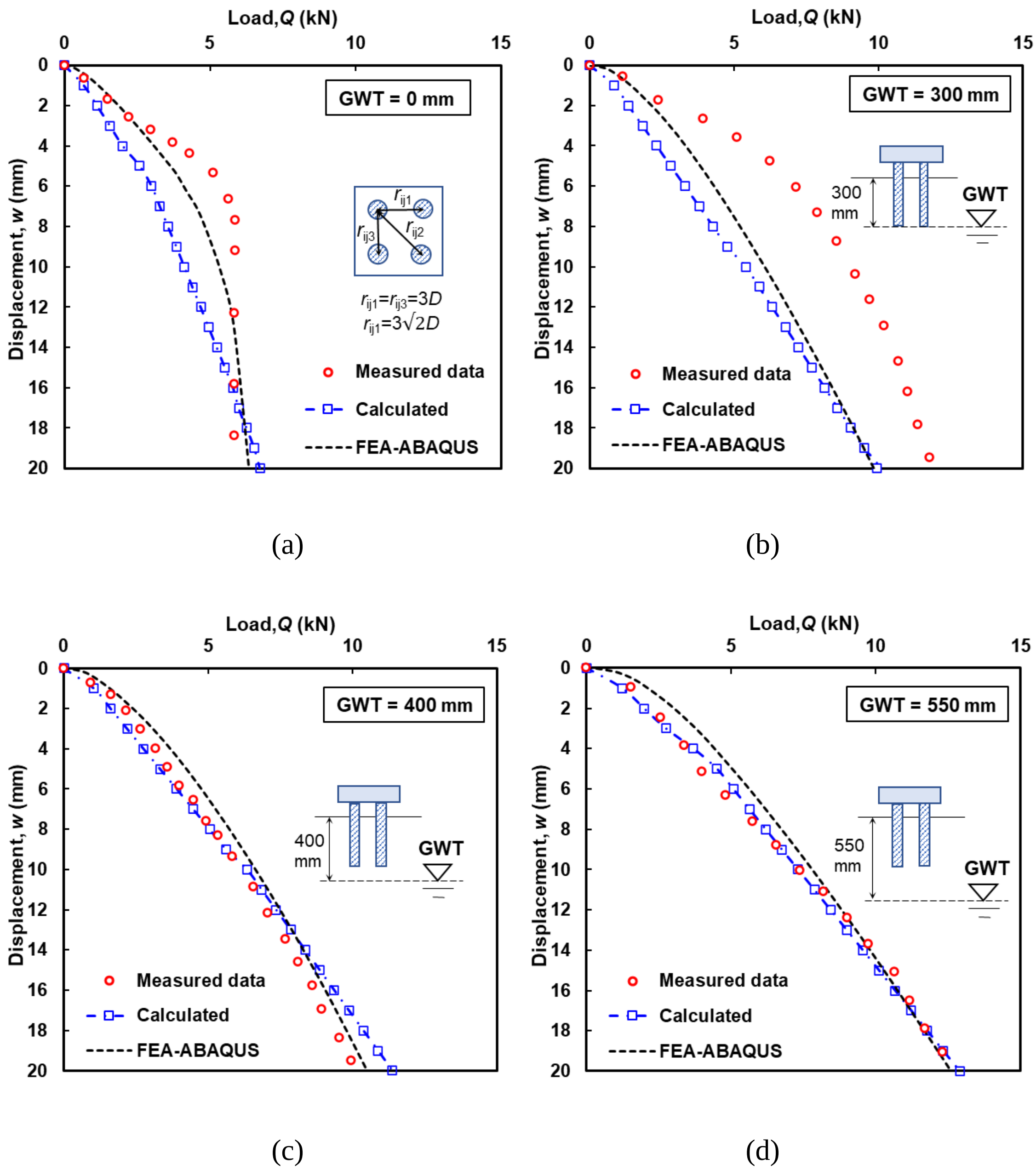

Figure 5.14 Load versus displacement curves of a pile group for different GWT scenarios ($s = 3D$)

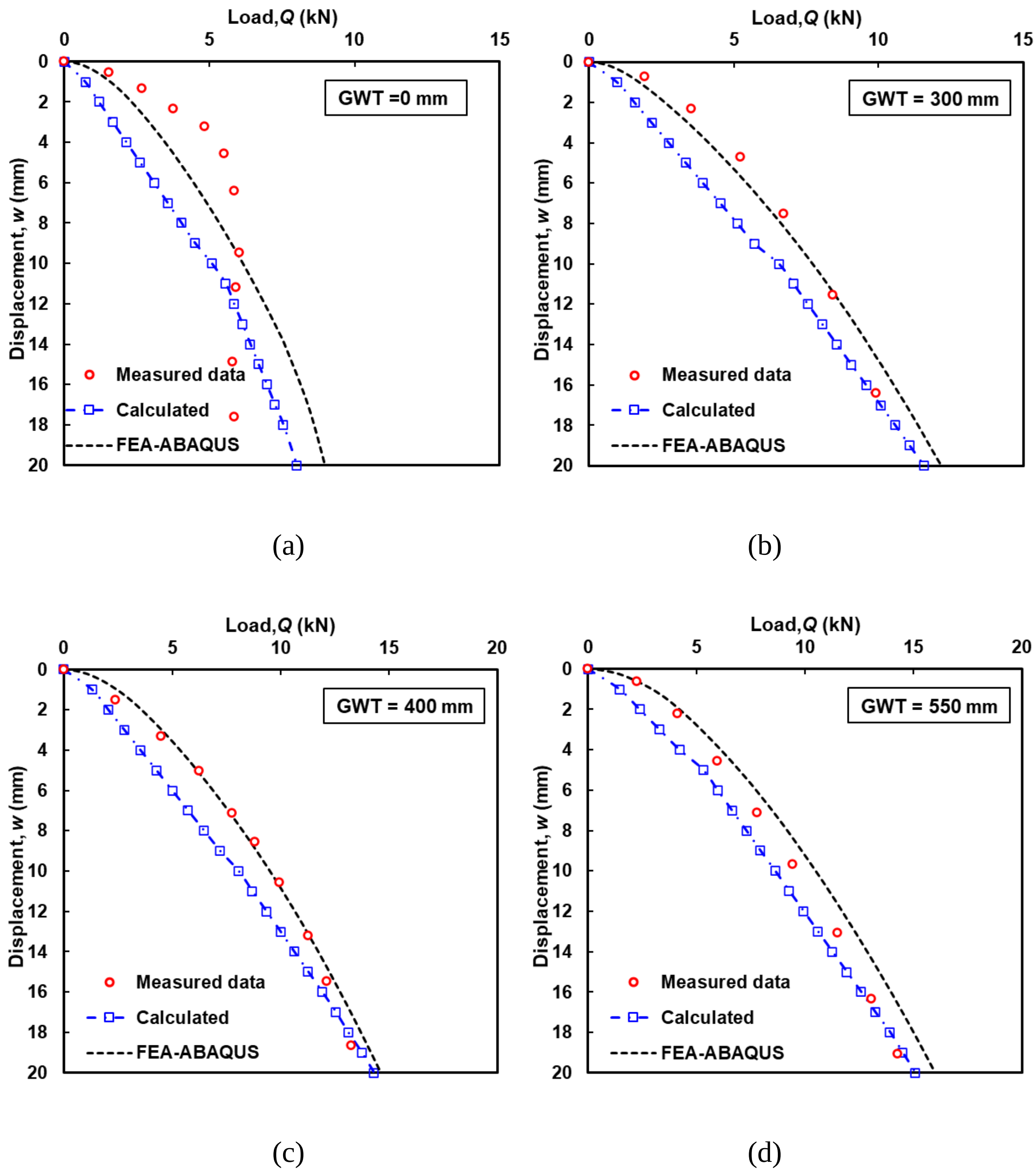

Figure 5.15 Load versus displacement curves of a pile group for different GWT scenarios ($s = 5D$)

The results from both the proposed approach and 3D numerical models highlight relatively good agreements with the experimental data for most cases. In addition, the load-displacement curves from the 3D FE model match more closely with the measured data compared to the present analytical method. This may be attributed to several factors. Firstly, numerical analysis considers the impact of dilation. Some research studies have been undertaken to study the dilation effect of unsaturated interfaces (Hamid and Miller 2008, 2009; Hossain and Yin 2014). From these studies, it is concluded that the unsaturated interface exhibits strain-hardening behavior prior to reaching peak strength due to the impact of dilation. As the GWT is lowered, sand dilatancy increases due to matric suction, resulting in a steeper slope in bearing capacity. However, in the proposed MLTM, this factor is not considered. Secondly, load transfer methods often involve simplifying assumptions and idealizations to model the soil-pile interaction. These assumptions may not fully capture the complex behavior of the soil and pile system, leading to discrepancies between predicted and measured responses.

5.7 Summary and conclusion

A better understanding of the load transfer mechanism using the principles of unsaturated soil mechanics is required for the rational design of pile foundations that are in soils that are not in a state of saturated condition. In this study, a modified load transfer method (MLTM) is first proposed to predict the nonlinear load-displacement behavior at the pile-soil interface for single piles in unsaturated soils considering the influence of matric suction. The nonlinear relationship between shaft shear stress and pile-soil relative shaft displacement is described by a modified hyperbolic load transfer model, while the relationship between pile base resistance and base displacement is described using a bilinear model. Two pile load tests performed in unsaturated residual soils are used to validate the reliability of the proposed method for predicting the load-displacement curve of single piles. In addition, the analysis for single piles is extended to pile group to account for the interaction effect between individual piles. Highly effective iterative procedures were developed using MATLAB to obtain the solution to load-displacement curves for both single piles and pile groups incorporating the input parameters. A model pile group test in various unsaturated conditions has also been used to provide the validity of the proposed approach. Lastly, a 3D numerical analysis of a 2×2 pile group using ABAQUS is undertaken to investigate the effects of varying GWT depths and interaction between piles in a group. Both FEA and analytical methods provide good comparisons with the measurements from the model pile group test. It is envisaged that both proposed numerical and analytical methods will be useful to geotechnical engineers for reliable estimates of the load-displacement response in the design of pile foundations in unsaturated soil conditions.

CHAPTER 6

NUMERICAL ANALYSIS OF PILE FOUNDATIONS IN SATURATED AND UNSATURATED SOILS

6.1 Introduction[5]

The analyses of pile foundations should be undertaken to ensure that pile can fulfill its functions under various working loading conditions taking account of both practical and economical factors. The determination of the ultimate bearing capacity of piles that is required in the analysis of pile foundations has always been a challenge to geotechnical engineers. Many attempts have been made to develop alternative methods for evaluating the behavior of pile foundations that are relatively low in cost and simple since the full-scale pile load tests are expensive and time-consuming. Theoretical approaches (e.g., total and effective stress approaches) have been proposed by researchers that utilize the shear strength parameters with simplified assumptions which provide reasonable agreements with full scale tests (Skempton 1959, Vesić 1963, Hansen 1970, Vijayvergiya and Focht 1972, Burland 1973). In-situ tests such as Standard Penetration Test (SPT) or Cone Penetration Test (CPT) also have been widely recognized as a useful technique that provide essential soil information in the design of pile foundations (Hong et al. 2010, Alkrooah and Nikraz 2012, Shooshpasha et al. 2013).

In many scenarios, pile foundations are placed either in part or fully in the vadose zone where the soil is typically in an unsaturated state. Some studies showed that soil suction has a significant influence on the bearing capacity and the settlement behavior of pile foundations (Douthitt et al. 1998, Uchaipichat 2012, Vanapalli and Taylan 2012, Fattah et al. 2014). Therefore, using conventional approaches based on saturated soil mechanics in the design of foundations in unsaturated soils can contribute to unrealistic estimations of both the bearing capacity and the settlement behavior of pile foundations. In recent years,

[5] The contents presented in this chapter are from a manuscript that has been submitted to an international journal for review: **Cheng, X**., & Vanapalli, S. K. Numerical analysis of pile foundations in saturated and unsaturated soils (*Under review with a Special Issue Journal*)

some investigations have been undertaken to estimate the behavior of pile foundations in unsaturated soils considering the influence of matric suction based on experimental studies (Vanapalli et al. 2018, Al-Khazaali and Vanapalli 2019, Fattah et al. 2020, Chung and Yang 2017) and analytical approaches (Vanapalli and Taylan 2012, Vanapalli et al. 2018, Cheng and Vanapalli 2021). Numerical analyses are also extensively used to model the nonlinear response of soils with the rapid growth of computational techniques. In the early stage of numerical analysis applications to piles in unsaturated soils, Georgiadis et al. (2003) developed a total stress constitutive model to investigate the influence of the degree of saturation on pile behavior. The model incorporates an equation for the yield and plastic potential surfaces and well reproduces the collapse and wetting characteristics of unsaturated soils. The studies showed that the finite element analysis (FEA) based on unsaturated soil mechanics provides more consistent results with the field data compared to conventional analysis based on saturated soil mechanics. Al-Khazaali et al. (2016) and Han et al. (2016) have focused on the load versus displacement behaviour of single piles in unsaturated sandy and clayey soils using PLAXIS 2D, respectively. The influence of matric suction on the shear strength and elastic modulus of unsaturated soils was considered. It is concluded that the pile bearing capacity and slope of load versus displacement curve increase significantly with an increase in matric suction. Chung and Yang (2021) performed the FEA of single piles in unsaturated clayey soils under vertical loads using PLAXIS 2D. The required soil parameters for the numerical model in this study were determined performing different tests. For example, matric suction was measured using the contact filter method. An interface direct shear test was conducted to determine the interface strength reduction factor ($R_{\text{interface}}$) and interface friction angle. Cheng and Vanapalli (2021) have undertaken numerical studies to simulate the behavior of single piles subjected to both vertical and lateral loads in unsaturated soils. A user-defined subroutine was developed in ABAQUS to take account of the nonlinear behavior of shear strength and the elastic modulus of unsaturated soils. Good comparisons were observed between the experimental tests gathered from the several model pile load tests from the literature and the FEA results.

In this Chapter, succinct theoretical background of how the shear strength and elastic modulus of unsaturated soils can be used as tools for predicting the behavior of pile foundations with respect to matric suction is first reviewed. Secondly, a numerical modelling technique is developed to analyze the nonlinear response of single piles in both saturated and unsaturated soils. A user-defined subroutine USDFLD (user subroutine to redefine field variables at a material point) is written and implemented in finite element software ABAQUS to model the nonlinear mechanical behavior of unsaturated soils with respect to matric suction. The numerical analyses were then performed on four pile load tests that include two model pile tests performed in the laboratory and the remainder two from the field tests that were gathered from the published literature. Good comparisons were observed between the measured data and numerical predictions, for all four cases. The proposed numerical technique in this study is a promising approach for practicing geotechnical engineers for modelling the load versus deformation of piles in both saturated and unsaturated soils.

6.2 The mechanical behavior of unsaturated soils

The ultimate bearing capacity of single piles in unsaturated soils is significantly influenced by the pile-soil interface and the soil properties surrounding the pile. There is a strong relationship between the shear strength and the bearing capacity of a soil. Due to this reason, several researchers have developed theoretical approaches for estimating the bearing capacity of foundations using the shear strength properties of soils. The determination of the shear strength of unsaturated soils (*SSUS*) from experimental studies requires elaborate testing equipment and can be costly and time-consuming. Hence, several researchers have developed empirical and semi-empirical approaches to predict the *SSUS* using the saturated shear strength parameters and the Soil-Water Characteristic Curve (SWCC) (e.g., Vanapalli et al. 1996, Rassam and Cook 2002, Vilar 2006).

The SWCC is defined as the relationship between the soil water content (volumetric or gravimetric) or degree of saturation and matric suction. There are three distinct zones of SWCC (i.e., boundary effect zone (BEZ), transition effect zone (TEZ) and residual zone of saturation (RZS)). All the pores are filled with water in BEZ when the soil is in a state of saturated condition. The soil behavior in this zone can be interpreted using saturated soil mechanics and the shear strength increases linearly. The value of matric suction at which air enters the largest pores of soil is referred to as the air-entry value (AEV). As the water content in the soil reduces rapidly in TEZ, there is a further increase in matric suction. The contribution of matric suction starts to decrease as the wetted contact of the area decreases. The shear strength increases nonlinearly as matric suction increases. The shear strength contribution due to matric suction (ϕ^b) in this zone is less than the angle of internal friction (ϕ'). In RZS, there are relatively small reduction in the degree of saturation despite the significant increase in the matric suction. The shear strength of unsaturated soils may increase, decrease, or remain constant depending on the type of soil. For example, the shear strength of unsaturated sand decreases beyond the residual zone since the sand desaturates at a faster rate than fine-grained soils and there is a limited wetted area of contact. However, fine-grained soils such as clays may not have a well-defined residual state. Considerable water remaining in clay at the residual stage may still transmit suction effectively. Therefore, the shear strength of clays typically increases in the RZS. In addition, shear strength of certain fine-grained soils such as silts decreases gradually over a large suction range. The above results suggest that the SWCC is a valuable tool for predicting the shear strength taking account of the influence of matric suction.

Vanapalli et al. (1996) proposed two different semi-empirical models to predict the nonlinear shear strength of unsaturated soils, τ_{unsat}, using the saturated shear strength parameters (c' and ϕ') and the SWCC (Equations 6.1a and 6.1b). In these models, the SWCC information is typically expressed as a relationship between either degree of saturation or volumetric water content versus suction:

$$\tau_{\mathrm{unsat}} = c' + (\sigma_{\mathrm{n}} - u_{\mathrm{a}})\tan\phi' + (u_{\mathrm{a}} - u_{\mathrm{w}})\left[\frac{(\theta - \theta_{\mathrm{r}})}{(\theta_s - \theta_{\mathrm{r}})}\tan\phi'\right] \tag{6.1a}$$

$$\tau_{\mathrm{unsat}} = c' + (\sigma_{\mathrm{n}} - u_{\mathrm{a}})\tan\phi' + (u_{\mathrm{a}} - u_{\mathrm{w}})(S^{\kappa})\tan\phi' \tag{6.1b}$$

where $(\sigma_{\mathrm{n}} - u_{\mathrm{a}})$ is net normal stress in which σ_{n} is the normal stress and u_{a} is the atmospheric pressure, u_{w} is pore water pressure, $(u_{\mathrm{a}} - u_{\mathrm{w}})$ is matric suction, θ is volumetric water content, θ_{s} and θ_{r} is saturated and residual volumetric water content, respectively, S is the degree of saturation and κ is the fitting parameter that related to the plasticity index, I_p (Garven and Vanapalli 2006). Several studies suggest that the effective friction angle is not influenced by matric suction for conventional soils (Vanapalli et al. 1996, Ho and Fredlund 1982, Fredlund and Rahardjo 1993). For this reason, the contribution of matric suction towards shear strength can be incorporated as apparent cohesion c_a, which can be written as:

$$c_{\mathrm{a}} = c' + \left(u_{\mathrm{a}} - u_{\mathrm{w}}\right)\left[\frac{\left(\theta - \theta_{\mathrm{r}}\right)}{\left(\theta_{\mathrm{s}} - \theta_{\mathrm{r}}\right)} \tan\phi'\right] \tag{6.2a}$$

$$c_{\mathrm{a}} = c' + \left(u_{\mathrm{a}} - u_{\mathrm{w}}\right)\left(S^{\kappa}\right)\tan\phi' \tag{6.2b}$$

Many studies suggest that the modulus of elasticity of unsaturated soils increases with matric suction (Miao et al. 2002, Oh et al. 2009, Rahardjo et al. 2011). Oh et al. (2009) proposed the following equation to predict the variation of modulus of elasticity of unsaturated soils (i.e., E_{unsat}) using saturated modulus of elasticity of soils (i.e. E_{sat}) and the information of SWCC:

$$E_{\mathrm{unsat}} = E_{\mathrm{sat}}\left[1 + \alpha \frac{\left(u_{\mathrm{a}} - u_{\mathrm{w}}\right)}{\left(P_a / 101.3\right)}\left(S^{\beta}\right)\right] \tag{6.3}$$

where P_{a} = atmosphere pressure (101.3 kPa). The fitting parameter α varies from 0.5 to 2.5 depending on the foundation size and plasticity index, I_p. The fitting parameter β=1 for coarse-grained soils and 2 for fine-grained soils.

6.3 Numerical analysis

Numerical analyses are performed to simulate the behavior of bored piles in unsaturated sandy soil, clayey soil and residual soils from four pile load tests (two performed in the laboratory and two from the field test) reported by Vanapalli et al. (2018), Al-Khazaali and Vanapalli (2019), Marques et al. (2021) and Fellenuis et al. (2007). A numerical modelling technique is developed to analyze the behavior of single piles considering the contribution of matric suction using finite element software ABAQUS. The input parameters for the numerical model include the shear strength parameters of saturated soil, saturated modulus of elasticity and the SWCC. As shown in Figure 6.1, the matric suction profile along the depth varies linearly or nonlinearly depending on the environmental activities such as water infiltration and evaporation. SWCC is a useful tool to predict the degree of saturation (or water content) based on matric suction or vise versa. Substituting matric suction, degree of saturation (or water content) and saturated shear strength parameters (c', ϕ') into Equations 6.2a or 6.2b, the variation of both apparent cohesion and unsaturated elastic modulus with respect to matric suction can be obtained. The nonlinear relationship between the apparent cohesion and matric suction can be implemented into ABAQUS by writing a user-defined subroutine (USDFLD) so that the nonlinear shear strength of unsaturated soil can be interpreted using appropriate constitutive models (i.e., Equations 6.1a, 6.1b, 6.2a and 6.2b). The USDFLD allows the user to define field variables at every integration point of an element and calculate the material properties taking account of the influence of field variables. It provides access to the solutions from the previous increment and allows the user to update field variables for the current increment. The material properties of the unsaturated soil are defined as functions of field variables such as pore water pressure or degree of saturation in a material point. In other words, the contribution of matric suction towards cohesion at any point can be incorporated into apparent cohesion via the USDFLD. The results from numerical models are compared with the measured data from experimental studies. The details of numerical analyses are summarized in the following sections.

6.3.1 Case 1

A model pile load test was performed by Vanapalli et al. (2018) in Unimin sand under saturated and unsaturated conditions. The size of the soil tank is 300 mm in diameter and 700 mm in height. Model piles with 38.3 mm in diameter and length of 200 mm were tested in the testing program as shown in Figure 6.2a. The soil properties of Unimin sand are summarized in Table 6.1. Three tensiometers were installed at depths of 50, 200 and 250 mm to measure and monitor the matric suction value. The water level was first raised to the soil surface to achieve the saturated condition. Later, the elevation of the water was adjusted and maintained at 450 mm and 650 mm deep from the soil surface through a pulley system that connected to a water container. After achieving equilibrium conditions with respect to targeted matric suction values, a vertical load at a rate of 0.7 mm/min was applied to ensure a drained loading condition.

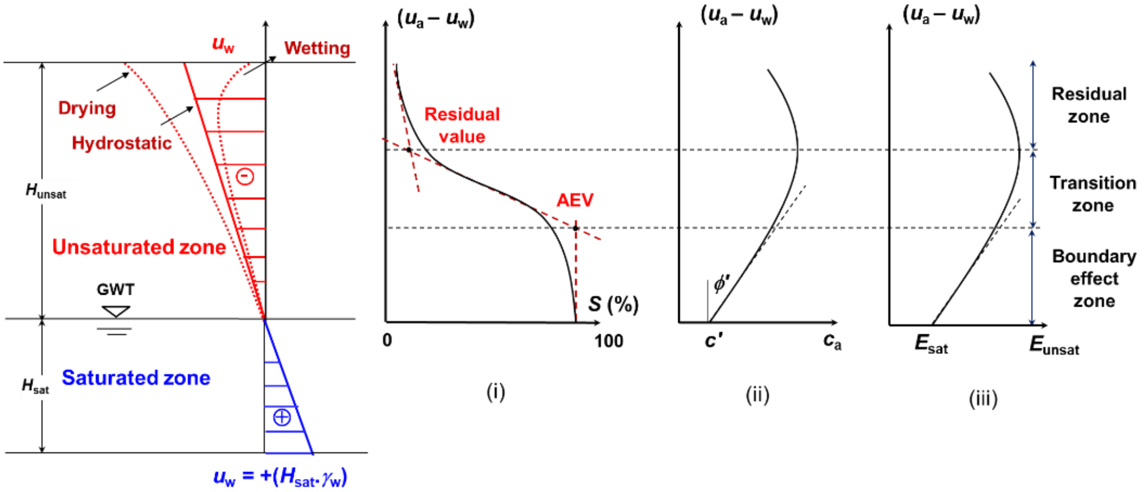

Figure 6.1 The influence of matric suction on the properties of unsaturated soils

In the present study, a 2D axisymmetric model was set up due to the symmetry of the pile-soil system. The pile is modelled as a linear elastic material with modulus of elasticity of 210 GPa and the Poisson's ratio of 0.15. The Unimin sand is modeled as an elastic-perfectly plastic material obeying Mohr-Coulomb failure criterion. The dilation angle of Unimin Sand was determined as 4.5°, which is slightly higher than 10% of ϕ'(DS415 1984) . The pile-soil interface friction angle (δ) was assumed to be $\delta = 2/3\phi' = 24.2°$. Figure 6.2b shows the details of the numerical model.

The drying path of SWCC of Unimin sand was fitted using Fredlund and Xing (1994)'s equation which yielded the fitting parameters a = 16.673, n = 4.341, m = 177.27 as follows:

$$S = \left[C(\psi)\right]\left[\frac{1}{\ln\left(e+\left(\frac{\psi}{a}\right)^{n}\right)}\right]^{m} \tag{6.4}$$

where $C(\psi)$ is the correction function, ψ is matric suction, e is Euler's number (2.71828), and a, n, m are fitting parameters. Figure 6.3 shows both the measured SWCC and the fitting curve.

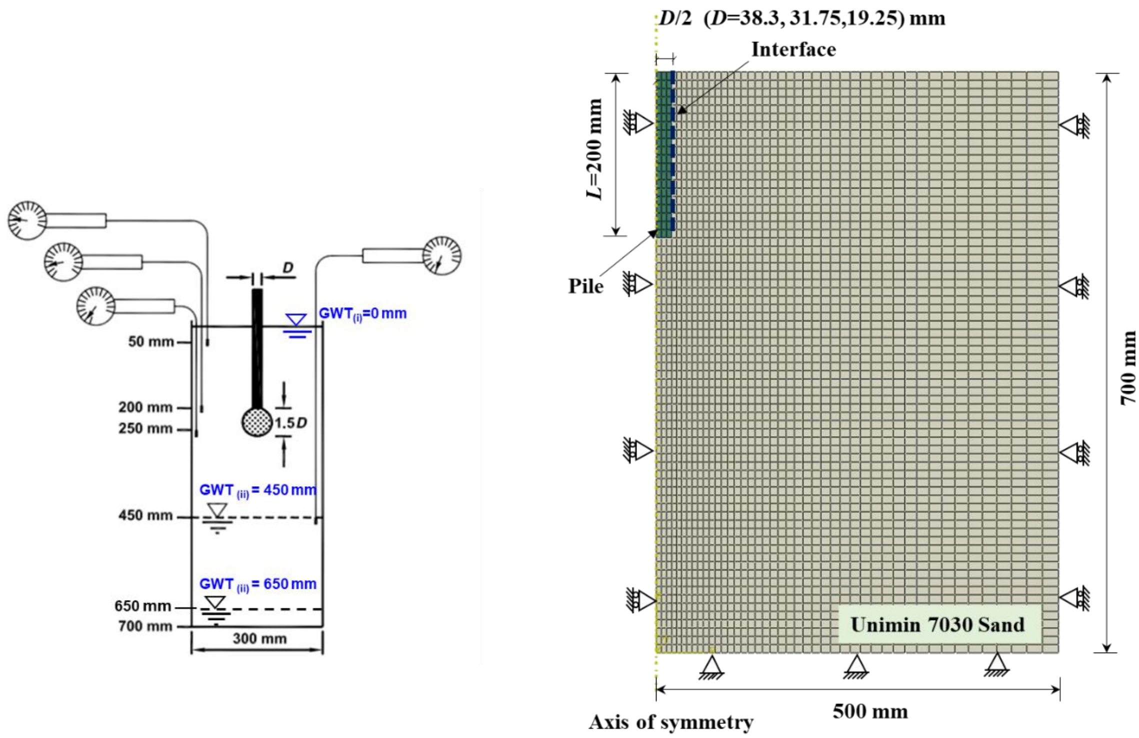

(a) (b)

Figure 6.2 Schematic pile-soil system in (a) Experimental study (modified after Vanapalli et al. 2018) (b) Numerical study

The sand is assumed to be in a state of hydrostatic conditions, thus the negative pore water pressure (i.e., matric suction) is linearly distributed above the GWT as shown in Figure 6.4a. Using the SWCC as a tool, the degree of saturation along the depth can be derived from matric suction profile (See Figure 6.4b). The apparent cohesion c_a is calculated using Equation 6.2b and the variation of shear strength of unsaturated soils corresponding to varying matric suction can be obtained as shown in Figure 6.5. The relationship between apparent cohesion and varying matric suction is implemented into ABAQUS with the aid of a subroutine USDFLD. The SWCC of Unimin sand was imported into ABAQUS by adding "sorption" in material properties with a range of degrees of saturation and corresponding matric suction values. The hydraulic conductivity of unsaturated soils can be obtained by the degree of saturation according to Brooks and Corey (1964)

$$k = k_{sat} S^{\lambda} \tag{6.5}$$

where the saturated permeability of Unimin Sand, k_{sat}, was 5×10^{-5}m/s (Ileme and Oh 2019). The parameter λ was equal to 2 for sand.

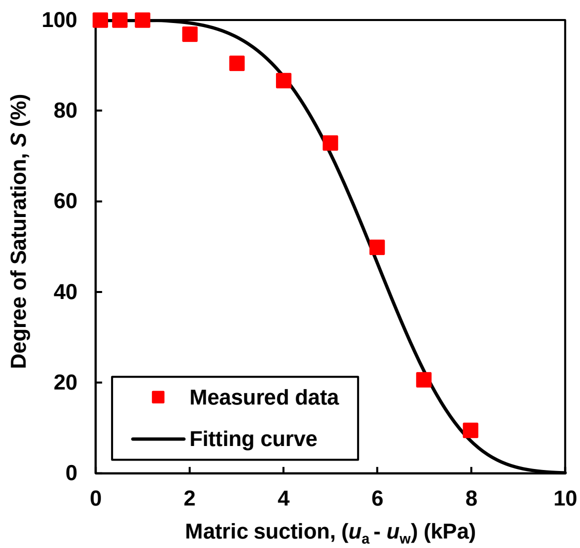

Figure 6.3 The SWCC of Unimin 7030 sand (modified from Vanapalli et al. 2018)

Table 6.1 Soil and interface properties (modified after Al Khazaali and Vanapalli 2019)

Soil Property	Value
Specific gravity, G_s	2.65
Dry unit weight, γ_d (kN/m^3)	16.3-16.7
Total unit weight, γ (kN/m^3)	18.6
Saturated unit weight, γ_{sat} (kN/m^3)	20.4
Average void ratio, e	0.606
Range of relative density, D_r (%)	60-70
Poisson's ratio	0.334
Effective cohesion, c (kPa)	0
Internal friction angle, ϕ'(°)	35.3
Pile-soil interface friction angle for smooth shaft surface, δ'(°)	24

The saturated elastic modulus, $E_{sat,}$ of Unimin Sand is estimated as 4000 kPa. For unsaturated soil, the E_{unsat} used for the numerical model is calculated using Equation 6.3. Since sand is a non-plastic soil, the fitting parameters α =1 and β = 1 were used in Equation 6.3. The variation of calculated E_{unsat} for different GWT depths is shown in Figure 6.6. An average value of E_{unsat} from the pile head to the bottom of stress bulb below the pile base (1.5D) was used as uniform elastic modulus of soil in the model. The average E_{unsat} for GWT = 450 and 650 mm is 15.82 and 17.05 MPa, respectively.

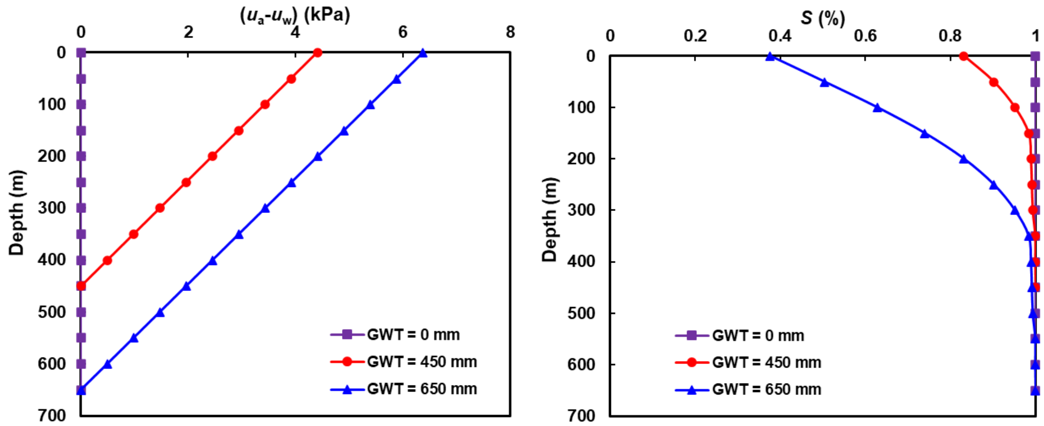

(a) (b)

Figure 6.4 Distribution of (a) matric suction (b) degree of saturation along the depth for different GWT scenarios

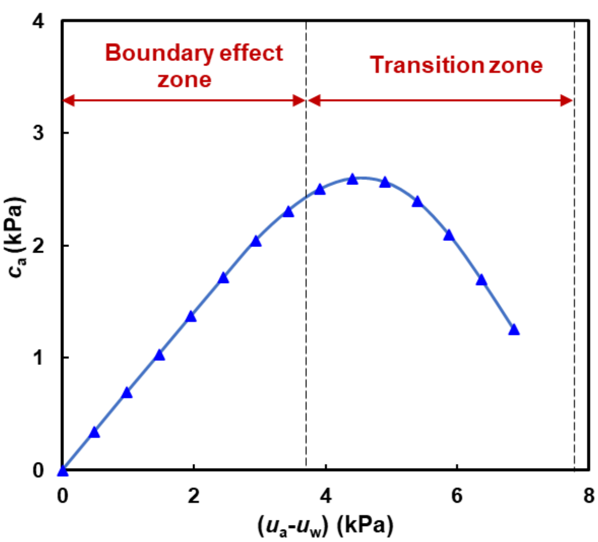

Figure 6.5 Variation of apparent cohesion with respect to matric suction

A surface-to-surface contact model was used to simulate small sliding and gapping at the pile-soil interface, in which the pile was regarded as the master surface and the soil as the slave surface. The pile-soil interface friction angle for smooth shaft surface (δ) is 24° and the coefficient of friction is set to 0.45. A displacement of 20 mm is applied to the top of the pile to simulate axial forces in the model tests.

Al-Khazaali et al. (2016) performed FEA using PLAXIS 2D software to simulate this experimental study. The average matric suction values were calculated at the centroid of the stress bulb zone below the pile base, which is at a depth of 1.5*D*. Average matric suction values of 2 and 4 kPa were used with the corresponding GWT at 450 mm and 650 mm depth, respectively. Comparisons between the measured data, FEA results using PLAXIS 2D and FEA results using ABAQUS from this study for piles with three different diameters are presented in Figure 6.7. Numerical results from Al-Khazaali et al. (2016) based on average matric suction values overestimate the ultimate bearing capacity of single piles in unsaturated sands. However, reliable comparisons between experimental results and the numerical predictions in this study were obtained since the variation of shear strength and modulus of elasticity of unsaturated soils corresponding to varying matric suction was considered in ABAQUS.

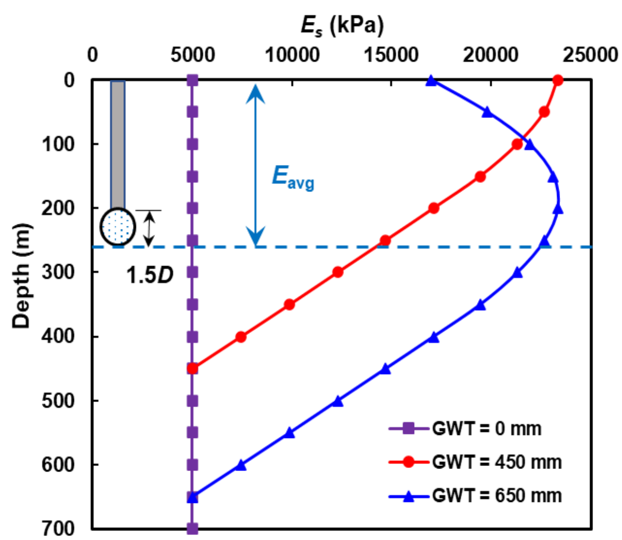

Figure 6.6 Variation of E_{unsat} with respect to depth due to the contribution of suction for different GWT depth

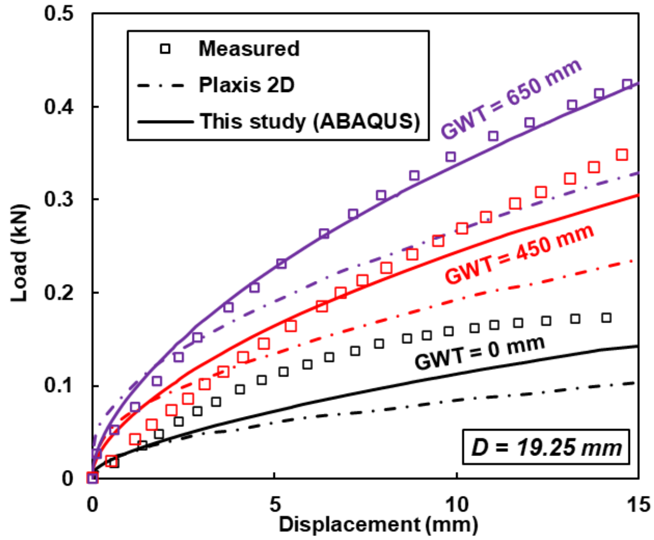

Measured
Plaxis 2D
This study (ABAQUS)
GWT = 650 mm
GWT = 450 mm
GWT = 0 mm
D = 19.25 mm
Load (kN)
Displacement (mm)

(a)

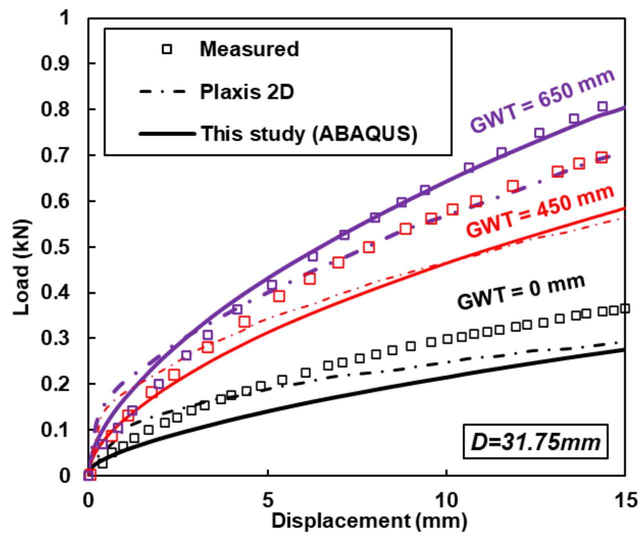

Measured
Plaxis 2D
This study (ABAQUS)
GWT = 650 mm
GWT = 450 mm
GWT = 0 mm
D=31.75mm
Load (kN)
Displacement (mm)

(b)

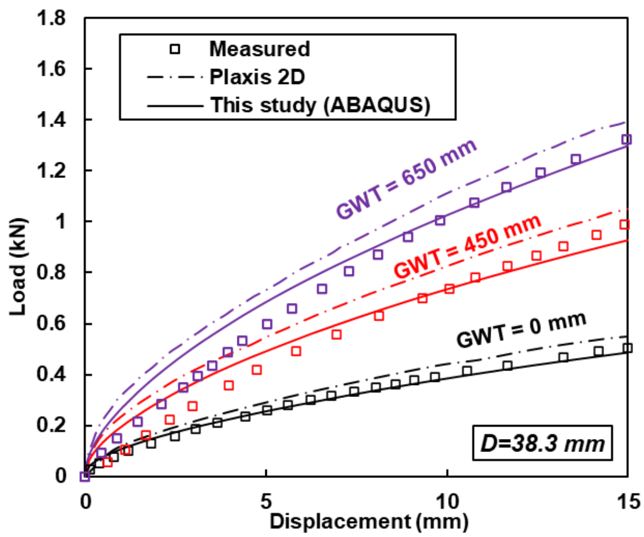

(c)

Figure 6.7 Comparisons between the measured data, FEA results using PLAXIS 2D (Al-Khazaali et al. 2016) and FEA results using ABAQUS

Comparisons of the variation of ultimate bearing capacity with respect to matric suction from different methods are shown in Figure 6.8. The ultimate bearing capacity can also be estimated using analytical method by summing the contribution of shaft carrying capacity using modified β method (Vanapalli and Taylan 2012) and end-bearing capacity using modified Terzaghi's method (Vanapalli et al. 2018). The ultimate bearing capacity increases nonlinearly with an increase in matric suction. The rate of increase in the bearing capacity reduces as the soil desaturates and approaches the residual zone. All three methods show good agreements with the measurements from the experimental study.

6.3.2 Case 2

Al Khazaali and Vanapalli (2019) performed model pile tests to investigate the influence of matric suction and the roughness of pile-soil interface on the behavior of single piles and pile groups in same soil with case 1 (i.e., Unimin sand). Model piles of 38 mm diameter and total length of 360 mm with an embedment depth of 300 mm with smooth and rough shafts were used in the tests. The pile load test was performed in both saturated and unsaturated sand at four varying ground water tables (GWTs) at 0, 300, 400 and 550 mm deep from the surface. The model pile was first placed in a prepared pit and supported by a wooden frame. The pile surrounding sand was then manually compacted to optimum moisture content. The water supply/drainage valve connected to the soil container was used to control the saturation and desaturation procedures in the sand. A vertical loading rate of 0.5 mm/s was applied at the top of the model pile or pile groups to simulate a drained loading condition. More details of the testing procedure are available in Al Khazaali and Vanapalli (2019).

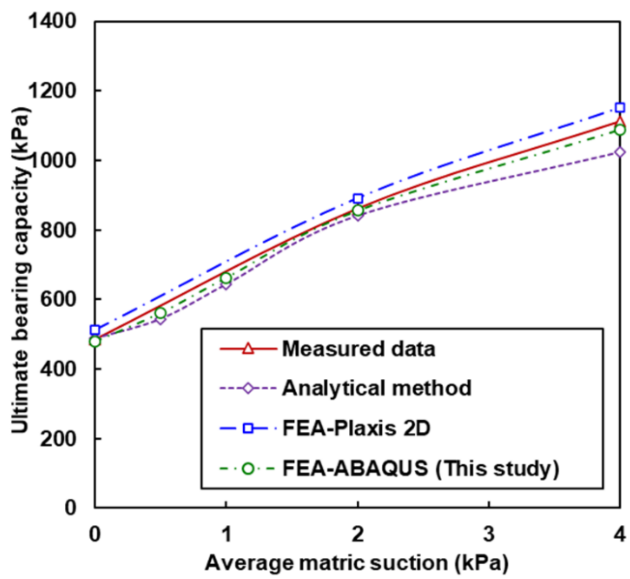

Figure 6.8 Comparisons of the variation of ultimate vertical bearing capacity with respect to average matric suction

A 2D axisymmetric model was set up due to the symmetry of the pile-soil system. The single pile was modelled as a linear-elastic material while the soil as a linear-elastic perfectly plastic material following Mohr-Coulomb failure criterion. The variation of shear strength corresponding to varying matric suction is considered in the model. The average E_{unsat} for GWT = 300, 400 and 550 mm is 12.3, 17 and 21.33 MPa, respectively. The rest of the modelling procedures are the same as case 1.

Figure 6.9 shows the comparisons of load-displacement curve between the measured data and numerical predictions. Good agreements are obtained between the measured results and numerical predictions by taking account of the influence of shear strength and modulus of elasticity with varying matric suction. As GWT moves deeper from the soil surface, a considerable increase in vertical load is observed compared to GWT at ground surface.

The ultimate bearing capacity can also be estimated using analytical method by summing the contribution of shaft carrying capacity using modified β method and end-bearing capacity using modified Janbu's method (Vanapalli et al. 2018). Comparisons of the variation of ultimate load capacity with respect to different GWT depths between the results from the experiment, numerical model and analytical methods are shown in Figure 6.10. The difference between the results using numerical modeling and the analytical method is less than 5% suggesting that there is a reasonably good agreement. The calculated bearing capacity using the analytical method underestimates the vertical bearing capacity of single piles. The difference between the analytical method and measured data varies from 9% to 24%. This may be attributed to the theoretical equations are based only on shear strength parameters and not considering the settlement behavior which is strongly related to the modulus of elasticity of unsaturated soils.

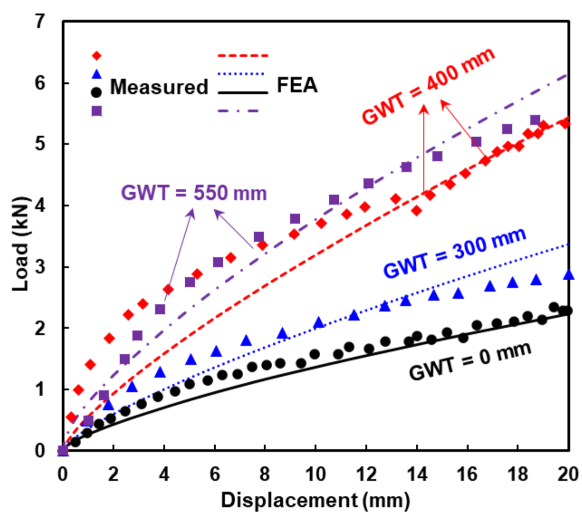

Figure 6.9 Comparisons between the measured data and FEA predictions using ABAQUS

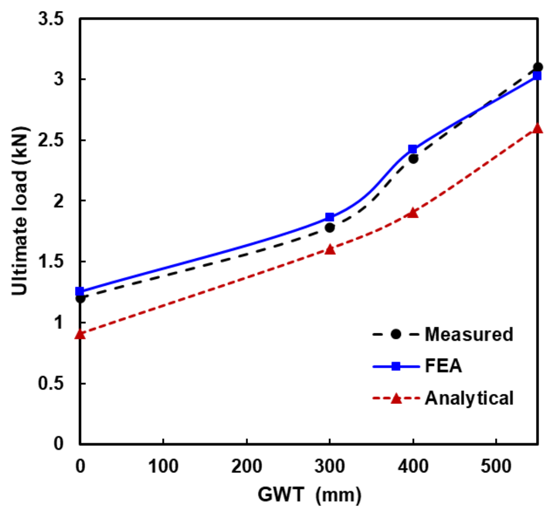

Figure 6.10 The variation of ultimate load with respect to GWT depths using different methods

6.3.3 Case 3

Marques et al. (2021) conducted a series of field tests to study the influence of water content on the pile behavior in Maringá region, which is in the northwest part of Paraná State, Brazil. The soil in the region consists of two layers of residual soils. The upper soil layer with a thickness of 8.5 m is characterized by matured, lateritic silty clay and the degree of saturation varies from 37% to 70%. The underlying soil is a less altered soil layer that can reach up to 30 m deep in some places. Bored cast-in-place piles of 4 m and 8 m in length with a nominal diameter of 250 mm were embedded in the upper soil layer. Table 6.2 shows some soil properties obtained from the comprehensive laboratory test performed by Gutierrez and Belincanta (2004). The groundwater table is at a depth of 15.7 m below the ground surface. To investigate the effect of water content, two pile load tests were conducted for each pile length: one under natural moisture condition and another in pre-moisten condition. In the case of the 4 m pile, the elevated moisture condition was achieved by manual pre-moistening, while in the case of the 8 m pile, it is achieved by natural pre-moistening since the pre-moistened test was done after a long period of precipitation, which thereby increased the soil moisture. The details of the test procedure and duration of the test can be found in Marques (2017).

Table 6.2 Properties of the Maringá subsoil (Marques et al. 2021)

Soil Property	Value
Clay fraction (%)	52-78
Silt fraction (%)	15-38
Sand fraction (%)	5-10
Unit weight, γ (kN/m^3)	12.5-16.5
Natural gravimetric water content (%)	29-35
Plastic index (PI)	14-22
Void ratio, e	1.5-2.3
Effective cohesion, c (kPa)	10-30
Internal friction angle, ϕ'(°)	27-32
Permeability coefficient (cm/s)	10^{-3}

The tested piles were regarded as floating pile. To further eliminate the end-bearing resistance, boring was made below the depth of pile base. Therefore, only the shaft resistance is considered significant and measured in the test. In the numerical study, a 20 mm depth gap under the base of the pile was set up. Following the similar procedure with Case 1 and 2, the numerical model is established. The total cohesion for each case is calculated using Equation 6.2b and presented in Table 6.3 using the given average matric suction. Figure 6.11 shows comparisons between the measured data and predictions using FEA. Good agreements are found between the measured and predicted results for all four cases.

Table 6.3 The input FEA parameters and results for four piles

Pile	Pile length (m)	Water content (%)	Average S (%)	Average (u_a - u_w) (kPa)	Total cohesion (kPa)	Measured Q_{ult} (kN)	FEA Q_{ult} (kN)	Difference (%)
P4n	4	33.6	53.4	813.5	102.14	122.43	135.04	10.2
P4p	4	39.4	62.5	442.6	83.67	94.47	99.37	5.2
P8n	8	34.1	54.2	768.9	100.28	284.51	298.35	4.8
P8p	8	36.7	58.3	579.4	91.28	224.65	238.68	6.2

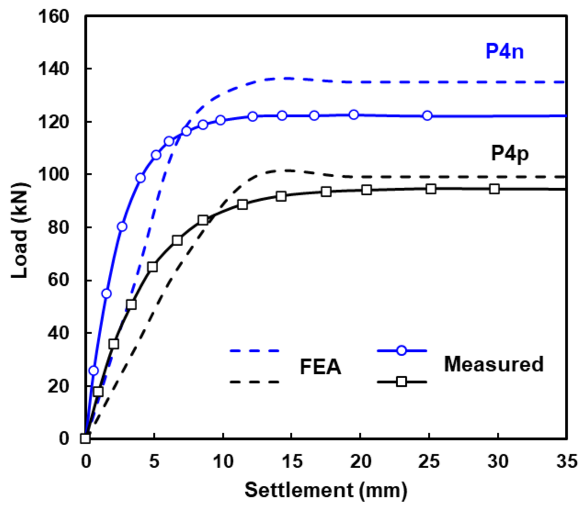

(a)

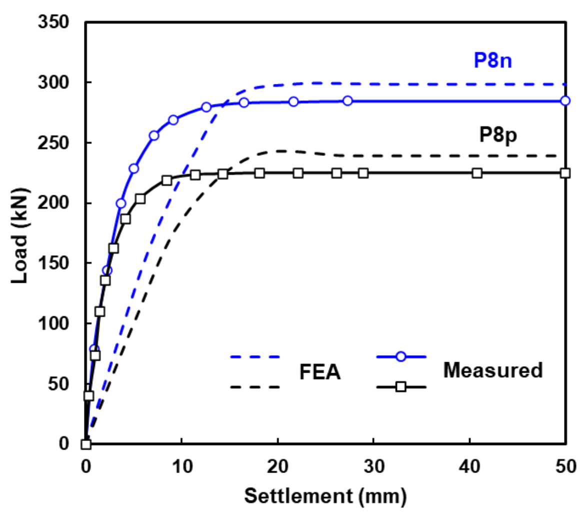

(b)

Figure 6.11 Comparisons between the measured data and predictions using FEA (P4n, P8n: Natural water content; P4p: artificially pre-moistened; P8p: Naturally pre-moistened after long rainfall period)

The ultimate vertical load can be evaluated from load versus settlement curve using double tangent method according to Prakash and Sharma (1990), which is defined as the vertical load at intersection point of the initial tangents to the load versus settlement curve and the tangent to or the extension to the final portion of the curve. Table 6.3 presents the ultimate load derived from the load-settlement curve from the measurement and FEA predictions with differences vary from 4.8 % to 10.2%.

6.3.4 Case 4

In the Fall of 2003, the Faculty of Engineering of the University of Porto (FEUP), Porto, Portugal and the High Technical Institute of the Technical University of Lisbon have initiated a prediction event on pile bearing capacity and load-settlement behavior. Static loading tests were performed on bored piles with 600 mm in diameter, 6 m in embedment depth in residual soils.

The soil at the site is a weathered granite that is subject to high mean annual precipitation. The grain-size analysis shows that the soil consists of 10% clay, 30% silt, 40% sand and 20% gravel, which are classified as “sand and silt with some gravel and some clay”. The fine content in the soil is non-plastic and the void ratio varies from 0.6 to 0.8. The ground water table is located at a depth of 11 m. The total density of the soil is 18 kN/m^3. The average cone resistance $q_{c,avg}$ in the influence zone is 5.1 MPa. The water content of the soil varies from 16.2% to 22.5% and the degree of saturation ranges from 56 % to 86%. The pore water pressure measurement within 8 m depth from the natural ground surface shows a negative value of 10 to 20 kPa (i.e., matric suction), indicating that the soil is unsaturated. The effective cohesion is estimated as 2 kPa according to Ortiz et al. (1986). A summary of the site characterization and the results of static loading tests was reported by Santos et al. (2005) and Fellenius et al. (2007). The internal friction angle ϕ' can also be obtained from CPT records using the following relationship provided by Kulhawy and Mayne (1990):

$$\phi'(\text{degrees}) = 17.6 + 11\log\frac{q_c}{\sqrt{100\sigma'_v}} \tag{6.6}$$

where q_c is cone tip resistance. The calculated ϕ' is 36°. Substituting the average matric suction of 15 kPa and average degree of saturation of 71% in Equation 6.2b, the apparent cohesion is estimated as 10.2 kPa.

Figure 6.12 shows good comparisons of the load-displacement curve between the measurement from field test and FEA predictions. These results suggest the proposed numerical method is reliable for predicting the load-settlement behavior of single piles taking account of the influence of matric suction.

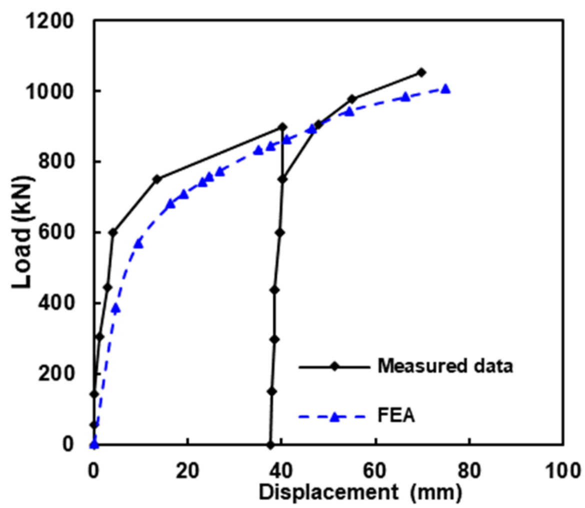

Figure 6.12 Comparisons between the measured data and predictions using FEA

6.4 Summary and conclusion

In this paper, a theoretical background of how the shear strength of unsaturated soils with respect to matric suction can be used for predicting the ultimate bearing capacity of pile foundations is summarized. Then, a numerical technique is proposed to simulate the nonlinear response of piles in saturated and unsaturated soils. A subroutine USDFLD that is developed based on the summarized theoretical background was implemented into ABAQUS for modeling the variation of load–displacement curves considering the influence of matric suction in the shear strength and the elastic modulus of unsaturated soils. The required information for modeling includes only the shear strength parameters of the saturated soil, saturated modulus of elasticity and the SWCC.

The proposed numerical method was validated using two model pile tests and two field tests from the literature. Satisfactory comparisons between FEA results and measured data were observed for all four cases. The studies presented in this chapter are simple and promising for the geotechnical engineers for use in practice for predicting the load-displacement behavior of single piles in both saturated and unsaturated soils.

CHAPTER 7

CONCLUSIONS AND SUGGESTIONS FOR FUTURE RESEARCH

7.1 Major conclusions

In this thesis, analytical and numerical approaches were developed to interpret the behavior of single pile and pile group foundations under axial and lateral loadings extending the mechanics of saturated and unsaturated soils. Major conclusions drawn from the studies undertaken in this thesis are summarized below.

7.1.1 State-of-the-art review

In recent years, several studies in literature focused on the load-displacement behavior of axially loaded single piles and pile groups in unsaturated soils considering the contribution of matric suction. Simple approaches that have been developed extending the conventional saturated soil mechanics principles are succinctly summarized based on experimental studies, theoretical approaches, and numerical simulations. More studies including large-scale field tests are necessary to better understand the strengths and limitations of the developed approaches for use in the design of foundations in unsaturated soils.

The studies for analyzing the behavior of laterally loaded piles in saturated soils are reviewed and discussed. These methods primarily focus on piles in either saturated cohesive ($c_u \neq 0$, $\phi_u = 0$) or cohesionless soils ($c' = 0$, $\phi' \neq 0$). There has been lack of research undertaken on investigating the lateral response of piles in unsaturated soils. The understanding of laterally loaded piles in unsaturated soils is still limited for geotechnical engineers to reliably use them in geotechnical engineering practice.

7.1.2 The nonlinear behavior of laterally loaded piles in unsaturated soils

An analytical method is proposed for predicting the lateral response of short rigid piles in unsaturated soils. Considering three distinct states (i.e., pre-tip yield state, post-tip yield state and ultimate limiting state) and incorporating the contribution of matric suction towards shear strength, the lateral load versus displacement is derived based on force and moment equilibrium equations. The predictive capability of the proposed analytical method is validated against two sets of published data from the literature (Truong 2017, Choi et al. 2013). The results suggest that the method can well predict the nonlinear behavior of laterally loaded rigid piles. In addition, a series of 3D FE analyses are undertaken to model the load-displacement behavior of laterally loaded piles using ABAQUS. The nonlinear shear strength and modulus of elasticity behavior of unsaturated soils with respect to matric suction are considered in FE models through a user-defined subroutine (USDFLD) using appropriate constitutive models. The proposed numerical method is validated using two sets of published pile model tests, one in unsaturated silty soil and the other in unsaturated sandy soil.

Both methods are reliable and promising for the geotechnical engineers to use in practice for the design of piles in unsaturated soils under lateral loading. Compared with the analytical method developed only for short rigid pile, the numerical method can be used for pile with varying lengths and stiffness, including short, intermediate, and for both long piles and non-rigid piles.

7.1.3 The end-bearing capacity of axially loaded piles in saturated and unsaturated soils

A new methodology is developed for predicting the end-bearing capacity of driven piles in saturated and unsaturated soils extending stress characteristics method (SCM). Eleven driven pile load tests conducted in saturated soils as well as two conducted in unsaturated soils are used to validate the proposed methodology. The comparisons suggest that the proposed model is capable of reliably estimating the end-bearing capacity of driven piles in both saturated and unsaturated soils. Moreover, numerical analyses have been performed to simulate the pile penetration and load tests using ABAQUS. The ultimate bearing capacity derived from FEA, along with the computed results using the proposed method, were compared against the experimental data from a published model pile test.

One advantage of using FEA is that it considers the dependency of friction angle and considers varying soil shear strength values for different stress levels. In addition, the FEA can provide comprehensive output data that include the load-displacement behavior and stress distribution along the pile under different displacements, whereas the proposed analytical method restricted to providing only the end-bearing capacity of the pile. However, solving large deformation geotechnical problems can be challenging especially when dealing with complex soil-structure interactions such as the driven piles behavior. Simulating a driven pile using FEA can contribute to problems in terms of convergence in both dynamic and static analyses. The proposed analytical method, on the other hand, is simple and provides relatively quick and reliable estimations of the bearing capacity for a driven pile embedded in unsaturated soils. The required input parameters only include pile properties (i.e., length, diameter, and material), soil properties (i.e., saturated shear strength parameters c', ϕ' and unit weight γ) and *SWCC*. The study highlights the need for considering the influence of matric suction in the rigorous design of pile foundations in both saturated and unsaturated soils.

7.1.4 The load-displacement behavior of single pile and pile groups in unsaturated soils

A simplified model is developed for studying the load-displacement behavior of single piles combining the principle of unsaturated soil mechanics and load transfer method (LTM). The proposed model is then extended to the analysis of pile groups accounting for the group effect and pile-soil interaction. The results of experiments on two single pile load tests (i.e., one bored pile in Piedmont residual soil in Atlanta and another in the residual soil in Portugal) and a pile group in unsaturated sandy soil provides the validity of the proposed approach. In addition, 3D numerical analysis is performed to investigate the axial response of pile groups in unsaturated soils with varying GWTs. Good comparisons were observed between both the analytical method and numerical analysis with the experimental data. The load-displacement curves from the 3D FE model match more closely with the measured data compared to the present analytical method. This may be attributed to several factors. Firstly, numerical analysis considers the dilation effect of unsaturated interfaces. As the GWT is lowered, sand dilatancy increases due to matric suction, resulting in a steeper slope in bearing capacity. However, in the proposed modified LTM, this factor is not considered. Secondly, load transfer methods often involve simplifying assumptions and idealizations to model the soil-pile interaction. These assumptions may not fully capture the complex behavior of the soil and pile system, leading to discrepancies between predicted and measured responses.

7.1.5 Numerical analysis of pile foundations in saturated and unsaturated soils

A numerical technique is developed to model the behavior of pile foundations in saturated and unsaturated soils using FEA. A user-defined subroutine is implemented into ABAQUS which considers the nonlinear shear strength and elasticity of modulus with respect to matric suction. The numerical technique is validated against two model pile tests and two field test and good comparisons are achieved. The results showed that the influence of matric suction on the ultimate bearing capacity of piles is significant. The numerical predictions are closer to experimental data compared to analytical method. This may be attributed to the theoretical equations are based only on shear strength parameters and not considering the settlement behavior which is strongly related to the modulus of elasticity of unsaturated soils. The proposed numerical technique is simple and only requires shear strength parameters of the saturated soil, saturated modulus of elasticity and the SWCC.

7.2 Recommendations for Future Work

The following recommendations are suggested for future research:

(1) In Chapter 3, an analytical method is proposed for investigating the lateral response of short rigid piles. Further studies focusing on the failure mechanisms of short, intermediate,

and long piles with free- and restrained-head conditions are required. This can be possibly accomplished by incorporating the proposed methodology into existing numerical technique that already consider the principle of unsaturated mechanics.

(2) In Chapter 4, given the absence of measured data, the end-bearing capacity values used to validate the model were back-calculated under certain assumptions, which may not have represented the actual value in the field. It is recommended to perform sensitivity analysis to investigate the range of validity and limitations of the proposed analytical method and FEA model.

(3) In Chapter 5, the soils used for validation of the numerical model of the axial response of pile groups in unsaturated soils with varying GWTs were cohesionless. It is recommended to extend the validation to include unsaturated cohesive soils in the future work.

(4) Experimental studies have showed that the interaction of unsaturated soils with different structures plays a curial role in many unsaturated interface problems in civil engineering. Therefore, numerical technique developed in this study can be modified considering more factors such as: (i) pile-soil interface shear strength concerning matric suction; (ii) the nonlinear variation of elastic modulus of unsaturated soils.

(5) The interaction effect of combined vertical and lateral loads on the pile response is of significant interest in geotechnical engineering practice applications. The mechanism of interaction effect of combined vertical and lateral loads is complex. Most studies in the published literature are only related to combined loads action on piles for saturated soils. Therefore, a generalized solution for axially and laterally loaded pile in unsaturated soils can be proposed extending the analysis of laterally loaded piles from this thesis. The transfer matrix approach can be used to provide solutions to the response of piles under combined axial and lateral loads.

REFERENCES

Abu-Farsakh, M. Y., and Titi, H. H. (2004). Assessment of direct cone penetration test methods for predicting the ultimate capacity of friction driven piles. *Journal of Geotechnical and Geoenvironmental Engineering*, 130(9), 935-944. https://doi.org/10.1061/(ASCE)1090-0241(2004)130:9(935)

Adem, H. H., and Vanapalli, S. K. (2013). Constitutive modeling approach for estimating 1-D heave with respect to time for expansive soils. *International Journal of Geotechnical Engineering*, 7(2), 199-204. https://doi.org/10.1179/1938636213Z.00000000024

Ahmadi, M. M., and Ahmari, S. (2009). Finite-element modelling of laterally loaded piles in clay. *Proceedings of the Institution of Civil Engineers-Geotechnical Engineering*, 162(3), 151-163.

Ai, Z. Y., and Han, J. (2009). Boundary element analysis of axially loaded piles embedded in a multi-layered soil. *Computers and Geotechnics*, 36(3), 427-434. https://doi.org/10.1016/j.compgeo.2008.06.001

Akrouch, G. A., Sánchez, M., and Briaud, J. L. (2016). An experimental, analytical and numerical study on the thermal efficiency of energy piles in unsaturated soils. *Computers and Geotechnics*, 71, 207-220. https://doi.org/10.1016/j.compgeo.2015.08.009

Almeida, M. S., Danziger, F. A., and Lunne, T. (1996). Use of the piezocone test to predict the axial capacity of driven and jacked piles in clay. *Canadian Geotechnical Journal*, 33(1), 23-41. https://doi.org/10.1139/t96-022

Alkroosh, I., and Nikraz, H. (2012). Predicting axial capacity of driven piles in cohesive soils using intelligent computing. *Engineering Applications of Artificial Intelligence*, 25(3), 618-627. https://doi.org/10.1016/j.engappai.2011.08.009

Al-Khazaali, M., Han, Z., and Vanapalli, S. K. (2016). Modelling the load-settlement behavior of model piles in unsaturated sand and glacial till. In *Geotechnical and Structural Engineering Congress 2016* (pp. 2075-2087). https://doi.org/10.1061/9780784479742.178

Al-Khazaali, M., and Vanapalli, S. K. (2019). Experimental Investigation of Single Model Pile and Pile Group Behavior in Saturated and Unsaturated Sand. *Journal of Geotechnical and Geoenvironmental Engineering*, 145(12), 04019112.

Alonso, E. E., Gens, A., and Josa, A. (1990). A constitutive model for partially saturated soils. *Géotechnique*, 40(3), 405-430.

Al-Omari, R. R., Fattah, M. Y., and Kallawi, A. M. (2019). Laboratory study on load carrying capacity of pile group in unsaturated clay. *Arabian Journal for Science and Engineering*, 44(5), 4613-4627.

Altaee, A., Fellenius, B. H., and Evgin, E. (1992). Axial load transfer for piles in sand. I. Tests on an instrumented precast pile. *Canadian Geotechnical Journal*, 29(1), 11-20. https://doi.org/10.1139/t92-002

American Petroleum Institute RP 2A (2011). *Planning, designing, and constructing fixed offshore platforms*. Washington, DC.

Arya, L. M., and Paris, J. F. (1981). A physicoempirical model to predict the soil moisture characteristic from particle-size distribution and bulk density data. *Soil Science Society of America Journal*, 45(6), 1023-1030.

Babu, G.L.S., Rao, R.S., Peter, J. (2005). Evaluation of shear strength functions based on soil water characteristic curves. *Journal of Testing and Evaluation* 33(6): 461-465.

Baguelin, F., Frank, R., Jezequel, J. F. (1982). Parameters for friction piles in marine soils. *Proceedings of 2nd International Conference Numerical Methods for Offshore Piling*, ASCE, Austin, Texas., Vol. 2, 421–430.

Banerjee, P. K., and Davies, T. G. (1978). The behaviour of axially and laterally loaded single piles embedded in nonhomogeneous soils. *Geotechnique*, 28(3), 309-326.

Basu, D., and Salgado, R. (2007). Elastic analysis of laterally loaded pile in multi-layered soil. *Geomechanics and Geoengineering*, 2(3), 183–196. doi:10.1080/17486020701401007

Basu, D., and Salgado, R. (2008). Analysis of laterally loaded piles with rectangular cross sections embedded in layered soil. *International Journal for Numerical and Analytical Methods in Geomechanics*, 32(7), 721-744.

Basarkar, S. S., and Dewaikar, D. M. (2006). Load transfer characteristics of socketed piles in Mumbai region. *Soils and foundations*, 46(2), 247-257.

Bazaraa, A. R., and Kurkur, M. M. (1986). N-values used to predict settlements of piles in Egypt. In *Use of In Situ tests in geotechnical engineering* (pp. 462-474).

Berezantzev, V.G., and Yaroshenko, V.A. (1962). Osobennosti deforminovania peschanych osnovanii pod fundamentami glubokogo zalozhenia. Osnovaniya I Fundamenty, 4: 3–7. [In Russian.]

Beringen, F. L., Windle, D., and Van Hooydonk, W. R. (1980). Results of loading tests on driven piles in sand. In *Recent developments in the design and construction of piles* (pp. 213-225). Thomas Telford Publishing.

Biot, M. A., (1937). Bending of an infinite beam on an elastic foundation. *Z. Angew. Math.*

Mech. 2(3), 165–184

Birid, K. C. (2017). Evaluation of ultimate pile compression capacity from static pile load test results. In *International Congress and Exhibition" Sustainable Civil Infrastructures: Innovative Infrastructure Geotechnology"* (pp. 1-14). Springer, Cham.

Bishop, R.F., Hill, R., and Mott, N.F. (1945). The theory of indentation and hardness tests. *Proceedings of the Physical Society*, 57: 147– 159.

Bishop, A. W. (1959). The principle of effective stress. Teknik Ukeblad, 39, 859–863.

Bishop, A. W., and Blight, G. E. (1963). Some aspects of effective stress in saturated and partly saturated soils. *Geotechnique*, 13(3), 177–197.

Blaney, G. W., and O'Neill, M. W. (1986). Measured lateral response of mass on single pile in clay. *Journal of geotechnical engineering*, *112*(4), 443-457. https://doi.org/10.1061/(ASCE)0733-9410(1986)112:4(443)

Bolton, M. D., and Lau, C. K. (1993). Vertical bearing capacity factors for circular and strip footings on Mohr–Coulomb soil. *Canadian Geotechnical Journal*, *30*(6), 1024-1033. https://doi.org/10.1139/t93-099

Bowles, J. E. (1996). *Foundation analysis and design*. 5th Edition, McGraw Hill.

Brødbæk, K. T., Møller, M., Sørensen, S. P. H., and Augustesen, A. H. (2009). Review of *p-y* relationships in cohesionless soil.

Broms, B. B. (1964a). Lateral resistance of piles in cohesive soils. *Journal of the soil mechanics and foundations division*, *90*(2), 27-63. https://doi.org/10.1061/JSFEAQ.0000611

Broms, B. B. (1964b). Lateral resistance of piles in cohesionless soils. *Journal of the Soil Mechanics and Foundations Division*, *90*(3), 123-156. https://doi.org/10.1061/JSFEAQ.0002132

Broms, B. B. (1965). Design of laterally loaded piles. *Journal of the Soil Mechanics and Foundations Division*, *91*(3), 79-99. https://doi.org/10.1061/JSFEAQ.0000751

Brooks, R. H., and Corey, A. T. (1964). Hydraulic properties of porous media. Colorado State University. Libraries.

Brown, D. A., and Shie, C. F. (1991). Some numerical experiments with a three dimensional finite element model of a laterally loaded pile. *Computers and Geotechnics*, *12*(2), 149-162. https://doi.org/10.1016/0266-352X(91)90004-Y

Buisman, A.S.K. (1935). De Weerstand van Paalpunten in Zand. De Ingenieur, 50(Bt. 25–28): 31–35. [In Dutch.]

Burland, J. (1973). Shaft friction of piles in clay--a simple fundamental approach. *Publication of: Ground Engineering/UK/*, *6*(3).

Bustamante, M., and Gianeselli, L. (1982). Pile bearing capacity predictions by means of static penetrometer, CPT, *2nd European Symposium on Penetration Testing*, ESOPT II, Amsterdam, 2, pp. 493–500.

Butler, H. D., and Hoy, H. E. (1977). *Users manual for the Texas quick-load method for foundation load testing* (No. FHWA-IP-77-8). United States. Federal Highway Administration. Office of Research and Development.

Campanella, R.G., Robertson, P.K., Davies, M.P., and Sy, A. (1989). Use of in-situ tests in pile design. In *Proc. of 12th Int. Conf. Soil Mech. Found. Engrg.* (ICSMFE), Rio de Janeiro, Brazil, 13–18. 1:199–203.

Canadian Geotechnical Society (CGS). (1992). *Canadian foundation engineering manual*, CFEM. 3rd ed. BiTech Publishers, Richmond, British Columbia, pp 512.

Caputo, V., and Viggiani, C. (1984). Pile foundation analysis: a simple approach to nonlinearity effects. Rivista Italiana di Geotecnica, 18(1), 32-51.

Caquot, A. (1934). *Equilibre des massifs à frottement interne*. Gauthier-Villars, Paris.

Caquot, A. I., and Lehuerou Kerisel, J. (1956). *Treatise on soil mechanics*.

Carsel, R. F., and Parrish, R. S. (1988). Developing joint probability distributions of soil water retention characteristics. *Water resources research*, *24*(5), 755-769. https://doi.org/10.1029/WR024i005p00755

Cecconi, M., Pane, V., Vecchietti, A., and Bellavita, D. (2019). Horizontal capacity of single piles: an extension of Broms' theory for c-ϕ soils. *Soils and Foundations*, *59*(4), 840-856. https://doi.org/10.1016/j.sandf.2019.01.007

Chatterjee, K., and Choudhury, D. (2013). Variations in shear wave velocity and soil site class in Kolkata city using regression and sensitivity analysis. *Natural hazards*, *69*(3), 2057-2082.

Chari, T. R., and Meyerhof, G. G. (1983). Ultimate capacity of rigid single piles under inclined loads in sand. *Canadian Geotechnical Journal*, *20*(4), 849-854.

Chik, Z. H., Abbas, J. M., Taha, M. R., and Shafiqu, Q. S. M. (2009). Lateral behavior of single pile in cohesionless soil subjected to both vertical and horizontal loads. *European Journal of Scientific Research*, *29*(2), 194-205.

Chin, F. K. (1970). Estimation of the ultimate load of piles from tests not carried to failure. In *Proc. 2nd Southeast Asian Conference on Soil Engineering, Singapore.*

Chin, K. B., Leong, E. C., and Rahardjo, H. (2010). A simplified method to estimate the soil-water characteristic curve. *Canadian Geotechnical Journal*, 47(12), 1382-1400.

Chen, J. C. (1984). Evaluation of strength parameters of partially saturated soils on the basis of initial suction and unconfined compression strength, M.Sc. thesis, Asian Institute of Technology Report, Bangkok, Thailand.

Cheng, X., Tan, M., and Vanapalli, S. (2021). Simple approaches for the design of shallow and deep foundations for unsaturated soils II: numerical Techniques. *Indian Geotechnical Journal*, *51*(1), 115-126. https://doi.org/10.1007/s40098-021-00500-3

Cheng, X., and Vanapalli, S. K. (2021). Prediction of the nonlinear behavior of laterally loaded piles in unsaturated soils. *Computers and Geotechnics*, 140, 104480.

Choi, H. Y., Lee, S. R., Park, H. I., and Kim, D. H. (2013). Evaluation of lateral load capacity of bored piles in weathered granite soil. *Journal of Geotechnical and Geoenvironmental Engineering*, *139*(9), 1477-1489. https://doi.org/10.1061/(ASCE)GT.1943-5606.0000831

Chow, Y. K. (1986). Discrete element analysis of settlement of pile groups. *Computers and structures*, 24(1), 157-166.

Chung, S. H., and Yang, S. R. (2017). Numerical analysis of small-scale model pile in unsaturated clayey soil. *International Journal of Civil Engineering*, *15*(6), 877-886. https://doi.org/10.1007/s40999-016-0065-7

Clough, G. W., and Duncan, J. M. (1971). Finite element analyses of retaining wall behavior. *Journal of the Soil Mechanics and Foundations Division*, 97(12), 1657-1673.

Colasanti, R. J., and Horvath, J. S. (2010). Practical subgrade model for improved soil-structure interaction analysis: software implementation. *Practice periodical on structural design and construction*, *15*(4), 278-286. https://doi.org/10.1061/(asce)sc.1943-5576.0000060

Comodromos, E. M., Papadopoulou, M. C., and Rentzeperis, I. K. (2009). Pile foundation analysis and design using experimental data and 3-D numerical analysis. *Computers and Geotechnics*, 36(5), 819-836.

Comodromos, E. M., Papadopoulou, M. C., and Laloui, L. (2016). Contribution to the design methodologies of piled raft foundations under combined loadings. *Canadian Geotechnical Journal*, 53(4), 559-577.

Costa, Y. D., Cintra, J. C., and Zornberg, J. G. (2003). Influence of matric suction on the results of plate load tests performed on a lateritic soil deposit. *Geotechnical Testing Journal*, 26(2), 219-227.

Cox, A. D., Eason, G., and Hopkins, H. G. (1961). Axially symmetric plastic deformations in soils. *Philosophical Transactions of the Royal Society of London. Series A, Mathematical and Physical Sciences*, *254*(1036), 1-45.

Coyle, H. M., and Reese, L. C. (1966). Load transfer for axially loaded piles in clay. *Journal of the Soil mechanics and Foundations Division*, 92(2), 1-26.

Coyle, H. M., and Castello, R. R. (1981). New design correlations for piles in sand. *Journal of the Geotechnical Engineering Division*, *107*(7), 965-986.

Cuomo, S., Moscariello, M., Manzanal, D., Pastor, M., and Foresta, V. (2018). Modelling the mechanical behaviour of a natural unsaturated pyroclastic soil within generalized plasticity framework. *Computers and Geotechnics*, 99, 191-202.

da Fonseca, A. J. P. V., Alberto, J., Esteves, E. C., and Massad, F. (2007). Analysis of piles in residual soil from granite considering residual loads.

Dai, A. (2013). Increasing drought under global warming in observations and models. *Nature climate change*, *3*(1), 52-58.

Davies, T. G., and Budhu, M. (1986). Non-linear analysis of laterally loaded piles in heavily overconsolidated clays. *Geotechnique*, *36*(4), 527-538.

Davisson, M. T., and Robinson, K. E. (1965). Bending and buckling of partially embedded piles. Sixth International Conference on Soil Mechanics and Foundation Engineering. Montreal. 2:243–246.

Davisson, M.T. (1972). High Capacity Piles. *Proceedings, Lecture Series, Innovations in Foundation Construction*, ASCE, Illinois Section, Chicago, pp. 81-112

de Albuquerque, P. J. R., Carvalho, D., and Fontaine, E. B. (2010). Pile capacity for Omega piles in an unsaturated Brazilian soil using the CPT. In *Proceedings of 2nd International Symposium on Cone Penetration Testing, Huntington Beach, CA, USA*.

de Albuquerque, P. J. R., Carvalho, D., Kassouf, R., and Fonte Jr, N. L. (2019). Behavior of laterally top-loaded deep foundations in highly porous and collapsible soil. *Journal of Materials in Civil Engineering*, *31*(2), 04018373.

De Beer, E.E. (1945). Etude des fondations sur pilotis et des fondations directes. Annales des Travaux Publics de Belqique, 46: 1–78.

De Beer, E. E. (1963). The scale effect in the transposition of the results of deep-sounding tests on the ultimate bearing capacity of piles and caisson foundations. *Geotechnique*, *13*(1), 39-75. https://doi.org/10.1680/geot.1963.13.1.39

De Beer, E.E. (1968). Proefondervindlijke bijdrage tot de studie van het grensdraag vermogen van zand onder funderingen op staal. Tijdshift der Openbar Verken van Belgie, No. 4, 5, and 6.

Decourt, L. (1999). Behavior of foundations under working load conditions. *11th Pan-American Conferenvce on Soil Mechanics and Geotechnical Engineering, Foz do Iguaçu*, *4*, 453-488.

de Ruiter, J., and Beringen, F. L. (1979). Pile foundations for large North Sea structures. *Marine Georesources and Geotechnology*, *3*(3), 267-314. https://doi.org/10.1080/10641197909379805

Dennis, N. D. and Olson, R . E. (1983). Axial Capacity of Steel Pipe Piles in Clay, In *Proceedings of the Geotechnical Practice in Offshore Engineering*, Austin, Texas, pp. 370-388.

Deng, Y., Wang, S., Bai, X., Luo, G., Wu, L., Chen, F., ... and Lu, Q. (2020). Vegetation greening intensified soil drying in some semi-arid

and arid areas of the world. *Agricultural and Forest Meteorology*, 292, 108103.

Desai, C. S., Drumm, E. C., and Zaman, M. M. (1985). Cyclic testing and modeling of interfaces. *Journal of Geotechnical Engineering*, 111(6), 793-815.

DNV (2014). *Design of Offshore Wind Turbine Structures*, DNV-OS-J101. Det Norske Veritas, Det Norske Veritas Classification A/S.

Donald, I. B., 1957. *Effective stresses in unsaturated noncohesive soils with controlled negative pore pressure*. M.Eng. Sc. Thesis, University of Melbourne, Melbourne, Australia

Douthitt, B., Houston, W., Houston, S. and Walsh, K. (1998). Effect of wetting on pile friction. In *Proc. of 2nd Int. Conf. unsaturated soils*, China, 1:219–224

Douglas, D. J., and Davis, E. H. (1964). The movement of buried footings due to moment and horizontal load and the movement of anchor plates. *Géotechnique*. 14(2), 115–132. https://doi.org/10.1680/geot.1964.14.2.115

DS 415. (1984). *The Danish code of practice for foundation engineering*. Danish Society of Civil Engineering.

Edil, T. B., Motan, S. E., and Toha, F. X. (1981). Mechanical behavior and testing methods of unsaturated soils. In *Laboratory shear strength of soil*. ASTM International.

Evans, L. T., and Duncan, J. M. (1982). *Simplified analysis of laterally loaded piles*. University of California, Department of Civil Engineering.

Escario, V., and Saez, J. (1986). The shear strength of partly saturated soils. *Geotechnique*, 36(3), 453-456. https://doi.org/10.1680/geot.1986.36.3.453

Escario, V., and Juca, J. F. T. (1989). Strength and deformation of partly saturated soils. In *Congrès international de mécanique des sols et des travaux de fondations*. 12 (pp. 43-46).

Eslami, A., and Fellenius, B. H. (1997). Pile capacity by direct CPT and CPTu methods applied to 102 case histories. *Canadian Geotechnical Journal*, *34*(6), 886-904. https://doi.org/10.1139/t97-056

Fattah, M. Y., Salim, N. M., and Mohsin, I. M. (2014). Behavior of single pile in unsaturated clayey soils. *Engineering and Technology Journal*, *32*(3), 763-787.

Fattah, M. Y., Al-Omari, R. R., and Fadhil, S. H. (2020). Load sharing and behavior of single pile embedded in unsaturated swelling soil. *European Journal of Environmental and Civil Engineering*, *24*(12), 1967-1992.

Fan, C. C., and Long, J. H. (2005). Assessment of existing methods for predicting soil response of laterally loaded piles in sand. *Computers and Geotechnics*, *32*(4), 274-289. https://doi.org/10.1016/j.compgeo.2005.02.004

Fellenius, B.H. (2005). What Capacity Value to Choose from the Results a Static Loading Test. *Deep Foundation Institute*. pp. 19 – 22.

Fellenius, B.H. (2006). The red book — *Basics of foundation design*. Available from http://www.fellenius.net/.

Fellenius, B. H., Santos, J. A., and Fonseca, A. V. D. (2007). Analysis of piles in a residual soil—The ISC'2 prediction. *Canadian Geotechnical Journal*, *44*(2), 201-220. https://doi.org/10.1139/t06-105

Fleming, W. G. K., Weltman, A. J., Randolph, M. F., and Elson, W. K. (1992). *Piling engineering*. Surrey University Press, London

Frank, R. (1982). Estimation par les paramètres pressiométriques de l'enfoncement sous charge axiale de pieux forés dans des sols fins. Bull Liaison Lab Ponts Chauss, (119).

Frank, R. (1988). Recent developments in the prediction of pile behaviour from pressuremeter results. *Building Science*, (2), 14-24.

Frank, R., Kalteziotis, N., Bustamante, M., Christoulas, S., and Zervogiannis, H. (1991). Evaluation of performance of two piles using pressuremeter method. *Journal of geotechnical engineering*, 117(5), 695-713.

Fredlund, D. G., Bergan, A. T., and Sauer, E. K. (1975). Deformation characterization of subgrade soils for highways and runways in northern environments. *Canadian Geotechnical Journal*, 12(2), 213-223.

Fredlund, D. G., Morgenstern, N. R., and Widger, R. A. (1978). The shear strength of unsaturated soils. Canadian geotechnical journal, 15(3), 313-321.

Fredlund, D. G., and Rahardjo, H. (1993). *Soil mechanics for unsaturated soils*. John Wiley & Sons.

Fredlund, D. G., and Xing, A. (1994). Equations for the soil-water characteristic curve. *Canadian geotechnical journal*, *31*(4), 521-532. https://doi.org/10.1139/t94-061

Fredlund, D. G., Rahardjo, H. and Fredlund, M. D. (2012). *Unsaturated Soil Mechanics in*

Engineering Practice. John Wiley & Sons, New York.

Fuller, F. M., and Hoy, H. E. (1970). Pile load tests including quick-load test method, conventional methods, and interpretations. *Highway Research Record*, (333).

Gabr, M. A., Lunne, T., and Powell, J. J. (1994). P-y analysis of laterally loaded piles in clay using DMT. *Journal of geotechnical engineering*, *120*(5), 816-837.

Gabr, M. A., Borden, R. H., Cho, K. H., Clark, S. C., and Nixon, J. B. (2002). Py curves for laterally loaded drilled shafts embedded in weathered rock. *Department of Civil Engineering North Carolina State University: Raleigh, NC, USA*.

Gan, J. K. M., Fredlund, D. G., and Rahardjo, H. (1988). Determination of the shear strength parameters of an unsaturated soil using the direct shear test. *Canadian Geotechnical Journal*, 25(3), 500-510.

Gan, J.K.M. and Fredlund, D.G. (1988). Multistage direct shear testing of unsaturated soils. American Society for Testing Materials. *Geotechnical Testing Journal* 11(2): 132-138.

Garven, E. A., and Vanapalli, S. K., (2006). Evaluation of empirical procedures for predicting the shear strength of unsaturated soils. In *Unsaturated Soils 2006*, pp. 2570–2592. https://doi.org/10.1061/40802(189)219

Gazioglu, S. M., and O'Neill, M. W. (1984). Evaluation of py relationships in cohesive soils. In *Analysis and design of pile foundations* (pp. 192-213). ASCE.

Georgiadis, M. (1983). Development of p-y curves for layered soils. In *Proc. of Geotechnical Practice in Offshore Engineering*, ASCE Specialty Conf., ASCE, Reston, Va., 536–545.

Georgiadis, K., Potts, D. M., and Zdravkovic, L. (2003). The influence of partial soil saturation on pile behaviour. *Géotechnique*, *53*(1),11-25..https://doi.org/10.1680/geot.2003.53.1.11

GeoSlope International Ltd., (2002). SLOPE/W, "Stability Analysis," Users Guide Version 5, GeoSlope Office, Canada.

Glick, G. W. (1948). Influence of soft ground on the design of long piles. *Proc. 2nd ICSMFE*. 4, 84–88.

Graham, J. (1968). Plane plastic failure in cohesionless soils. *Geotechnique*, *18*(3), 301-316. https://doi.org/10.1680/geot.1968.18.3.301

Gregersen, O. S., Aas, G., and Dibiagio, E. (1973). Load tests on friction piles in loose sand. *VIII International Conference on Soil Mechanics and Foundation Engineering* 19-27.

Guan, G. S., Rahardjo, H., and Choon, L. E. (2010). Shear strength equations for unsaturated soil under drying and wetting. *Journal of Geotechnical and*

Geoenvironmental Engineering, *136*(4), 594-606. https://doi.org/10.1061/(ASCE)GT.1943-5606.0000261

Gui, M. W. (2006). Bearing capacity of foundations on sand using the method of slip line. *Journal of Marine Science and Technology*, *14*(1), 1. https://doi.org/10.51400/2709-6998.2074

Guo, W. D., and Lee, F. H. (2001). Load transfer approach for laterally loaded piles. *International Journal for Numerical and Analytical Methods in Geomechanics*, *25*(11), 1101-1129.https://doi.org/10.1002/nag.169

Guo, W. D. (2008). Laterally loaded rigid piles in cohesionless soil. *Canadian Geotechnical Journal*, *45*(5), 676-697. https://doi.org/10.1139/T07-110

Haar, A., and von Karman, T. (1909). Zur Theorie der Spannungszustaende in plastichen und sandartigen Medien. *Nachrichten von der Gesellschaft der Wissenschaften zu Göttingen, Mathematisch-Physikalische Klasse*, 204-218.

Han, Z., Vanapalli, S. K., and Kutlu, Z. N. (2016). Modeling behavior of friction pile in compacted glacial till. *International Journal of Geomechanics*, *16*(6), D4016009. https://doi.org/10.1061/(ASCE)GM.1943-5622.0000659

Hansen B. J., (1961). The ultimate resistance of rigid piles against transversal forces. Bull. No. 12, Danish Geotechnical Institute.

Hansen, B. J., (1963) Discussion on hyperbolic stress-strain response. Cohesive soils. Journal for Soil Mechanics and Foundation Engineering, 89, 241–242.

Hansen, J. B. (1970). A revised and extended formula for bearing capacity. *Bulletin* 28, Danish Geotechnical Institute, Copenhagen. pp. 5-11.

Hara, A., Ohta, T., Niwa, M., Tanaka, S., and Banno, T. (1974). Shear modulus and shear strength of cohesive soils. *Soils and Foundations*, *14*(3), 1-12.

Harr, M. E. (1966). *Foundation of theoretical soil mechanics.* New York.

Harris, D. E., and Mayne, P. W. (1994). Axial compression behavior of two drilled shafts in Piedmont residual soils. In *Proceedings of International Conference on Design and Construction of Deep Foundation* (pp. 352-367).

Hasancebi, N., and Ulusay, R. (2007). Empirical correlations between shear wave velocity and penetration resistance for ground shaking assessments. *Bulletin of Engineering Geology and the Environment*, *66*(2), 203-213.

Hatanaka, M., and Uchida, A. (1996). Empirical correlation between penetration resistance and internal friction angle of sandy soils. *Soils and foundations*, *36*(4), 1-9.

Haverkamp, R., Leij, F. J., Fuentes, C., Sciortino, A., and Ross, P. J. (2005). Soil water retention: I. Introduction of a shape index. *Soil Science Society of America Journal*, 69(6), 1881-1890.

Helmers, M. J. (1997). *Use of ultimate load theories for design of drilled shaft sound wall foundations*. Doctoral dissertation, Virginia Tech.

Hery, P. (1983). *Residual stress analysis in WEAP*. Master thesis, Department of Civil. Engineering and Architecture Engineering., University of Colorado.

Hilf, J. W., 1956. *An investigation of pore-water pressure in compacted cohesive soils*. University of Colorado at Boulder.

Hirayama, H. (1990). Load-settlement analysis for bored piles using hyperbolic transfer functions. *Soils and Foundations*, 30(1), 55-64. https://doi.org/10.3208/sandf1972.30.55

Ho, D. Y., and Fredlund, D. G. (1982). A multistage triaxial test for unsaturated soils. *Geotechnical Testing Journal*, *5*(1/2), 18-25. https://doi.org/10.1520/GTJ10795J.

Hoerling, M., and Kumar, A. (2003). The perfect ocean for drought. *Science*, *299*(5607), 691-694.

Hong Kong Geotechnical Engineering Office (HKGEO). (2005). *Foundation design and construction*. Draft ed. Government of Hong Kong.

Hong, S. J., Lee, M., Kim, J., and Lee, W. (2010). Evaluation of undrained shear strength of Busan clay using CPT. In *Proceedings of the 2nd International Symposium on Cone Penetration Testing*, CPT (Vol. 10).

Huang, J., Ji, M., Xie, Y., Wang, S., He, Y., and Ran, J. (2016). Global semi-arid climate change over last 60 years. *Climate Dynamics*, *46*(3), 1131-1150.

IS 2911. (2010). *Indian Standard Code of Practice for Design and Construction of Pile Foundations*, Part I: Concrete Piles, Section 2: Bored Cast In Situ Concrete Piles (Second Revision).

Jaky, J., (1944). The coefficient of earth pressure at rest. In *Hungarian. J. Soc. Hung. Eng. Arch.* 355–358

Jáky, J. 1948. Pressure in silos. In *Proceedings of the 2nd International Symposium on Soil Mechanics and Foundation Engineering* (ICSMFE). Vol. 1, pp. 103–107.

Jamiolkowski, M., Lo Presti, D. C. F., and Manassero, M. (2003). Evaluation of relative density and shear strength of sands from CPT and DMT. *Soil behavior and soft ground construction*, 7(119), 201-238.

Janbu, N. (1976). Static bearing capacity of friction piles. In *Sechste Europaeische Konferenz Fuer Bodenmechanik Und Grundbau* (Vol. 1).

Jardine, R., Chow, F., Overy, R., and Standing, J. (2005). *ICP design methods for driven piles in sands and clays* (Vol. 112). London: Thomas Telford.

Jennings, J. E. B., and Burland, J. B. (1962). Limitations to the use of effective stresses in partly saturated soils. *Geotechnique*, 12(2), 125–144.

Joo, J. S. (1985). *Behaviour of large scale rigid model piles under inclined loads in sand* (Doctoral dissertation, Memorial University of Newfoundland).

Kalantary, F., Ardalan, H., and Nariman-Zadeh, N. (2009). An investigation on the Su–NSPT correlation using GMDH type neural networks and genetic algorithms. *Engineering Geology*, *104*(1-2), 144-155.

Kallehave, D., Thilsted, C. L., and Liingaard, M. A. (2012). Modification of the API py formulation of initial stiffness of sand. In *Offshore site investigation and geotechnics: integrated technologies-present and future*.

Kampitsis, A. E., Giannakos, S., Gerolymos, N., and Sapountzakis, E. J. (2015). Soil–pile interaction considering structural yielding: Numerical modeling and experimental validation. *Engineering Structures*, *99*, 319-333. https://doi.org/10.1016/j.engstruct.2015.05.004

Karlsrud, K., Clausen, C. J. F., and Aas, P. M. (2005). Bearing capacity of driven piles in clay, the NGI approach. In *Proc., 1st Int. Symp. on Frontiers in Offshore Geotechnics* (pp. 677-681). London: Taylor and Francis.

Karlsrud, K., Jensen, T. G., Lied, E. K. W., Nowacki, F., and Simonsen, A. S. (2014, May). Significant ageing effects for axially loaded piles in sand and clay verified by new field load tests. In *Offshore Technology Conference*. https://doi.org/10.4043/25197-MS

Kawaguchi, T., Mitachi, T., Shibuya, S., 2001. Evaluation of shear wave travel time in laboratory bender element test. In *Proceedings of 15th International Conference on Soil Mechanics and Foundation Engineering*, Istanbul, Turkey, 155–158.

Kerisel, J. (1965). Vertical and horizontal bearing capacity of deep foundation in clay, *Proceedings of Symposium on Bearing Capacity of Settlement of Foundations*, (pp. 45-52). Durham: Duke University.

Khalili, N., and Khabbaz, M. H. (1998). A unique relationship for χ for the determination of the shear strength of unsaturated soils. *Geotechnique*, *48*(5), 681-687.

Khalili-Tehrani, P., Ahlberg, E. R., Rha, C., Lemnitzer, A., Stewart, J. P., Taciroglu, E., and Wallace, J. W. (2014). Nonlinear load-deflection behavior of reinforced concrete drilled piles in stiff clay. *Journal of Geotechnical and Geoenvironmental Engineering*, *140*(3), 04013022.

Khodair, Y., and Abdel-Mohti, A. (2014). Numerical analysis of pile–soil interaction under axial and lateral loads. *International Journal of Concrete Structures and Materials*, *8*(3), 239-249.

Khoury, N. N., and Zaman, M. M. (2004). Correlation between resilient modulus, moisture variation, and soil suction for subgrade soils. *Transportation research record*, 1874(1), 99-107. https://doi.org/10.3141/1874-11

Kim, S., Jeong, S., Cho, S., and Park, I. (1999). Shear load transfer characteristics of drilled shafts in weathered rocks. *Journal of Geotechnical and Geoenvironmental Engineering*, 125(11), 999-1010. https://doi.org/10.1061/(ASCE)1090-0241(1999)125:11(999)

Kim, Y., and Jeong, S. (2011). Analysis of soil resistance on laterally loaded piles based on 3D soil–pile interaction. *Computers and geotechnics*, *38*(2), 248-257. https://doi.org/10.1016/j.compgeo.2010.12.001

Klar, A., and Frydman, S. (2002). Three-dimensional analysis of lateral pile response using two-dimensional explicit numerical scheme. *Journal of geotechnical and geoenvironmental engineering*, *128*(9), 775-784.

Kovacs, W. D., and Salomone, L. A. (1982). SPT hammer energy measurement. *Journal of the Geotechnical Engineering Division*, *108*(4), 599-620.

Kraft Jr, L. M., Ray, R. P., and Kagawa, T. (1981). Theoretical t-z curves. *Journal of the Geotechnical Engineering Division*, 107(11), 1543-1561. https://doi.org/10.1061/AJGEB6.0001207

Kuhlemeyer, R. L. (1979). Static and dynamic laterally loaded floating piles. *Journal of the Geotechnical Engineering Division*, *105*(2), 289-304.

Kumar, J., and Chitikela, S. (2002). Seismic passive earth pressure coefficients using the method of characteristics. *Canadian Geotechnical Journal*, *39*(2), 463-471. https://doi.org/10.1139/t01-103

Kulhawy, F.H., and Mayne, P.W. (1990). *Manual on estimating soil properties for foundation design.* Report EPRI EL6800, Electric Power Research Institute, Palo Alto, CA, 306p.

Ladhane, K. B., and Sawant, V. A. (2016). Effect of pile group configurations on nonlinear dynamic response. *International Journal of Geomechanics*, 16(1), 04015013.

Lalicata, L. M., Desideri, A., Casini, F., and Thorel, L. (2019). Experimental observation on laterally loaded pile in unsaturated silty soil. *Canadian Geotechnical Journal*, *56*(11), 1545-1556. https://doi.org/10.1139/cgj-2018-0322

Lee, J. H., and Salgado, R. (1999). Determination of pile base resistance in sands. *Journal of Geotechnical and Geoenvironmental Engineering*, 125(8), 673-683.

Lee, K. M., and Xiao, Z. R. (2001). A simplified nonlinear approach for pile group settlement analysis in multilayered soils. *Canadian Geotechnical Journal*, 38(5), 1063-1080.

Lee, S. J., Lee, S. R., and Kim, Y. S. (2003). An approach to estimate unsaturated shear strength using artificial neural network and hyperbolic formulation. *Computers and Geotechnics*, *30*(6), 489-503. https://doi.org/10.1016/j.compgeo.2004.08.001

Lee, J. S., and Santamarina, J. C. (2005). Bender elements: performance and signal interpretation. *Journal of geotechnical and geoenvironmental engineering*, 131(9), 1063-1070.

Lehane, B. M., Schneider, J. A., and Xu, X. (2005). The UWA-05 method for prediction of axial capacity of driven piles in sand. *Frontiers in offshore geotechnics: ISFOG*. 683-689.

Leij, F. J. (1996). *The UNSODA unsaturated soil hydraulic database: user's manual* (Vol. 96, No. 95). National Risk Management Research Laboratory, Office of Research and Development, US Environmental Protection Agency.

Leung, Y. F., Soga, K., Lehane, B. M., and Klar, A. (2010). Role of linear elasticity in pile group analysis and load test interpretation. *Journal of geotechnical and geoenvironmental engineering*, 136(12), 1686-1694.

Li, L., Li, J., Wang, Y., and Gong, W. (2020). Analysis of nonlinear load-displacement behaviour of pile groups in clay considering installation effects. *Soils and Foundations*, 60(4), 752-766.

Li, Y., and Vanapalli, S. K. (2022). Prediction of soil-water characteristic curves using two artificial intelligence (AI) models and AI aid design method for sands. *Canadian Geotechnical Journal*, 59(1), 129-143. https://doi.org/10.1139/cgj-2020-0562

Lin, H., Ni, L., Suleiman, M. T., and Raich, A. (2015). Interaction between laterally loaded pile and surrounding soil. *Journal of geotechnical and geoenvironmental engineering*, *141*(4), 04014119.

Liu, J., Xiao, H. B., Tang, J., and Li, Q. S. (2004). Analysis of load-transfer of single pile in layered soil. *Computers and Geotechnics*, 31(2), 127-135. https://doi.org/10.1016/j.compgeo.2004.01.001

Liu, Y., and Vanapalli, S. K. (2019). Load displacement analysis of a single pile in an unsaturated expansive soil. *Computers and Geotechnics*, *106*, 83-98. https://doi.org/10.1016/j.compgeo.2018.10.007

Long, J. H., and Vanneste, G. (1994). Effects of cyclic lateral loads on piles in sand. *Journal of Geotechnical Engineering*, 120(1), 225-244.

Lu, Z. (1992). The relationship of shear strength to swelling pressure for unsaturated soils. *Chinese journal of geotechnical engineering*, 14(3), 1-8.

Lu, N., and Likos, W. J. (2006). Suction stress characteristic curve for unsaturated soil. *Journal of geotechnical and geoenvironmental engineering*, *132*(2), 131-142.

Lu, N., and Kaya, M. (2014). Power law for elastic moduli of unsaturated soil. *Journal of Geotechnical and Geoenvironmental Engineering*, 140(1), 46-56.

Ma, Z., and Yang, Q. (2017). Global patterns of aridity trends and time regimes in transition. In *Aridity Trend in Northern China* (pp. 67-90).

Mahmood, M. R., Salim, N. M., and Abood, M. H. (2018). The behavior of laterally loaded single pile model in unsaturated cohesionless soil. In *IOP Conference Series: Materials Science and Engineering* (Vol. 454, No. 1, p. 012175). IOP Publishing. https://doi.org/10.1088/1757-899X/454/1/012175

Mahmoudabadi, V., and Ravichandran, N. (2019). A procedure for incorporating climatic and water table data in the geotechnical design of driven pile subjected to axial load." In *Geo-Congress 2019: Geotechnical Materials, Modeling, and Testing* (pp. 711-721). https://doi.org/10.1061/9780784482124.072

Mancuso, C., Vassallo, R., and d'Onofrio, A. (2002). Small strain behavior of a silty sand in controlled-suction resonant column torsional shear tests. *Canadian Geotechnical Journal*, 39(1), 22-31. https://doi.org/10.1139/t01-076

Mares, M. A., 2017. *Encyclopedia of deserts*. University of Oklahoma Press.

Martin, C.M. (2004). *User guide for ABC – analysis of bearing capacity version 1.0.* UK:University of Oxford.

Martin, C. M. (2005). Exact bearing capacity calculations using the method of characteristics. *Proc. IACMAG. Turin, 11*, 441-450.

Matlock, H., and Reese, L. C. (1960). Generalized solutions for laterally loaded piles. *Journal of the Soil Mechanics and foundations Division*, *86*(5), 63-92. https://doi.org /10.1061/TACEAT.0008439

Matlock, H. (1970). Correlation for design of laterally loaded piles in soft clay. In: *Offshore Technology in Civil Engineering's Hall of Fame Papers from the Early Years*. 77–94. https://doi.org/10.4043/1204-MS

Matyas, E. L., and Santamarina, J. C. (1994). Negative skin friction and the neutral plane. *Canadian Geotechnical Journal*, 31(4), 591-597. https://doi.org/10.1139/t94-069

Matyas, E. L., and Radhakrishna, H. S. (1968). Volume change characteristics of partially saturated soils. *Géotechnique*, 18(4), 432-448.

Mayne, P. W., and Harris, D. E. (1993). Axial load-displacement behavior of drilled shaft foundation in Piedmont residium. Technical Repeport. No. 41-30-2175, Federal Highway Administration, Washington, D.C

Mayne, P.W. and Elhakim, A. (2002). Axial pile response evaluation by geophysical piezocone tests. In: *Proc. 9th. International Conference On piling and deep foundations.* June 3-5.

Mayne, P. W. (2005). Integrated ground behavior: in-situ and labs tests. In *Deformation characteristics of geomaterials* (pp. 162-185). CRC Press.

Mayne, P. W. (2007). *Cone penetration testing* (Vol. 368). Transportation Research Board.

Mayne P.W., Peuchen, J., and Bouwmeester, D. (2010). Estimation of soil unit weight from CPTs. *Proc. 2nd International Symposium on Cone Penetration Testing*. Vol 2. 169-176

Mazurkiewicz, B. K. (1972). Test Loading of Piles According to Polish Regulations. *Royal Swedish Academy of Engineering Sciences Commission on Pile Research*, Report No. 35, Stockholm, 20

McCarthy, D. F. (1977). Essentials of soil mechanics and foundations (p. 505). Virginia: Reston Publishing Company.

Mendonca, A. V., and Paiva, J. B. D. (2003). An elastostatic FEM/BEM analysis of vertically loaded raft and piled raft foundation. *Engineering analysis with boundary elements*, 27(9), 919-933. https://doi.org/10.1016/S0955-7997(03)00061-4

Mendoza, C. E., and Colmenares, J. E. (2006). Influence of the suction on the stiffness at very small strains. In *Unsaturated Soils 2006* (pp. 529-540). https://doi.org/10.1061/40802(189)40

Meslier, V., and DiRuggiero, J., (2019). Endolithic microbial communities as model systems for ecology and astrobiology. In *Model ecosystems in extreme environments* (pp. 145-168). Academic Press. https://doi.org/10.1016/B978-0-12-812742-1.00007-6

Meyerhof, G.G. (1951). The ultimate bearing capacity of foundations. *Géotechnique*. 2(4): 301–332. https://doi:110.1680/geot.1951.2.4.301

Meyerhof, G. G. (1976). Bearing capacity and settlement of pile foundations, *Journal of the Geotechnical Engineering Division*, 102 (GT3), 197-228.

Miao, L., Liu, S., and Lai, Y. (2002). Research of soil-water characteristics and shear strength features of Nanyang expansive soil. Engineering Geology, 65(4): 261–267.

Mindlin, R. D. (1936). Force at a point in the interior of a semiinfinite solid. *Physics 7*, May, 195–202.

Mohamedzein, Y. E., Mohamed, M. G., and El Sharief, A. M. (1999). Finite element analysis of short piles in expansive soils. *Computers and Geotechnics*, *24*(3), 231-243. https://doi.org/10.1016/S0266-352X(99)00008-7

Mokwa, R. L., Duncan, J. M., and Helmers, M. J., (2000). Development of *p-y* curves for partly saturated silts and clays. Proceedings of Sessions of Geo-Denver 2000 - New Technological and Design Developments in Deep Foundations, GSP 100, 288, 224–239. https://doi.org/10.1061/40511(288)16

Morales, L., Romero, E., Jommi, C., Garzón, E., and Giménez, A. (2015). Ageing effects on the small-strain stiffness of a bio-treated compacted soil. *Géotechnique Letters*, 5(3), 217-223.

Morgenstern, N. R. (1979). Properties of compacted soils, *Proceedings of the Sixth Pan American Conference on Soil Mechanics and Foundation Engineering*, Lima, Vol. 3, pp. 349–354.

Murff, J. D., and Hamilton, J. M. (1993). P-ultimate for undrained analysis of laterally loaded piles. *Journal of Geotechnical Engineering*, *119*(1), 91-107.

Murphy, G., Igoe, D., Doherty, P., and Gavin, K. (2018). 3D FEM approach for laterally loaded monopile design. *Computers and Geotechnics*, *100*, 76-83.

Mwindo, M., (1992). Strain dependent soil modulus of horizontal subgrade reaction. M.Sc. thesis, Univ. of Missouri-Rolla, Rolla, Mo

Nasr, A. M. (2014). Experimental and theoretical studies of laterally loaded finned piles in sand. *Canadian Geotechnical Journal*, *51*(4), 381-393.

Niazi, F. S., and Mayne, P. W. (2013). Cone penetration test based direct methods for evaluating static axial capacity of single piles. *Geotechnical and Geological Engineering*, *31*(4), 979-1009. https://doi.org/10.1007/s10706-013-9662-2

Noor, S. T., Hanna, A., and Mashhour, I. (2013). Numerical modeling of piles in collapsible soil subjected to inundation. *International Journal of Geomechanics*, *13*(5), 514-526.

Ng, C. W. W., and Menzies, B., (2007). *Advanced unsaturated soil mechanics and engineering*. CRC Press.

Ng, C. W., and Zhang, L. M. (2001). Three-dimensional analysis of performance of laterally loaded sleeved piles in sloping ground. *Journal of Geotechnical and Geoenvironmental Engineering*, *127*(6), 499-509.

Nottingham, L. C. (1975). Use of quasi-static friction cone penetrometer data to predict load capacity of displacement piles. PhD Thesis. University of Florida.

Öberg, A. L., and Sällfors, G. (1997). Determination of shear strength parameters of unsaturated silts and sands based on the water retention curve. *Geotechnical Testing Journal*, *20*(1), 40-48.

Oh, W. T., Vanapalli, S. K., and Puppala, A. J. (2009). Semi-empirical model for the prediction of modulus of elasticity for unsaturated soils. *Canadian Geotechnical Journal*, *46*(8), 903-914. https://doi.org/10.1139/T09-030

Oh, W. T., and Vanapalli, S. K. (2009). A simple method to estimate the bearing capacity of unsaturated fine-grained soils. In *Proc. 62nd Canadian Geotechnical Conference* (pp. 234-241).

Oh, W. T., and Vanapalli, S. K. (2011). Modelling the applied vertical stress and settlement relationship of shallow foundations in saturated and unsaturated sands. *Canadian Geotechnical Journal*, *48*(3), 425-438. https://doi.org/10 .1139/T10-079.

Oh, W. T., and Vanapalli, S. K. (2014). Semi-empirical model for estimating the small-strain shear modulus of unsaturated non-plastic sandy soils. *Geotechnical and Geological Engineering*, 32, 259-271.

O'Neill, M. W., Hawkins, R. A. and Mahar, L. J. (1981). Field study of pile group action.

O'Neill, M.W. (1988). *Pile group prediction symposium*. Summary of prediction results. U.S. Federal Highway Administration (FHWA), Washington, D.C. Draft report.

Ortiz, J.M.R, J Serra, and C. Oteo. (1986). *Curso Aplicado de Cementations*. Third ed. Colegio de Arquitectos de Madrid. Madrid.

Pando, M., Filz, G., Ealy, C., and Hoppe, E. (2003). Axial and lateral load performance of two composite piles and one prestressed concrete pile. *Transportation research record*, *1849*(1), 61-70. https://doi.org/10.3141/1849-08

Paik, K., Salgado, R., Lee, J., and Kim, B. (2003). Behavior of open-and closed-ended piles driven into sands. *Journal of Geotechnical and Geoenvironmental Engineering*, *129*(4), 296-306. https://doi.org/10.1061/(ASCE)1090-0241(2003)129:4(296)

Parry, R. H. G., and Swain, C. W. (1977). Effective stress methods of calculating skin friction on driven piles in soft clay. *Ground Engineering*, 10 (Analytic).

Peck, R. B. (1958). A study of the comparative behaviour of friction piles, *Highway Research Board*, Special Report 36.

Peranić, J., Arbanas, Ž., Cuomo, S., and Maček, M. (2018). Soil-water characteristic curve of residual soil from a flysch rock mass. *Geofluids*, 2018. https://doi.org/10.1155/2018/6297819.

Petrasovits, G., and Awad, A. (1972). Ultimate lateral resistance of a rigid pile in cohesionless soil. In *Fifth Eur Conf On Soil Proc/Sp/* .Vol.3, 407-412.

Pham, K., Kim, D., Yoon, Y., and Choi, H. (2019). Analysis of neural network based pedotransfer function for predicting soil water characteristic curve. *Geoderma*, 351, 92-102. https://doi.org/10.1016/j.geoderma.2019.05.013.

Phanikanth, V. S., Choudhury, D., and Srinivas, K. (2013). Response of flexible piles under lateral loads. *Indian Geotechnical Journal*, *43*(1), 76-82. https://doi.org/10.1007/s40098-012-0030-6

Potyondy, J. G. (1961). Skin friction between various soils and construction materials. *Geotechnique*, *11*(4), 339-353. https://doi.org/10.1680/geot.1961.11.4.339

Potts, D. M., and Zdravković, L. (2001). *Finite element analysis in geotechnical engineering: application* (Vol. 2). London: Thomas Telford.

Poulos, H. G., and Davis, E. H. (1968). The settlement behaviour of single axially loaded incompressible piles and piers. *Géotechnique.* 18(3), 351-371. https://doi.org/10.1680/geot.1968.18.3.351

Poulos, H. G. (1971a). Behavior of laterally loaded piles: I-single piles. *Journal of the Soil Mechanics and Foundations Division*, *97*(5), 711-731.

Poulos, H. G. (1971b). Behavior of laterally loaded piles: II-pile groups. *Journal of the Soil Mechanics and Foundations Division*, *97*(5), 733-751.

Poulos, H. G., and Davis, E. H. (1980). *Pile foundation analysis and design* (Vol. 397). New York: Wiley.

Powell, J. M., Lunne, T., and Frank, R. (2001). Semi empirical design procedures for axial pile capacity in clays. In *International Conference on soil mechanics and geotechnical engineering* (pp. 991-994).

Power, K. C., Vanapalli, S. K., and Garga, V. K. (2008). A revised contact filter paper method. *Geotechnical Testing Journal*, *31*(6), 461-469.

Prakash, S., and Sharma, H. D. (1990). *Pile foundations in engineering practice*. John Wiley & Sons.

Prakash, S., and Kumar, S. (1996). Nonlinear lateral pile deflection prediction in sands. *Journal of Geotechnical Engineering*, *122*(2), 130-138. https://doi.org/10.1061/(asce)0733-9410(1996)122:2(130)

Prandtl, L. (1920). Über die Härte plastischer Körper. In Nachrichten von der Königlichen Gesellschaft der Wissenschaften zu Göttingen. Mathematisch–physikalische Klasse aus dem Jahre. Berlin. pp.74–85. [In German.]

Prasad, Y. V., and Chari, T. R. (1999). Lateral capacity of model rigid piles in cohesionless soils. *Soils and Foundations*, *39*(2), 21-29.

Pressley, J. S., and Poulos, H. G. (1986). Finite element analysis of mechanisms of pile group behaviour. *International journal for numerical and analytical methods in geomechanics*, 10(2), 213-221. https://doi.org/10.1002/nag.1610100208

Pujiastuti, H., Rifa'i, A., Adi, A. D., and Fathani, T. F. (2022). Single piles and pile groups capacity in unsaturated sandy clay based on laboratory test. *ASEAN Engineering Journal.* 12(1), 165-171. https://doi.org/10.11113/aej.v12.17520

Radhakrishna, H. S., and Adams, J. I. (1973). Long-term uplift capacity of augered footings in fissured clay. *Canadian Geotechnical Journal*, *10*(4), 647-652.

Rafraf, S., Guellouz, L., Guiras, H., and Bouhlila, R. (2016). A new model using dynamic contact angle to predict hysteretic soil water retention curve. *Soil Science Society of America Journal*, 80(6), 1433-1442. https://doi.org/10.2136/sssaj2016.01.0006

Rahardjo, H., Melinda, F., Leong, E. C., and Rezaur, R. B. (2011). Stiffness of a compacted residual soil. Engineering geology, 120(1-4), 60-67.

Randolph, M. F., and Wroth, C. P. (1978). Analysis of deformation of vertically loaded piles. *Journal of the geotechnical engineering division*, 104(12), 1465-1488. https://doi.org/10.1061/AJGEB6.0000729

Randolph, M. F. (1981). The response of flexible piles to lateral loading. *Géotechnique*. 31(2), 247–259. https://doi.org/10.1680/geot.1981.31.2.247

Randolph, M. F., and Houlsby, G. T. (1984). The limiting pressure on a circular pile loaded laterally in cohesive soil. *Geotechnique*, 34(4), 613-623.

Randolph, M. F., Dolwin, R., and Beck, R. (1994). Design of driven piles in sand. *Géotechnique.* 44(3), 427-448. https://doi.org/10.1680/geot.1994.44.3.427

Rassam, D. W., and Cook, F. (2002). Predicting the shear strength envelope of unsaturated soils. *Geotechnical Testing Journal*, *25*(2), 215-220.

Rausche, F., Goble, G. G., and Likins Jr, G. E. (1985). Dynamic determination of pile capacity. *Journal of Geotechnical Engineering*, *111*(3), 367-383. https://doi:10.1061/(ASCE)0733-9410(1985)111:3(367).

Reese, L.C., Cox, W. R., and Koop, F. D., (1974). Analysis of laterally loaded piles in sand. In *Offshore Technology Conference. Offshore Technology Conference*. https://doi.org/10.4043/2080-MS

Reese, L. C., and Welch, R. C. (1975). Lateral loading of deep foundations in stiff clay. *Journal of the Geotechnical engineering division*, *101*(7), 633-649.

Reese, L. C., Wright, S. G., and Aurora, R. P. (1984). Analysis of a pile group under lateral loading. *Laterally Loaded Deep Foundations: Analysis and Performance*, 56-71.

Reese, L. C., Wang, S. T., and Long, J. H. (1989). Scour from cyclic lateral loading of piles. In *Offshore Technology Conference*. OnePetro.

Reese, L. C. (1997). Analysis of laterally loaded piles in weak rock. *Journal of Geotechnical and Geoenvironmental engineering*, *123*(11), 1010-1017. https://doi.org/10.1061/(ASCE)1090-0241(1997)123:11(1010)

Reese, L.C., Van Impe, W. F., (2000). *Single piles and pile groups under lateral loading*. CRC Press.

Reissner, H. (1924). Zum Erddruck problem. In *Proceedings of the 1st International Congress of Applied Mechanics*, Delft, the Netherlands, 22–26 April 1924. Edited by C.B. Biezeno and J.M. Burgers. pp. 295–311. [In German.]

Ridley, A. M. (1993). *The measurement of soil moisture suction* (Doctoral dissertation, Imperial College London (University of London)).

Robertson, P. K., and Campanella, R. G. (1983). Interpretation of cone penetration tests. Part I: Sand. *Canadian geotechnical journal*, *20*(4), 718-733.

Robertson, P. K., 2016. Cone penetration test (CPT)-based soil behaviour type (SBT) classification system—an update. Can. Geotech. J. 53(12), 1910-1927. https://doi.org/10.1139/cgj-2016-0044

Robertson, P. K., and Cabal, K. L., 2015. Guide to cone penetration testing for geotechnical engineering. Gregg Drilling Testing. Inc, 6.

Rollins, K. M., Gerber, T. M., Lane, J. D., and Ashford, S. A. (2005). Lateral resistance of a full-scale pile group in liquefied sand. *Journal of Geotechnical and Geoenvironmental Engineering*, *131*(1), 115-125. https://doi.org/10.1061/(ASCE)1090-0241(2005)131:1(115)

Rollins, K. M., Clayton, R. J., Mikesell, R. C., and Blaise, B. C. (2005). Drilled shaft side friction in gravelly soils. *Journal of Geotechnical and Geoenvironmental Engineering*, 131(8), 987-1003. https://doi.org/10.1061/(ASCE)1090-0241(2005)131:8(987)

Russo, G. (2016). A method to compute the non-linear behaviour of piles under horizontal loading. *Soils and foundations*, *56*(1), 33-43. https://doi.org/10.1016/j.sandf.2016.01.003

Santhoshkumar, G., and Ghosh, P. (2021). Closed-form solution for seismic earth pressure on bilinear retaining wall using method of characteristics. *Journal of Earthquake Engineering,* 25(6), 1171-1190. https://doi.org/10.1080/13632469.2019.1570880

Sawangsuriya, A., Edil, T. B., and Bosscher, P. J. (2009). Modulus-suction-moisture relationship for compacted soils in postcompaction state. Journal of Geotechnical and geoenvironmental engineering, 135(10), 1390-1403. https://doi.org/10.1061/(ASCE)GT.1943-5606.0000108

Salgado, R. (2006). The role of analysis in non-displacement pile design. In *Modern trends in geomechanics* (pp. 521-540). Springer, Berlin, Heidelberg.

Schaap, M. G., Leij, F. J., and Van Genuchten, M. T. (2001). Rosetta: A computer program for estimating soil hydraulic parameters with hierarchical pedotransfer functions. *Journal of hydrology*, 251(3-4), 163-176. https://doi.org/10.1016/S0022-1694(01)00466-8

Schaap, M. G., and Bouten, W. (1996). Modeling water retention curves of sandy soils using neural networks. *Water Resources Research*, 32(10), 3033-3040.

Schmertmann, J. H. (1978). *Guidelines for cone penetration test: performance and design* (No. FHWA-TS-78-209). United States. Federal Highway Administration

Schneider, J. A., Xu, X., and Lehane, B. M. (2008). Database assessment of CPT-based design methods for axial capacity of driven piles in siliceous sands. *Journal of geotechnical and geoenvironmental engineering*, *134*(9), 1227-1244. https://doi.org/10.1061/(ASCE)1090-0241(2008)134:9(1227)

Schnellmann, R., Rahardjo, H., and Schneider, H. R. (2013). Unsaturated shear strength of a silty sand. *Engineering Geology*, *162*, 88-96. https://doi.org/10.1016/j.enggeo.2013.05.011

Seed, H. B., and De Alba, P. (1986). Use of SPT and CPT tests for evaluating the liquefaction resistance of sands. In *Use of in situ tests in geotechnical engineering* (pp. 281-302).

Sedano, J. I., Vanapalli, S. K., and Garga, V. K. (2007). Modified ring shear apparatus for unsaturated soils testing. *Geotechnical Testing Journal*, 30(1), 39-47. https://doi.org/10.1520/GTJ100002

Shariatmadari, N., Eslami A. A., and Karim P. F. M. (2008). Bearing capacity of driven piles in sands from SPT–applied to 60 case histories. *Iranian Journal of Science and Technology transactions of civil engineering*, 32.125-140.

Sheng, D., Gens, A., Fredlund, D. G., and Sloan, S. W. (2008). Unsaturated soils: from constitutive modelling to numerical algorithms. *Computers and Geotechnics*, *35*(6), 810-824.

Sheng, D., Zhou, A., and Fredlund, D. G. (2011). Shear strength criteria for unsaturated soils. *Geotechnical and Geological Engineering*, *29*(2), 145-159. https://doi.org/10.1007/s10706-009-9276-x

Shioi, Y., and Fukui, J. (1982). Application of N-value to design of foundations in Japan. In *Penetration testing* (pp. 159-164). Routledge.

Shooshpasha, I., Hasanzadeh, A., and Taghavi, A. (2013). Prediction of the axial bearing capacity of piles by SPT-based and numerical design methods. *Geomate Journal*, *4*(8), 560-564.

Sivrikaya, O. S. M. A. N., and Toğrol, E. (2006). Determination of undrained strength of fine-grained soils by means of SPT and its application in Turkey. *Engineering geology*, *86*(1), 52-69.

Sladen, J. A. (1992). The adhesion factor: applications and limitations, *Canadian Geotechnical Journal*, 29, 322-326.

Skempton, A. W., Yassin, A. S., and Gibson, R.E. (1953). Théorie de la force partante des pieux dans le sable, *Annales de l'Institut Technique du Bâtiment et des Travaux Publics*, vol 16. pp 285-290.

Skempton, A. W. (1959). Cast in-situ bored piles in London clay. *Géotechnique*. 9(4), 153-173. https://doi.org/10.1680/geot.1959.9.4.153

Skempton, A. W. (1986). Standard penetration test procedures and the effects in sands of overburden pressure, relative density, particle size, ageing and overconsolidation. *Géotechnique*. 36(3), 425–447. https://doi.org/10.1680/geot.1986.36.3.425

Soet, M., and Stricker, J. N. M. (2003). Functional behaviour of pedotransfer functions in soil water flow simulation. *Hydrological processes,* 17(8), 1659-1670. https://doi.org/10.1002/hyp.1207

Sørensen, S. P. H., Ibsen, L. B., and Augustesen, A. H. (2010). Effects of diameter on initial stiffness of py curves for large-diameter piles in sand. In *The European Conference on Numerical Methods in Geotechnical Engineering* (pp. 907-912). CRC Press.

Sowers, G. F. (1979). *Introductory soil mechanics and foundations*. The Macmillan Company, 4th edition, New York.

Stacul, S., Squeglia, N., and Morelli, F. (2017). Laterally loaded single pile response considering the influence of suction and non-linear behaviour of reinforced concrete sections. *Applied Sciences*, *7*(12), 1310. https://doi.org/10.3390/app7121310

Stevens, J. B., and Audibert, J. M. E. (1979). Re-examination of py curve formulations. In *Offshore technology conference*.

Su, D., Huang, J. J., and Yan, W. M. (2018). Parametric investigation on the responses of laterally loaded piles in overconsolidated clay using nondimensional solutions addressing nonlinear soil-pile interaction. *Computers and Geotechnics,* 96, 203-214.

Suleiman, M. T., Ni, L., Helm, J. D., and Raich, A. (2014). Soil-pile interaction for a small diameter pile embedded in granular soil subjected to passive loading. *Journal of Geotechnical and Geoenvironmental Engineering*, *140*(5), 04014002. https://doi.org/10.1061/(ASCE)GT.1943-5606.0001081

Sullivan W. (1977). *Development and evaluation of a unified method for the analysis of laterally loaded piles in clay.* University of Texas. MS Thesis.

Sun, K. (1994). Laterally loaded piles in elastic media. *Journal of Geotechnical Engineering*, *120*(8), 1324-1344.

Suzuki, Y., Goto, S., Hatanaka, M., and Tokimatsu, K. (1993). Correlation between strengths and penetration resistances for gravelly soils. *Soils and Foundations*, *33*(1), 92-101.

Sokolovskii, V.V. (1960). *Statics of soil media*. (Translated by D.H. Jones and A.N. Schofield.) Butterworths, London

Tekinsoy, M. A., Kayadelen, C., Keskin, M. S., and Söylemez, M. (2004). An equation for predicting shear strength envelope with respect to matric suction. *Computers and*

Geotechnics, *31*(7), 589-593. https://doi.org/10.1016/j.compgeo.2004.08.001

Tavenas, F. A. (1971). Load test results on friction piles in sand. *Canadian Geotechnical Journal*. 8(1). 7-22. https://doi.org/10.1139/t71-002

Terzaghi, K. (1943). *Theoretical soil mechanics.* New York: Wiley.

Terzaghi, K., and Peck, R.B. (1948). *Soil Mechanics in Engineering Practice.* John Wiley & Sons.

Terzaghi, K. (1955). Evaluation of coefficients of subgrade reaction. *Géotechnique*. 5(4), 297–326. https://doi.org/10.1680/geot.1955.5.4.297

Tomlinson, M., Woodward, J., (2007). *Pile design and construction practice*. CRC press.

Tomlinson, M. J. (1957). The adhesion of piles driven in clay soils. In *Proceedings of the 4th International Conference on Soil Mechanics and Foundation Engineering* (Vol. 2, pp. 66-71).

Truong, P. (2017). *Experimental investigation on the behaviour of laterally loaded piles in soft clay, sand and residual soils* (Doctoral dissertation, PhD thesis, The University of Western Australia, Perth, Australia).

Tzivakos, K. P., and Kavvadas, M. J. (2014). Numerical investigation of the ultimate lateral resistance of piles in soft clay. *Frontiers of Structural and Civil Engineering*, *8*(2), 194-200.

Uchaipichat, A. (2012). Variation of pile capacity in unsaturated clay layer with suction. *Electronic Journal of Geotechnical Engineering*, *17*, 2425-2433.

Uma Maheswari, R., Boominathan, A., and Dodagoudar, G. R. (2010). Use of surface waves in statistical correlations of shear wave velocity and penetration resistance of Chennai soils. *Geotechnical and Geological Engineering*, *28*(2), 119-137.

Vahedifard, F., and Robinson, J. D. (2016). Unified method for estimating the ultimate bearing capacity of shallow foundations in variably saturated soils under steady flow. *Journal of Geotechnical and Geoenvironmental Engineering*, *142*(4), 04015095. https://doi.org/10.1061/(ASCE)GT.1943-5606.0001445

Valikhah, F., Eslami, A., and Veiskarami, M. (2019). Load–displacement behavior of driven piles in sand using CPT-based stress and strain fields. *International Journal of Civil Engineering*, *17*(12), 1879-1893. https://doi.org/10.1007/s40999-018-0388-7

Van der Veen, C. (1953). The bearing capacity of pile. In *Proc. 3rd ICSMFE* (Vol. 2, pp. 84-90).

Van Dijk, B. F. J., and Kolk, H. J. (2011). CPT-based design method for axial capacity of offshore piles in clays. *Frontiers in offshore geotechnics II*, 555-560.

van Genuchten, M. T. (1980). A closed-form equation for predicting the hydraulic conductivity of unsaturated soils. *Soil science society of America journal*, *44*(5), 892-898. https://doi.org/10.2136/sssaj1980.03615995004400050002x.

Vanapalli, S.K., Wright, A., and Fredlund, D.G. (2000). Shear strength of two unsaturated silty soils over the suction range from 0 to 1,000,000 kPa. *Proc. 53rd Canadian Geotechnical Conference*, Montreal, October 15-18: 1161-1168.

Vanapalli, S. K., Fredlund, D. G., Pufahl, D. E., and Clifton, A. W. (1996). Model for the prediction of shear strength with respect to soil suction. *Canadian geotechnical journal*, *33*(3), 379-392. https://doi.org/10.1139/t96-060

Vanapalli, S. K., Sillers, W. S., and Fredlund, M. D. (1998). The meaning and relevance of residual state to unsaturated soils. In *51st Canadian Geotechnical Conference* (pp. 4-7). Alberta, Canada: Edmonton.

Vanapalli, S. K., and Catana, M. C. (2005). Estimation of the soil-water characteristic curve of coarse-grained soils using one point measurement and simple properties. In *Proceedings of an International Symposium on Advanced Experimental Unsaturated Soil Mechanics* (pp. 401-410).

Vanapalli, S. K., and Mohamed, F. M. (2007). Bearing capacity of model footings in unsaturated soils. In *Experimental unsaturated soil mechanics*. Springer, Berlin, 483–493. http://dx.doi. org/10.1007/3-540-69873-6_48.

Vanapalli, S. K. (2009). Shear strength of unsaturated soils and its applications in geotechnical engineering practice. In *Keynote Address. Proc. 4th Asia-Pacific Conf. on Unsaturated Soils. New Castle, Australia* (pp. 579-598).

Vanapalli, S., and Oh, W. (2010). A model for predicting the modulus of elasticity of unsaturated soils using the soil-water characteristic curve. *International Journal of Geotechnical Engineering*, 4(4), 425-433. https://doi.org/10.3328/IJGE.2010.04.04.425-433

Vanapalli, S. K., and Taylan, Z. N. (2012). Design of single piles using the mechanics of unsaturated soils. *International Journal of GEOMATE.* 2(1), 197–204.

Vanapalli, S. K., Sheikhtaheri, M., and Oh, W. T. (2018). Experimental and simple semi-empirical methods for interpreting the axial load versus settlement behaviors of single model piles in unsaturated sands. *Geotechnical Testing Journal*, *41*(4), 698-716. https://doi.org/10.1520/GTJ20170152

Van Der Veen, C., (1953). The bearing capacity of the pile. In: *Proceedings of the third ICSM FE*, pp 84–90

Vardanega, P. J., Williamson, M. G., & Bolton, M. D. (2012). Bored pile design in stiff clay II: mechanisms and uncertainty. *Proceedings of the Institution of Civil*

Engineers-Geotechnical Engineering, 165(4), 233-246. https://doi.org/10.1680/geng.11.00063

Veiskarami, M., Eslami, A., and Kumar, J. (2011). End-bearing capacity of driven piles in sand using the stress characteristics method: analysis and implementation. *Canadian geotechnical journal*, *48*(10), 1570-1586. https://doi.org/10.1139/t11-057

Verbrugge, J. C. (1981). Évaluation du tassement des pieux à partir de l'essai de pénétration statique. Revue Française de Géotechnique, (15), 75-82. https://doi.org/10.1051/geotech/1981015075

Verruijt, A. and Kooijman, A. P. (1989). Laterally loaded piles in a layered elastic medium. *Geotechnique*, 39, No. 1, 39–46.

Vesić, A.S. (1963). Bearing capacity of deep foundations in sand. *Highway Research Record*. 39: 112–153

Vesić, A.S. (1967). Ultimate load and settlement of deep foundations in sand. In *Proceedings of the Symposium on Bearing Capacity and Settlement of Foundations*, Durham, N.C., 5–6 April 1965. Edited by A.S. Vesić. Duke University, Durham, N.C. pp. 53–68.

Vesić, A. S. (1970). Tests on instrumented piles, Ogeechee River site. *Journal of the Soil Mechanics and Foundations Division*, *96*(2), 561-584. https://doi.org/10.1061/JSFEAQ.0001404

Vesic, A. S. (1975). Principles of pile design. *Lecture Series on Deep Foundations Sponsored by the Geotechnical Group, BSCES/ASCE in cooperation with Massachusetts Institute of Technology*.

Vijayvergiya, V. N., and Focht, J. A. (1972). A new way to predict capacity of piles in clay. *Offshore Technology Conference,* Dallas.

Vijayvergiya, V. N. (1977). Load-movement characteristics of piles. *Ports '77: 4th Annual Symp. of the Waterway, Port, Coastal, and Ocean Division*, ASCE, Los Angeles, 269–284.

Vilar, O. M. (2006). A simplified procedure to estimate the shear strength envelope of unsaturated soils. *Canadian Geotechnical Journal*, *43*(10), 1088-1095.

Vlasov, V. Z. and Leontev, N. N. (1966). *Beams, plates and shells on elastic foundations*. Jerusalem: Israel Program for Scientific Translations.

Wang, Z., Xie, X., and Wang, J. (2012). A new nonlinear method for vertical settlement prediction of a single pile and pile groups in layered soils. *Computers and Geotechnics*, 45, 118-126. https://doi.org/10.1016/j.compgeo.2012.05.011

Wei, B. Z., Pezeshk, S., Chang, T. S., Hall, K. H., and Liu, H. P. (1996). An empirical method to estimate shear wave velocity of soils in the New Madrid seismic zone. *Soil Dynamics and Earthquake Engineering*, *15*(6), 399-408.

Wheeler, S. J., Sharma, R. S., and Buisson, M. S. R. (2003). Coupling of hydraulic hysteresis and stress–strain behaviour in unsaturated soils. *Géotechnique*, *53*(1), 41-54.

Winkler, E. (1867). Die Lehre von der Elastizit at und Festigkeit. Domimicus. Prague

Wong, K. S., and Teh, C. I. (1995). Negative skin friction on piles in layered soil deposits. *Journal of Geotechnical Engineering*, 121(6), 457-465.

Wösten, J. H. M., Lilly, A., Nemes, A., and Le Bas, C. (1999). Development and use of a database of hydraulic properties of European soils. *Geoderma*, 90(3-4), 169-185. https://doi.org/10.1016/S0016-7061(98)00132-3

Yanamandra, G., and Oh, W. T. (2021). Influence of Excavation Time, Tension Crack, and Rainfall on the Stability of Unsupported Vertical Cuts in Unsaturated Soil. *International Journal of Geomechanics*, 21(10), 04021199.

Yang, K., and Liang, R. (2006). Numerical solution for laterally loaded piles in a two-layer soil profile. *Journal of Geotechnical and Geoenvironmental Engineering*, *132*(11), 1436-1443. https://doi.org/10.1061/(asce)1090-0241(2006)132:11(1436)

Yang, J., Tham, L. G., Lee, P. K. K., Chan, S. T., and Yu, F. (2006). Behaviour of jacked and driven piles in sandy soil. *Géotechnique*, 56(4), 245-259. https://doi:10.1680/geot. 2006.56.4.245

Yang, Z. X., Guo, W. B., Zha, F. S., Jardine, R. J., Xu, C. J., and Cai, Y. Q. (2015). Field behavior of driven prestressed high-strength concrete piles in sandy soils. American Society of Civil Engineers. https://doi.org/10.1061/(ASCE)GT.1943-5606.0001303

Yasufuku, N., and Hyde, A. F. L. (1995). Pile end-bearing capacity in crushable sands. *Geotechnique*, *45*(4), 663-676.

Yen, T. L., Lin, H., Chin, C. T., and Wang, R. F. (1989). Interpretation of instrumented driven steel pipe piles. *Proc. Foundation Eng. Cong.: Current Principle and Practices*, *GSP No*, *22*, 1293-1308.

Yoshida, I., and Yoshinaka, R. (1972). A method to estimate modulus of horizontal subgrade reaction for a pile. *Soils and Foundations*, *12*(3), 1-17.

Yu, J., Huang, M., and Zhang, C. (2015). Three-dimensional upper-bound analysis for ultimate bearing capacity of laterally loaded rigid pile in undrained clay. *Canadian Geotechnical Journal*, *52*(11), 1775-1790.

Zdravković, L., Taborda, D. M., Potts, D. M., Abadias, D., Burd, H. J., Byrne, B. W., ...

and Ushev, E. (2020). Finite-element modelling of laterally loaded piles in a stiff glacial clay till at Cowden. *Géotechnique*, *70*(11), 999-1013.

Zhang, L., McVay, M. C., and Lai, P. W. (1999). Centrifuge modelling of laterally loaded single battered piles in sands. *Canadian Geotechnical Journal*, *36*(6), 1074-1084.

Zhang, L., Silva, F., and Grismala, R. (2005). Ultimate lateral resistance to piles in cohesionless soils. *Journal of Geotechnical and Geoenvironmental Engineering*, *131*(1), 78-83.

Zhang, L. (2009). Nonlinear analysis of laterally loaded rigid piles in cohesionless soil. *Computers and geotechnics*, *36*(5), 718-724. https://doi.org/10.1016/j.compgeo.2008.12.001

Zhang, G., and Zhang, J. M. (2009). Constitutive rules of cyclic behavior of interface between structure and gravelly soil. *Mechanics of materials*, 41(1), 48-59.

Zhang, L., and Ahmari, S. (2013). Nonlinear analysis of laterally loaded rigid piles in cohesive soil. *International Journal for Numerical and Analytical Methods in Geomechanics*, *37*(2), 201-220. https://doi.org/10.1002/nag.1094

Zhang, L. L., Fredlund, M. D., Fredlund, D. G., Lu, H., and Wilson, G. W. (2015). The influence of the unsaturated soil zone on 2-D and 3-D slope stability analyses. *Engineering Geology*, 193, 374-383.

Zhang, Q. Q., Zhang, Z. M., and He, J. Y. (2010). A simplified approach for settlement analysis of single pile and pile groups considering interaction between identical piles in multilayered soils. *Computers and Geotechnics*, 37(7-8), 969-976. https://doi.org/10.1016/j.compgeo.2010.08.003

Zhang, Q. Q., and Zhang, Z. M. (2012). A simplified nonlinear approach for single pile settlement analysis. *Canadian Geotechnical Journal*, 49(11), 1256-1266. https://doi.org/10.1139/t11-110

Zhang, Q. Q., Li, S. C., Liang, F. Y., Yang, M., and Zhang, Q. (2014). Simplified method for settlement prediction of single pile and pile group using a hyperbolic model. *International Journal of Civil Engineering*, 12(2), 146-159.

Zhang, C., Yan, Q., Zhao, J., and Wang, J. (2020). Formulation of ultimate bearing capacity for strip foundations based on the Meyerhof theory and unsaturated soil mechanics. *Computers and Geotechnics*, *126*, 103734. https://doi.org/10.1016/j.compgeo.2020.103734

Zhou, A. N., Sheng, D., and Carter, J. P. (2012). Modelling the effect of initial density on soil-water characteristic curves. *Géotechnique*, 62(8), 669-680. https://doi.org/10.1680/geot.10.P.120

Zhou, A., Huang, R., and Sheng, D. (2016). Capillary water retention curve and shear strength of unsaturated soils. *Canadian Geotechnical Journal*, *53*(6), 974-987.

https://doi.org/10.1139/cgj-2015-0322

Zhu, H., and Chang, M. F. (2002). Load transfer curves along bored piles considering modulus degradation. *Journal of Geotechnical and Geoenvironmental Engineering*, 128(9), 764-774. https://doi.org/10.1061/(ASCE)1090-0241(2002)128:9(764)

Zong-Ze, Y., Hong, Z., and Guo-Hua, X. (1995). A study of deformation in the interface between soil and concrete. *Computers and Geotechnics*, 17(1), 75-92. https://doi.org/10.1016/0266-352X